DISS. ETH NO. 26137

Nickel-Catalyzed Cyclopropanation with Lithiomethyltrimethylammonium Triflate

A thesis submitted to attain the degree of

DOCTOR OF SCIENCES of ETH ZURICH

(Dr. sc. ETH Zurich)

presented by

Stefan Alexander Künzi

MSc in Chemistry ETH

born on 12.11.1988

citizen of Linden, BE

accepted on the recommendation of

Prof. Dr. Peter Chen, examiner
Prof. Dr. Bill Morandi, co-examiner

2019

Front cover: Lucas Jennis, in *De Lapide Philosophico*, 1625, Frankfurt.

Acknowledgment

I would like to thank Prof. Dr. Peter Chen for giving me a space in his lab, a challenging but fascinating research topic and the freedom to explore it wherever my ideas led me. It was a true inspiration working in a group with such a diverse interest. Your mentoring made me a better scientist.

I would like to thank Prof. Dr. Bill Morandi for taking on the role as co-examiner, for his mentorship early on in my studies and all throughout the years. Black t-shirts and shorts are more than clothes, it's a way of a life.

Armin Limacher is gratefully acknowledged for his tireless effort to help. Without Armin's support, the work presented in this thesis would have been much harder to accomplish. Be it GCs, glove boxes, or computers, Armin was more than willing to bring things back to working conditions. Your help was always greatly appreciated and never taken for granted.

It was a great pleasure to have such an amicable administrative staff over years. Anke Witten, Gabriela Schenk, and Barbara Loepfe, thank you very much for all the nice conversation over yet another coffee in the group room. It was always a true joy coming to the office for a Schöggeli. Your help made life much easier.

Many thanks go to Dr. Juan Manuel Sarria Toro for initiating me into the beautiful world of ammonium ylides and teaching me the art of making glass-coated stir bars.

I thank Dr. Renana Gershoni-Poranne for all the calculations in thesis and many more.

To all the members of G220 over the years, Dr. Augustin Tchawou, Dr. Krista Vikse, Miao Yanan, Kevin Breitwieser and Maurice Andrey, thank you for creating a motivating atmosphere in the lab. To the students who were willing to try out my ideas, Mathias Ginterseder, Lucas Schaus, and André Bütikofer, I hope you learned just as much as I did during your projects. André Bütikofer is additionally acknowledged for correcting the Zusammenfassung.

Abstract

Cyclopropanes are prevalent structures in natural and synthetic molecules and are of interest due to their unique reactivity and geometry.

To install a cyclopropane by transfer of a methylene unit CH_2 to an alkene, three reaction classes are known. The transition metal-catalyzed decomposition of diazomethane CH_2N_2, the Simmons-Smith reaction, commonly involving zinc carbenoid species such as the classic $IZnCH_2I$, and the transfer of a methylene unit from an ylide such as the Corey-Chaykovsky reagent $Me_2S(O)CH_2$. While the latter is only applicable in cases where the double bond is activated by an electron-withdrawing group, the former two are more broadly applicable to unactivated and/or electron-rich alkenes. Especially on large scale, several drawbacks plague the cyclopropanation of unactivated alkenes. The Simmons-Smith reaction often employs a superstoichometric amount of the carbenoid reagent, creating a large amount of metal salt waste. From an atom-economy standpoint, diazomethane is almost ideal. The reaction usually proceeds in the presence of very low catalyst loadings with N_2 as the only by-product. Nevertheless, the hazardous nature of diazomethane, a toxic and explosive gas, precludes its use on anything but small-scale reactions. An alternative, safe and easy to handle reagent would be of synthetic use.

Reported in 1960 by Franzen and Wittig to cyclopropanate an unactivated alkene, cyclohexene, lithiomethyltrimethylammonium salts appear to be such candidates. Unfortunately, four years later this result was declared irreproducible by Wittig and Krauss. Previous work in our group established lithiomethyltrimethylammonium triflate as a methylene donor in uncatalyzed reactions with styrenes and stilbenes, which are weakly activated alkenes, but not with unactivated alkenes.

The present work introduces nickel as a uniquely active catalyst for the cyclopropanation of unactivated alkenes with lithiomethyltrimethylammonium triflate as methylene donor, including Franzen and Wittg's original substrate cyclohexene. In an initial optimization phase, $(Ph_3P)_2NiBr_2$ was established as the most effective and convenient precatalyst source. Several odd features of the cyclopropanation were observed during this phase as well. Most notably, a pronounced substrate dependence on the product yield and a strong non-linear effect of the catalyst loading on the yield gave rise to a bell-shaped curve for the plot of catalyst concentration versus yield for the cyclopropanation of cylooctene. Additionally, we observed the formation of

polyethylene and cyclopropane. These side products likely stem from initial homocoupling of two carbene fragments to give ethene, followed by subsequent polymerization or cyclopropanation, respectively. We proposed a catalytic cycle based on these observations, which is supported by literature precedent for all involved steps, including a nickel carbene species. These studies are summarized in chapter 2.

Our initial hypothesis was reversible formation of this nickel carbene, analogous to the persistent radical effect, which could explain some of the observed effects. In a first set of mechanistic experiments, no proof for reversibility could be established. This prompted us to study the mechanism more extensively by kinetic, physical-organic and computational methods to rationalize the observed effects and improve the reaction in a mechanism-guided fashion. These efforts are discussed in chapter 3.

Norbornene, the highest yielding alkene with 79 – 83% yield, was chosen as substrate for the kinetic studies. We observed approximately 0th order in norbornene and PPh$_3$, and 1st order in catalyst for both the cyclopropanation and homocoupling in the absence of added alkene. The order in ylide appeared more complex and hints at a change from 0th to 1st order during the reaction progress. Additionally, a secondary KIE of 2.1 ± 0.3 was observed using the perdeuterated ammonium reagent [LiCD$_2$N(CD$_3$)$_3$)]OTf. This secondary KIE implies a rehybridization of the ylidic carbon from sp^3 to sp^2 in the rate-limiting transition state relative to the resting state.

Taking these results together, we proposed a catalytic cycle for the cyclopropanation with the substrate already coordinated in the resting state. This is followed by rate-determining extrusion of NMe$_3$ from the nickel ylide adduct to give the nickel carbene. This species undergoes intramolecular cycloaddition with the substrate and subsequent reductive elimination gives the cyclopropane.

Additionally, we proposed that a pre-equilibrium between alkene and phosphine binding to Ni(0) exists in the resting state manifold. This pre-equilibrium intersects the product-forming cycle with the parasitic homocoupling cycle. If no alkene is bound before the nickel carbene is formed, homocoupling and/or subsequent side reactions occur that reduce the cyclopropanation yield. We developed this mechanistic proposal into a mathematical model, with the pre-equilibrium at its core, based on Tolman's binding constants of alkenes to Ni(0).

This insight led to the design of new ligands with remote steric hindrance as introduced by Wu and Doyle in a recent publication. These ligands allow for the coordination of the alkene by virtue of their small buried volume but prevent saturation of the catalyst with ligands by their large cone angle. This rationale was investigated via a multivariate regression analysis. This strategy almost doubled the yield for cyclooctene from 25 % to 48 %. This design strategy is discussed in chapter 4.

Chapter 5 concludes this thesis and offers several rationales to improve the reaction based on our mechanistic insights.

Zusammenfassung

Cyclopropane sind häufige Strukturen in natürlichen und synthetischen Molekülen und interessant wegen ihrer einzigartigen Reaktivität und Geometrie.

Um ein Cyclopropan durch Transfer einer Methyleneinheit CH_2 auf ein Alken zu synthetisieren, sind drei Reaktionsklassen bekannt. Die Übergangsmetall-katalysierte Zersetzung von Diazomethan CH_2N_2, die Simmons-Smith-Reaktion, normalerweise Zinkcarbenoid-Spezies, wie das klassische $IZnCH_2I$, involvierend, und den Transfer einer Methyleneinheit eines Ylids, wie das Corey-Chaykosky-Reagenz $Me_2S(O)CH_2$. Während das letztgenannte nur anwendbar ist für Doppelbindungen, die durch eine elektronenziehende Gruppe aktiviert sind, sind die ersten Beiden breiter anwendbar auf nicht-aktivierte und/oder elektronenreiche Alkene. Die Simmons-Smith-Reaktion verwendet häufig eine überstöchiometrische Menge des Carbenoidreagenzes, was zu einer grossen Menge an Metallsalzabfällen führt. Diazomethan ist vom Standpunkt der Atomökonomie her fast ideal. Die Reaktion verläuft normalerweise in Anwesenheit einer sehr kleinen Katalysatormenge mit N_2 als einzigem Nebenprodukt. Nichtsdestotrotz, die gefährlichen Eigenschaften von Diazomethan, einem giftigen und explosiven Gas, verhindern dessen Verwendung ausserhalb des Labormassstab. Ein alternatives, sicheres und einfach handhabbares Reagenz wäre von synthetischem Interesse.

Lithiomethyltrimethylammoniumsalze scheinen aufgrund einer 1960 von Franzen und Wittig berichteten Cyclopropanierung eines nicht-aktiviertes Alkens, Cyclohexen, solche idealen Kandidaten zu sein. Leider wurde dieses Resultat vier Jahre später von Wittig und Krauss für nicht reproduzierbar erklärt. Vorherige Arbeiten in unserer Gruppe haben Lithiomethyltrimethylammoniumtriflat als Methylendonor in einer unkatalysierten Reaktion mit Styrol und Stilben, schwach aktivierten Alkenen, etabliert, jedoch nicht für unaktivierte Alkene.

Die vorliegende Arbeit führt Nickel als einzigartig aktiven Katalysator für die Cyclopropanierung von unaktivierten Alkenen mit Lithiomethyltrimethylammoniumtriflat als Methylendonor ein, inklusive dem ursprünglichen Substrat von Franzen und Wittig, Cyclohexen. In einer anfänglichen Optimisierungsphase wurde $(Ph_3P)_2NiBr_2$ als die effektivste und praktischste Katalysatorvorstufenquelle etabliert. Mehrere eigenartige Merkmale wurden ebenfalls

in dieser Phase beobachtet. Am wichtigsten, eine ausgeprägte Substratabhängigkeit auf die Produktausbeute und ein starker nicht-linearer Effekt der Katalysatormenge auf die Ausbeute, was in einer glockenförmigen Kurve für den Katalysatorkonzentration-Ausbeute-Graphen für die Cyclopropanierung von Cycloocten resultierte. Zusätzlich beobachteten wir die Bildung von Polyethen und Cyclopropan. Nebenprodukte, die wahrscheinlich von anfänglicher Homokupplung zweier Carbenfragmente zu Ethen, gefolgt von anschliessender Polymerisation respektive Cyclopropanierung, stammen. Wir schlugen basierend auf diesen Beobachtungen und Literaturpräzedenz aller involvierten Schritte inklusive einer Nickelcarbenspezies einen katalytischen Zyklus vor. Diese Studien sind in Kapitel 2 zusammengefasst.

Unsere anfängliche Hypothese war eine reversible Bildung dieses Nickelcarbens, analog zum persistenten Radikal-Effekt, die einige der beobachteten Effekte erklären könnte. In einer ersten Reihe von mechanistischen Experimenten konnte kein Beweis einer Reversibilität festgestellt werden. Dies veranlasste uns den Mechanismus umfassender mittels kinetischen, physikalisch-organischen und rechnergestützten Methoden zu untersuchen, um die beobachteten Effekte zu rationalisieren und die Reaktion auf einem Mechanismus-gelenkten Weg zu verbessern. Diese Anstrengungen werden im Kapitel 3 diskutiert.

Norbornen, das Alken mit der höchsten Ausbeute zwischen 79 und 83 %, wurde als Substrat für die kinetischen Studien ausgewählt. Wir beobachteten ungefähr eine Reaktion nullter Ordnung für Norbornen und PPh_3 und eine Reaktion erster Ordnung für den Katalysator für die Cyclopropanierung respektive die Homokupplung in Abwesenheit eines hinzugefügten Alkens. Die Reaktionsordnung des Ylides erschien komplizierter und weist auf einen Wechsel zwischen nullter und erster Ordnung während des Fortschrittes der Reaktion hin. Zusätzlich wurde ein sekundärer KIE von 2.1 ± 0.3 für das perdeuterierte Ammoniumreagenz $[LiCD_2N(CD_3)_3]OTf$ beobachtet. Dies impliziert eine Rehybridisierung des ylidischen Kohlenstoffs von sp^3 zu sp^2 im geschwindigkeitsbestimmenden Übergangszustand relativ zum Ruhezustand.

Diese Resultate zusammennehmend haben wir einen katalytischen Zyklus für die Cyclopropanierung vorgeschlagen in dem das Substrat bereits im Ruhezustand koordiniert vorliegt. Dem folgt eine geschwindigkeitsbestimmende Extrusion des NMe_3 aus dem Nickel-Ylid-Addukt, um das Nickelcarben zu erhalten. Diese Spezies geht

eine Cycloaddition mit dem Substrat ein mit anschliessender reduktiven Eliminierung um das Cyclopropan zu erhalten.

Zusätzlich postulierten wir, dass ein Vorgleichgewicht zwischen Alken- und Phosphin-Koordination an das Ni(0) in der Ruhezustandsmenge existiert, welches den produktiven Zyklus mit dem parasitären Homokupplungszyklus verbindet. Falls kein Alken gebunden ist bevor sich das Nickelcarben bildet, erfolgen eine Homokupplung und/oder weitere Nebenreaktionen, welche die Cyclopropanierungsausbeute reduzieren. Wir haben diesen mechanistischen Vorschlag in ein mathematisches Modell überführt in dessen Mitte sich das Vorgleichgewicht befindet, welches auf Tolman's Bindungskonstanten von Alkenen an Ni(0) basiert.

Diese Einsicht führte zu einem Entwurf für neue Liganden mit entfernter sterischer Hinderung, wie sie von Wu und Doyle in einer kürzlich erschienenen Publikation eingeführt wurde. Diese Liganden erlauben die Koordination des Alkens aufgrund ihrer kleinen vergrabenen Volumina, verhindern aber die Sättigung des Katalysators mit Liganden mittels ihrer grossen Kegelwinkel. Diese Begründung wurde mittels einer multivariaten Regressionsanalyse untersucht. Diese Strategie verdoppelte beinahe die Ausbeute für Cyclooocten von 25 % zu 48 %. Diese Entwurfsstrategie wird in Kapitel 4 diskutiert.

Kapitel 5 schliesst diese Dissertation ab und offeriert einige Überlegungen, um die Reaktion, basierend auf unseren mechanistischen Erkenntnissen, zu verbessern.

Publications

(1) <u>Künzi, S. A.</u>; Sarria Toro, J. M.; den Hartog, T.; Chen P. Nickel-Catalyzed Cyclopropanation with NMe_4OTf and nBuLi. *Angew. Chem. Int. Ed.* **2015**, *54*, 10670-106704.

(2) <u>Künzi, S. A.</u>; Sarria Toro, J. M.; den Hartog, T.; Chen, P. A Case for Mechanisms. *Isr. J. Chem.* **2015**, *56*, 53-61.

(3) <u>Künzi, S. A.</u>; Poranne-Gershoni, R.; Chen, P. Mechanistic Studies on the Nickel-Catalyzed Cyclopropanation with Lithiomethyltrimethylammonium Triflate. *Organometallics* **2019**, *38*, 1928-1938*.*

Presentations

ISRIUM, Ascona, Switzerland   July 2018
Poster Presentation

SSCI Symposium, ETH Zürich, Zürich, Switzerland   January 2018
Poster Presentation

Gordon Research Conference: Organometallic   July 2016
Chemistry, Newport, RI, USA
Poster Presentation

SSCI Symposium, ETH Zürich, Zürich, Switzerland   January 2016
**Poster Presentation**

Contents

1 Introduction

1.1 Nickel

Nickel was first isolated by the Swedish chemist Axel Frederic Cronstedt in 1751 from the NiAs mineral niccolite, or known by its German names *Rotnickelkies* or *Kupfernickel*.[1] The name *Kupfernickel* in turn, came from its deceiving appearance; metallic red in color it fooled miners of the sixteenth century into believing it to be copper. Upon smelting, only toxic fumes (As compounds!) emanated, leaving behind a, then unknown, silver-grey substance instead of copper metal. Thus it was believed to be the work of an evil demon or kobold (cf. cobalt), who had changed or cursed the ore.[2]

As one of the so-called base metals, it is relative common in the earth's crust at 150 ppm as compared to the heavier members of the nickel triad, Pd (0.011 ppm) and Pt (0.005 ppm), yet still relatively rare when compared to iron (47000 ppm).

Today, metallic nickel is most commonly produced from nickel sulfide ores. The ore is first roasted to give nickel oxide, which is reduced in a second step with coke to the metal.

$$2\ NiS \xrightarrow[-\ 2\ SO_2]{+\ 3\ O_2,\ \Delta} 2\ NiO \xrightarrow[-\ CO_2]{+\ C,\ \Delta} Ni \qquad (1.1)$$
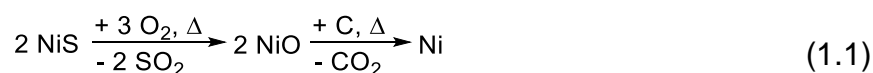
If needed, the nickel metal can be further refined by the Mond process discovered in 1890 by Ludwig Mond and coworkers.[3] First, carbon monoxide is passed over the nickel powder heated to 80 °C. The volatile $Ni(CO)_4$ is subsequently directed to another chamber heated to 180 °C, where it decomposes again to pure metallic nickel and CO.

$$Ni \xrightarrow[80\ °C]{+\ 4\ CO} Ni(CO)_4 \xrightarrow[180\ °C]{-\ 4\ CO} Ni \qquad (1.2)$$

Nickel(II) chloride is moderately toxic, slightly more so then the 'heavy metal' salts $PdCl_2$ and $PtCl_2$.[4] Additionally, nickel salts can lead in many cases to skin sensitization and are potentially carcinogenic. Counterintuitively, the carcinogenicity is higher for insoluble nickel compounds such as Ni_3S_2. Dissolved nickel ions bind already in the

extracellular environment to proteins or single amino acids and do not enter the nucleus as such a complex. Insoluble nickel particles, on the other hand, enter the cell via endocytosis, dissolve inside the lysosomes close to the nucleus, and can subsequently enter the nucleus more easily and cause DNA damage.

1.2 Cyclopropanes and Their Synthesis

The first synthesis of cyclopropane, C_3H_6, was accomplished by August Freund in 1881.[5] The compound was synthesized by an intramolecular Wurtz coupling of 1,3-dibromopropane with sodium. Since then, many more naturally occurring or man-made cyclopropanes have been discovered or synthesized.

$$Br\diagdown\diagup Br \xrightarrow{\text{Na}} \triangle \qquad (1.3)$$

A very brief selection of cyclopropanes is given in **Figure 1.1**. The complexity of the cyclopropanes can vary significantly. The pentacyclopropane FR-900848 (**1.1**) is an antifungal compound isolated from the bacterium *Streptoverticillium fervens*.[6] The bicyclic monoterpene thujene (**1.3**) is a component of many plants and can be found in essential oils derived from them.[7] 1-Aminocyclopropane-1-carboxylic acid (ACC, **1.2**) is the smallest possible cyclopropyl amino acid and is the direct precursor for ethylene in plants, where it acts as a plant hormone. Lastly, Javanol (**1.4**) is a fragrance molecule by Givaudan with a creamy, warm sandalwood smell.[8]
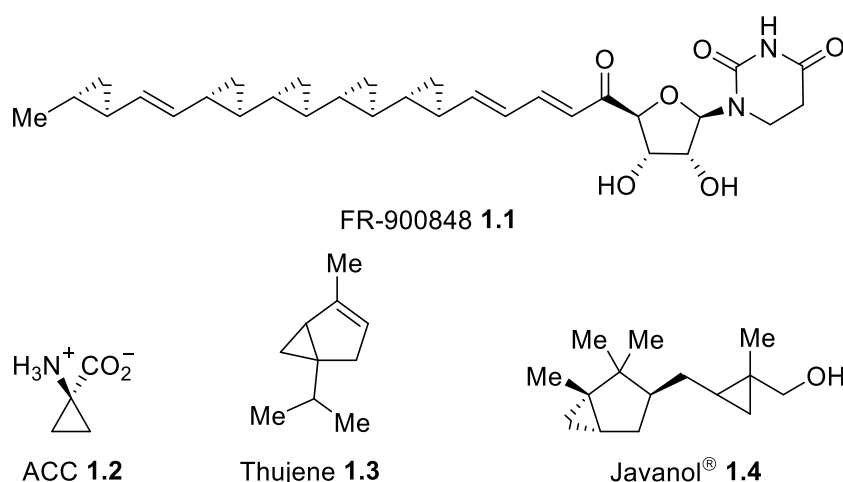

FR-900848 **1.1**

ACC **1.2**   Thujene **1.3**   Javanol® **1.4**

Figure 1.1. .Selection of naturally occurring and man-made cyclopropanes of different structural complexity.

Not entirely surprising, the biosynthesis of cyclopropanes does not proceed via carbenes or carbenoids to the best of our knowledge.

Broadly speaking, biosynthetic pathways can be divided into mechanisms containing carbocationic or carbanionic intermediates.[6] Two examples are shown below.

Figure 1.2 shows a carbocationic rearrangement sequence starting from geranyl pyrophosphate (**1.5**) to give thujene (**1.3**).
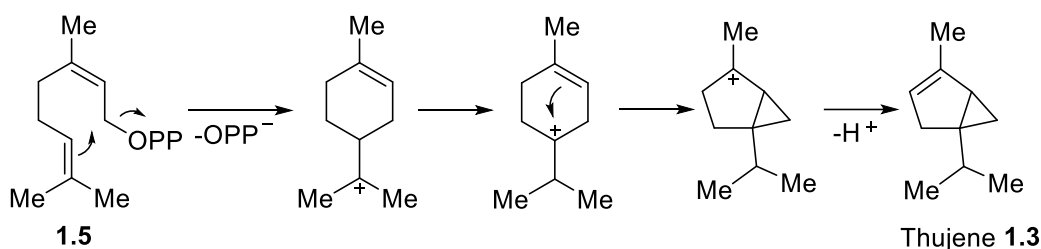

Figure 1.2. A sequence of cationic rearrangements starting from geranyl pyrophosphate leads to the cyclopropane thujene.

A formally carbanionic cyclopropane synthesis pathway is shown in **Figure 1.3**. After activation of S-adenosyl methionine (SAM) by a coenzyme to give aldimine **1.6**, the nucleophilic α-C displaces the sulfide leaving group in an intramolecular reaction. Hydrolysis leads then to ACC (**1.2**).
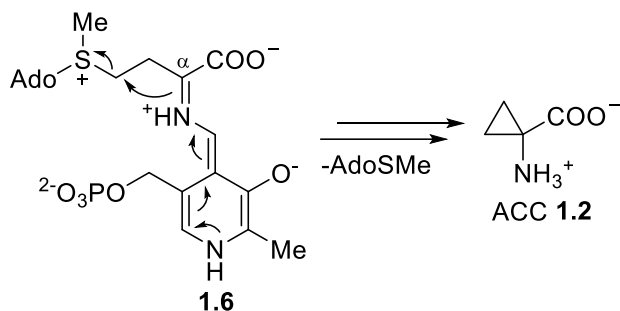

Figure 1.3. Activation of S-adenosyl methionine (SAM) is followed by nucleophilic displacement of the sulfide leaving group.

Cyclopropanes are not only interesting due to their occurrence in nature, but also for their unique bonding properties.[9] The three-membered ring necessitates C-C-C bond angles of 60°, deviating significantly from those expected from either sp^2- or sp^3-carbons and resulting in a rather high strain energy of 27.4 kcal/mol. The C-C bond lengths in C_3H_6 with 1.51 Å is closer to that of ethane (1.54 Å) than that of ethene (1.34 Å), yet, contains some double bond character with π-type orbitals (see below and **Figure 1.4**).[10] Additionally, because of their rigid nature, they can act as a well-defined

structural element. For example, a *cis-* or *trans-*1,2-disubstituted cyclopropane can mimic a double bond without its increased reactivity.[7]

An often-used model for the bonding in cyclopropane are the Walsh orbitals. An sp^2-hybridization of the carbon atoms in the ring is assumed. Omitting the six sp^2-orbital involved in the C-H (or C-R) bonds leaves a set of three sp^2- and three p-orbitals for the bonding within the ring plane. These can be combined in a set of three Hückel-aromatic and three Möbius-aromatic molecular orbitals from sp^2- and p-orbitals, respectively, as shown in **Figure 1.4**.
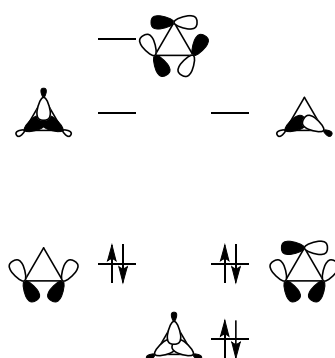
Figure 1.4. MO and energy level diagram for cyclopropane with Walsh orbitals.

As shown above for the biosynthesis of cyclopropanes (also eq (1.3)), viable synthetic methods for cyclopropanes include cyclizations of linear precursors. With respect to the scope of this thesis, only (formal) transfers of a CR_2 unit (R = H, alkyl, aryl), specifically CH_2, to a double bond shall be discussed in the following.
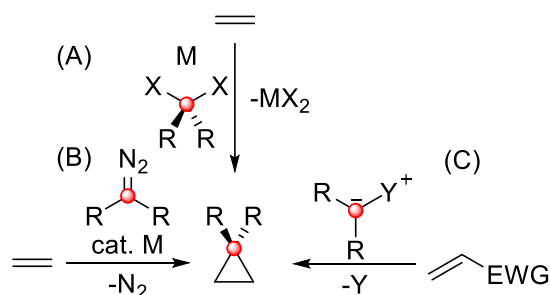

Figure 1.5. General synthetic pathways to access cyclopropanes via formal CR_2 transfer.

For the cyclopropanation via methylene transfer, three general pathways can be identified (**Figure 1.5**).[11-12]

Method (A) is the Simmons-Smith reaction or its derivatives that proceeds via a metal carbenoid intermediate. The metal carbenoid in turn is usually formed in situ from a

low-valent metal in stoichiometric quantities by oxidative addition or via transmetallation with a dihalomethane.

Method (B) is the decomposition of a diazo compound in the presence of a metal catalyst and is thought to proceed, in contrast to (A), via a metal carbene instead of a carbenoid.

Method (C) is the reaction of an ylide with an activated, i.e., electron-poor double bond and proceeds in two distinct steps. First, an addition of the ylide to the double bond, followed by ring closure. Hence, this reaction type is also known as Michael initiated ring closure (MIRC).

The literature review presented below is meant to be illustrative rather than exhaustive with an eye particularly on the scope of this thesis.

1.2.1 Simmons-Smith Reaction and Derivatives

Since the seminal discovery by Simmons and Smith in 1958/59, the eponymous reaction and its modifications have become a mainstay of cyclopropanation chemistry, especially on larger scale.[13-14] In the original publication, a Zn-Cu couple was use together with CH_2I_2 as methylene source (**Figure 1.6**). The reaction is most likely proceeding via a zinc carbenoid species that transfers its methylene group in a single step to the substrate. Since then, efforts have been made to replace the Zn-Cu couple, e.g., with $ZnEt_2$ (Furukawa modification), or other metal alkyls engaging in metal-halogen exchange, resulting in homogenous condition[8, 15] or the methylene source for cheaper and more stable ones, e.g., CH_2Br_2 or even CH_2Cl_2.[16-18]
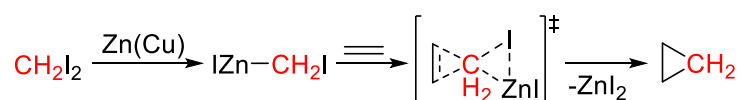

Figure 1.6. General reaction scheme of the Simmons-Smith reaction with a concerted methylene transfer step.

Of particular interest in this respect is work by Uyeda et al. that has been published during the time span of this thesis (**Figure 1.7**).[17-18] These Simmons-Smith-type reactions are catalyzed by Ni and Co, respectively, and offer different selectivities than under the classic Simmons-Smith conditions.
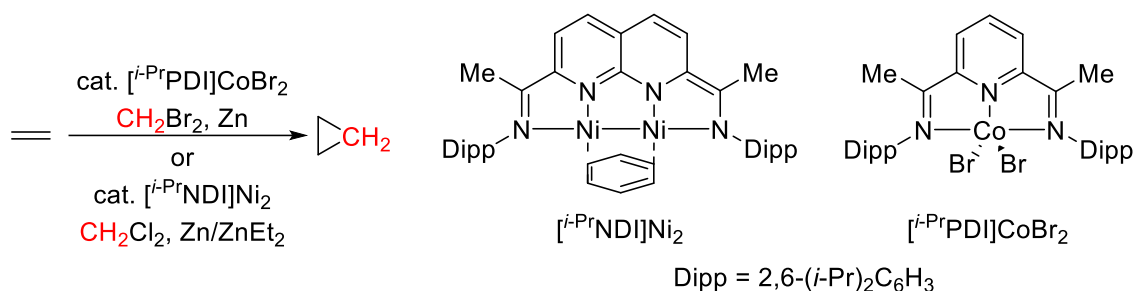
Figure 1.7. Ni- and Co-catalyzed Simmons-Smith-type reactions reported by Uyeda et al.

1.2.2 Transition Metal-Catalyzed Decomposition of Diazo Compounds

In terms of atom economy, it is hard to compete with the use of diazomethane as a methylene donor.[19] Unfortunately, this significant advantage is overshadowed by the hazardous nature of this gaseous, toxic, and explosive reagent.[20] Glassware used to prepare diazomethane needs to be flame polished and free of scratches. Contact with even innocuous seeming metal salts such as $CaCl_2$, Na_2SO_4, $MgSO_4$ or the exposure to strong light can lead to detonations. Thus, storage is not recommended and an immediate synthesis from precursors prior to its use is required. These precursors are often themselves hazardous compounds. With these limitations at hand, only cyclopropanation reactions on relatively small scale are feasible.

Cyclopropanation reaction using diazomethane are most commonly catalyzed by Cu or Pd, although other metals can be employed as well. Additionally, the reaction also proceeds photochemically, albeit with lower yields and selectivity.[20-21]
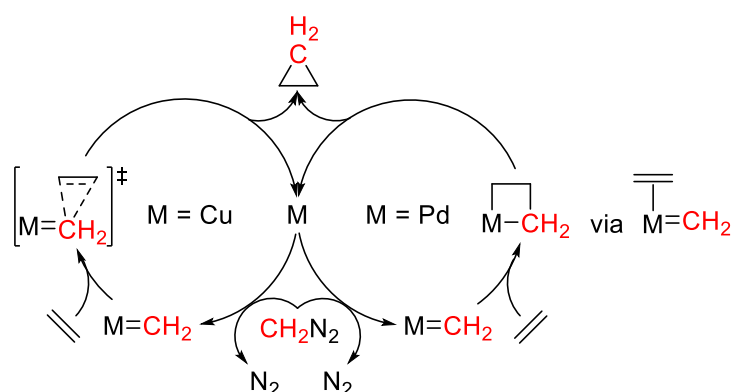

Figure 1.8. General mechanistic scheme for the Cu- or Pd-catalyzed cyclopropanation with diazomethane.

Pd is usually a more active catalyst for electron-poor and strained alkenes, Cu is more active for very electron-rich substrates.[21] This difference can easily be appreciated from the mechanistic sketch in **Figure 1.8**. Both species undergo a turnover-limiting

extrusion of N_2 to form the metal carbene. The electrophilic Cu carbene transfers its methylene group directly to the alkene in a single step without any intermediate coordination of the substrate (outer-sphere mechanism). The Pd carbene on the other hand, forms an intermediate palladacyclobutane before reductive elimination affords the cyclopropane (inner-sphere mechanism).[22-25]

Due to the very useful but fickle properties of diazomethane, much effort has been spent on in its situ[26] or in flow[27] generation, or alternative reagents for cyclopropanation altogether.[28-31]

1.2.3 Michael Initiated Ring Closure Reactions

The substrate scope of cyclopropanation reactions using ylides is highly dependent on their nucleophilicity. For any but the most nucleophilic ylides, the alkene has to be activated by an electron-withdrawing group, i.e., Michael acceptors. (For a highly nucleophilic ylide capable of cyclopropanating only weakly activated alkenes, see **Figure 1.12**.)

The seminal report for this type of reaction was published by Corey and Chaykovsky in 1965.[32] Dimethyloxosulfonium methylide adds selectively to α,β-unsaturated ketones, followed by dimethylsulfoxide extrusion to give the cyclopropane product (**Figure 1.9**).
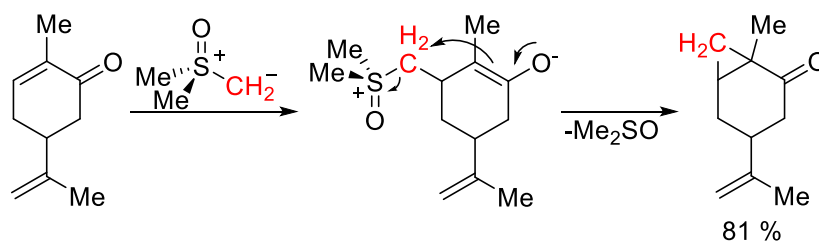

Figure 1.9. Cyclopropanation of carvone with dimethyloxosulfonium methylide according to Corey and Chaikovsky.

Since then, many variants have been developed employing S-, N-, P-, Te-ylides.[33-34]

1.3 Ammonium Ylides and the Franzen Story

The term ylide is defined by IUPAC as "*compounds in which an anionic site Y⁻ […] is attached directly to a heteroatom X⁺ […] carrying a formal positive charge.*"[35]Thus, they represent 1,2-dipolar species. Both the use of the heteroatom X element name, e.g.,

nitrogen ylide or *N*-yilde, as well as the –onium terminology to stress the formal positive charge on the heteroatom, e.g., ammonium ylide, are correct names and will be used exchangeable throughout this thesis. The term *ylide* was coined by Georg Wittig in 1944 as an alternative to an older proposal, *ylidide*, and was meant to signify both the 'homopolar valence' (-yl) and the 'heteropolar' bond (-ide).[36-37]

Ylides are nucleophiles of varying strength. In the case of tetramethylammonium, the pK_a was estimated to be 42 for the hypothetical free ylide,[38] making the corresponding ylide a strong base/nucleophile.

In a short communication in 1960, Franzen and Wittig reported on the cyclopropanation of cyclohexene using trimethylammonium methylide as methylene donor (**Figure 1.10**).[39] The reaction was thought to proceed via a free carbene by decomposition of the ammonium ylide.
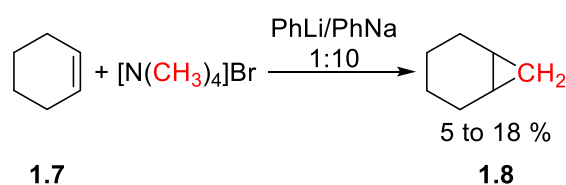

Figure 1.10. Synthesis of norcarane with trimethylammonium methylide as methylene donor according to Franzen and Wittig.

A solution of PhLi/PhNa (1:10) in Et_2O was added to a suspension of $[NMe_4]Br$ in neat cyclohexene (**1.7**). The product of the reaction was then separated by distillation, characterized by its IR spectrum, GC retention time, and refractive index, and found to be identical to an authentic sample of norcarane (**1.8**). Even though it was mentioned that the reaction outcome was somewhat capricious, the yield varied between 5 and 18 %, it appeared to be reproducible.

Four years later, Krauss and Wittig reported on attempts to reproduce the original work without any success and concluded that trimethylammonium methylide was not a viable cyclopropanation reagent.[40]

The only product isolated was dimethylethylamine in 49 % yield, along with traces of ethene and polyethylene or polymethylene in their terminology).
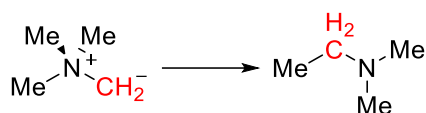
Figure 1.11. Stevens rearrangement of tetramethylammonium methylide.

Ammonium ylides are prone to decomposition via the Stevens rearrangement, in the case of trimethylammonium methylide to dimethylethylamine, a [1,2]-sigmatropic rearrangement (**Figure 1.11**).[41-42]

It appears that after the 1964 report by Krauss and Wittig no further attempts were published to use trimethylammonium methylide as methylene donor. These historical events have been summarized in more depth elsewhere.[43]

1.4   Previous Work with Tetramethylammonium Salts in the Chen Group

Previous work in this group has dealt with the reevaluation of trimethylammonium methylide as methylene donor.[44-45] The first key issue identified was the general insolubility of tetramethylammonium salts in solvents that allow for the deprotonation to form the ammonium ylide. Several lipophilic anions were tested (tetrakis(3,5-bis(trifluoromethyl)phenyl)borate, bis(trifluoromethane)sulfonamide, pivalate, triflate), of which triflate proved to be the best performing counteranion. Even though [NMe$_4$]OTf is not (completely) soluble in THF, the resulting ammonium ylide is fully soluble at the concentrations employed.

The ammonium ylide was shown to act as a methylene donor for ketones, aldehydes, imines, styrenes, and stilbenes to form the corresponding three-membered rings (**Figure 1.12**). However, an unactivated alkene, i.e., cyclohexene, the original substrate of Franzen and Wittig, was not a viable substrate (cf. **Figure 1.10**).
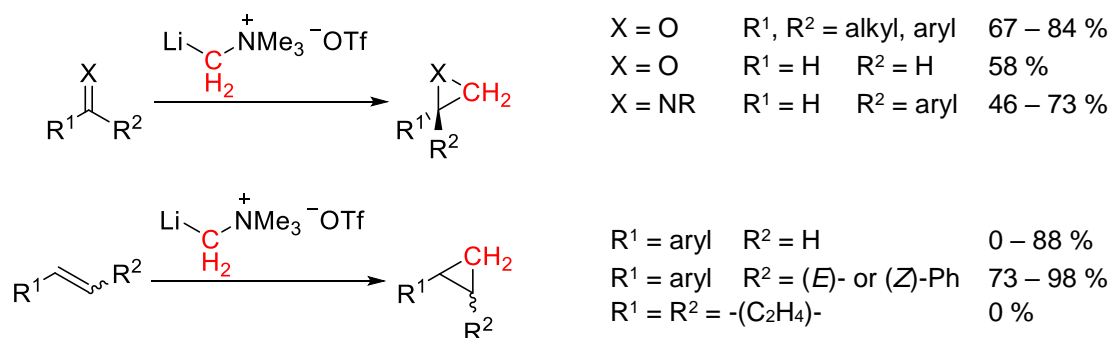

X = O	R^1, R^2 = alkyl, aryl	67 – 84 %
X = O	R^1 = H R^2 = H	58 %
X = NR	R^1 = H R^2 = aryl	46 – 73 %

R^1 = aryl	R^2 = H	0 – 88 %
R^1 = aryl	R^2 = (*E*)- or (*Z*)-Ph	73 – 98 %
R^1 = R^2 = -(C$_2$H$_4$)-		0 %

Figure 1.12. Lithiomethyltrimethylammonium triflate serves as methylene donor to several unsaturated system to give the corresponding three-membered rings.

A mechanistic study of the cyclopropanation reaction was consistent with a two-step mechanism. First, a rate-limiting carbolithiation, followed by fast ring closure with concomitant extrusion of NMe$_3$ (**Figure 1.13**), at least for electron-rich styrenes. Electron-withdrawing substituents (4-NO$_2$, 4-F) resulted in low yields, 0 and 17 %, respectively. It was hypothesized that the benzylic carbanion after initial carbolithiation is too stable for the intramolecular ring closure and instead undergoes intermolecular side-reactions, possibly polymerization.
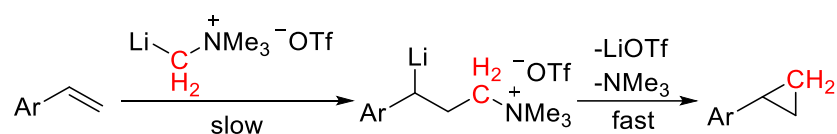

Figure 1.13. Two-step mechanism for the cyclopropanation with lithiomethyltrimethylammonium as methylene donor.

A concomitant computational study on the ammonium ylide and its heavier homologue [Me$_3$PCH$_2$Li] was performed and indicated the integral role of Li for the stability of the ammonium yilde. In contrast, the phosphonium ylide is able to redistribute the negative charge over the entire framework, as evidenced for example by the P-CH$_2$ bond shortening upon removal of Li. Indeed, Me$_3$P=CH$_2$ is a thermally stable liquid which can be purified by distillation at 210 °C.[46] Hence, *lithiomethyltrimethylammonium* more accurately describes the bonding situation for the nitrogen ylide, it cannot be accessed salt-free. A circumstance already observed previously, i.e., the use of a chelating diether solvent, dimethoxyethane, or the use of Na instead of Li insufficiently stabilizes the ylide and accelerate its decomposition.[47]

1.5 The Lewis Acidity of Ni(0)

Ni(0) can be considered a very electron-rich and nucleophilic metal. Nevertheless, many complexes in which Ni(0) formally acts as a Lewis acid are known in the literature. The most relevant examples, many of them reported by Pörschke and Wilke, shall be discussed here in summary.[48-53]
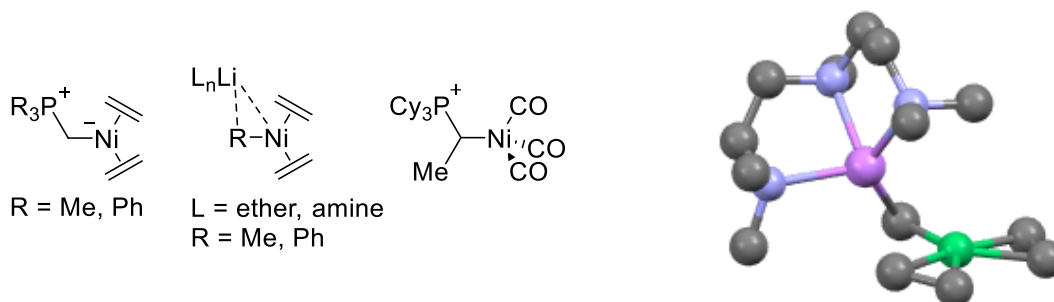
Figure 1.14. Left: Selection of characterized carbanion adducts of Ni(0). Right: Crystal structure of [(PMDTA)Li][MeNi(C₂H₄)₂]. Hydrogen atoms are omitted for clarity.[48] PMDTA = pentamethylethylenetriamine.

The complexes shown in **Figure 1.14** feature the common motive of π-accepting ligands, carbon monoxide or ethene, on nickel. These ligands play the important role of accepting and redistributing the negative charge of the carbanion in the niccolate(0) complexes. On the other hand, the stability of the adducts are also dictated by the nucleophilicity of the carbanion. These two trends of donor and acceptor strength are depicted in **Figure 1.15** for the relevant nucleophiles and ligands.
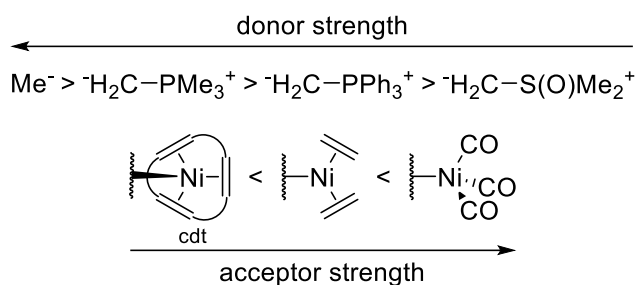

Figure 1.15. Qualitative scale of nucleophilicity for carbanions and electrophilicity for several Ni(0) fragments. cdt = *trans,trans, trans*-1,5,9-cyclododecatriene.

The donor strength of the carbanion follows the basicity of the carbanion and diminishes from the strongly basic methide anion to the rather weakly basic dimethylsulfoxonium methylide. The π-acceptor strength of the ligand set on nickel, weakens from the strongly π-accepting CO ligands to the cyclic triene cdt (cdt = *trans,trans,trans*-1,5,9-cyclododecatriene). The weak acceptor ability of cdt can be understood in terms of poor orbital overlap. Due to the ethylene bridges between the *trans* double bonds in cdt, the alkenes cannot be coplanar with respect to the alkene-nickel plane. Additionally, upon coordination of a fourth ligand perpendicular to the Ni-cdt plane, the nickel atom is removed out of the triene plane, further reducing the orbital overlap and thus π-backbonding (**Figure 1.16**).[54-55]
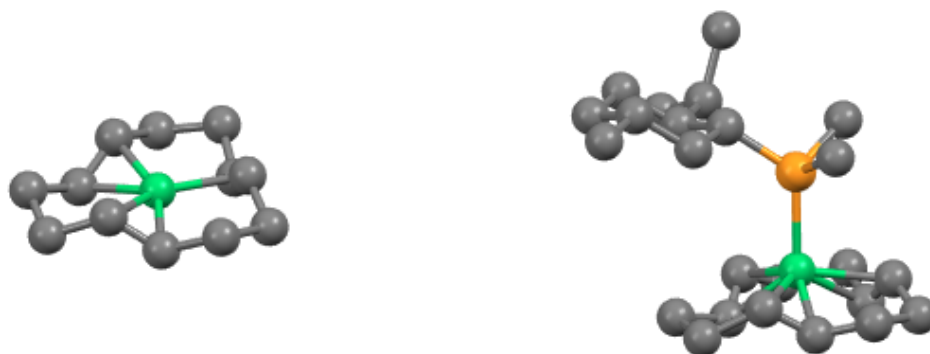
11

Figure 1.16. Crystal structures of Ni(cdt) and Ni(cdt)(PMe$_2$(menthyl)).[54-55] Hydrogen atoms are omitted for clarity.

The adduct formation is highly temperature sensitive. The compounds shown in **Figure 1.14**, with the exception of the triscarbonyl complex, are highly thermally labile and often decompose already well below 0 °C. As an extreme example based on the affinity scale in **Figure 1.15**, [Me$_2$S(O)CH$_2$] does not form an adduct with Ni(cdt) at all, while the Ni(C$_2$H$_4$)$_2$ adduct is only stable below 0 °C and the Ni(CO)$_3$ adduct decompose at room temperature within a day.[50] The complex formation can thus be characterized as a push-pull-type behavior between a σ-donating nucleophile and a π-accepting ligand (set) on Ni(0).
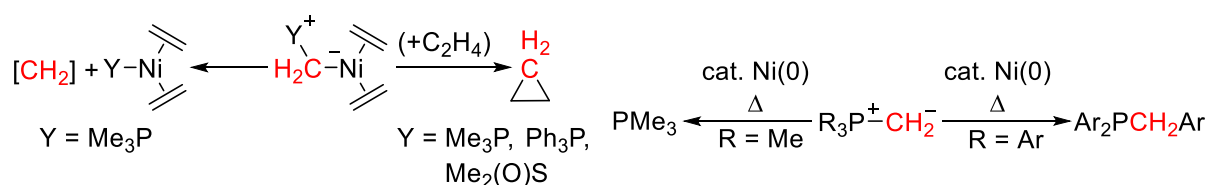

Figure 1.17. Decomposition pathways for several ylide Ni(0) complexes.

The usual decomposition pathways for the (C$_2$H$_4$)$_2$Ni(ylide) complexes is the formation of cyclopropane, among other decomposition products, especially under an atmosphere of ethene (**Figure 1.17**, left side). In the case of (C$_2$H$_4$)$_2$Ni(CH$_2$PMe$_3$), the resulting phosphine complex is stable enough to give the identifiable, major nickel-containing product (C$_2$H$_4$)$_2$Ni(PMe$_3$).

At higher temperatures, catalytic amounts of Ni(0) (e.g., Ni(alkene)$_n$, Ni(PR$_3$)$_n$) effect the rearrangement of phosphorus ylides in a Stevens-like reaction for aryl substituted ylides, while the alkyl substituted ylide [Me$_3$PCH$_2$] does not lead to the analogous phosphine, Me$_2$PEt (**Figure 1.17**, right).[51] These reactions presumably also proceed via the intermediacy of Ni(0)-ylide adducts presented in this chapter, but the mechanism has not been studied in detail.
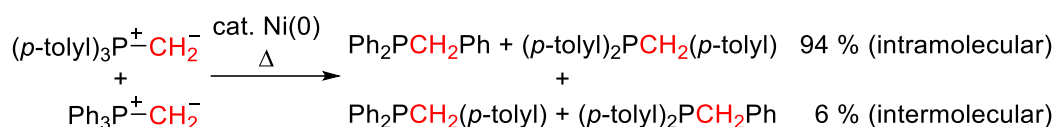
$(p\text{-tolyl})_3P^+\!\!-\!\!CH_2^- \quad \xrightarrow[\Delta]{\text{cat. Ni(0)}} \quad Ph_2PCH_2Ph + (p\text{-tolyl})_2PCH_2(p\text{-tolyl}) \quad 94\ \%\ (\text{intramolecular})$

$+$

$Ph_3P^+\!\!-\!\!CH_2^- \qquad\qquad Ph_2PCH_2(p\text{-tolyl}) + (p\text{-tolyl})_2PCH_2Ph \quad 6\ \%\ (\text{intermolecular})$

Figure 1.18. Cross-over experiment for the nickel-catalyzed phospha-Stevens rearrangement. 6 % of the total amount of phosphine products stem from an intermolecular cross-over.

The active catalyst appears to be a Ni(0) species. Ni(II) precatalysts (NiCl$_2$, Ni(acac)$_2$) showed no activity for the rearrangement. A cross-over experiment with differently substituted arylphosphonium ylides and 4 mol% Ni(cod)$_2$ resulted mostly in the formation of the intramolecular rearrangement products shown in **Figure 1.18**. Nevertheless, a small amount of cross-over products were identified. Two possible pathways for the rearrangement are presented in **Figure 1.19**.
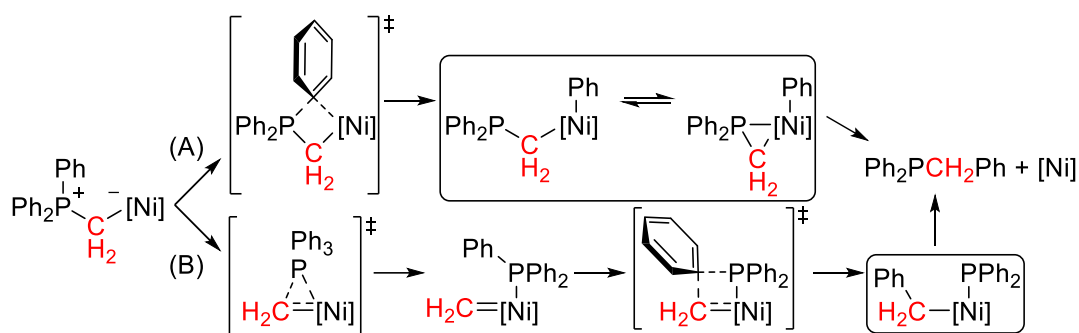

Figure 1.19. Two plausible pathways for the Ni(0)-catalyzed ylide rearrangement.

Starting from the initial Ni(0)-ylide adduct on the left side in **Figure 1.19** (at least) two pathways can be envisioned. Pathway (A) proceeds via an initial β-aryl transfer to Ni via a P-C bond cleavage to give a Ni(II)(Ph)(κ^1C-CH$_2$PPh$_2$) species or its (κ^2C,P) isomer. Reductive elimination would result in the observed product, Ph$_2$PCH$_2$Ph.

Alternatively, pathway (B) proceeds via a 1,2-phosphine migration to give a nickel carbene intermediate. Aryl group transfer to the carbenic carbon, also via P-C bond cleavage, results in a Ni(II)(CH$_2$Ph)(PPh$_2$) species. Finally, reductive elimination leads to the same phosphine product.

Both pathways postulate intermediates (highlighted in boxes) that could explain the observed cross-over products, i.e., via a bimolecular aryl or diarylphosphide transfer.
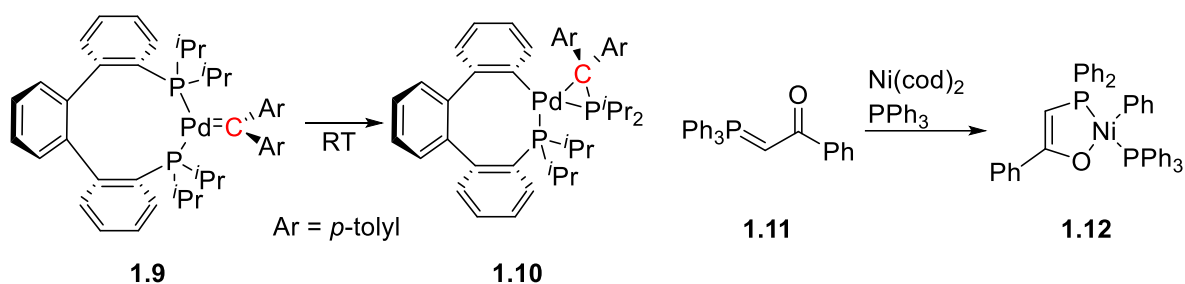
13

Figure 1.20. Left: Decomposition of a Pd carbene via aryl-P bond cleavage. Right: Aryl-P bond cleavage of a phosphonium ylide with Ni(0).

A related, interesting observation of a Pd carbene reaction is shown in **Figure 1.20** (left).[56] The Pd carbene **1.9** reacts within several hours at room temperature to the P-C bond activated compound **1.10**, reminiscent of the postulated ($\kappa^2 C,P$) isomer for pathway (A) in **Figure 1.19**. The Pd complex could thus represent an arrested intermediate on the way to the formal carbene insertion into the P-aryl bond. For the stabilized phosphonium ylide **1.11** a similar reaction was observed in the presence of Ni(0) to give the Ni(II) complex **1.12** after P-C bond activation (**Figure 1.20**, right).[57] Arguably, complex **1.12** is stable towards reductive elimination due to the delocalized charge in the $\kappa O,\kappa P$-chelate (cf. **Figure 1.19**, pathway (A)).

In another rare example of a phospha-Stevens rearrangement, Ni(0) complex **1.13** was treated with the sulfur ylide [Ph$_2$SCH$_2$] (**Figure 1.21**).[58] Ylide adduct formation and subsequent nickel carbene formation were proposed as reactive intermediates. The first observable, new species was characterized by NMR as the phosphorus ylide adduct **1.14**, which rearranged over several hours at room temperature to **1.15**.
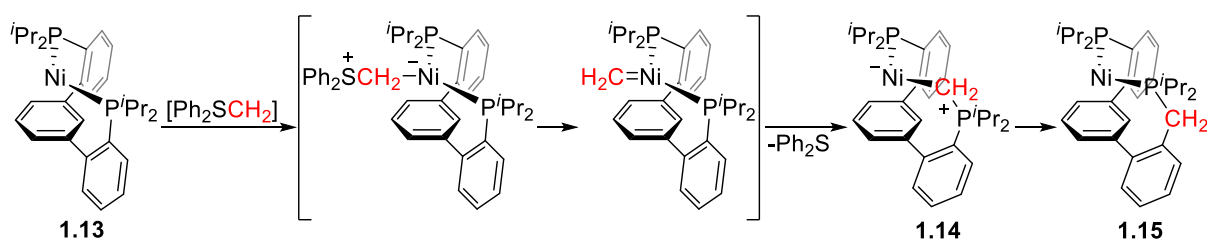

Figure 1.21. Phospha-Stevens rearrangement of a ligand bound to Ni(0) after methylene transfer from a sulfur ylide.

14

1.6 Stable Nickel Carbenes and Nickelacyclobutanes

Terminal, non-Fischer carbenes for nickel are exceedingly rare. The Hillhouse group has reported on three isolable nickel carbenes (**Figure 1.22**).[59-60] All complexes are kinetically stabilized with bulky, bidentate phosphine ligands and feature (large) aryl groups on the carbenic carbon to further sterically protect the carbene moiety from decomposition.
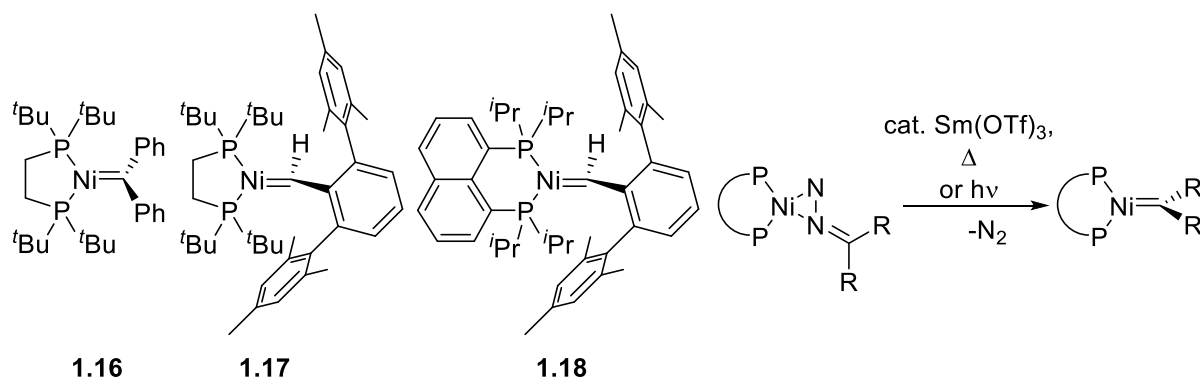

Figure 1.22. Stable nickel carbenes reported by Hillhouse and co-workes (left) and their general syntheses from diazo precursors (right).

The carbenes were synthesized from their respective Ni(0)-η^2-diazo precursors either via a thermal extrusion catalyzed by Sm(OTf)$_3$ (**1.16**) or a photochemical extrusion (**1.17**, **1.18**) of N$_2$ (**Figure 1.22**, right). These compounds are best described as nucleophilic carbenes, i.e., the double bond is polarized towards the carbene center, as has been suggested in a related case of nickel-catalyzed cyclopropanation with diazo compounds.[61] DFT calculations on a model complex in lieu of **1.17**, (1,2-bis(dimethylphosphino)ethane)Ni=C(H)Ph, showed the HOMO to be bonding orbital with π-symmetry between the d$_{x^2-y^2}$ on nickel and the p$_x$ orbital on carbon.[60]

1.17 and **1.18** do not react with strong bases/nucleophiles such as BuLi, NaHMDS, LDA, or MeLi.[60] A Brønsted acid ([HNMe$_2$Ph][B(C$_6$F$_5$)$_4$]), on the other hand, protonates **1.16** at the carbenic carbon to give the corresponding cationic alkylnickel(II) species.[59] Most importantly for the present work, **1.16** acted as a carbene transfer reagent under an athmosphere of ethene (110 °C, 5 d, 85% yield), or even catalytically (10 mol %, TON =4.1) in the presence of diphenyldiazomethane (**Figure 1.23**, right).[62] No intermediates were detected by NMR, nevertheless, a [2+2] cycloaddition to form a nickelacyclobutane with subsequent reductive elimination was suggested as a viable mechanistic pathway for the cyclopropane formation.

In a related study by the Hillhouse group, nickelacyclobutanes **1.19^{Me}** and **1.19^{Ph}** were synthesized using a route not proceeding through a nickel carbene species (**Figure 1.23**, left).[63] These complexes underwent facile reductive elimination to give the corresponding cyclopropanes in quantitative yields at much milder condition than for the catalytic process (45 °C, 30 min).
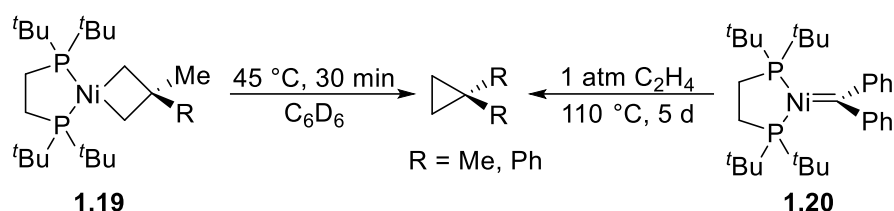

Figure 1.23. Cyclopropane formation from isolated nickelacyclobutanes or nickel carbene.

Not entirely surprising, the stable nickel carbenes shown in **Figure 1.22** have not been observed to undergo bimolecular homocoupling reactions of the two carbene fragments to form the corresponding ethene derivatives. Presumably this is due to the steric protection of the nickel carbene.

For other metals, methylidene complexes are known and even isolable in certain cases. Two instructive cases of an electrophilic rhenium and a nucleophilic tantalum carbene are discussed below, which both do undergo bimolecular homocoupling to give ethene.
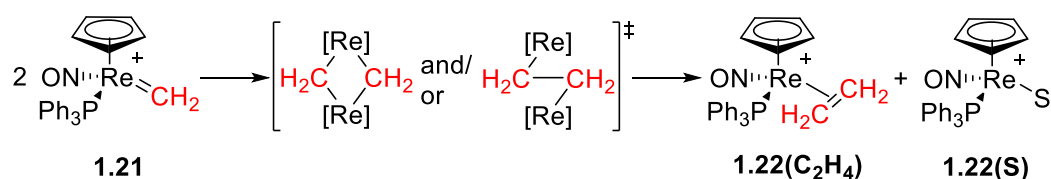

Figure 1.24. Homocoupling of an electrophilic rhenium carbene via a proposed bimolecular coupling step.

The cationic rhenium carbene **1.21** is synthesized from its methyl precursor by hydride abstraction using [Ph$_3$C][PF$_6$]. The resulting electrophilic rhenium carbene decomposes subsequently at room temperature in a homocoupling reaction to give a rhenium-ethylene complex (**1.22(C$_2$H$_4$)**) (**Figure 1.24**).[64] The other equivalent of Re can be trapped by addition of CH$_3$CN (**1.22(S)**, S = CH$_3$CN). It has been unequivocally shown that the homocoupling proceeds via a bimolecular rate-determining step. The decomposition is 2nd order in rhenium carbene and exhibits a large inverse secondary

isotope effect for [Re]=CD$_2$/CH$_2$ of 0.39. This implies a hybridization change of the carbenic carbon from sp^2 to sp^3 in the rate-determining transition state. Additionally, a large negative entropy of activation $\Delta S^{\neq}$ = -32.2 cal mol^{-1} K^{-1} was measured, in line with a highly ordered, bimolecular transition state. Intriguingly, the homocoupling showed a strong preference for a homochiral vs heterochiral homocoupling transition state when an isotopically labelled pseudo-racemate of the chiral-at-metal carbenes were used (**Figure 1.25**). Indeed, the analogous rhenium carbene with the sterically more demanding and electron-rich C$_5$Me$_5$ as ligand is stable as solid above 100 °C.[65] The chiral self-recognition (and stability) thus seem to be of steric and electronic nature. Cyclopropanation was not observed under an atmosphere of ethene.
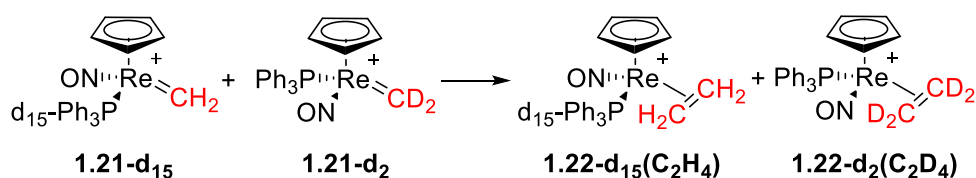

Figure 1.25. Chiral self-recognition for the bimolecular homocoupling of a pseudo-racemate of chiral-at-metal rhenium carbenes.

The nucleophilic tantalum carbene **1.23** was synthesized from TaCp$_2$Me$_3$ by methyl abstraction with [Ph$_3$C][BF$_4$] and subsequent deprotonation of one of the methyl ligands with a base, [Me$_3$PCH$_2$] or LiN(SiMe$_3$)$_2$.[66]
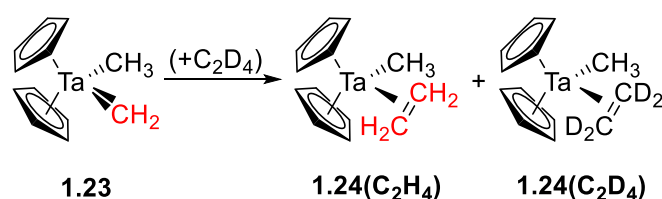

Figure 1.26. Homocoupling of a nucleophilic tantalum carbene.

Complex **1.23** can be isolated in pure form but does decompose in solution over several days at room temperature to give the corresponding ethene complex **1.24(C$_2$H$_4$)** via carbene homocoupling (**Figure 1.25**). Analogous to the rhenium carbene homocoupling in **Figure 1.24**, this reaction is also 2nd order in Ta. When an additional ligand is present during the decomposition, the second equivalent of Ta can be trapped as shown in **Figure 1.24** with C$_2$D$_4$ (**1.24(C$_2$D$_4$)**). No metathesis, H/D scrambling, or cyclopropanation occurred during the reaction. Additionally, it was shown that PMe$_3$, PMe$_2$Ph, and CO are also able to serve as a trap.

Grubbs and Miyashita studied extensively the reactivity of metallacycles of nickel of various ring sizes.[67-70] They prepared the metallacycle **1.26** by (formally) intramolecular deprotonation of the γ-H of the neopentyl ligand of **1.25** (**Figure 1.27**). **1.26** is thermally unstable and decomposes above -20 °C to give, among other products, 1,1-dimethylcylopropane in up to 47 % yield depending on the reaction conditions.[70] The same reductive elimination can be achieved by oxidation of **1.26** either by O_2 or Ce(IV).
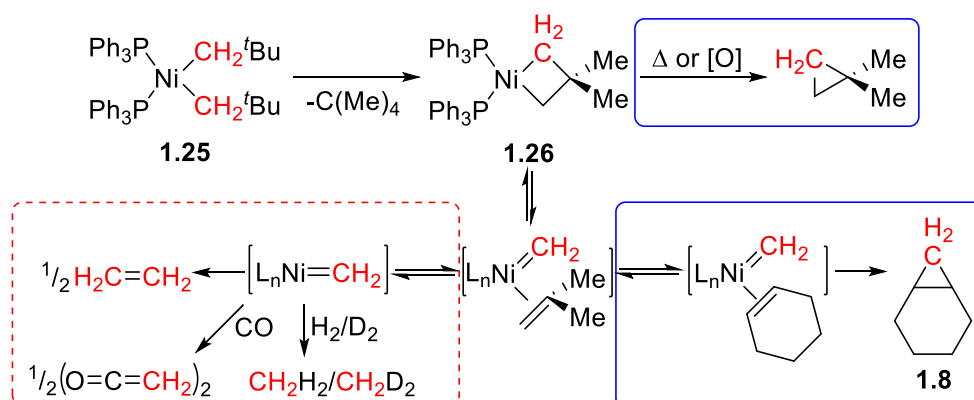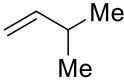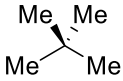

Figure 1.27. Synthesis of metallacycle **1.26,** its cyclorpopanation (solid blue boxes), and decomposition (dashed red box) pathways. Postulated intermediates are shown in brackets.

Depending on the exact reaction condition under which the decomposition proceeds, other products can be obtained stemming from carbene transfer. This reactivity led the authors to propose nickel carbene intermediates, highlighted in brackets in **Figure 1.27**, being in equilibrium with the nickelacyclobutane **1.26**. Decomposition under an atmosphere of CO resulted in carbene transfer to CO to give the ketene dimer in 8 % yield. Under an atmosphere of H_2 or D_2 hydrogenation took place to give methane or methane-d_2, respectively (38 % yield with H_2). In the presence of an excess cyclohexene, an apparent alkene exchange takes place, isobutene for cyclohexene, to finally give norcarane (**1.8**) in 8 % yield.

Additionally, when an excess of PPh3 (5 equiv per Ni) is added to the decomposition of **1.26**, the product distribution is changed quite significantly away from cyclopropane formation towards homocoupling to give ethene (**Table 1.1**).

18

Table 1.1. Decomposition of Nickelacyclobutane **1.26** with Additional PPh₃.[a]

Compound	Yield product / %				
	$=$	(Me)₂C=CH₂	cyclopropane-Me₂	CH₂=CH–CH(Me)₂	(Me)₂C=C(Me)₂
1.26	15	26	47	6	6
1.26 + 5 PPh₃	28	52	11	7	2

[a] 15 h at 24 °C in toluene, see ref. [70].

1.7 Ligand Binding to Ni(0)

1.7.1 Alkene Binding to Ni(0)

Binding of alkenes (and other π-bonds) can be understood in terms of the Chatt-Dewar-Duncanson model (**Figure 1.28**).[71-73] An empty orbital on the metal with the appropriate symmetry (d_{z^2} or $d_{x^2-y^2}$) can interact with the filled π-orbital of the alkene (σ-donation). Concomitantly, a filled orbital on the metal (d_{xz} or d_{xy}) can donate electron density into the empty π^*-orbital (π-back donation). Depending on the metal and its oxidation state, a continuum of η^2-alkene complex and metallacyclopropane can exist. With increasing π-back donation from electron-rich metals, the C-C bond length, C-C stretch frequency, and C-H out-of-plane angle increase.[74-75]
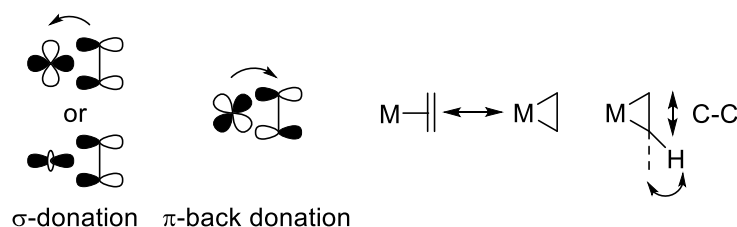

σ-donation   π-back donation

Figure 1.28. Chatt-Dewar-Duncanson model for the binding of alkenes to transition-metals. Left: Orbital interaction for σ-donation and π-back donation (Arrows mark flow of electron density). Middle: Resonance extremes for η^2-alkene complex and metallacyclopropane. Right: C-C bond length and C-H out-of-plane angle increase with increasing metallacyclopropane character.

Tolman has extensively studied the binding of alkenes to Ni(0) phosphite and phosphine complexes (and to a lesser degree to Pd(0) and Pt(0)). It was shown that the stability of the alkene complexes are dominated by the interaction of the HOMO on Ni(0) and the π^*-orbital on the alkene, i.e., π-back donation.[76] This leads to electron-poor olefins, such as maleic anhydride, binding much more strongly to Ni(0) than electron-rich ones, such as trialkyl-substituted alkenes. The binding constants have been shown to be rather sensitive to the substitution pattern on the double bond and

correlate well with the Hammett parameter σ_p^+, leading to values spanning a range of over twelve orders of magnitude (**Figure 1.29**).
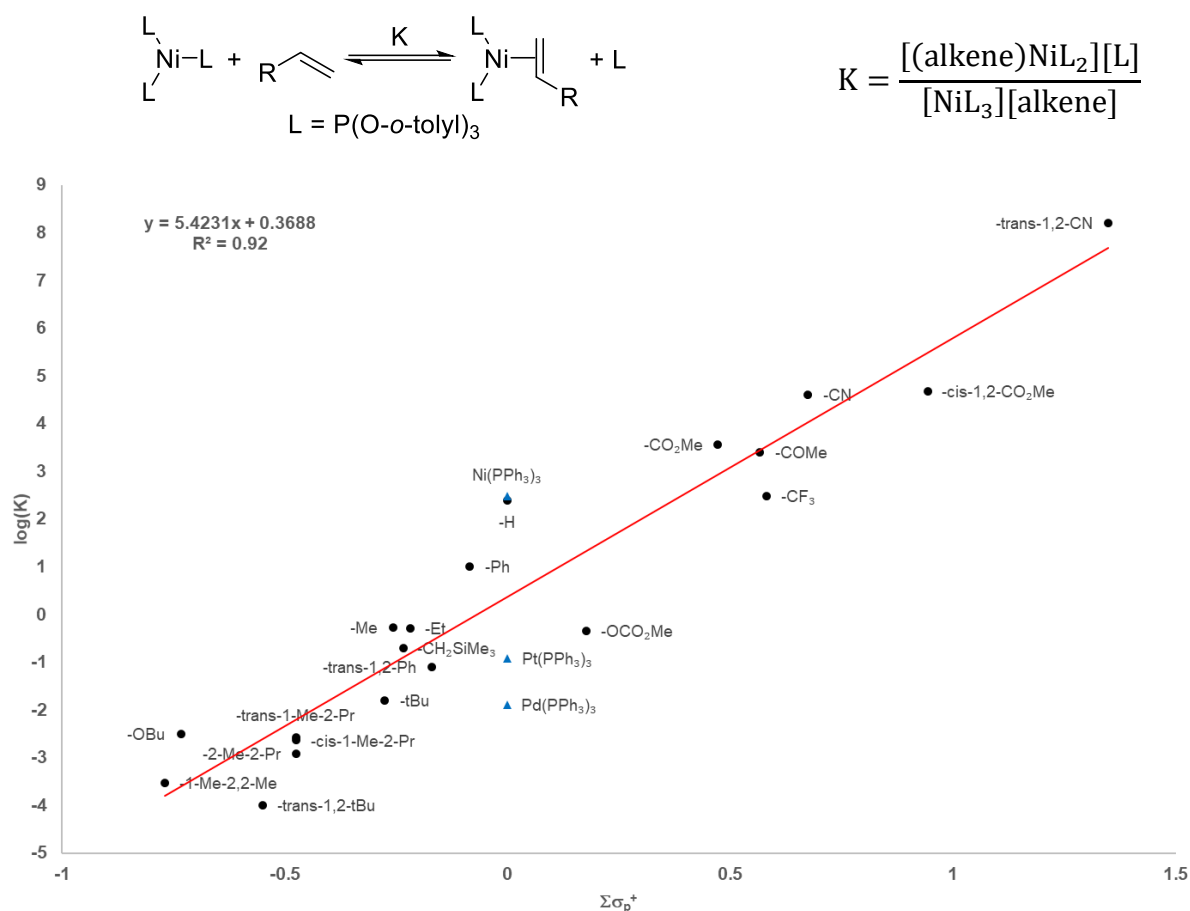

Figure 1.29. Top: Definition of equilibrium binding to Ni(0) of alkene and P(O-*o*-tolyl)$_3$. Bottom: Alkene binding constants K (logarithmic values) for selected alkenes versus Hammett constant σ_p^+. (Figure adapted from ref. [76] and additional data from ref. [77]) Data point labels denote substitution pattern of ethene. Ethene is denoted by –H. Blue Triangles are for the same equilibrium with ethene but with complexes as indicated in the data point labels. Note: Ni(0) complexes of P(O-*o*-tolyl)$_3$ and PPh$_3$ result in very similar K values, 250 and 300, respectively.

The sensitivity to the alkene substitution is much less pronounced for other metals (**Figure 1.30**). This trend follows the π-back donation strength of these metals.[75] The apparent insensitivity to the *cis-trans* substitution pattern for Ni(0) compared to Ag(I) and Rh(I) is noteworthy.
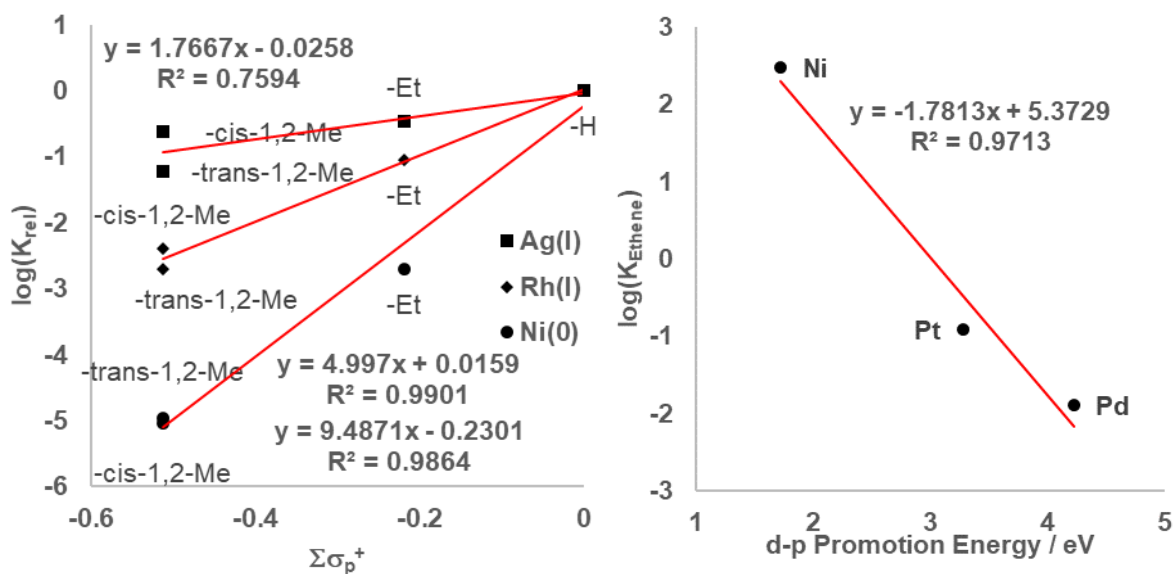
Figure 1.30. Comparison of Ni(0) to other metals. Left: Relative binding constants (logarithmic values) for several alkenes and three different metals versus Hammett constant σ_p^+. Squares: $(C_2H_4)Ag^+$, Diamonds: $(acac)Rh(C_2H_4)_2$, Circles: $(C_2H_4)Ni(P(O\text{-}o\text{-tolyl})_3)_2$. (Data adapted from ref. [76] and references therein). Data point labels denote substitution pattern of ethene. Ethene is denoted by –H. Right: Binding constants of ethene to nickel triade complexes $M(PPh_3)_3$ versus the M $(n\text{-}1)d^{10} \rightarrow (n\text{-}1)d^9 np^1$ promotion energy. (Data adapted from ref. [77] and reference therein).

The consequence of this, as noted by Tolman, is that more electron-withdrawing (phosphite) ligands decrease the binding constant of alkenes and make it less sensitive to the substitution pattern of the alkene.[78] Additionally, it was shown that the binding constant is higher for phosphite ligand with a larger cone angle. This is a direct effect of a lower binding constant of the ligand itself due to steric crowding around the metal (see 1.7.2).

In line with the above-presented bonding behavior, Pd(0) and Pt(0) have lower binding constants (at least for the pair PPh_3/ethene), because they are less electron-rich and thus less π-donating (**Figure 1.29**, blue triangles, and **Figure 1.30**, right) as evidenced by their $(n\text{-}1)d^{10} \rightarrow (n\text{-}1)d^9 np^1$ promotion energy.[77] Promotion energies have been found to be more predictive for coordination behavior than ionization potentials of the gaseous ions.[74]

1.7.2 Phosphine Binding to Ni(0) and Parametrization

Since the seminal work of Tolman, mainly on phosphorus-based ligands in Ni(0) complexes, the use of steric and electronic parameters have had a tremendous impact on the rationalization of ligand effects in organometallic and coordination chemistry.[79] Initially, the Tolman electronic parameter (TEP, ν) has been determined by measuring the A_1 stretch frequency of $(R_3P)Ni(CO)_3$ complexes, and the Tolman cone angle (TCA,

θ) by building physical models of the ligand and determining the cone angle by hand. Since Tolman's early work, other parameters and ligand classes have been extensively examined and adapted to other metals, often with the help of modern computational methods, and applied especially in the field of catalysis.[80-82]

Two modern, complementary descriptors for ligand steric demands of particular relevance for this thesis shall be briefly introduced here.

Allen and coworkers and derived a mathematical formalism for an exact ligand solid cone angle.[83] A sphere is drawn around the metal-ligand complex of interest with the metal atom at the center of the sphere. Next, for every ligand atom a shadow is cast on the sphere. Subsequently, all single shadow areas are summed up, normalized to the total sphere area, and transformed into the exact solid cone angle $\Theta°$. Thus, this parameter is *insensitive* to the distance of the ligand atom from the metal center.

The buried volume parameter $\%V_{Bur}$ developed by Cavallo et al. is calculated by drawing a sphere around the central metal atom. Then, the volume *occupied* by the ligand of interest is divided by the total sphere volume to give $\%V_{Bur}$.[84] In contrast to the exact solid cone angle $\Theta°$, $\%V_{Bur}$ *is sensitive* to the distance from the central metal atom. Although a sphere radius of 3.5 Å has been establish as standard value, one could in principal change this parameter to suit the needs of the system at hand. Additionally, the buried volume can be visualized by a steric map of a chosen half-sphere.

Conveniently, both parameter can be easily calculated and visualized by freely-available tools, a program package for $\Theta°$ and a web tool for $\%V_{Bur}$, respectively.

In general, Tolman has observed that for many ligand exchange equilibria with phosphine ligands sterics, as measured by ligand cone angles, play a dominant role.[78-79, 85-86]
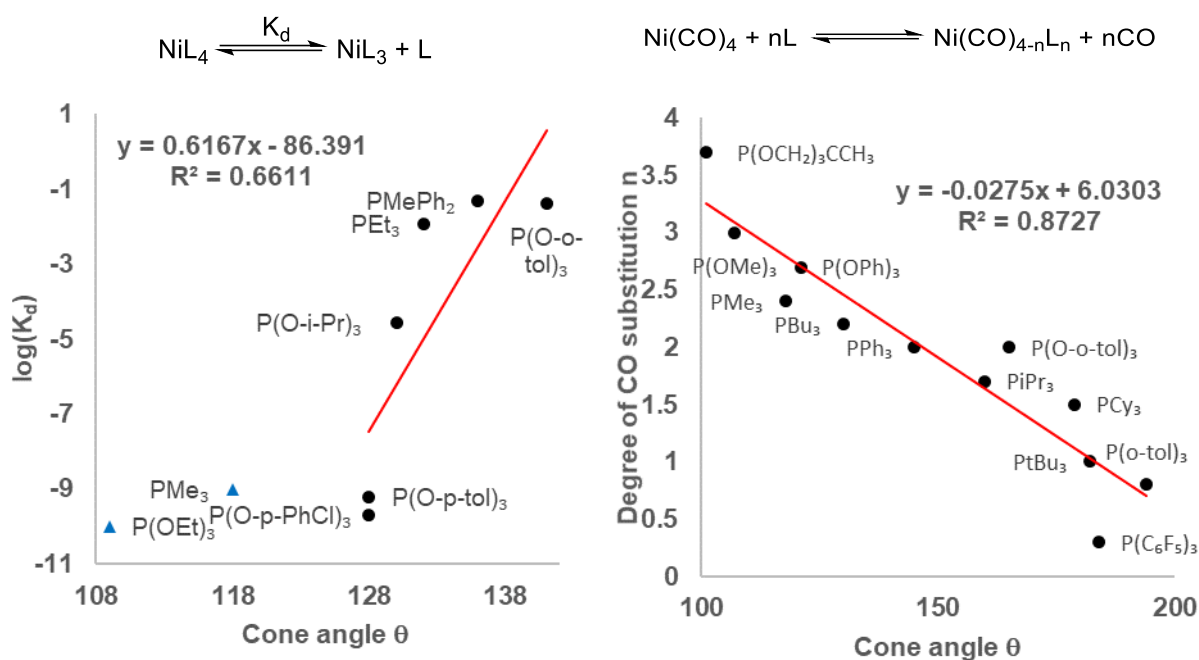
Figure 1.31. Left: Dissociation equilibrium constants for NiL_4 complexes versus cone angles for several phosphine ligands. (Data adapted from ref. [79].) Black circles were measured at 25 °C. Blue triangles were measured at 70 °C and are excluded from the linear regression. Right: (Fractional) degrees of dissociation as estimated by IR intensities versus ligand cone angle for several phosphine ligands. (Data adapted from ref. [85].)

Figure 1.31 shows two exemplary equilibria involving Ni(0) and a variety of phosphine ligands plotted solely against a steric parameter.[79, 85] Despite their rather different electronic properties, a moderate to good correlation can already be achieved with ligand cone angles.

1.8   References

1. Sicius, H., Einzeldarstellungen. In *Nickelgruppe: Elemente der zehnten Nebengruppe*, Springer Fachmedien Wiesbaden: Wiesbaden, 2017; pp 9-40.
2. Davidson, J. P.; Duffin, C. J. *Folklore* **2012,** *123*, 99-109.
3. Mond, L.; Langer, C.; Quincke, F. *Journal of the Chemical Society, Transactions* **1890,** *57*, 749-753.
4. Egorova, K. S.; Ananikov, V. P. *Organometallics* **2017,** *36*, 4071-4090.
5. Freund, A. *Journal für Praktische Chemie* **1882,** *26*, 367-377.
6. Thibodeaux, C. J.; Chang, W.-c.; Liu, H.-w. *Chem. Rev.* **2012,** *112*, 1681-1709.
7. Wessjohann, L. A.; Brandt, W.; Thiemann, T. *Chem. Rev.* **2003,** *103*, 1625-1648.
8. Schroder, F. *Chem Biodivers* **2014,** *11*, 1734-1751.
9. Structure and Reactivity of the Cyclopropane Species. In *Cyclopropanes in Organic Synthesis*.
10. de Meijere, A. *Angewandte Chemie International Edition in English* **1979,** *18*, 809-826.
11. Synthesis of Cyclopropanes. In *Cyclopropanes in Organic Synthesis*.

12. Lebel, H.; Marcoux, J.-F.; Molinaro, C.; Charette, A. B. *Chem. Rev.* **2003,** *103*, 977-1050.
13. Simmons, H. E.; Smith, R. D. *J. Am. Chem. Soc.* **1958,** *80*, 5323-5324.
14. Simmons, H. E.; Smith, R. D. *J. Am. Chem. Soc.* **1959,** *81*, 4256-4264.
15. Furukawa, J.; Kawabata, N.; Nishimura, J. *Tetrahedron Letters* **1966,** *7*, 3353-3354.
16. Friedrich, E. C.; Domek, J. M.; Pong, R. Y. *The Journal of organic chemistry* **1985,** *50*, 4640-4642.
17. Zhou, Y. Y.; Uyeda, C. *Angewandte Chemie* **2016,** *55*, 3171-3175.
18. Werth, J.; Uyeda, C. *Chem Sci* **2018,** *9*, 1604-1609.
19. Trost, B. M. *Angewandte Chemie International Edition in English* **1995,** *34*, 259-281.
20. Diazomethane. In *Encyclopedia of Reagents for Organic Synthesis.*
21. Metal Catalysed Cyclopropanation. In *The Chemistry of the Cyclopropyl Group.*
22. Rasmussen, T.; Jensen, J. F.; Østergaard, N.; Tanner, D.; Ziegler, T.; Norrby, P.-O. *Chemistry – A European Journal* **2002,** *8*, 177-184.
23. Straub, B. F.; Gruber, I.; Rominger, F.; Hofmann, P. *Journal of Organometallic Chemistry* **2003,** *684*, 124-143.
24. Straub, B. F. *J. Am. Chem. Soc.* **2002,** *124*, 14195-14201.
25. Berthon-Gelloz, G.; Marchant, M.; Straub, B. F.; Marko, I. E. *Chemistry – A European Journal* **2009,** *15*, 2923-2931.
26. Morandi, B.; Carreira, E. M. *Science* **2012,** *335*, 1471-1474.
27. Mastronardi, F.; Gutmann, B.; Kappe, C. O. *Org. Lett.* **2013,** *15*, 5590-5593.
28. Gai, Y.; Julia, M.; Verpeaux, J.-N. *Synlett* **1991,** *1991*, 56-57.
29. Gai, Y.; Julia, M.; Verpeaux, J. N. *Bull Soc Chim Fr* **1996,** *133*, 817-829.
30. den Hartog, T.; Toro, J. M.; Chen, P. *Organic letters* **2014,** *16*, 1100-1103.
31. Tchawou, A. A. S. W.; Raducan, M.; Chen, P. *Organometallics* **2017,** *36*, 180-191.
32. Corey, E. J.; Chaykovsky, M. *J. Am. Chem. Soc.* **1965,** *87*, 1353-1364.
33. Recent Advances in Synthesis of Cyclopropanes. In *The Chemistry of the Cyclopropyl Group.*
34. Roiser, L.; Zielke, K.; Waser, M. *Asian J Org Chem* **2018,** *7*, 852-864.
35. IUPAC Gold Book, https://goldbook.iupac.org/ (last access: 6.6.2019)
36. Wittig, G.; Felletschin, G. *Justus Liebigs Annalen der Chemie* **1944,** *555*, 133-145.
37. Ingold, C. K.; Jessop, J. A. *Journal of the Chemical Society (Resumed)* **1930**, 713-718.
38. Zhang, X. M.; Bordwell, F. G. *J. Am. Chem. Soc.* **1994,** *116*, 968-972.
39. Franzen, V.; Wittig, G. *Angew. Chem.* **1960,** *72*, 417-417.
40. Wittig, G.; Krauss, D. *Justus Liebigs Annalen der Chemie* **1964,** *679*, 34-41.
41. Stevens, T. S.; Creighton, E. M.; Gordon, A. B.; MacNicol, M. *Journal of the Chemical Society (Resumed)* **1928**, 3193-3197.
42. Sweeney, J. B. *Chemical Society Reviews* **2009,** *38*, 1027-1038.
43. Kunzi, S. A.; Toro, J. M. S.; den Hartog, T.; Chen, P. *Israel Journal of Chemistry* **2016,** *56*, 53-61.
44. den Hartog, T.; Sarria Toro, J. M.; Couzijn, E. P.; Chen, P. *Chem Commun (Camb)* **2014,** *50*, 10604-10607.
45. Sarria Toro, J. M.; den Hartog, T.; Chen, P. *Chem Commun (Camb)* **2014,** *50*, 10608-10610.
46. Schmidaur, H.; Tronich, W. *Chemische Berichte* **1968,** *101*, 595-603.
47. Wittig, G.; Polster, R. *Justus Liebigs Annalen der Chemie* **1956,** *599*, 1-12.
48. Pörschke, K.-R.; Jonas, K.; Wilke, G.; Benn, R.; Mynott, R.; Goddard, R.; Krüger, C. *Chemische Berichte* **1985,** *118*, 275-297.

49. Pörschke, K.-R.; Wilke, G.; Mynott, R. *Chemische Berichte* **1985,** *118*, 298-312.

50. Pörschke, K.-R. *Chemische Berichte* **1987,** *120*, 425-427.

51. Heydenreich, F.; Mollbach, A.; Wilke, G.; Dreeskamp, H.; Hoffmann, E. G.; Schroth, G.; Seevogel, K.; Stempfle, W. *Israel Journal of Chemistry* **1972,** *10*, 293-319.

52. Nattmann, L.; Lutz, S.; Ortsack, P.; Goddard, R.; Cornella, J. *J. Am. Chem. Soc.* **2018,** *140*, 13628-13633.

53. Barnett, B. L.; Krüger, C. *Journal of Crystal and Molecular Structure* **1972,** *2*, 271-279.

54. Brauer, D. J.; Krüger, C. *Journal of Organometallic Chemistry* **1972,** *44*, 397-402.

55. Wilke, G. *Angewandte Chemie International Edition in English* **1988,** *27*, 185-206.

56. Barrett, B. J.; Iluc, V. M. *Organometallics* **2017,** *36*, 730-741.

57. Keim, W.; Kowaldt, F. H.; Goddard, R.; Krüger, C. *Angewandte Chemie International Edition in English* **1978,** *17*, 466-467.

58. Herbert, D. E.; Lara, N. C.; Agapie, T. *Chemistry - A European Journal* **2013,** *19*, 16453-16460.

59. Mindiola, D. J.; Hillhouse, G. L. *J. Am. Chem. Soc.* **2002,** *124*, 9976-9977.

60. Iluc, V. M.; Hillhouse, G. L. *J. Am. Chem. Soc.* **2014,** *136*, 6479-6488.

61. Nakamura, A.; Yoshida, T.; Cowie, M.; Otsuka, S.; Ibers, J. A. *J. Am. Chem. Soc.* **1977,** *99*, 2108-2117.

62. Waterman, R.; Hillhouse, G. L. *J. Am. Chem. Soc.* **2003,** *125*, 13350-13351.

63. Kitiachvili, K. D.; Mindiola, D. J.; Hillhouse, G. L. *J. Am. Chem. Soc.* **2004,** *126*, 10554-10555.

64. Merrifield, J. H.; Lin, G. Y.; Kiel, W. A.; Gladysz, J. A. *J. Am. Chem. Soc.* **1983,** *105*, 5811-5819.

65. Patton, A. T.; Strouse, C. E.; Knobler, C. B.; Gladysz, J. A. *J. Am. Chem. Soc.* **1983,** *105*, 5804-5811.

66. Schrock, R. R.; Sharp, P. R. *J. Am. Chem. Soc.* **1978,** *100*, 2389-2399.

67. Grubbs, R. H.; Miyashita, A. *J. Am. Chem. Soc.* **1978,** *100*, 7418-7420.

68. Grubbs, R.; Miyashita, A., Reactions of Metallacycles of Nickel, Metallacyclopentanes, Hexanes and Butanes. In *Fundamental Research in Homogeneous Catalysis*, Tsutsui, M., Ed. Springer US: 1979; pp 151-163.

69. Miyashita, A.; Grubbs, R. H. *Tetrahedron Letters* **1981,** *22*, 1255-1256.

70. Miyashita, A.; Ohyoshi, M.; Shitara, H.; Nohira, H. *Journal of Organometallic Chemistry* **1988,** *338*, 103-111.

71. Dewar, M. J. S. *Bull. Soc. Chim. Fr.* **1951,** *18*.

72. Chatt, J.; Duncanson, L. A. *Journal of the Chemical Society (Resumed)* **1953**, 2939-2947.

73. Frenking, G.; Fröhlich, N. *Chem. Rev.* **2000,** *100*, 717-774.

74. Ugo, R. *Coordination Chemistry Reviews* **1968,** *3*, 319-344.

75. Tolman, C. A.; Seidel, W. C. *J. Am. Chem. Soc.* **1974,** *96*, 2774-2780.

76. Tolman, C. A. *J. Am. Chem. Soc.* **1974,** *96*, 2780-2789.

77. Tolman, C. A.; Seidel, W. C.; Gerlach, D. H. *J. Am. Chem. Soc.* **1972,** *94*, 2669-2676.

78. Tolman, C. A.; Seidel, W. C.; Gosser, L. W. *Organometallics* **1983,** *2*, 1391-1396.

79. Tolman, C. A. *Chem. Rev.* **1977,** *77*, 313-348.

80. Durand, D. J.; Fey, N. *Chemical reviews* **2019**.

81. Santiago, C. B.; Guo, J.-Y.; Sigman, M. S. *Chemical Science* **2018,** *9*, 2398-2412.

82. Brown, T. L.; Lee, K. J. *Coordination Chemistry Reviews* **1993,** *128*, 89-116.

83. Bilbrey, J. A.; Kazez, A. H.; Locklin, J.; Allen, W. D. *Journal of Chemical Theory and Computation* **2013,** *9*, 5734-5744.

84. Falivene, L.; Credendino, R.; Poater, A.; Petta, A.; Serra, L.; Oliva, R.; Scarano, V.; Cavallo, L. *Organometallics* **2016,** *35*, 2286-2293.
85. Tolman, C. A. *J. Am. Chem. Soc.* **1970,** *92*, 2956-2965.
86. Tolman, C. A.; Reutter, D. W.; Seidel, W. C. *Journal of Organometallic Chemistry* **1976,** *117*, C30-C33.

2 Discovery and Development

Parts of this chapter have been published as and figures adapted or reprinted with permission from:

Künzi, S. A.; Sarria Toro, J. M.; den Hartog, T.; Chen, P. Nickel-Catalyzed Cyclopropanation with NMe_4OTf and *n*BuLi. *Angew. Chem. Int. Ed.* **2015**, *54*, 10670-106704.

2.1   Introduction – Nickel-Catalyzed Cyclopropanations

At the outset of the project, it was suspected that a (transition) metal impurity might have acted as a hidden catalyst in Franzen's 1960 result (see chapter 1), or at least that there could be an active catalyst for this transformation. Although, no such catalyst had been found at that point.

Nickel has been known to catalyze or promote cyclopropanation reactions with several methylene donors. Seminal examples can be seen in **Figure 1.8**.[1-4] Treating Ni(cdt) (**2.1**) with diazomethane resulted in the formation of cyclopropane **2.2** and cyclopentane **2.3**.[1] The product ratio depends on the amount of excess diazomethane used. Interestingly, rather than forming a bis- or triscyclopropanes, the selective formation of cyclopentane **2.3** was observed instead.

Otsuka and Ibers reported on the Ni(0)-catalyzed cyclopropanation of electron-poor alkenes.[2] For alkyl or aryl substituted alkenes (1-hexene, cyclohexene, styrene) only trace amounts of product were obtained.
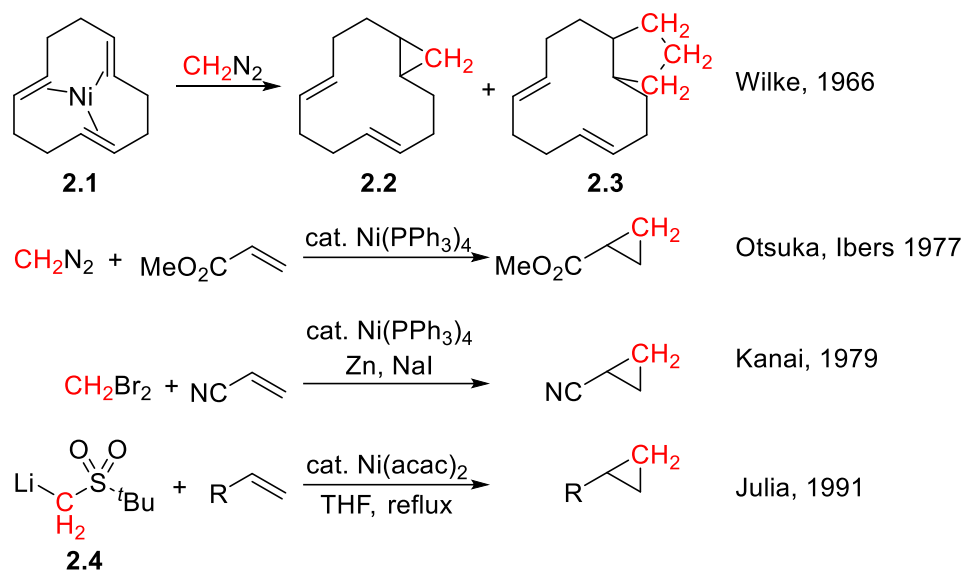
Figure 2.1. Examples of nickel-promoted or –catalyzed cyclopropanation reactions with different methylene donors.

Kanai and coworkers demonstrated a nickel-catalyzed Simmons-Smith reaction with a shifted substrate scope towards electron-poor alkenes not accessible with standard Simmons-Smith conditions.[3]

The most significant early indication that nickel could be a viable catalyst is shown in **Figure 1.8** on the bottom. Julia et al. reported on the nickel-catalyzed cyclopropanation of alkyl and aryl substituted alkenes using lithiomethyl *tert*-butyl sulfone (**2.4**) as methylene donor in refluxing THF.[4]

2.2 Reaction Discovery and Optimization

The standard test conditions for the cyclopropanation were chosen as follows. For the formation of the methylene donor lithiomethyltrimethylammonium triflate, the protocol established previously in our group by Sarria Toro and den Hartog was adopted, i.e., deprotonation of tetramethylammonium triflate with BuLi in THF at 0 °C.[5] The substrate cyclooctene was not expected to be very biased or activated and easier to handle as high-boiling liquid (b.p. 144 °C) as opposed to Franzen's original substrate, cyclohexene (b.p. 83 °C).

2.2.1 Initial Hit and Catalyst Screening

As outlined above, nickel was targeted as potential catalyst based upon literature precedent of cyclopropanation reactions. Especially the conditions employed by Julia

and coworker were very similar to the conditions established previously in our group by Sarria Toro and den Hartog for the deprotonation of tetramethylammonium triflate, i.e., THF as solvent and BuLi as base.[5-6]

Indeed, the use of 5 mol% Ni(OTf)$_2$ and 15 equiv cyclooctene (COE) relative to in situ formed ylide provided the cyclopropane product, bicyclo[6.1.0]nonane, in 6 % yield (**Table 1.1**, entry 1).
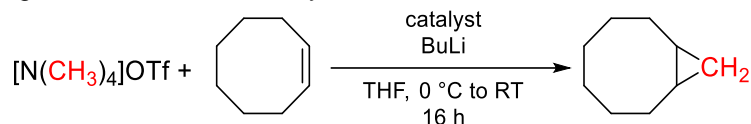
Table 2.1. Screening of Different Nickel Precatalysts.[a]
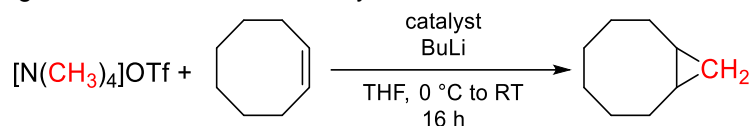
Entry	Catalyst	Yield / %
1[b]	5 mol% Ni(OTf)$_2$	6
2	1 mol% (Ph$_3$P)$_2$NiBr$_2$	23
3	1 mol% (Ph$_3$P)$_2$NiCl$_2$	25
4	1 mol% Ni(cod)$_2$ / 2 mol% PPh$_3$	19
5	1 mol% CpNi(PPh$_3$)Cl	22
6	0.5 mol% (dme)NiBr$_2$	16
7	1 mol% (dme)NiBr$_2$ / 2 mol% PPh$_3$	19
8	1 mol% Ni(acac)$_2$ / 2 mol% PPh$_3$	20
9	None	0
10[c]	1 mol% (dme)NiBr$_2$ / 2 mol% PPh$_3$	14
11[d]	1 mol% (Ph$_3$P)$_2$NiBr$_2$	25

[a]Standard conditions: 1 equiv [NMe$_4$]OTf, 1.05 equiv BuLi, 5 equiv COE, 0.05 M in THF. [b]15 equiv COE. [c]3 equiv [NMe$_4$]OTf, 1 equiv COE. [d]Slow addition of BuLi over 5.5 h, 0.5 mmol scale.

Several other nickel sources were viable precatalysts. A control experiment in the absence of any catalyst resulted in no background reaction (**Table 2.1**, entry 9). Both nickel(II) and nickel(0) precatalyst were active for the cyclopropanation (e.g., **Table 2.1**, entry 2 vs entry 4). Even though the cyclopropanation of COE proceeded under 'ligandless' conditions (entry 1 and 6), the addition of a ligand proved highly beneficial for the reaction. First, most ligandless nickel(II) salts are usually rather insoluble in organic solvents; Ni(OTf)$_2$ is very poorly soluble in THF and (dme)NiBr$_2$ is only poorly so. Second, the use of (dme)NiBr$_2$ without any additional ligand resulted in capricious reaction outcomes with widely varying yields. In these cases, the formation of a black colloid was often observed, likely the precipitation of nickel black had occurred, presumably inactive for this transformation. Thus, it can be concluded that in absence of a stabilizing ligand the active catalyst is not stable towards aggregation and deactivation making the reaction poorly reproducible. This makes the interpretation of any mechanistic insights under ligandless condition, at least with cyclooctene, unreliable.

Neither slow addition of BuLi (entry 11) nor the use of excess ylide with respect to 1 equiv COE (entry 10) improved the yield.

Table 2.2. Screening of other Metal Precatalysts.[a]

$$[N(CH_3)_4]OTf \; + \; \text{(cyclooctene)} \quad \xrightarrow[\substack{THF, \; 0\,°C \text{ to RT} \\ 16\ h}]{\substack{catalyst \\ BuLi}} \quad \text{(bicyclic)}CH_2$$

Entry	Catalyst	Yield / %
1	0.5 mol % $Cu(OTf)_2 \cdot C_6H_6$ / 2 mol% PPh_3	0
2	1 mol% $Fe(acac)_3$ / 2 mol% PPh_3	0
3	1 mol% $Co(acac)_3$ / 2 mol% PPh_3	0
4	1 mol% $(Ph_3P)_2PdCl_2$	0
5	1 mol% $Rh_2(OAc)_4$	0
6	1 mol% $[(cod)(Ph_3P)_2Rh]PF_6 \cdot CH_2Cl_2$	0
7	1 mo% $Zn(OTf)_2$ / 2 mol% PPh_3	0
8	1 mol% $(Ph_3P)_2Re(O)Cl_3$	0
9	1 mol% $Cp^*_2ZrCl_2$	0
10	1 mol% Cp_2TiCl_2	0

[a]Standard conditions: 1 equiv $[NMe_4]OTf$, 1.05 equiv BuLi, 5 equiv COE, 0.05 M in THF.

A variety of other metals known to be active cyclopropanation catalysts were screened as well. Interestingly, none of the tested metals yielded any product. Neither, the metal employed in the Simmons-Smith reactions (**Table 2.2**, entry 7), albeit here in catalytic amounts, nor any of the commonly used metal catalysts (Cu, Rh, Pd) for the cyclopropanation with diazomethane and other diazo compounds (entries 1, 4, 5, and 6) afforded any cyclopropane.[7] Especially the absence of any reactivity of Pd (entry 4) should be highlighted here despite being the heavier homologue of Ni with often similar reactivity. Both have been shown to catalyze the cyclopropanation with diazomethane.[2]

Thus, **Table 2.2** rather drastically shows the unique ability of nickel to catalyze the reaction at hand.

2.2.2 Ligand Screening

After nickel was established as an active catalyst, we turned to screening (commercially available) ligands (**Table 2.3**).

Table 2.3. Screening of Ligands.[a]
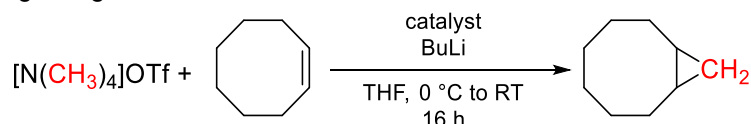
Entry	Catalyst	Yield / %
1	1 mol% (PPh₃)₂NiBr₂	23
2	1 mol% Ni(cod)₂ / 1 mol% IPr	<1
3	1 mol% Ni(cod)₂ / 1 mol% IMes	<1
4	1 mol% Ni(acac)₂ / 1 mol% IPr·HBF₄	1
5	1 mol% Ni(acac)₂ / 1 mol% SIPr·HBF₄	3
6	1 mol% Ni(acac)₂ / 1 mol% I^{t}Bu·HBF₄	5
7	1 mol% (dme)NiBr₂ / 2 mol% PCy₃	6
8	1 mol% (dme)NiBr₂ / 2 mol% PBu₃	11
9	1 mol% (dme)NiBr₂ / 2 mol% PPh₂Me	0.3
10	1 mol% (dme)NiBr₂ / 2 mol% PPhMe₂	3
11	1 mol% (dme)NiBr₂ / 2 mol% P(o-tolyl)₃	4
12	1 mol% Ni(cod)₂ / 2 mol% P(3,5-CF₃Ph)₃	8
13	1 mol% (dme)NiBr₂ / 2 mol% P(2-MeOPh)₃	1
14	1 mol% (dme)NiBr₂ / 2 mol% P(4-MePh)₃	6
15	1 mol% (dme)NiBr₂ / 2 mol% PPh₂Cy	21
16	1 mol% (dme)NiBr₂ / 1 mol% BINAP	12
17	1 mol% (dme)NiBr₂ / 1 mol% dppf	0
18	1 mol% (dme)NiBr₂ / 1 mol% dcpe	5
19	1 mol% (dme)NiBr₂ / 1 mol% dppp	4
20	1 mol% (dme)NiBr₂ / 1 mol% dppb	11
21	1 mol% (dppe)NiCl₂	9
22	1 mol% (dme)NiBr₂ / 2 mol% AsPh₃	2
23	1 mol% (dme)NiBr₂ / 1 mol% 4,4'-DiMebpy	3
24	1 mol% Ni(TPP)	1

[a]Standard conditions: 1 equiv [NMe₄]OTf, 1.05 equiv BuLi, 5 equiv COE, 0.05 M in THF. 4,4'-diMebpy = 4,4'-dimethyl-2,2'-bipyridine. TPP = 5,10,15,20-Tetraphenyl-21H,23H-porphine.

Several different, commonly used ligand classes were tested, such as phosphines, both monodentate (**Table 2.3**, entry 7 to 15) and bidentate (entry 16 to 21), NHCs (entry 2 to 6), and a diimine-based ligand (entry 23). Out of these screening efforts a general picture emerged. Phosphines were by far the best ligand class tested, while for example NHCs produced inactive catalyst systems. Within the class of phosphine ligands, monodentate, triarylphophshines performed best, while chelating phosphine generally performed much worse, with PPh₃ being the best performing ligand.

From the screening efforts presented above, (Ph₃P)₂NiBr₂ crystallized as the catalyst system of choice. Its commercial availability and solubility in THF, together with the best performing ligand already precomplexed as a one-component system, made it the most convenient choice as precatalyst.

### 2.2.3 Solvents, Counteranions and Alternative Cations

Tetramethylammonium salts are in general poorly soluble in solvents that allow for their deprotonation. Hence, the choice of solvent and the counteranion is intimately

connected. For the triflate salt, the solvent window is rather narrow and mostly limited to THF. Although a small amount of less polar co-solvent (toluene) is tolerated (**Table 2.4**, entry 1 and 2 vs 3 to 5).

More solubilizing counteranions have been tested. Both the BArF$_{24}$ and nonaflate salts are considerably more soluble in organic solvents, even in less polar solvents such as toluene and diethyl ether. While the BArF$_{24}$ gave much lower yields (entry 9 and 10), the longer chain analogue of triflate, nonaflate, performed similar to triflate even in low-polarity solvents (entry 6 to 8).

Because the higher solubility offered no advantage in terms of yield, the triflate salt was chosen as the simpler reagent. Although in specific instances, the nonaflate might be an interesting alternative to be considered.

Table 2.4. Solvent and Counteranion Screening.[a]
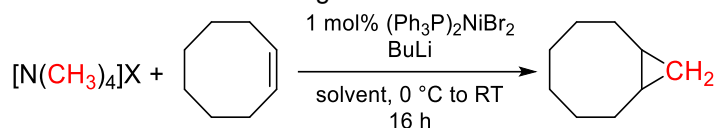
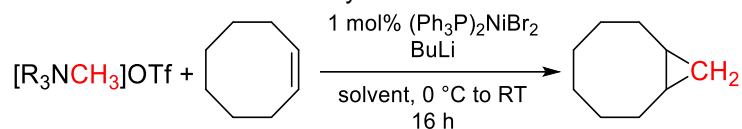| Entry	X$^-$	Solvent	Yield / %
1	OTf	THF	23
2	OTf	3:1 THF/PhCH$_3$	24
3	OTf	1:1 THF/PhCH$_3$	15
4	OTf	1:3 THF/PhCH$_3$	15
5	OTf	1:9 THF/1,4-Dioxane	3
6	ONf	THF	20
7	ONf	Et$_2$O	24
8	ONf	PhCH$_3$	22
9	BArF$_{24}$	THF	3
10	BArF$_{24}$	Et$_2$O	0.4
11	TFA	THF	0.3

[a]Standard conditions: 1 equiv [NMe$_4$]X, 1.05 equiv BuLi, 5 equiv COE. ONf = Perfluorooctanoic sulfonate, BArF$_{24}$ = Tetrakis(3,5-bis(trifluoromethyl)phenyl)borate, TFA = Trifluoroacetate

The ammonium cation itself can in principal also be varied. Analogous to changing the anion, the solubility of the salt can be increased with more lipophilic groups (cf. long-chain tetraalkylammonium phase transfer agents, e.g., [NBu$_4$]$^+$). At the same time, this introduces several complicating factors. First, for asymmetrically substituted ammonium salts, the question of selectivity regarding which substituent is transferred arises. Second, new decomposition pathways are possible or the probability of existing ones are increased, e.g., Stevens or Sommelet-Hauser rearrangements and Hofmann eliminations.

Having multiple methyl groups to deprotonate should favor the methylene transfer kinetically, while secondary alkyl anions should be disfavored thermodynamically and thus disfavor the transfer of groups other than methylene. The proclivity of the ylide to

decompose on the other hand is mostly dictated by the availability of β-hydrogen, ring strain etc. and might be prevented by the proper choice of substituents.

Table 2.5. Alternative Ammonium Salts as Methylene Donor.[a]

[R₃NCH₃]OTf + (cyclooctene) → (bicyclic cyclopropane CH₂)

1 mol% (Ph₃P)₂NiBr₂
BuLi
solvent, 0 °C to RT
16 h

Entry	Ammonium Salt	Yield / %
1	*N,N*-Dimethylpyrrolidinium Triflate	0
2	*N,N*-Dimethylmorpholinium Triflate	0
3	*N,N,N*-Trimethyl-1-adamantylammonium Triflate	3
4	*N,N,N*-Trimethylneopentylammonium Triflate	1
5[b]	*N,N,N*-Trimethylbutylammonium Triflate	22

[a]Standard conditions: 1 equiv [NR₄]OTf, 1.05 equiv BuLi, 5 equiv COE. [b]5 equiv NBE.
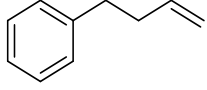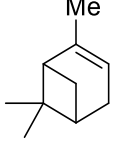
Despite the above considerations, no other ammonium cation besides tetramethylammonium yielded product in any significant amount (**Table 2.5**). Although, these reactions were usually not followed up in detail, the accelerated decomposition compared to lithiomethyltrimethylammonium was sometimes noticed.

2.3   Substrate Scope

Having preliminary optimized conditions in hand, we turned to survey the substrate scope for a small set of differently substituted alkenes (**Table 2.6**). The yield for the strained bicyclic alkene norbornene (NBE, entry 1) and terminal alkenes (entry 2 and 3) ranged from good to moderate. The rather low yield of 4-phenylbutene (entry 3) compared to 1-octene (entry 2) seems to stem from side-reactions not present for the latter. Indeed, for all substrates and conditions tested, side-products derived from the alkene itself has not observed except for 4-phenylbutene. Only starting material or cyclopropane product was observed. These side-products have not been identified for the reaction with 4-phenylbutene.

Table 2.6. Small Substrate Scope.[a]

$$[N(CH_3)_4]OTf + R\diagdown \xrightarrow[\substack{THF,\ 0\ °C\ to\ RT \\ 16\ h}]{\substack{1\ mol\%\ (Ph_3P)_2NiBr_2 \\ BuLi}} R\triangle CH_2$$

Entry	Alkene	Yield / %	Entry	Alkene	Yield / %
1		79	5		8
2	Hex	62	6		0
3		40	7		0
4		23			

[a]Standard conditions: 1 equiv [NMe$_4$]OTf, 1.05 equiv BuLi, 5 equiv alkene, 0.05 M in THF.

The cyclic alkenes cyclooctene and cyclohexene (entry 4 and 5) gave low yields. But very importantly, Franzen's original substrate cyclohexene was cyclopropanated for the first time using lithiomethyltrimethylammonium as methylene donor since the original report, at least to the best of our knowledge.

Unfortunately, the electron-rich cyclic enol ether 3,4-dihydro-2*H*-pyrane (entry 6) and the trisubstituted, highly sterically encumbered double bond of α-pinene (entry 7) did not yield any product.
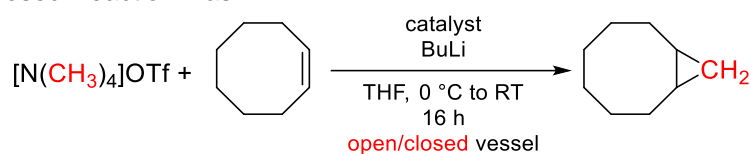
2.4 'Odd' Observations

During our initial optimization studies presented above, we discovered several unusual features of the cyclopropanation reaction. These are discussed in the following.

2.4.1 Open versus Closed

During previous work with lithiomethyltrimethylammonium triflate in this group, it was noted that the reagent is only stable in a closed vessel.[8] To see whether this is also the case in the present reaction and could make a difference, we conducted the standard reaction in a flask open to an argon Schlenk line. Under standard conditions, the reaction was run in a closed reaction vessel to allow no gas exchange. Indeed, a small difference was observed using (Ph$_3$P)$_2$NiBr$_2$ as catalyst (**Table 2.7**, entry 1 vs 2). Using (dme)NiBr$_2$ as catalyst, the difference was more pronounced (entry 3 vs 4).

Although keeping the capricious nature of the ligandless reaction conditions in mind, one should not put too much weight on any effects observed under the latter. Nevertheless, all reaction were generally conducted in a sealed flask to prevent any possible influence of this variable.

Table 2.7. Open/closed Reaction Flask.[a]

$[N(CH_3)_4]OTf$ + [cyclooctene] $\xrightarrow[\substack{THF, 0\ °C\ to\ RT \\ 16\ h \\ open/closed\ vessel}]{\substack{catalyst \\ BuLi}}$ [bicyclic]CH_2

Entry	Catalyst	Open/closed[b]	Yield / %
1	1 mol% $(Ph_3P)_2NiBr_2$	Closed	23
2	1 mol% $(Ph_3P)_2NiBr_2$	Open	16
3	0.5 mol% $(dme)NiBr_2$	Closed	16
4	0.5 mol% $(dme)NiBr_2$	Open	<1

[a]Standard conditions: 1 equiv $[NMe_4]OTf$, 1.05 equiv BuLi, 5 equiv COE, 0.05 M in THF. [b]Flask was open or closed to an argon Schlenk line.

2.4.2 Catalyst loading effect

Varying the catalyst loading for $(Ph_3P)_2NiBr_2$, we noticed a bell-shaped curve for the cyclopropanation yield of cyclooctene. Both at low and at high loading of precatalyst, the product yield is low, while there is an optimal loading in terms of product formation around 0.5 to 1 mol% of catalyst.
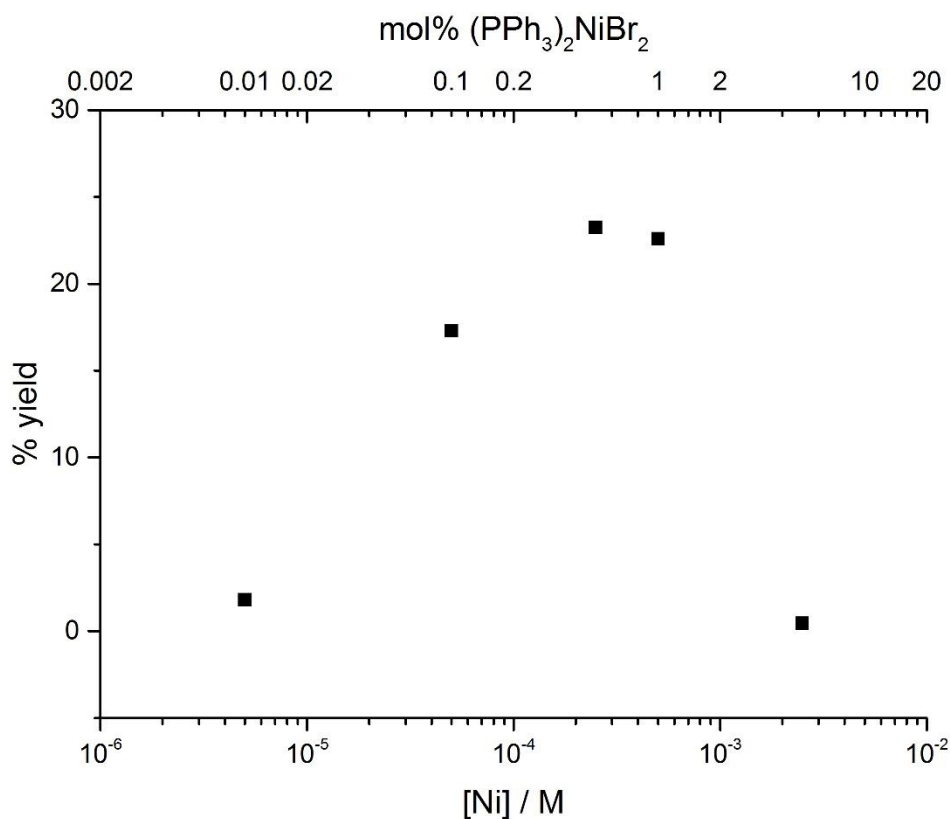
Figure 2.2. Varying catalyst loading [(Ph₃P)₂NiBr₂] versus cyclopropanation yield for cyclooctene.

2.4.3 Side-Products

For the substrates presented in **Table 2.6** we have not observed any side-products derived from the alkenes themselves, except for 4-phenylbutene as discussed above. To gain insight into the fate of the ylide, we synthesized the ^{13}C-enriched tetramethylammonium salt [(H₃C)₃N($^{13}CH_3$)]OTf. ^{13}C NMR spectra overlay of the cyclopropanation conducted in a J. Young NMR tube with the natural abundance and the ^{13}C-enriched reagent, respectively, is shown in **Figure 2.3**. An additional overlay of the reaction and the authentic product bicyclo[6.1.0]nonane is shown in **Figure 2.4**. Comparing the peak intensity in **Figure 2.3** shows incorporation of the $^{13}CH_2$ unit into the expected position of the cyclopropane product. Additionally, the formation of cyclopropane C_3H_6 was observed.

As expected, also some small amounts of remaining starting material [NMe₄]⁺ and the by-product NMe₃ show an increased peak intensity in the ^{13}C NMR spectrum.
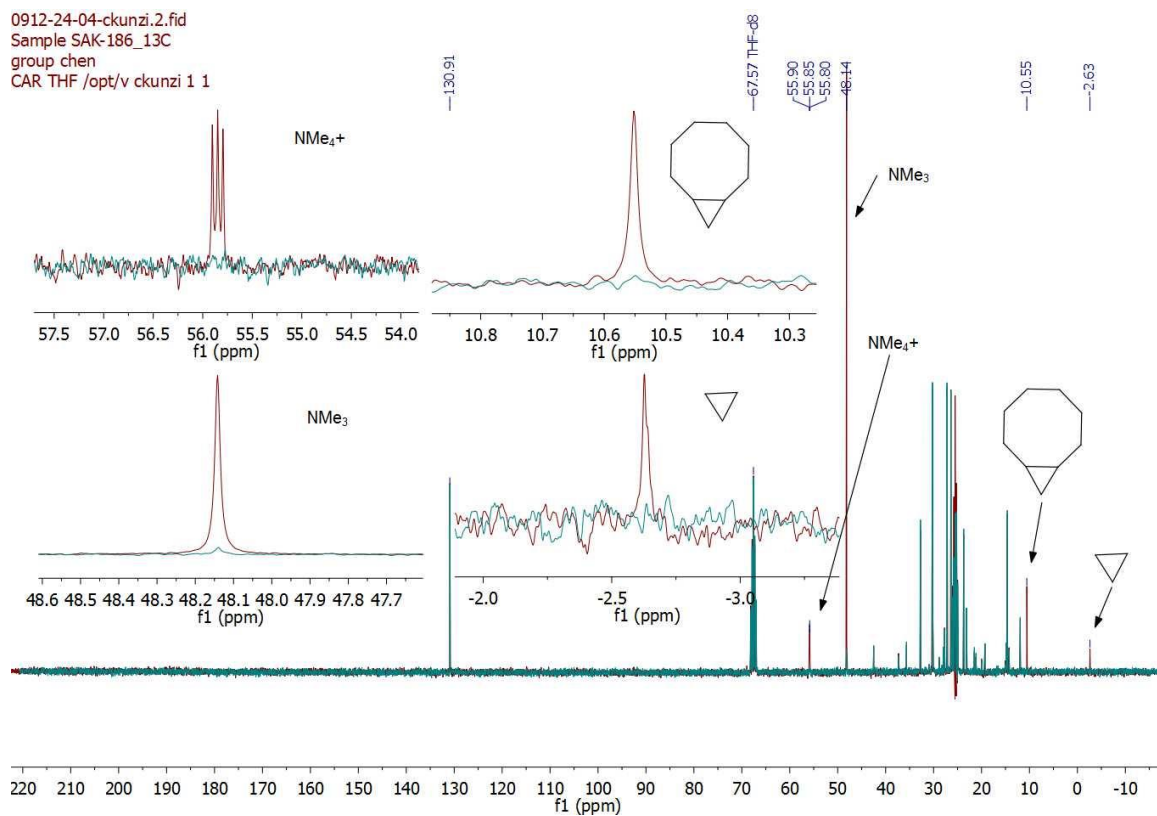
Figure 2.3. Comparison of ^{13}C NMR spectra of reactions with unlabeled and ^{13}C-enriched tetramethylammonium triflate. Spectrum in red shows reaction with ^{13}C-enriched reagent, spectrum in blue with natural abundance. Insets show peaks which are not or only weakly present in the reaction with unlabeled reagent
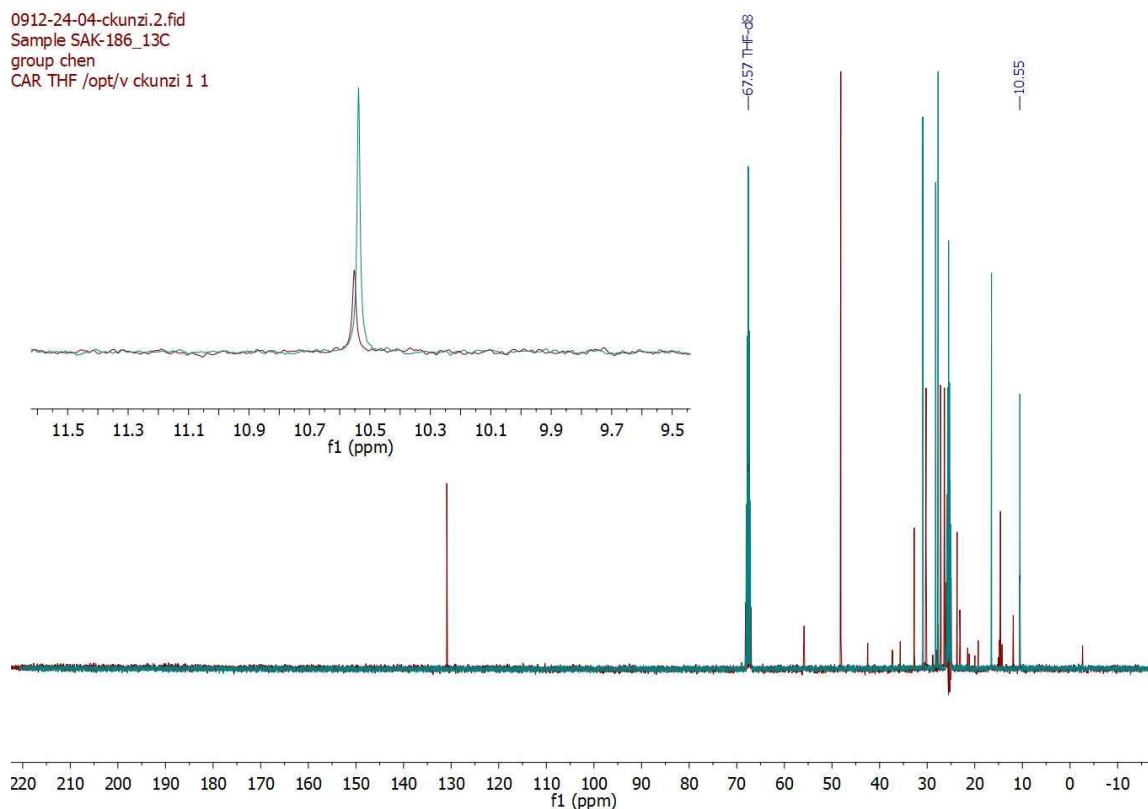
0912-24-04-ckunzi.2.fid
Sample SAK-186_13C
group chen
CAR THF /opt/v ckunzi 1 1

Figure 2.4. Overlay of ^{13}C NMR spectra of reaction with ^{13}C-enriched NMe$_4$OTf (red) and authentic bicyclo[6.1.0]nonane (blue). Inset shows the position of ^{13}C incorporation into the product.

At the end of the reaction, small amounts of an amorphous, white solid can be visually identified. Scale-up of the reaction and subsequent isolation of this material led to the identification of polyethylene by NMR, IR, and high-temperature GPC in 17 % yield. The IR spectrum of the isolated material and that of an authentic polyethylene reference substance is shown in **Figure 2.5**.
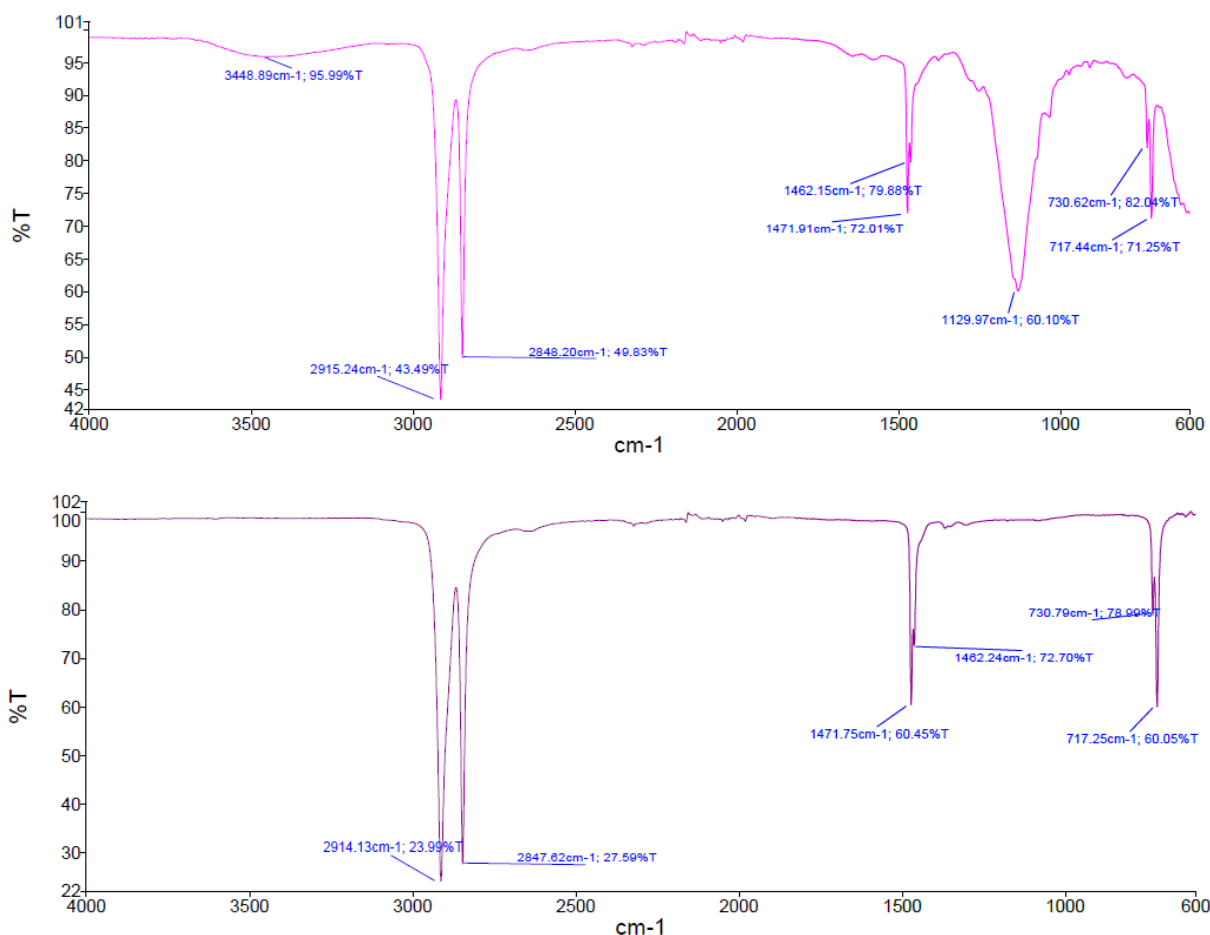
Figure 2.5. Top: IR spectrum (neat solid) of the isolated polymer. Bottom: IR spectrum (neat solid) of polyethylene standard (M_w = 153'000) as reference.

Both of these side-products, i.e., cyclopropane and polyethylene, likely stem from in situ produced ethene via nickel carbene homocoupling (see below).

2.5 Proposed Catalytic Cycle

Combining the gathered insights presented in this chapter, as well as literature precedent, we proposed the catalytic cycle sketched out in **Figure 2.6**.

We begin the cycle with the Ni(0) species **2.5** with L = PR_3 or alkene as the most likely ligand in this system for a Ni(0) species. In the case of a Ni(II) precatalyst, the nickel can first be reduced either by BuLi or potentially by the ylide itself, if it has been preformed before the addition of the catalyst. The reduction of Ni(II) to Ni(0) by BuLi is a known process.[9] In the case of a Ni(0) precatalyst, this activation step is not necessary.

The Ni(0) species **2.5** can than form an adduct with lithiomethyltrimethylammonium to give the niccolate(0) complex **2.6**. This step and intermediate is modelled after Pörschke's work on the Lewis acidity of Ni(0) compounds, specifically the isolated methyl adducts Li[(H$_3$C)Ni(C$_2$H$_4$)$_2$] presented in the Introduction.[10]

Extrusion of NMe$_3$ would lead to the nickel carbene species **2.7** as a reactive intermediate. Several reactions steps branching out from this intermediate can be postulated. Reaction with an alkene would lead in a [2+2] cycloaddition to the nickelacyclobutane **2.8** and subsequent reductive elimination would lead to the product and close the catalytic cycle. These product formation steps are proposed in analogy to the work of Hillhouse et al. on isolable nickel carbenes and nickelacyclobutanes and the work of Miyashita et al. on nickelacyclobutanes as presented in the Introduction chapter.[11-14]

Nickel carbene **2.7** could potentially also undergo homocoupling to give ethene and regenerate **2.5** (**Figure 2.6**, red arrow), thus, essentially short circuiting the product cycle and decomposing the ylide unproductively. Bimolecular homocoupling of isolable metal carbenes to form ethene has been reported for both an electrophilic rhenium carbene as well as a nucleophilic tungsten carbene (see Introduction).[15-16]
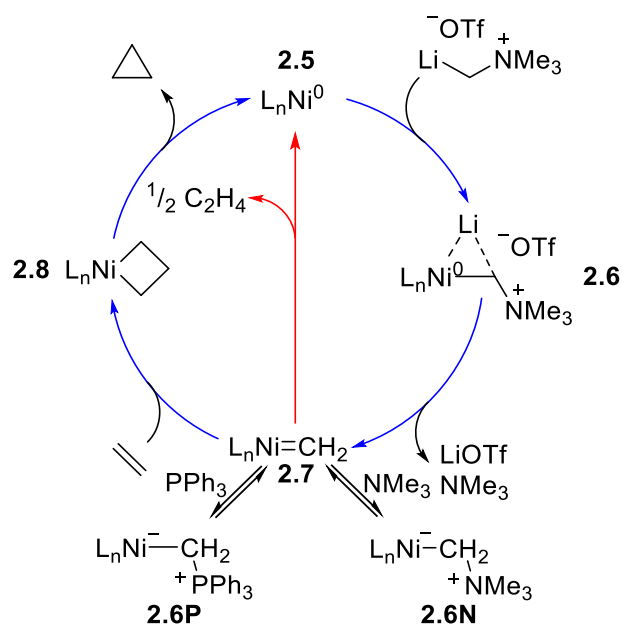

Figure 2.6. Proposed catalytic cycle.

In addition to homocoupling, we also speculated that the nickel carbene could potentially undergo (reversible) trapping with a nucleophile, such as the phosphine

ligand or liberated NMe$_3$ to give **2.6P** and **2.6N**, respectively. These off-cycle reaction pathways could have a significant influence on the reaction outcome (see chapter 3). Agnostic about the turnover-limiting step, nickel carbene **2.7** could be the reason for the observed catalyst loading effect. At low concentration, the cyclopropanation pathway, kinetically 1st order in carbene, is still kinetically competent, while at higher loadings the homocoupling, kinetically 2nd order in carbene, outcompetes the reaction with alkene. The ylide is then decomposed unproductively.

The influence of an open versus closed reaction flask could be due to volatile compounds formed during the proposed cycle, e.g., trimethylamine (b.p. 3 °C) or ethene, which might escape the open flask and change the course of the reaction. The hypothetical equilibrium between **2.7** and **2.6N** would be shifted by escaping trimethylamine, for example, in favor of more carbene, which would then favor homocoupling over cyclopropanation. This is reminiscent of the persistent radical effect, in which the 2nd order self-termination reaction of a radical is suppressed by reversible trapping with a persistent radical.[17]

2.6 Conclusions

In this chapter, the initial discovery, a nickel catalyst, and a preliminary reaction optimization for the cyclopropanation of unactivated olefins using lithiomethyltrimethylammonium triflate as methylene donor has been presented. Nickel precatalysts showed unique activity and PPh$_3$ proved to be the best performing ligand so far. In the absence of an ancillary ligand, at least in the cyclopropanation of cyclooctene with (dme)NiBr$_2$, the reaction outcome has been fickle.

A small substrate scope has been presented that features a wide variety of double bond substitution patterns. The reaction does not proceed for a trisubstituted, highly sterically congested double bond and a cyclic enol ether. Cyclic alkenes can be cyclopropanated in low yields, while terminal alkenes and a strained bicyclic alkene give moderate to good yields based on the methylene donor.

Several important observations have been made. Namely, there is a certain difference whether the reaction is open to an argon Schlenk line or completely sealed without gas exchange; i.e., the yield is lower when the flask is open.

There is a pronounced influence of the catalyst loading on the cyclopropane yield using cyclooctene as substrate. This results in a bell-shaped curve with a maximum between 0.5 to 1 mol% of (Ph$_3$P)$_2$NiBr$_2$.

We have isolated polyethylene and observed cyclopropane (C_3H_6) by NMR as side-products. Both likely stem from initial ethene formation via carbene homocoupling and subsequent polymerization and cyclopropanation, respectively.

With these observations in mind and a wealth of literature precedent of analogous, isolated intermediates, we proposed a preliminary mechanism that could explain our observations and the general reaction pattern of this cyclopropanation.

2.7   References

1. Bogdanović, B.; Kröner, M.; Wilke, G. *Justus Liebigs Annalen der Chemie* **1966,** *699*, 1-23.
2. Nakamura, A.; Yoshida, T.; Cowie, M.; Otsuka, S.; Ibers, J. A. *J. Am. Chem. Soc.* **1977,** *99*, 2108-2117.
3. Hiroyoshi, K.; Nobuyuki, H. *Chemistry Letters* **1979,** *8*, 761-762.
4. Gai, Y.; Julia, M.; Verpeaux, J.-N. *Synlett* **1991,** *1991*, 56-57.
5. Sarria Toro, J. M.; den Hartog, T.; Chen, P. *Chem Commun (Camb)* **2014,** *50*, 10608-10610.
6. Gai, Y.; Julia, M.; Verpeaux, J.-N. *Synlett* **1991,** *1991*, 269-270.
7. Anciaux, A. J.; Hubert, A. J.; Noels, A. F.; Petiniot, N.; Teyssie, P. *The Journal of organic chemistry* **1980,** *45*, 695-702.
8. den Hartog, T.; Sarria Toro, J. M.; Couzijn, E. P.; Chen, P. *Chem Commun (Camb)* **2014,** *50*, 10604-10607.
9. Jolly, P. W.; Wilke, G., Preface. In *The Organic Chemistry of Nickel*, Jolly, P. W.; Wilke, G., Eds. Academic Press: 1974; pp xi-xii.
10. Pörschke, K.-R.; Jonas, K.; Wilke, G.; Benn, R.; Mynott, R.; Goddard, R.; Krüger, C. *Chemische Berichte* **1985,** *118*, 275-297.
11. Mindiola, D. J.; Hillhouse, G. L. *J. Am. Chem. Soc.* **2002,** *124*, 9976-9977.
12. Kitiachvili, K. D.; Mindiola, D. J.; Hillhouse, G. L. *J. Am. Chem. Soc.* **2004,** *126*, 10554-10555.
13. Iluc, V. M.; Hillhouse, G. L. *J. Am. Chem. Soc.* **2014,** *136*, 6479-6488.
14. Miyashita, A.; Ohyoshi, M.; Shitara, H.; Nohira, H. *Journal of Organometallic Chemistry* **1988,** *338*, 103-111.
15. Merrifield, J. H.; Lin, G. Y.; Kiel, W. A.; Gladysz, J. A. *J. Am. Chem. Soc.* **1983,** *105*, 5811-5819.
16. Schrock, R. R.; Sharp, P. R. *J. Am. Chem. Soc.* **1978,** *100*, 2389-2399.
17. Fischer, H. *Chem. Rev.* **2001,** *101*, 3581-3610.

3 Mechanistic Studies

Parts of this chapter have been published as and figures adapted or reprinted with permission from:

Künzi, S. A.; Sarria Toro, J. M.; den Hartog, T.; Chen, P. Nickel-Catalyzed Cyclopropanation with NMe$_4$OTf and *n*BuLi. *Angew. Chem. Int. Ed.* **2015**, *54*, 10670-106704.
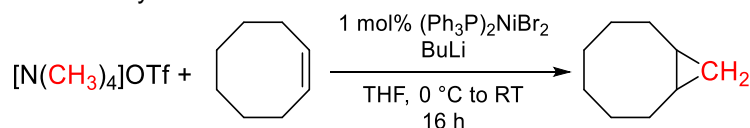
Künzi, S. A.; Gershoni-Poranne, R.; Chen, P. Mechanistic Studies on the Nickel-Catalyzed Cyclopropanation with Lithiomethyltrimethylammonium Triflate. *Organometallics* **2019**, *38*, 1928-1938.

3.1 Introduction – Nickel-Catalyzed Cyclopropanation Reactions

In chapter 2, we presented our initial optimization studies as well as some interesting observations we made during the process. We then decided to study the reaction mechanism in more depth to explain these findings and develop a rational way forward to design optimal reaction conditions.

3.2 Nickel Carbene Trapping

In our proposed catalytic cycle (**Figure 2.6**) we speculated that nickel carbene **2.7** might undergo reversible trapping with trimethylamine (or another nucleophile), essentially reversing the carbene formation step to go back to the ylide species (**2.6N**). To test this possibility, we added excess amounts of trimethylamine at the outset of the reaction.

Table 3.1. Addition of Trimethylamine.[a]

$$[N(CH_3)_4]OTf + \text{(cyclooctene)} \xrightarrow[\substack{THF, 0\,°C\ to\ RT \\ 16\ h}]{\substack{1\ mol\%\ (Ph_3P)_2NiBr_2 \\ BuLi}} \text{(bicyclic-}CH_2)$$

Entry	Additive	Yield / %
1	0 mol% NMe$_3$	23
2	20 mol% NMe$_3$	23
3	50 mol% NMe$_3$	22
4	100 mol% NMe$_3$	23
5	0 mol% NMe$_3$ / 50 mol% LiOTf	24
6	5 mol% NMe$_3$ / 5 mol% LiOTf	23
7	50 mol% NMe$_3$ / 50 mol% LiOTf	20

[a]Standard conditions: 1 equiv [NMe$_4$]OTf, 1.05 equiv BuLi, 5 equiv COE, 0.05 M in THF.

Neither the addition of NMe$_3$ alone, nor in combination with LiOTf (to compensate the formal negative charge on nickel after carbene trapping) had any influence on the cyclopropanation yield (**Table 3.1**).

Franzen showed that trimethylammonium-9-fluorenylide (**3.1**) decomposes at elevated temperature in neat *N,N*-dimethylbenzylamine to give 9-dimethylamino-9-benzylfluorene (**3.4**) (**Figure 3.1**).[1] It was postulated that the reaction proceeds via initial carbene formation (**3.2**) and subsequent carbene trapping with the amine solvent to give ylide **3.3**, which rearranges to **3.4**.[2] The rearrangement to **3.4** is irreversible and its formation was taken as proof for the intermediacy of the carbene **3.2**.

The ylide **3.1** is stable at room temperature and only decomposes at elevated temperatures (100 °C) with loss of NMe$_3$.[2] In contrast, the ylide **3.3** undergoes a Stevens rearrangement already at room temperature to give **3.5**.
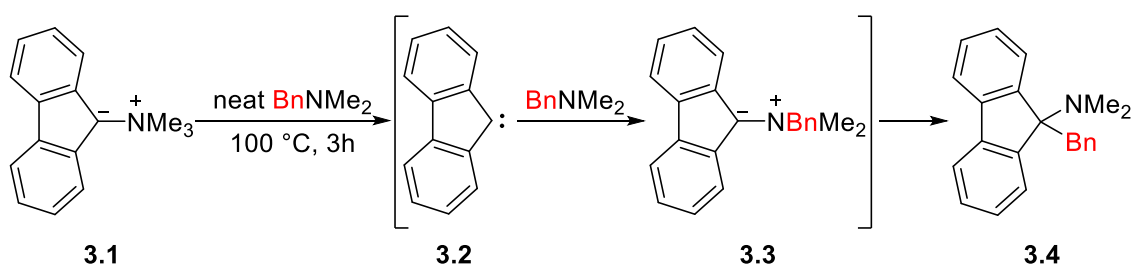
Figure 3.1. Trapping of fluorenyl carbene **3.2** with *N,N*-dimethylbenzylamine and subsequent Stevens rearrangement according to Franzen.[1]

In attempt to conduct the analogous trapping experiment as evidence for nickel carbene formation, an excess of *N,N*-dimethylbenzylamine was added to the standard cyclopropanation reaction in the presence and absence of norbornene (**Table 3.2**). The obtained cyclopropanation yield was comparable to a reaction without added

44

amine and neither in the presence nor absence of norbornene any rearrangement products were observed (entry 1 and 2). A control experiment with [BnNMe$_3$]OTf in the absence of alkene or catalyst but otherwise identical conditions showed rapid rearrangement of the in situ formed ylide to give the benzylamines shown in **Table 3.2**. To test for the viability of a phosphonium ylide as methylene donor and thus the possibility of reversible trapping of nickel carbene **2.7** with PPh$_3$ to give **2.6P** (**Figure 2.6**), [Ph$_3$PMe]OTf was used as methylene donor under otherwise identical conditions. In this case, neither product formation nor a rearrangement from a putative *N*-ylide formed in situ was observed (entry 3 and 4), additionally suggesting that lithiomethyltrimethylammonium is the methylene donor.

Table 3.2. Addition of *N,N*-Dimethylbenzylamine.[a]
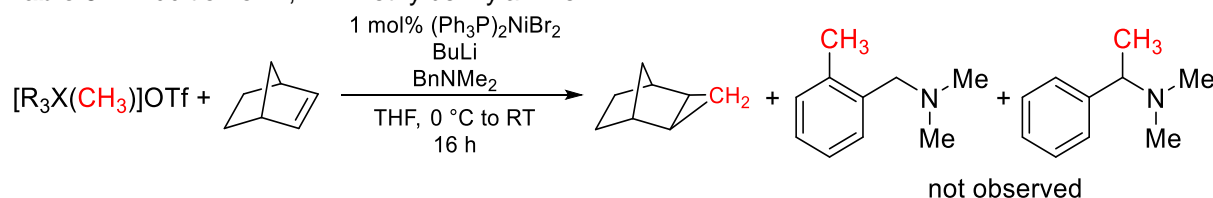
Entry	Methylene Donor	Additive	Yield Cyclopropane / %
1	[NMe$_4$]OTf	10 equiv BnNMe$_2$	71
2[b]	[NMe$_4$]OTf	10 equiv BnNMe$_2$	N/A
3[b,c]	[Ph$_3$PCH$_3$]OTf	10 equiv BnNMe$_2$	0
4[b,c]	[Ph$_3$PCH$_3$]OTf	10 equiv BnNMe$_2$	N/A

[a]Standard conditions: 1 equiv [R$_3$XMe]OTf, 1.05 equiv BuLi, 5 equiv NBE, 0.05 M in THF. [b]Without norbornene. [c]Up to 50 °C.

In the Introduction, the case of an isolable rhenium carbene was presented, which underwent selective homocoupling with chiral self-recognition of the chiral-at-metal carbene to give ethene (**Figure 1.25**).[3]

We hypothesized that we could potentially recreate this self-recognition behavior by using a chiral ligand, instead of the chiral-at-metal complex, to obtain a chiral complex. This would allow to probe for a kinetically relevant homocoupling step.

Technically a carbene 'trapping' with itself, it was hypothesized that the homocoupling rate could be selectively altered by varying the enantiomeric excess of a chiral phosphine nickel complex and thus serve as an indirect evidence of nickel carbene formation. The cyclopropanation rate would not be affected as long as the substrate is achiral. The underlying rationale is that the homocoupling rate can be selectively tuned while the cyclopropanation rate is kept constant. The cyclopropane yield should vary

with the enantiomeric excess as long as there is an analogous chiral self-recognition operative for the homocoupling transition state and this step is kinetically relevant.

If the heterochiral homocoupling transition state were to be lower in energy, one would expect a dip in the yield for the racemic catalyst mixture due to the highest homocoupling rate.

If the homochiral homocoupling transition state were to be lower in energy, one would expect a maximum for the racemic catalyst mixture.

To this end enantiomerically pure (BINAP)NiBr$_2$ complexes of either chirality were synthesized and used in varying ratios as catalyst for the cyclopropanation of cyclooctene. No effect of the enantiomeric excess of the ligand on the cyclopropanation yield was observed (**Figure 3.2**).
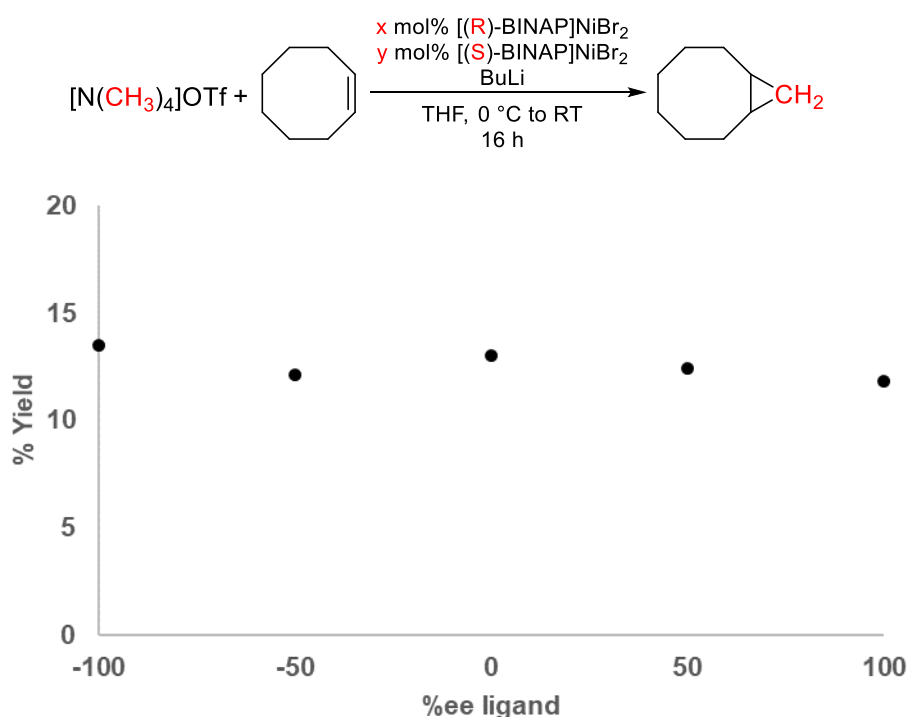

Figure 3.2. Cyclopropanation of cyclooctene with varying enantiomeric excess of the catalyst (1 mol% [(R/S)-BINAP]NiBr$_2$). (R)-BINAP = (R)-(+)-2,2'-bis(diphenylphosphino)-1,1'-binaphthyl. (S)-BINAP = (S)-(-)-2,2'-bis(diphenylphosphino)-1,1'-binaphthyl.

3.2.1 Attempts at Isolating Nickel Carbenes

Attempts were undertaken to isolate or observe a nickel carbene spectroscopically from an ammonium salt precursor (**Figure 3.3**). This would be a very strong indication

that under the standard conditions for cyclopropanation with tetramethylammonium ylide a nickel carbene is formed as well.
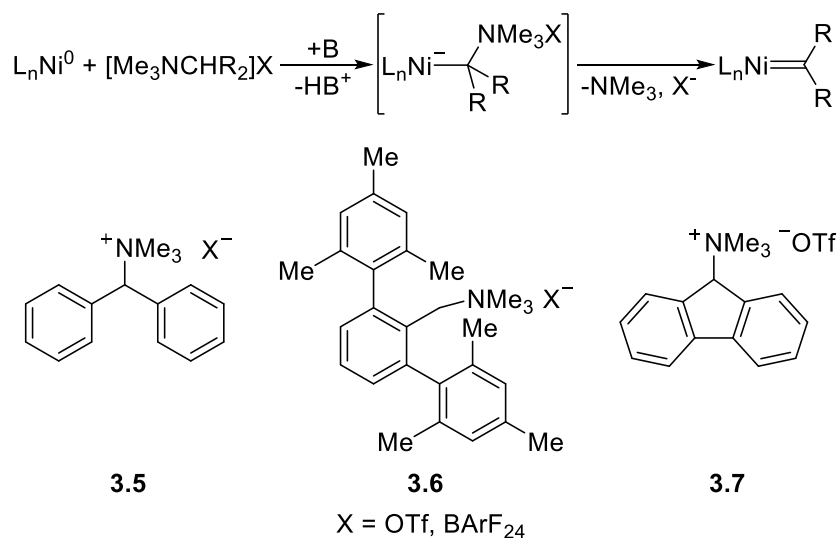

Figure 3.3. Attempted isolation of stable nickel carbenes.

Ammonium salts **3.5** and **3.6** were chosen in analogy to Hillhouse's diazo compounds that led to the isolation of the respective nickel carbenes.[4-5] Ammonium salt **3.7** was chosen due to the ylide's observed amine transfer reactivity (**Figure 3.1**) and a report of an alleged Pd carbene species from 9-diazofluorene of the composition Pd(PPh$_3$)$_2$(C$_{13}$H$_8$) (no other characterization was given).[1, 6]

Unfortunately, despite extensive efforts by changing the above-shown ammonium salts, solvent (THF, Et$_2$O, toluene, benzene), base (BuLi, LiHMDS, LiNMe$_2$, KHMDS, KO^{t}Bu), temperature (-110 to 0 °C), Ni precursor (Ni(II), Ni(0)), and ligand (mono- or bidentate phosphines of differing donor/acceptor ability) no nickel carbene was observed.

3.3   Kinetic Investigations

The experiments in section 3.2 had shown no indication for carbene trapping or the kinetic relevance of a bimolecular carbene homocoupling. This is suggestive of only a fleeting existence of a nickel carbene in solution and it not being the resting state of our catalytic cycle. Therefore, we turned to kinetic investigations of the cyclopropanation with norbornene, the highest-yielding substrate, to gain further

insights. The yilde decomposition, i.e. homocoupling, was also studied in the absence of any added substrate to isolate this side reaction and study it separately.

3.3.1 Kinetic Order in Catalyst

For the generation of the active methylene transfer reagent lithiomethyltrimethylammonium triflate we used two different methods of preparation (**Figure 3.4**).

Method A used an in situ formation of the ylide by deprotonation of a slight excess of the tetramethylammonium salt with BuLi in the presence of alkene and catalyst.

For method B, the ammonium salt was allowed to be deprotonated for 15 minutes before the catalyst was added to initiate the reaction.

No major difference was observed between these two methods. For method A, a small induction phase for the product formation was observed, which was absent in method B. This is likely due to the non-instantaneous deprotonation of the salt. In addition, the precatalyst activation efficiency appeared to be higher for method A than B as can be seen in the slightly lower cyclopropanation rates for method B in **Figure 3.5**.

At this point, we can only speculate what might be the reason for this difference in precatalyst activation. A possible explanation is the lack of β-hydrogen in the ylide, thereby excluding the formation of Ni(0) via a β-hydride elimination pathway. (For the reduction of a Ni(II) complex to Ni(0) with 3 equivalents of BuLi, the formation of butane , 1-butene, and octane was observed.[7]) Possible (minor) catalyst deactivation due to the activation method can also not be ruled out.

For the sake of simplicity, we opted to use method A whenever possible, that is, unless the decomposition of ylide was tracked. In that case, having the maximal concentration of ylide at the point of catalyst addition was beneficial, and method B was employed.
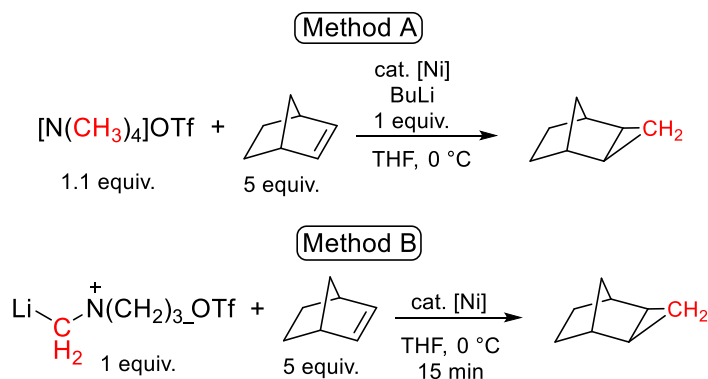
Figure 3.4. Preparation of ylide in situ (method A) or by preformation before addition of catalyst (method B).

Figure 3.5 shows the order plot for three different catalyst systems for the cyclopropanation with of norbornene as outlined in **Figure 3.4**. The precatalyst $(Ph_3P)_2NiBr_2$ was used in combination with method A and B. Additionally, $Ni(PPh_3)_4$ was used as an already reduced Ni(0) catalyst (with method A).
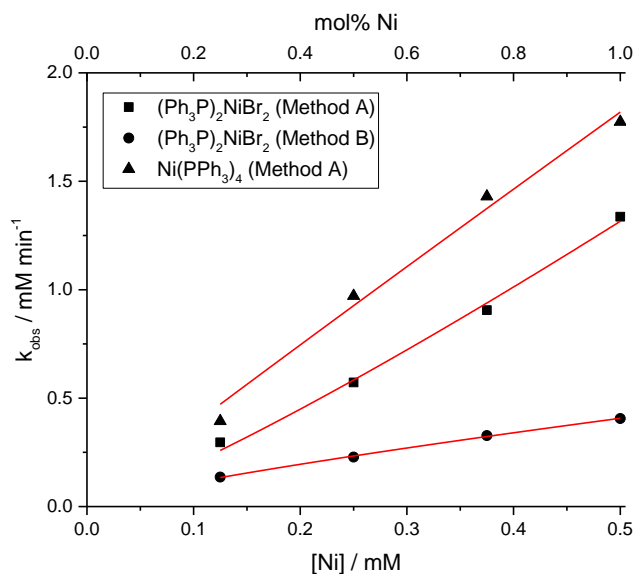

Figure 3.5. Plot of k_{obs} versus [catalyst] using $(Ph_3P)_2NiBr_2$ and Method A (squares) or Method B (circles) as precatalyst or $Ni(PPh_3)_4$ (Method A, triangles) with NBE. The red curves depict a fit to the function $y = ax^b$ to establish the order in [Ni] as follows: $b = 1.17 \pm 0.08$ (squares), $b = 0.80 \pm 0.02$ (circles), $b = 1.0 \pm 0.1$ (triangles).

All three systems display a close to first order dependence on catalyst concentration, albeit with slightly different observed rates. This difference in activity of the catalyst depending on the ylide formation method has been discussed above.

The homocoupling rate was measured in the absence of any added substrate by tracking the disappearance of ylide after a protic quench and measuring the amount of

remaining tetramethylammonium. For this set of experiments, method B and Ni(PPh$_3$)$_4$ as catalyst were chosen. The use of (Ph$_3$P)$_2$NiBr$_2$ caused the reaction to become immediately turbid and the reaction profile was less clean than in the case of a Ni(0) precatalyst.

The order in catalyst in the absence of added alkene also displays approximatively first order kinetics for the disappearance of ylide (**Figure 3.6**). This is contrary to a turnover-limiting bimolecular homocoupling step, which would be second order in catalyst as we had initially expected.
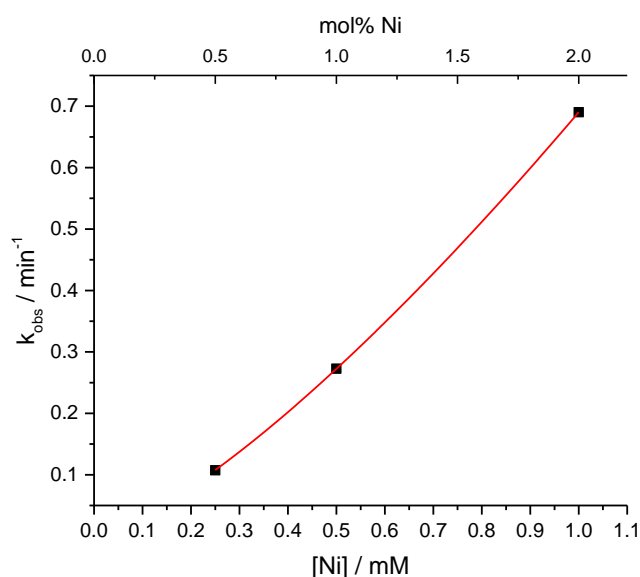

Figure 3.6. Plot of [Ni(PPh$_3$)$_4$] versus k_{obs} for the consumption of ylide in the absence of alkene. The red curve depicts a fit to the function $y = ax^b$ to establish the order in [Ni], $b = 1.34 \pm 0.01$.

3.3.2 Kinetic Orders in NBE and PPh$_3$

Next, we looked at the kinetic order for norbornene and triphenylphosphine. For the substrate norbornene between 1.25 – 10 equiv with respect to ylide, we observed an order of 0.18 ± 0.02, i.e., close to an idealized zeroth order in norbornene (**Figure 3.7**, left). This is suggestive of a saturation behavior in substrate analogous to Michaelis-Menten kinetics in enzymes.

For the ligand triphenylphosphine, we observed an order of 0.17 ± 0.05, i.e., also close to idealized order of zero (**Figure 3.7**, right) for the range of 0.5 – 4 mol%. This translates to a ratio of Ni:PPh$_3$ of 1:1 to 1:8.

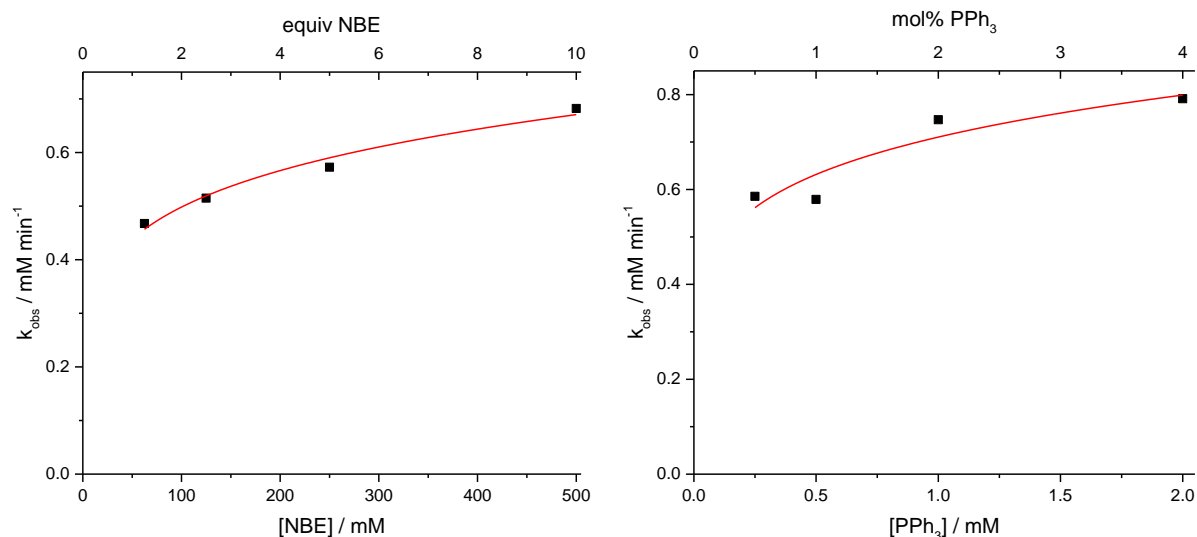**Figure 3.7.** Left: Plot of k_{obs} versus [NBE] using 0.5 mol% (Ph$_3$P)$_2$NiBr$_2$ (Method A). The red curve depicts a fit to the function $y = ax^b$ to establish the order in norbornene, b = 0.18 ± 0.02. Right: Plot of k_{obs} versus [PPh$_3$] using 0.5 mol% Ni(acac)$_2$ (Method A). The red curve depicts a fit to the function $y = ax^b$ to establish the order in PPh$_3$, b = 0.17 ± 0.05.

3.3.3 Kinetic Order in Ylide

The order in ylide was determined by preforming the ylide before catalyst addition, i.e., method B (**Figure 3.4**). The ylide concentration was varied between 25 – 100 mM, which translates to 0.5 – 2 equivalent of ylide based on the standard conditions. The order plot is shown in **Figure 3.8**. From this data it appears that at high concentration, the order in ylide changes from 1, observed at lower concentration, to 0. The data was accordingly fitted in a low concentration (solid curve) and a high concentration (dashed curve) regime as can be seen in **Figure 3.8**. Although the data density is too low to be certain, it is likely that there is an additional equilibrium for the ylide binding to Ni(0) that is saturated in favor of the adduct at high concentration and changes during the conversion of the ylide within the concentration range of the standard reaction conditions.

This can also be inferred from the reaction profile in **Figure 3.13** for example. The reaction rate stays constant, i.e., the concentration increases linearly, for longer than would be expected for a purely 1st order reaction in ylide. Only at high conversion when most of the ylide is consumed (with excess alkene still present) does the reaction rate slow down.
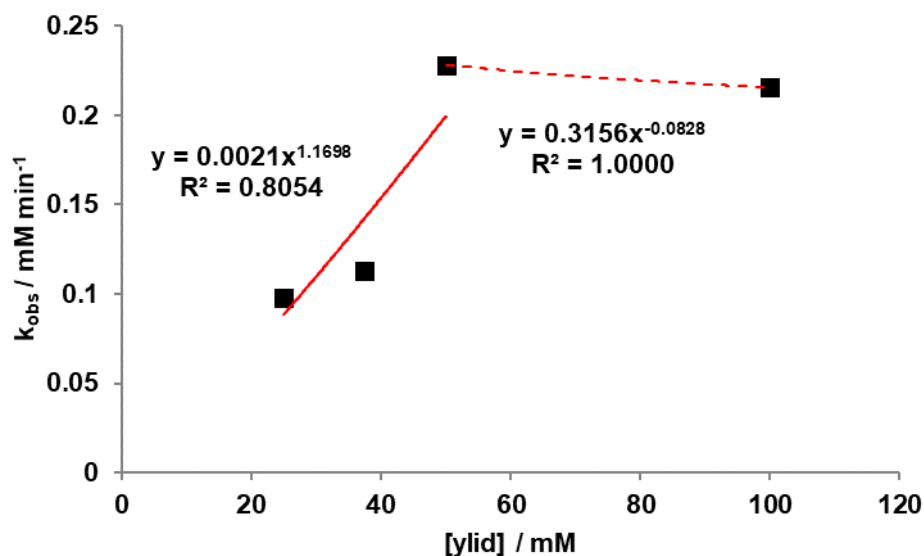
Figure 3.8. Plot of k_{obs} versus [ylide] using 0.5 mol% $(Ph_3P)_2NiBr_2$ (Method B). The red curve depicts a fit to the function $y = ax^b$ to establish the order in ylide in two regimes for low concentration (25 – 50 mM, solid curve) and high concentration (50 – 100 mM, dashed curve), respectively.

That there is or could be such an equilibrium is not entirely surprising given the extensive work of Pörschke et al. regarding the Lewis acidity of Ni(0) (see chapter 1 for an extensive discussion). The equilibrium was shown to be dependent on the nucleophilicity of the carbanion, and the π-acidity of the ligands (alkenes and CO). The nucleophilicity of lithiomethyltrimethylammonium should be closer to their strongest nucleophile, MeLi, then the next weaker carbanion, trimethylphosphonium methylide.[8-9]

3.3.4 Kinetic Isotope Effect

Kinetic isotope effects (KIE) are a powerful tool for reaction mechanism elucidation in organic and organometallic chemistry.[10] Secondary isotope effects reflect the hybridization change of the reaction center to which the isotopically labeled element is attached, in the present case hydrogen and deuterium. Thus, the isotopically labeled bond itself is not cleaved. In a catalytic cycle, KIEs probe the turnover-limiting transition state relative to the resting state, as do kinetic orders,[11] except under certain circumstances.[12]

A rehybridization from sp^3 to sp^2 in the transition state results in normal secondary KIE ($k_H/k_D > 1$). The opposite is true for a rehybridization from sp^2 to sp^3 giving an inverse secondary KIE ($k_H/k_D < 1$). This is mainly due the difference in zero point energy of the out-of-plane bending vibrations of the respective C-H/C-D bonds ($C(sp^3)$-H: 1350 cm⁻

^{1} vs C(sp^2)-H: 800 cm^{-1}) between the reactant and transition state, which are energetically closer for sp^2 than sp^3.[10]
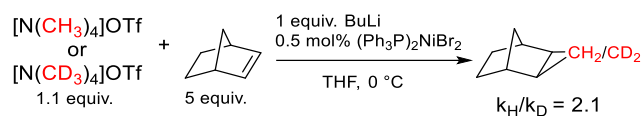

Figure 3.9. Determination of a secondary KIE using perdeuterated tetramethylammonium triflate.

To establish a secondary KIE for the reagent, we used the perdeuterated tetramethylammonium salt under otherwise identical conditions (**Figure 3.9**). This resulted in an observed secondary KIE of 2.1 ± 0.3. This indicates a rehybridization of sp^3 to sp^2 for the isotopically labeled carbon of the ylide.

Previous computational work in our group has shown that the carbanion of trimethylammonium methylide is pyramidal with and without coordination to lithium, while the analogous phosphonium ylide significantly flattens to approach an almost trigonal planar structure upon removal of the lithium ion.[13] Additionally, a crystal structure of a phosphonium ylide coordinated to Ni(CO)$_3$ shows a tetrahedral geometry for the ylidic carbon (see chapter 1).[14]

3.3.5 Temperature-Dependence of the Reaction Rate

Initial rate data for the cyclopropanation of norbornene was obtained between -30 and 0 °C under otherwise standard conditions. An Arrhenius plot was constructed as shown in **Figure 3.10** and the activation energy was obtained as E_a = 16.5 kcal mol^{-1}. This number compares favorably to the calculated barrier for our model system (see section 3.5).
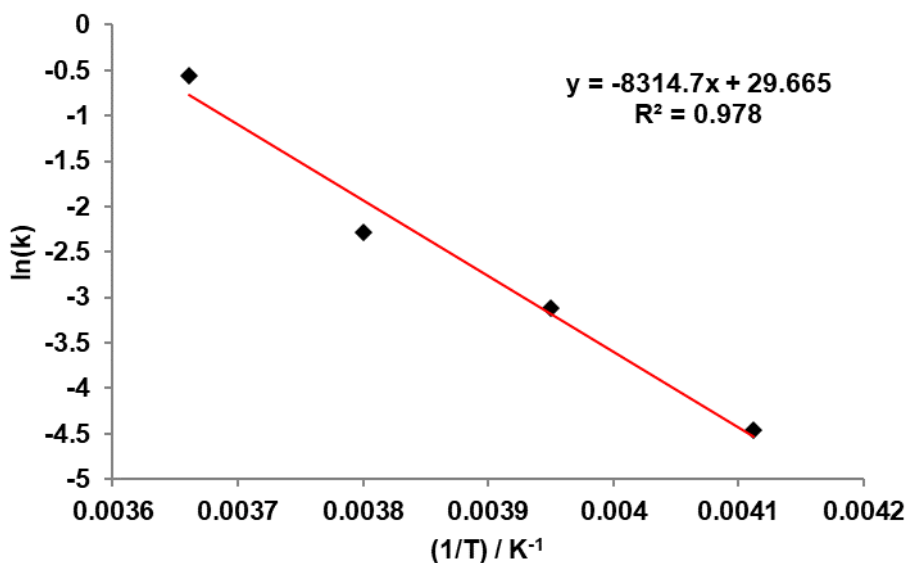
Figure 3.10. Arrhenius plot for the cyclopropanation of norbornene between -30 and 0 °C.

3.3.6 Solvent Polarity – Order in THF

Under certain circumstances, it is possible to determine the order in THF, even as the solvent.[11] To do so, THF is partially replaced by a second solvent and the reaction is run in a solvent mixture, in our case Et_2O. The obtained reaction profiles are shown in **Figure 3.11** (top). The induction phase is prolonged for the less polar solvent mixtures. This is likely caused by an extended deprotonation time of the sparingly soluble [NMe$_4$]OTf. After the induction phase, the cyclopropanation rate is little affected by the change is solvents.
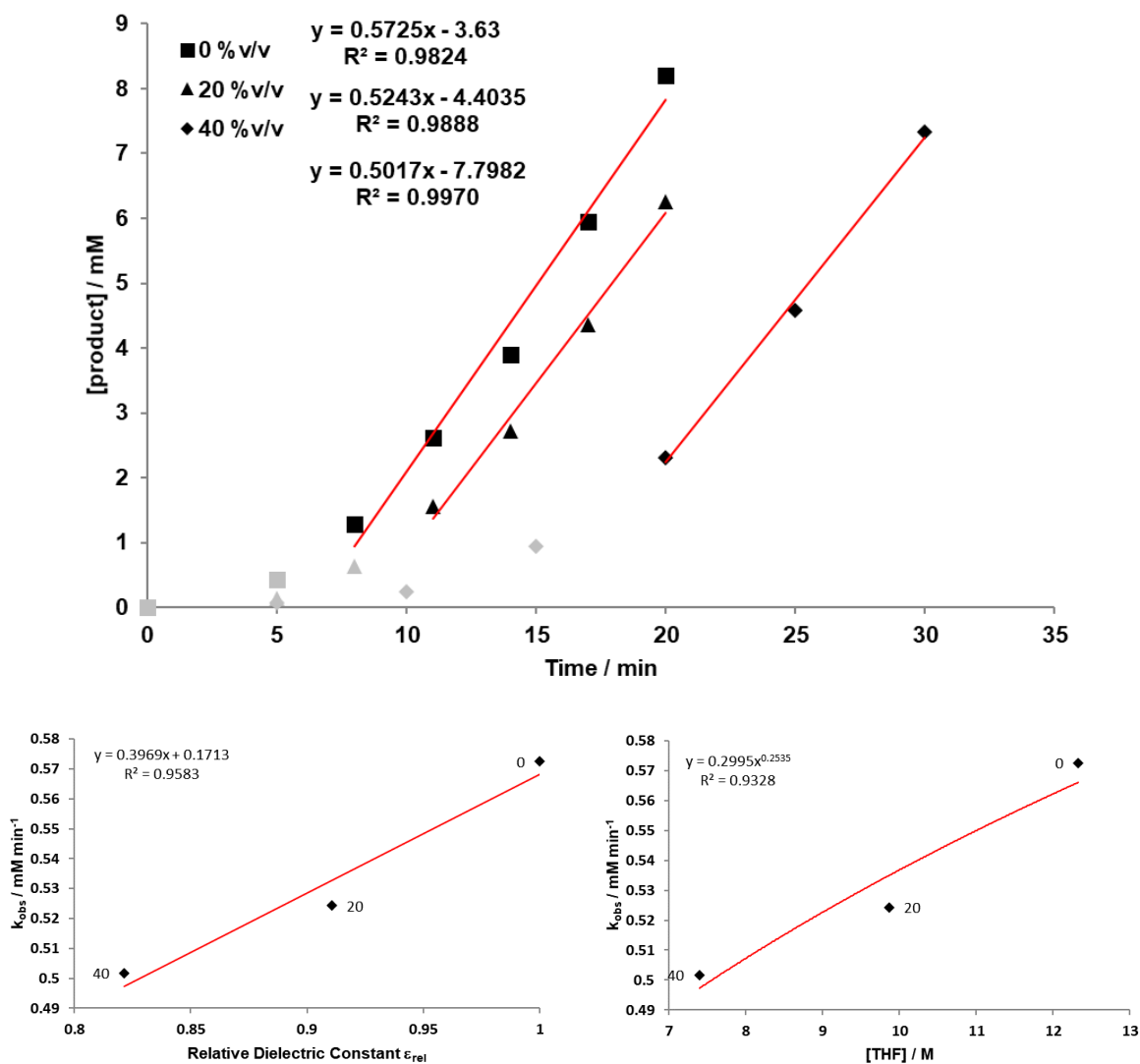
Figure 3.11. Top: Reaction profiles for the cyclopropanation of norbornene in Et_2O/THF solvent mixture with 0.5 mol% $(Ph_3P)_2NiBr_2$ as catalyst. The amount of Et_2O is given as %v/v in the legend. Red line depicts linear fit to obtain the initial rate excluding the gray data points of the induction phase. Bottom left: Plot of relative dielectric constant ε_{rel} versus k_{obs} for the cyclopropanation of norbornene in solvent mixtures of Et_2O/THF. Data labels refer to %v/v Et_2O for the solvent mixture. The relative dielectric constant ε_{rel} is taken as the dielectric constant of the mixture relative to that of pure THF ((%v/v $Et_2O \cdot \varepsilon_{Et2O}$ + %v/v THF$\cdot \varepsilon_{THF}$)/ε_{THF}).[15] Bottom right: Plot of THF concentration versus k_{obs} as left.

Figure 3.11 (bottom) shows the obtained rate data k_{obs} fitted to the average bulk solvent polarity (left) and the THF concentration (right). There is little influence of either variable on the reaction rate except a prolonged induction phase as mentioned above, and the order in THF appears to be zero.

3.4 Alkene Competition Experiment

Unfortunately, substrates other than norbornene gave relatively low yields and thus incomplete mass balances; the side products are not easily trackable in a quantitative manner (e.g., polyethylene). This makes an accurate kinetic study on these substrates unattainable. To gain further insights into the cyclopropanation of other olefins we opted for a competition experiment between two substrates, usually between norbornene and another alkene. The competition between 1-octene and 1-nonene serves as internal validation (black triangles). By varying the alkene ratios and plotting the mole fraction of one alkene against the product ratios Job plots were created as shown in **Figure 3.12**.[16]
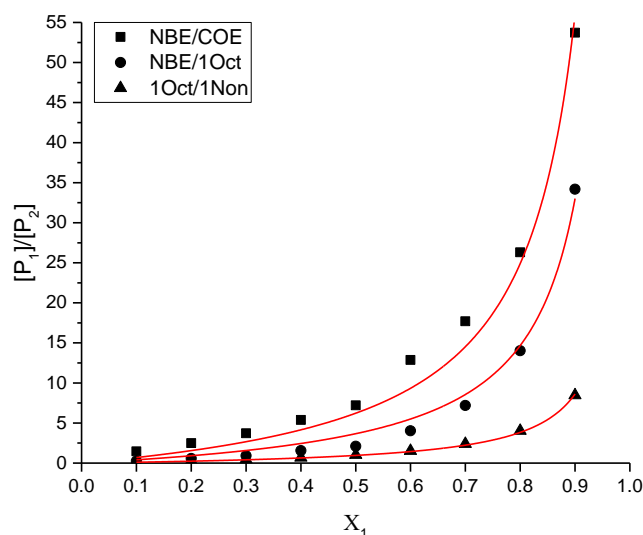

Figure 3.12. Plot of mole fraction of alkene 1, X_1, versus product ratio, $[P_1]/[P_2]$, derived from alkene 1 and alkene 2, respectively, with the following pairs of alkenes. 1: norbornene, 2: cyclooctene (squares); 1: norbornene, 2: 1-octene (circles); 1: 1-octene, 2: 1-nonene (triangles). 0.5 mol% $(Ph_3P)_2NiBr_2$ was used as precatalyst. The red curves depict a fit to the function $y = aX_1/(1-X_1)$ (see eq (1) and Discussion). $a = 6.2 \pm 0.2$ (squares), $a = 3.7 \pm 0.1$ (circles), $a = 0.96 \pm 0.01$ (triangles).

Additionally, we also examined the full kinetic profile for one ratio of norbornene and cyclooctene (ratio of 1:1, but with double the total concentration of substrates) (**Figure 3.13**). The product ratio P_1/P_2, i.e. P_{NBE}/P_{COE}, varies slightly with the conversion but stays between 10.9 and 7.7. This range is comparable to the value of 7.3 from **Figure 3.12** ($X_1 = 0.5$, black square).
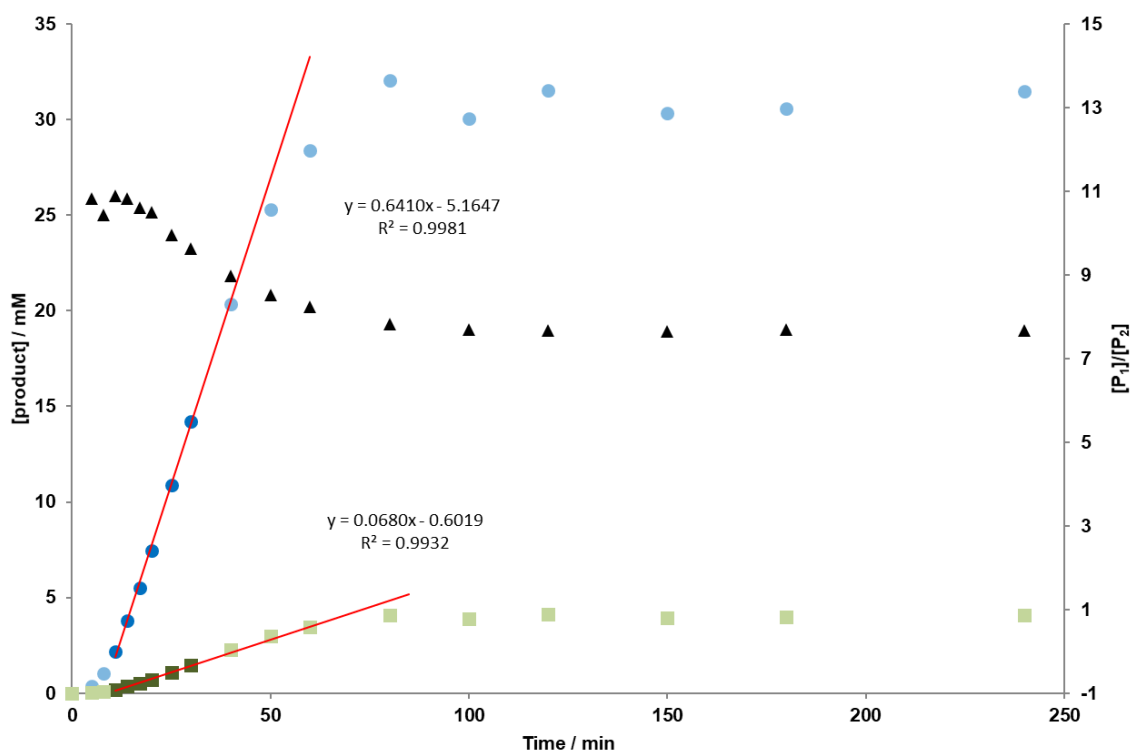
Figure 3.13. Left axis: Plot of time versus product concentration using norbornene (1) and cyclooctene (2) as substrates in a competition experiment. The red lines depict an initial rate fit with omission of the first few data points of the induction phase and the later data points at high conversions (lightly shaded) to obtain k_{obs}. The products are tricyclo[3.2.1.0^{2,4}]octane (blue circles) and bicyclo[6.1.0]nonane (green squares). Right axis: Plot of time versus product ratio [P$_1$]/[P$_2$] (black triangles).

3.5 Computational Studies

The computations in this thesis have been performed by Dr. Renana Gershoni-Poranne.

To corroborated our experimental finding and assess the viability of the kinetically invisible steps after the rate-limiting transition state, we performed DFT studies on the catalytic cycle using a truncated system with ethene as substrate and PH$_3$ as ancillary ligand (**Figure 3.14**). The structures were optimized at the M06L/def2-SVP level of theory using Gaussian 09, Revision D.[17] KIEs were calculated using the ISOEFF software based on the Bigeleisen equation.[18]
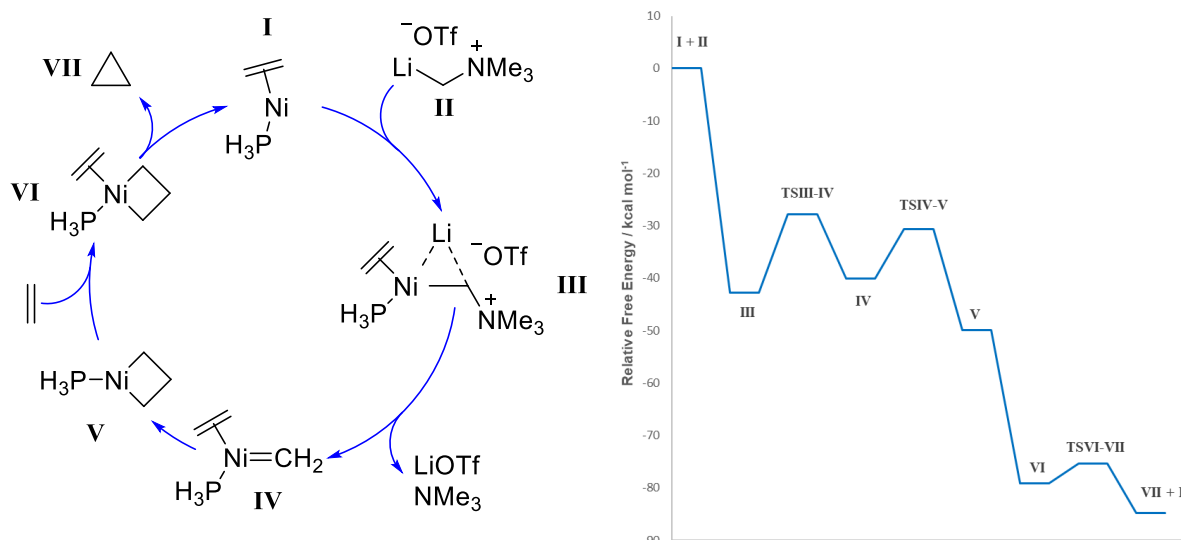
57

Figure 3.14. Left: Computed catalytic cycle with one alkene and one phosphine ligand. Right: Energy profile for the cycle shown on the left.

The energy profile shown in **Figure 3.14** in agreement with our experimental observations. The experimental activation energy of 16.5 kcal mol^{-1} (section 3.3.5) compares favorably to the computed energy barrier of the rate-determining step of 15.0 kcal mol^{-1} (III to IV, **Figure 3.14**). The calculations give also insights into the kinetically invisible steps after the nickel carbene formation and show these steps to be energetically feasible.

Importantly, calculation of the secondary KIEs with the perdeuterated reagent [LiCD$_2$N(CD$_3$)$_3$]OTf were performed on the relevant steps of the catalytic cycle in **Figure 3.14**. These values are shown in **Table 3.3**. Our experimental KIE (2.1) is most in agreement with the computed KIE for the nickel carbene formation (entry 1), while the KIEs for nickelacyclobutane formation (entry 2) and reductive elimination (entry 3) are either inverse or closer to 1 than nickel carbene formation, respectively. This is a strong indication that we correctly identified the rate-limiting transition state for the cyclopropanation and that the computations match the experiment.

Table 3.3. Computed KIEs with [LiCD$_2$N(CD$_3$)$_3$]OTf.

Entry	Step	KIE
1	III to IV	2.50
2	IV to V	0.63
3	VI to I	1.11

Calculations performed on a cycle with two PH$_3$ ligands showed that the nickel carbene formation is lower in energy with the more strongly σ-donating phosphine ligands compared to the catalyst with one ethene and one PH$_3$.

Additional calculation are shown in the experimental section.

3.6 Mechanistic Model

After having presented all the mechanistic work above, it is now time to piece together the puzzle to arrive at the catalytic cycle(s) shown in **Figure 3.15**. We will discuss the results from the previous sections and argue for the validity of the mechanism shown **Figure 3.15** and contrast it with our initial mechanistic proposal.
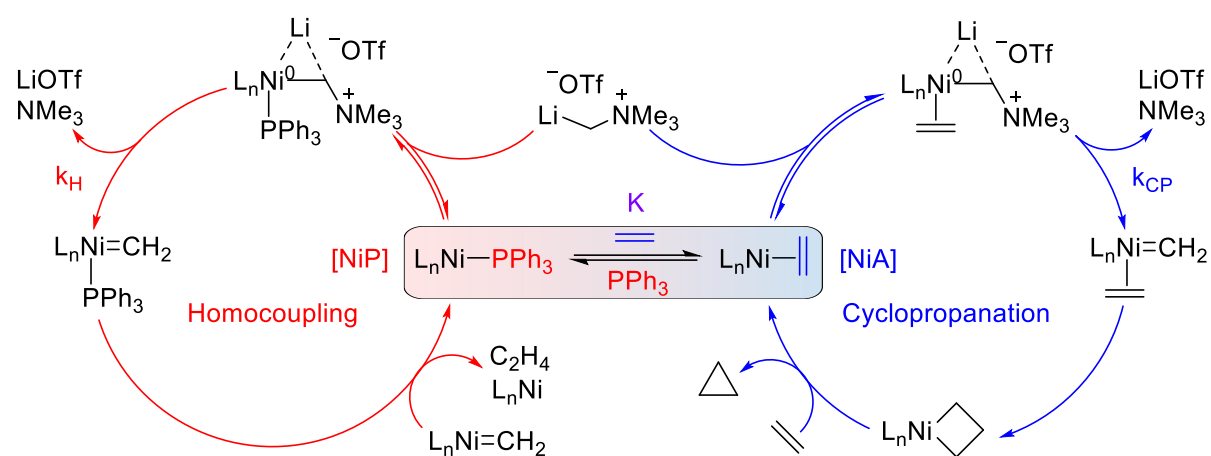

Figure 3.15. Proposed catalytic cycle. Central to the reaction is the highlighted equilibrium between ligand and alkene binding.

3.6.1 Catalyst Resting State and Rate-Limiting Step

At the outset of the kinetic investigation, we hypothesized that the reaction should be first order in catalyst for cyclopropane formation, but the bimolecular homocoupling would give a second order in catalyst. Overlaying these two processes could then give the observed non-linearity of the yield based on catalyst loading.

As expected, we observed first order in catalyst for the cyclopropanation. Taken together with the zeroth order in both norbornene and triphenylphosphine for the product formation, this implies saturation of the active catalyst with the substrate before the rate-limiting transition state and no dissociation of the phosphine between the resting state and the rate-limiting transition state.

Against our initial assumption, we also observed first order in catalyst for the homocoupling in absence of any substrate. This strongly suggests that the actual homocoupling step is not rate-limiting nor reversible, as suggested by the lack of influence of added amines or ligand chirality (**Table 3.1**, **Table 3.2**, and **Figure 3.2**).

The observed secondary KIE using a perdeuterated tetramethylammonium reagent implies a rehybridization from sp^3 to sp^2 in the rate-limiting transition state relative to the resting state. The only such step in our proposed catalytic cycle is the formation of the nickel carbene from the ylide adduct. This has been corroborated by computations of all relevant steps in the cycle (**Figure 3.14**, **Table 3.3**).

Considering all the results above, we propose that both the cyclopropanation and the homocoupling cycle have a shared Ni(0) resting state manifold with subsequent rate-limiting, irreversible nickel carbene formation. That is, the substrate and/or PPh$_3$ is already coordinated in the resting state of the catalyst before the ylide binds and NMe$_3$ is extruded in the rate-limiting step to give the nickel carbene.

There appears to be another pre-equilibrium of ylide binding involved. Nevertheless, this has little bearing on the cyclopropanation versus homocoupling competition, at least to a first approximation. Both reaction pathways necessarily need to bind the ylide first for the reaction to turnover. Therefore, we omit this added complexity in the further discussion below.

The kinetic results presented above and the substrate dependency of the reaction we noted earlier (**Table 2.6**) led us to consider the binding affinity of alkenes to Ni(0). A discussion of alkene binding to Ni(0) has been presented in chapter 1. Seminal work by Tolman has dealt with measuring the binding constant of a variety of alkenes to Ni[(P(O-*o*-tolyl)$_3$] by displacement of one of the phosphite ligands.[19] Selected values for relevant alkenes together with the yields are given in **Table 3.4**. As can be seen, the cyclopropanation yield correlates qualitatively with the binding constant of the substrate. More strongly bound alkenes (e.g., norbornene) resulted in higher cyclopropanation yields than weakly bound substrates (e.g., cyclohexene).

This observation is consistent with our proposed pre-equilibrium binding of the substrate *before* the rate-limiting step (denoted as K in **Figure 3.15**).

Table 3.4. Tolman's Alkene Equilibrium Constants.

$$A + NiL_3 \underset{}{\overset{K}{\rightleftharpoons}} (A)NiL_2 + L \qquad \begin{array}{l} A = \text{Alkene} \\ L = [P(O\text{-}o\text{-tolyl})_3] \end{array} \qquad K = \frac{[(A)NiL_2][L]}{[NiL_3][A]}$$

Alkene	K^a	Yield / %
Norbornene	4.4	83
1-Hexene[b]	5.0×10^{-1}	62
Cyclooctene	6.2×10^{-2}	25
Cyclohexene	3.5×10^{-4}	8

[a]Values taken from ref. [19]. [b]Used for all 1-alkenes.

Similar observations regarding the importance of the binding affinity of alkenes to low-valent metals have been noted previously. An similar scenario was proposed for the (ligandless) Pd-catalyzed cyclopropanation of alkenes with diazomethane in a DFT study by Straub.[20] An alkene ligated Pd(0) was proposed as resting state with a rate-limiting N_2 extrusion from diazomethane to form a Pd carbene and a subsequent intramolecular palladacyclobutane formation.

Higher cyclopropanation yields for more π-acidic alkenes have been noted for Ni- and Pd-catalyzed reactions.[21-23] A qualitative trend between Tolman's K values and yield has also been noted for a nickel-catalyzed cyclopropanation with α-lithiated sulfones as methylene donors.[24]

The importance of the alkene binding constant could also explain why Ni is so uniquely active for the cyclopropanation. K for ethene is four orders of magnitudes higher for Ni than it is for Pd (**Table 3.5**, see also discussion of alkene binding in chapter 1), thus it is likely that cyclooctene simply does not bind strongly enough to Pd under our conditions to be cyclopropanated (**Table 2.2**, entry 4).

Table 3.5. Tolman's Alkene Equilibrium Constants for Ethene and the Nickel Triade.

$$C_2H_4 + ML_3 \underset{}{\overset{K}{\rightleftharpoons}} (C_2H_4)ML_2 + L \qquad \begin{array}{l} A = \text{Alkene} \\ L = PPh_3 \end{array} \qquad K = \frac{[(C_2H_4)ML_2][L]}{[ML_3][C_2H_4]}$$

M	K^a
Ni	300 ± 40
Ni[b]	250
Pd	$(1.3 \pm 0.2) \times 10^{-2}$
Pt	$(1.22 \pm 0.03) \times 10^{-1}$

[a]Values taken from ref.[25]. [b]For L = P(O-o-tolyl)$_3$ instead. Data from ref. [19].

3.6.2 Derivation of a Mathematical Model

With the above-introduced mechanistic scheme, we can first look at the competition experiment between two alkenes disregarding any phosphine ligand present in the

reaction. With the assumption of a pre-equilibrium between the two alkenes, we arrive at a Curtin-Hammett-like scenario. The yield is then determined by how well the respective alkene binds to Ni(0) (K) *before* the rate-limiting nickel carbene formation (with the rate constants k_1, k_2). This followed by a fast [2+2] cycloaddition and reductive elimination. We make here the assumption that the *intermolecular* alkene exchange *after* the nickel carbene formation is much slower than the *intramolecular* nickelacyclobutane-reductive elimination sequence. In other words, the yield depends on how much alkene is bound (K) and how fast that complexes react (k_1, k_2). This is simplified reaction scheme is shown in **Figure 3.16**.
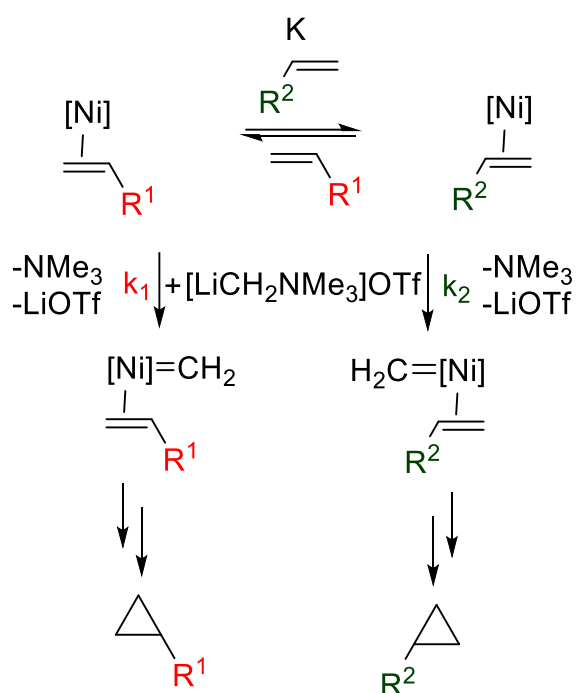

Figure 3.16. Simplified mechanistic scenario with an alkene exchange equilibrium before cyclopropanation.

Standard mathematical treatment of this scheme gives rise to the product ratio [P_1/P_2] expressed in equation (3.1) (see chapter 6 for full derivation),

$$\frac{[P_1]}{[P_2]} = \frac{k_1 K_1}{k_2 K_2} \frac{X_1}{(1 - X_1)} \tag{3.1}$$

where k_i denotes the rate constant for cyclopropane formation, K_i denotes the binding constant of alkene i to Ni(0), and X_i denotes the mole fraction of alkene i (in eq (3.1) solved for alkene 1). Using Tolman's values for K we essentially reference the binding

affinity of both alkenes to a hypothetical Ni[P(O-*o*-tolyl)$_3$] complex to arrive at a relative binding affinity to Ni(0).

We can now compare the fit equation used in **Figure 3.12** with equation (3.1) and arrive at equation (3.2)

$$a = \frac{k_1 K_1}{k_2 K_2} \qquad (3.2)$$

where a is the fit parameter from **Figure 3.12**. Defining k_{NBE} as $k_{rel} = 1$, we arrive at the relative cyclopropanation rates shown in **Table 3.6**.

Table 3.6. Relative Cyclopropanation Rates k_{rel}.

Alkene	K^a	k_{rel}
Norbornene	4.4	1^c
1-Octene^b	5.0 x 10^{-1}	2.4
Cyclooctene	6.2 x 10^{-2}	11.4

^{a}Values taken from ref.[19]. ^{b}Value for 1-hexene. ^{c}krel for NBE set to 1.

Table 3.6 shows that weakly binding alkenes (e.g. cyclooctene) react faster than strongly bound ones (e.g. norbornene). This is logically consistent with our proposed mechanism. The identified rate-limiting step is formally an oxidative process at nickel going from the Ni(0) ylide adduct to the Ni(II) carbene. Strongly bound alkenes are more π-acidic and therefore stabilize the ground state more, i.e., the Ni(0) complex, then they stabilize the transition state going to the Ni(II) carbene. Thus, increasing the energy barrier for this step.

An ESCA study (Electron Spectroscopy for Chemical Analysis) by Tolman showed an increased Ni 2p$_{3/2}$ binding energy with more π-acidic alkenes, i.e., higher binding constant K, for the corresponding (alkene)Ni(P(O-*o*-tolyl)$_3$)$_2$ complexes, at least for complexes that were air-stable enough to be correctly analyzed.[26] Additionally, the ethene complexes (C$_2$H$_4$)NiL$_2$ have higher binding energies that their NiL$_3$ counterparts (L = PPh$_3$ or P(O-*o*-tolyl)$_3$). From these examples, it can be concluded that alkenes remove more electron density from Ni(0), and thereby increase the Ni 2p$_{3/2}$ binding energy, than either PPh$_3$ or P(O-*o*-tolyl)$_3$ and do so according to their π-acidity as represented by Tolman's binding constants. This corroborates and explains the trend of k_{rel} as seen in **Table 3.6** when the nickel carbene formation is seen as a reductive cleavage of the C-N bond, which should proceed faster at a more electron-rich metal.

We can now extend and generalize the Curtin-Hammett scenario from above to a single alkene in competition with a phosphine ligand in a pre-equilibrium denoted with K *before* the rate-limiting step (**Figure 3.17**). Thus, alkene and phosphine compete for the available Ni(0) in a resting state manifold. This gives rise to an alkene coordinated complex (NiA) and a phosphine ligated complex (NiP). From both species a nickel carbene is formed in the rate-limiting NMe_3 extrusion with rate constant k_{CP} for cyclopropanation and k_H for homocoupling (and further side reactions) to form the nickel carbene.
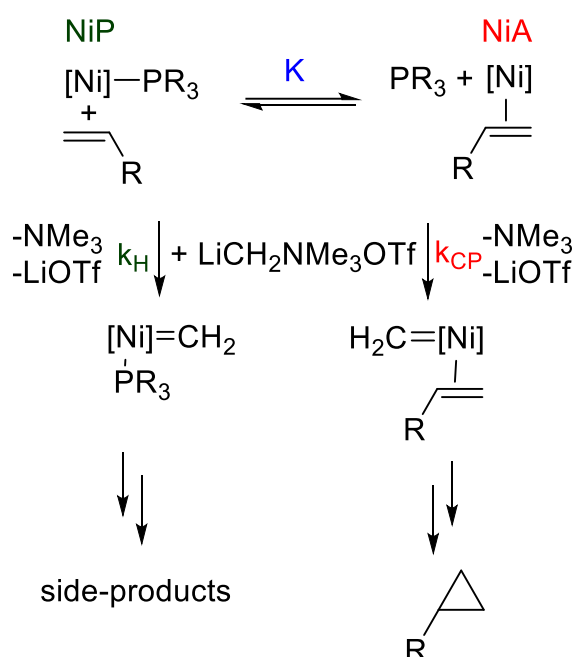

Figure 3.17. Simplified mechanistic scenario with an alkene-phosphine exchange equilibrium before cyclopropanation.

Assuming that all ylide is either consumed via cyclopropanation or the homocoupling, we can determine the yield by calculating which fraction of the ylide is converted to the cyclopropane. Here we make the approximation that both reaction pathways have the same dependency on ylide, i.e., that rates are given as k_{CP}[ylide][NiA] and k_H[ylide][NiP]. Standard mathematical treatment gives equation (3.3)

$$\% \text{ yield} = 100 \cdot \frac{\frac{k_{CP}}{k_H}([Ni]_{tot} - [NiP])}{\frac{k_{CP}}{k_H}[Ni]_{tot} + \left(1 - \frac{k_{CP}}{k_H}\right)[NiP]} \tag{3.3}$$

where the yield is dependent on the ratio of rate constants k_{CP}/k_H, the total concentration of Ni, $[Ni]_{tot}$, and $[NiP]$, which itself is a function of the binding constant K, and the total concentrations $[Ni]_{tot}$, $[P]_{tot}$, and $[A]_{tot}$.

This formalism can also be expanded to the observed cyclopropanation rate k_{obs}, giving equation (3.4).

$$k_{obs} = k_{CP}[NiA] = k_{CP}([Ni]_{tot} - [NiP]) \tag{3.4}$$

Because the absolute value of k_{CP} is not known, one can define a relative rate constant as shown in equation (3.5).

$$k_{obs,rel,n} = \frac{k_{CP}([Ni]_{tot,n} - [NiP]_n)}{k_{CP}([Ni]_{tot,1} - [NiP]_1)} = \frac{[NiA]_n}{[NiA]_1} \tag{3.5}$$

Here, we normalize the rate constant to the lowest concentration of catalyst ($[NiA]_1$).

3.6.3 Fit of Mathematical Model to Experimental Data

With equation (3.3) in hand, we can fit this mathematical model to the experimental data. The three concentration parameters contained in equation (3.3), $[Ni]_{tot}$, $[P]_{tot}$, and $[A]_{tot}$, are determined by the amount of added catalyst and alkene. We approximate the alkene concentration to be constant based on the observed 0th order in norbornene and the low conversion for other alkenes relative to the fivefold excess employed. For the equilibrium constant K, we used Tolman's values introduced earlier in **Table 3.4**. While these values have not been determined under the same conditions as our reaction, i.e., in benzene at 25 °C versus THF at 0 °C and with a different ligand, P(O-o-tolyl)$_3$ versus PPh$_3$, we argue that their use is justified.

First, K has been measured for ethene for both ligands and is essentially the same within experimental error (**Table 3.5**, entry 1 versus 2). Second, the entropy of the equilibrium is very small (e.g. $\Delta S = 2 \pm 3$ cal mol^{-1} K^{-1} for 1-hexene)[19], and thus makes the equilibrium, especially within the small temperature difference, almost temperature independent. Third, the ligand exchange does not generate any charged or highly polar species (or transition states) and is therefore not dependent on the stabilization of a polar solvent (benzene versus THF). (During our ligand design studies, we measured

some binding constants in THF at room temperature with PPh$_3$ and have seen a good agreement with Tolman's value, see chapter 4.)

By using Tolman's values, we have a large library of K values at hand, additionally giving the model predictive ability.
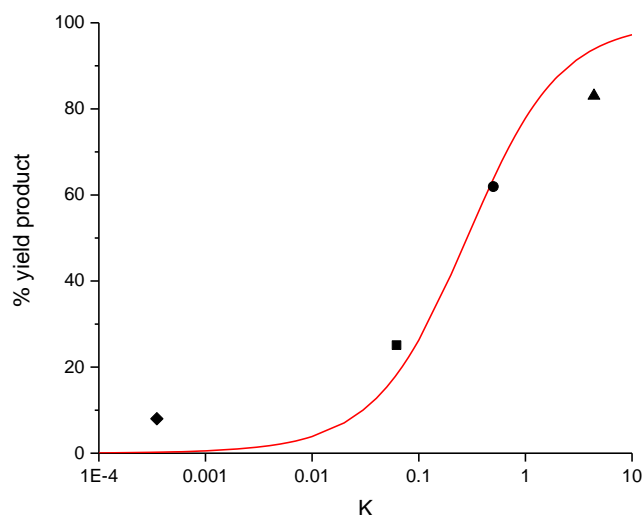

Figure 3.18. Plot of K (from Tolman,[13] log scale) versus the experimental yield (black symbols, 1.0 mol% (Ph$_3$P)$_2$NiBr$_2$) and the predicted yield (red line) based on our mechanistic model for the cyclopropanation of cyclohexene (diamond), COE (square), 1-octene (circle), and NBE (triangle). The ratio k_{CP}/k_H was used as a parameter to fit the experimental data according to eq (2) to give k_{CP}/k_H = 0.014. [Ni]$_{tot}$ = 0.5 mM, [P]$_{tot}$ = 1 mM, [A]$_{tot}$ = 250.

Figure 3.18 shows the fit of equation (3.3) to our experimental yields for different alkenes at a single concentration of the precatalyst (Ph$_3$P)$_2$NiBr$_2$. The *sole* fit parameter is the ratio of rate constants k_{CP}/k_H introduced in our model in **Figure 3.17**. This gives a value for k_{CP}/k_H of 0.014. Thus, the first significant insight from our model is that the homocoupling rate constant is higher than the cyclopropanation rate constant (k_H > k_{CP}).

Note that our model approximates this ratio to be constant over all alkenes. While k_H is likely independent of the alkene, i.e., the homocoupling proceeds via the species NiP, which is not ligated by the substrate, this is not necessarily the case for the cyclopropanation rate constant k_{CP} via NiA. Indeed, we have already seen that this is not the case as evidenced by k_{rel} derived from alkene competition experiments (**Table 3.6**).

3.6.4 Comparison of Fitted Model to Further Experimental Data

As pointed out above, k_{CP}/k_H is the *sole* fit parameter for our model. All further comparisons to experimental data are based on the fit in **Figure 3.18** with *no* further adjustment of parameters.

Figure 3.19 shows the comparison of the model to the order plots for catalyst, norbornene, and triphenylphosphine. The agreement between model and experiment is not entirely surprising. The model was constructed to fit the mechanism derived from this data. Nevertheless, the agreement serves as reassurance.
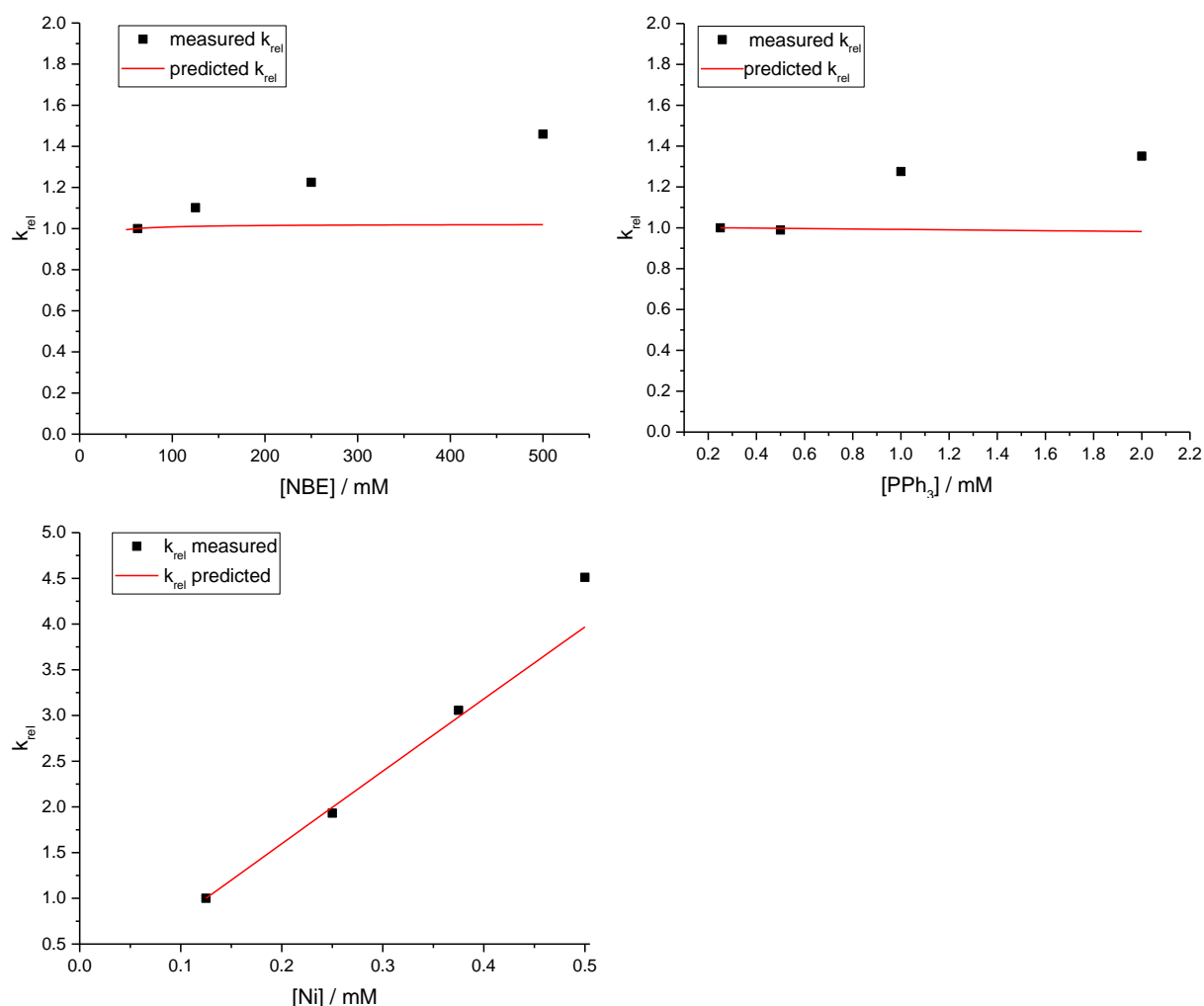

Figure 3.19. Top, left: Plot of NBE concentration versus the normalized measured rate (squares) and predicted rate (red curve) based on our model (eq (3.5)) for cyclopropanation with no further adjustment of parameters. k_{CP}/k_H = 0.014, $[Ni]_{tot}$ = 0.25 mM, $[P]_{tot}$ = 0.5 mM. **Top, right**: Plot of ligand (PPh₃) concentration versus the normalized measured rate (squares) and predicted rate (red curve) based on our model (eq (3.5)) for the cyclopropanation of NBE with no further adjustment of parameters. k_{CP}/k_H = 0.014, $[Ni]_{tot}$ = 0.25 mM, $[A]_{tot}$ = 250 mM. **Bottom, left**: Plot of catalyst, $(Ph_3P)_2NiBr_2$, concentration versus the measured rate (squares) using method A and predicted rate (red curve) based on our model (eq (3.5)), with no further adjustment of parameters. k_{CP}/k_H = 0.014, $[P]_{tot}$ = 2$[Ni]_{tot}$, $[A]_{tot}$ = 250 mM.

In contrast to the data shown above, **Figure 3.20** shows for the first time an extrapolation of the model to data that was not directly used to fit the k_{CP}/k_H parameter. Even though the fit is not quantitatively exact, the model is accurate enough to 'predict' the behavior of the reaction, in this case the cyclopropanation of cyclooctene with varying concentration of the substrate.
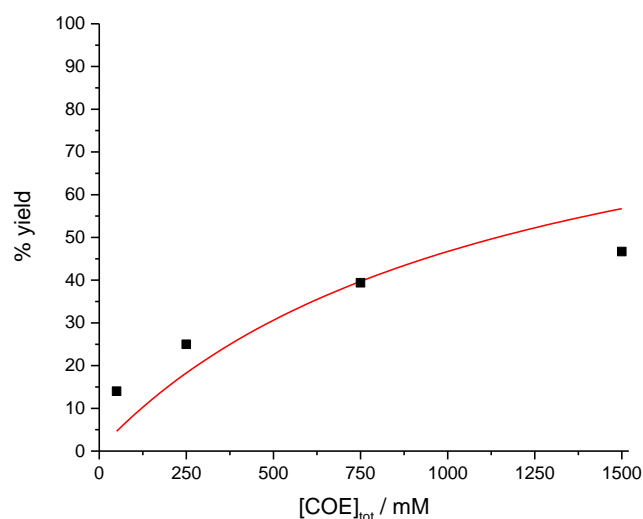

Figure 3.20. Plot of COE concentration versus the measured yield (squares) and predicted yield (red curve) based on our model (eq (3.3)) for cyclopropanation of COE using 1.0 mol% $(Ph_3P)_2NiBr_2$. k_{CP}/k_H = 0.014, $[Ni]_{tot}$ = 0.5 mM, $[P]_{tot}$ = 1 mM with no further adjustment of parameters.

For norbornene as substrate, the model also correctly predicts the behavior of varying the Ni/PPh$_3$ ratio as depicted in the Job plot in **Figure 3.21**. Despite that there is an exchange of substrate and ligand in the resting state, the model predicts that the rate (approximated as initial yield after 30 min) increases with increasing concentration of nickel present in solution (increasing mole fraction X_{Ni}). A possible explanation for the deviation at higher X_{Ni} (low concentration of PPh$_3$) is catalyst deactivation at low concentration of the stabilizing ancillary ligand.
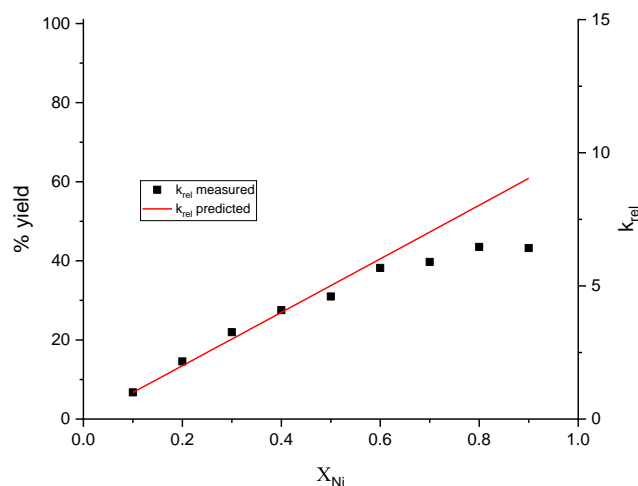
Figure 3.21. Plot of mole fraction of nickel X_{Ni} (using $Ni(acac)_2$) versus the measured rate (squares) and predicted rate (red solid curve) (approximated as initial yield after 30 min) based on our model (eq (3.5)) for the cyclopropanation of NBE, all with no further adjustment of parameters. $k_{CP}/k_H = 0.014$, $[Ni]_{tot} + [P]_{tot} = 0.5$ mM, $[A]_{tot} = 250$ mM.

One of the main observations we set out to explain with this mechanistic study was the observed non-linear catalyst loading effect on the cyclopropanation yield for cyclooctene. We have extended this line of inquiry to more alkenes (1-octene and norbornene) and more precatalysts ($Ni(cod)_2$, $Ni(PPh_3)_4$) as shown in **Figure 3.22**. We juxtaposed the experimental results with the prediction from our mathematical model. In the framework of our model, the yield decreases with increasing catalyst loading for the cyclopropanation of cyclooctene due to the fact that the alkene concentration ($[A]_{tot}$) stays constant but the amount of PPh_3 ($[P]_{tot}$) in the system increases. The substrate has to compete with increasingly more phosphine in solution which for COE is a losing game. Thus, the concentration of NiP increases and more ylide is shunted towards the unproductive homocoupling reaction, which in turns lowers the cyclopropanation yield. Norbornene is an interesting study case in this matter (**Figure 3.22**, triangles). For an already reduced precatalyst ($Ni(cod)_2$ or $Ni(PPh_3)_4$), the yield stays approximately constant over the range of catalyst loadings employed. Norborne has a relatively large binding constant ($K = 4.4$) and is competitive in binding to Ni(0) in a pre-equilibrium with PPh_3. This gives norbornene a markedly different behavior with respect to catalyst loading than cyclooctene.

An additional complication is the reduction to the active catalyst from a Ni(II) precatalyst (**Figure 3.22**, green triangles). The concentration dependence on this potential deactivation pathway might hint at an inactive dimeric species. Both monomeric and dimeric Ni(I) species are known to form under certain conditions in cross-coupling reactions and have been shown to be less active than their Ni(0) counterparts.[27-28] In

69

the present case, this could happen by comproportionation of the Ni(II) precatalyst and the already reduced Ni(0) to give a less active or inactive Ni(I) species.

Turning to a weakly binding alkene, cyclooctene (K = 0.062) (**Figure 3.22**, squares), we see that cyclooctene cannot effectively compete for the increasing amount of PPh$_3$ ([P]$_{tot}$) whether a Ni(II) (green triangles) or a Ni(0) precatalyst (red squares) is used.
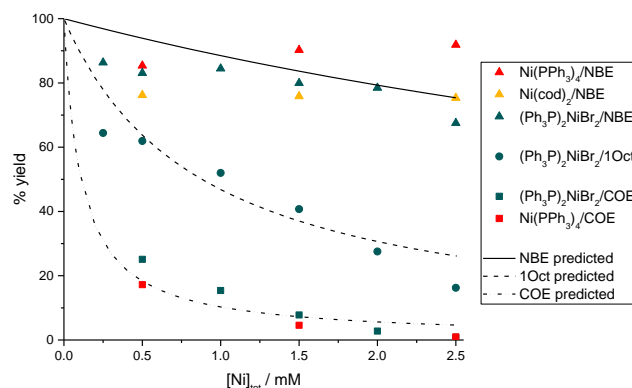

Figure 3.22. Plot of catalyst concentration versus yield for COE (squares), 1-octene (circles) and norbornene (triangles). The black curves depict the predicted yield based on our model (eq (3.3)), with no further adjustment of parameters. $k_{CP}/k_H = 0.014$, [P]$_{tot}$ = 2[Ni]$_{tot}$, [A]$_{tot}$ = 250 mM.

3.7 Conclusions

Through mechanistic experiments, most importantly kinetic investigations, and corroborations by DFT calculations we were able to propose a catalytic cycle (**Figure 3.15**). The main feature of the mechanism we propose is an intersection in the resting state manifold of the catalyst via a pre-equilibrium between substrate and a ligand. If the alkene binds only weakly (e.g. cyclooctene) to Ni(0), then a large fraction of the catalyst is not ligated by the substrate and decomposes the ylide unproductively via carbene homocoupling. This results in a low product yield because the methylene donor is shunted to this parasitic side reaction. If the alkene binds strongly to Ni(0), it can effectively replace a phosphine ligand in the resting state manifold. The resting state is shifted towards a substrate-ligated Ni(0) complex, which engages in an intramolecular [2+2] cycloaddition/reductive elimination sequence to give the product, thus outcompeting the homocoupling.

The relevant physical quantity to describe the pre-equilibrium has been identified as Tolman's alkene binding constants K to Ni[P(O-*o*-tolyl)$_3$]. Although these values have been measured with a different ligand than we employ under slightly different

conditions, we have presented arguments for the appropriateness to use them in our system.

Based on our proposed catalytic cycle, we developed a mathematical model to described and predict the reaction outcomes in terms of yield. Albeit a strongly simplified model, it allows for the explanation of many of the odd observations we had made at the outset of our mechanistic investigations.

1) As outlined above, the substrate must bind strongly to the Ni(0) resting state in order to outcompete homocoupling and thereby unproductive ylide decomposition.

2) A fit of our mathematical model to the experimental yields gave a ratio of rate constants $k_{CP}/k_H < 0$. The homocoupling rate constant k_H is significantly larger than the cyclopropanation rate constant k_{CP}. Unless the resting state manifold is significantly populated by the alkene-ligated complex, homocoupling outcompetes cyclopropanation.

3) Competition experiments and calculations have shown that the less π-accepting/more σ-donating ligands are faster for nickel carbene formation (PPh$_3$/PH$_3$ > NBE). This is logically consistent with an oxidative process at the metal center to go from the Ni(0) ylide adduct to the Ni(II) carbene.

4) Within our mechanistic framework, the catalyst loading effect can be explained by increasing phosphine concentration in solution, while the alkene concentration was kept constant. Thus, the substrate has to compete with more phosphine for the nickel catalyst. This effect is dependent on K and accordingly less pronounced for norbornene than cyclooctene.

5) Ethene, initially formed in the homocoupling reaction, is itself a very good ligand for Ni(0). Leaving the flask open to the Schlenk line might allow for its escape thereby possibly exerting an effect on the reaction and explain the small effect of an open reaction vessel. An effect of the volatile NMe$_3$ (b.p. 3 °C) seems less likely; addition of excess amines had no effect on the reaction.

The insights gathered during the mechanistic studies have been applied to a rational ligand design with the goal of a mechanism-guided improvement of the cyclopropanation yield throughout the progress of these studies. These efforts will be laid out in the next chapter.

3.8   References

1. Franzen, V. *Chemische Berichte* **1960,** *93*, 557-559.
2. Wittig, G.; Felletschin, G. *Justus Liebigs Annalen der Chemie* **1944,** *555*, 133-145.
3. Merrifield, J. H.; Lin, G. Y.; Kiel, W. A.; Gladysz, J. A. *J. Am. Chem. Soc.* **1983,** *105*, 5811-5819.
4. Mindiola, D. J.; Hillhouse, G. L. *J. Am. Chem. Soc.* **2002,** *124*, 9976-9977.
5. Iluc, V. M.; Hillhouse, G. L. *J. Am. Chem. Soc.* **2014,** *136*, 6479-6488.
6. Otsuka, S.; Nakamura, A.; Koyama, T.; Tatsuno, Y. *Justus Liebigs Annalen der Chemie* **1975,** *1975*, 626-635.
7. Morrell, D. G.; Kochi, J. K. *J. Am. Chem. Soc.* **1975,** *97*, 7262-7270.
8. Pörschke, K.-R.; Jonas, K.; Wilke, G.; Benn, R.; Mynott, R.; Goddard, R.; Krüger, C. *Chemische Berichte* **1985,** *118*, 275-297.
9. Pörschke, K.-R.; Wilke, G.; Mynott, R. *Chemische Berichte* **1985,** *118*, 298-312.
10. Gómez-Gallego, M.; Sierra, M. A. *Chem. Rev.* **2011,** *111*, 4857-4963.
11. Collum, D. B.; McNeil, A. J.; Ramirez, A. *Angewandte Chemie International Edition* **2007,** *46*, 3002-3017.
12. Simmons, E. M.; Hartwig, J. F. *Angewandte Chemie International Edition* **2012,** *51*, 3066-3072.
13. den Hartog, T.; Sarria Toro, J. M.; Couzijn, E. P.; Chen, P. *Chem Commun (Camb)* **2014,** *50*, 10604-10607.
14. Heydenreich, F.; Mollbach, A.; Wilke, G.; Dreeskamp, H.; Hoffmann, E. G.; Schroth, G.; Seevogel, K.; Stempfle, W. *Israel Journal of Chemistry* **1972,** *10*, 293-319.
15. Appendix A. Properties, Purification, and Use of Organic Solvents. In *Solvents and Solvent Effects in Organic Chemistry*.
16. Renny, J. S.; Tomasevich, L. L.; Tallmadge, E. H.; Collum, D. B. *Angewandte Chemie International Edition* **2013,** *52*, 11998-12013.
17. Frisch, M. J.; Trucks, G. W.; Schlegel, H. B.; Scuseria, G. E.; Robb, M. A.; Cheeseman, J. R.; Scalmani, G.; Barone, V.; Petersson, G. A.; Nakatsuji, H.; Li, X.; Caricato, M.; Marenich, A. V.; Bloino, J.; Janesko, B. G.; Gomperts, R.; Mennucci, B.; Hratchian, H. P.; Ortiz, J. V.; Izmaylov, A. F.; Sonnenberg, J. L.; Williams; Ding, F.; Lipparini, F.; Egidi, F.; Goings, J.; Peng, B.; Petrone, A.; Henderson, T.; Ranasinghe, D.; Zakrzewski, V. G.; Gao, J.; Rega, N.; Zheng, G.; Liang, W.; Hada, M.; Ehara, M.; Toyota, K.; Fukuda, R.; Hasegawa, J.; Ishida, M.; Nakajima, T.; Honda, Y.; Kitao, O.; Nakai, H.; Vreven, T.; Throssell, K.; Montgomery Jr., J. A.; Peralta, J. E.; Ogliaro, F.; Bearpark, M. J.; Heyd, J. J.; Brothers, E. N.; Kudin, K. N.; Staroverov, V. N.; Keith, T. A.; Kobayashi, R.; Normand, J.; Raghavachari, K.; Rendell, A. P.; Burant, J. C.; Iyengar, S. S.; Tomasi, J.; Cossi, M.; Millam, J. M.; Klene, M.; Adamo, C.; Cammi, R.; Ochterski, J. W.; Martin, R. L.; Morokuma, K.; Farkas, O.; Foresman, J. B.; Fox, D. J. *Gaussian 09 Rev. D.01*, Wallingford, CT, 2016.
18. Anisimov, V.; Paneth, P. *J. Math. Chem.* **1999,** *26*, 75-86.
19. Tolman, C. A. *J. Am. Chem. Soc.* **1974,** *96*, 2780-2789.
20. Straub, B. F. *J. Am. Chem. Soc.* **2002,** *124*, 14195-14201.
21. Nakamura, A.; Yoshida, T.; Cowie, M.; Otsuka, S.; Ibers, J. A. *J. Am. Chem. Soc.* **1977,** *99*, 2108-2117.
22. Anciaux, A. J.; Hubert, A. J.; Noels, A. F.; Petiniot, N.; Teyssie, P. *The Journal of organic chemistry* **1980,** *45*, 695-702.

23. Berthon-Gelloz, G.; Marchant, M.; Straub, B. F.; Marko, I. E. *Chemistry – A European Journal* **2009,** *15*, 2923-2931.

24. Gai, Y.; Julia, M.; Verpeaux, J. N. *Bull Soc Chim Fr* **1996,** *133*, 817-829.

25. Tolman, C. A.; Seidel, W. C.; Gerlach, D. H. *J. Am. Chem. Soc.* **1972,** *94*, 2669-2676.

26. Tolman, C. A.; Riggs, W. M.; Linn, W. J.; King, C. M.; Wendt, R. C. *Inorg. Chem.* **1973,** *12*, 2770-2778.

27. Ge, S.; Hartwig, J. F. *J. Am. Chem. Soc.* **2011,** *133*, 16330-16333.

28. Yin, G.; Kalvet, I.; Englert, U.; Schoenebeck, F. *J. Am. Chem. Soc.* **2015,** *137*, 4164-4172.

4 Ligand Design

Parts of this chapter have been published as and figures adapted or reprinted with permission from:

Künzi, S. A.; Gershoni-Poranne, R.; Chen, P. Mechanistic Studies on the Nickel-Catalyzed Cyclopropanation with Lithiomethyltrimethylammonium Triflate. *Organometallics* **2019**, *38*, 1928-1938.

4.1 Introduction

Throughout our mechanistic studies, we used the gathered insights to design new generations of ligands. Each of the ligand generations display a different approach to improve the reaction based on the current understanding of the system.

The bonding nature of phosphine to Ni(0) has been extensively discussed in the Introduction (chapter 1), mainly based on Tolman's seminal work. Several important conclusions for the present work will be highlighted accordingly throughout this chapter.

4.2 1st Generation - Hemilabile Ligands

The initial hypothesis was that nickel carbene formation might be reversible and that lowering its concentration might suppress bimolecular side reactions such as homocoupling. This rational is in analogy to the persistent radical effect.[1] We reasoned that a hemilabile ligand could serve as a 'placeholder' for the incoming alkene and additionally serve as an intramolecular trap of the carbene in a reversible reaction thereby lowering the concentration of the free nickel carbene in solution.

To this end, we tested several bidentate diphenylphosphinoamine ligands under our standard conditions. Unfortunately, no improvement of the cyclopropane yield was observed (**Table 4.1**). Given the results in chapter 3 - no effect of added free amine was observed - this outcome is not entirely surprising. Indeed, an isolated nickel carbene by Hillhouse and coworkers underwent intramolecular carbene trapping by the ligand to give the corresponding *P*-ylide only after one-electron oxidation, presumably to give an electrophilic, formally Ni(III) carbene species, which triggered the 1,2-shift.[2]
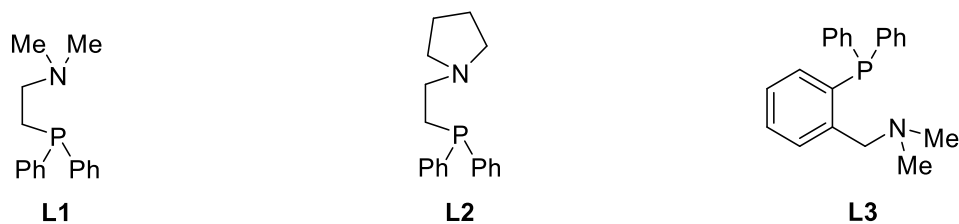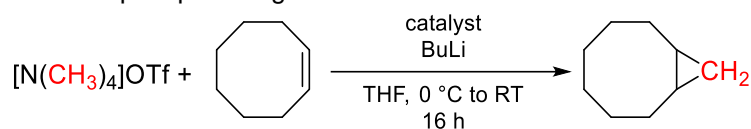
Figure 4.1. Hemilabile diphenylphosphinoamine ligands.

Table 4.1. Hemilabile Aminophosphine Ligands.[a]

Entry	Catalyst	Yield / %
1	1 mol% $(Ph_3P)_2NiBr_2$	25
2	1 mol% (dme)$NiBr_2$ / 1 mol% **L1**	8
3	1 mol% (dme)$NiBr_2$ / 2 mol% **L1**	11
4	1 mol% (dme)$NiBr_2$ / 1 mol% **L2**	4
5	1 mol% (dme)$NiBr_2$ / 2 mol% **L2**	9
6	1 mol% (dme)$NiBr_2$ / 1 mol% **L3**	2
7	1 mol% (dme)$NiBr_2$ / 2 mol% **L3**	2

[a]Standard conditions: 1 equiv [NMe₄]OTf, 1.05 equiv BuLi, 5 equiv COE, 0.05 M in THF.

The ligands presented in **Figure 4.1** are all based on a nucleophilic hemilabile arm. Given that the general reactivity of these nickel carbenes hint at a nucleophilic carbenic carbon (see chapter 1), it would be interesting to test bidentate ligands, which contain a Z-type ligand atom (e.g., B) or even metalloligands. This idea will be further discussed in the chapter 5.

4.3   2nd Generation - Strong π-Acceptor Ligands

The reasoning behind using strongly π-accepting ligands is two-fold. Alkene binding to Ni(0) is largely dominated by orbital interactions between the HOMO on Ni(0) and the alkene LUMO, i.e., the π^*-orbital (see discussion of alkene binding to Ni(0) in the Introduction).[3] This results in the observed trend in binding constants as measured by Tolman. Electron-poor olefins bind much more strongly to Ni(0) than electron-rich ones (e.g., acrylonitrile vs propene: $K_{rel} \approx 7.5 \cdot 10^4$). Our hypothesis was that removing electron density from the metal center would diminish the π-backbonding and concomitantly increase the interaction via σ-donation from the alkene. This could increase the bond strength of unactivated alkenes without a low-lying π^*-orbital by increasing the relative amount of σ-donation to the overall bonding interaction.

Additionally, a strong π-acceptor could also remove electron density from the nickel carbene carbon. This could potentially render it more electrophilic and more selective for electron-rich alkenes as well.

The second reasoning concerns the formation of the nickel carbene. We have argued in the last chapter that carbene formation is an oxidative process at nickel. Among other reasons, we made this claim based on the relative rates k_{rel} for cyclopropanation from our alkene competition experiments (see chapter 3). Alkenes with large K had smaller k_{rel} values. Translated into the above picture, this means that more strongly binding alkenes remove electron density from the nickel center thus increasing the barrier for (oxidative) nickel carbene formation. If the ancillary ligand(s) were electron-withdrawing enough, the ylide adduct might be stable under the reaction conditions, especially if multiple ligands are bound to Ni. The carbene formation would only be triggered once the less π-accepting substrate binds.

Common π-acidic ligands react with strong nucleophiles such as organolitihum reagents to give insertion products and/or are not modifiable (CO, RNC, PF_3, etc.).[4-5] Instead, we identified $RP(CF_3)_2$ as strongly π-accepting ligands that should be inert under our conditions. The ligands are easily synthesized from their respective $RP(OR)_2$ precursors and $TMSCF_3$/CsF.[6] Albeit, the separation of the volatile ligands **L4** and **L5** from a by-product proved difficult. Both distilled compounds contained a large amount (equimolar and more) of an impurity. Likely TMSOPh, which is a by-product under the reaction conditions. For ligands L6 and L7 this was less problematic. Nevertheless, the results in the presence of this impurity have to be interpreted with caution.

CO stretch frequencies, often used as measure for the π-acceptor strength of ligands, indicate the CF_3-based ligands to be strong acceptors. Indeed, values for $Mo(CO)_5L$ complexes place $MeP(CF_3)_2$ (ν_{CO} = 2094 cm^{-1}) closer to PF_3 (ν_{CO} = 2103 cm^{-1}) than to PPh_3 (ν_{CO} = 2072 cm^{-1}) or even $P(OPh)_3$ (ν_{CO} = 2083 cm^{-1}), another classic π-acidic P(III)-based ligand.[7]

Despite the outlined rationale, this ligand class was not successful in improving the cyclopropanation yield with cyclooctene as substrate (**Table 4.2**). Neither, a bidentate (entry 2 and 3) nor monodentate ligand, both small (entry 4) and steric more demanding (entry 5 to 7) were more effective ligands than the standard PPh_3.
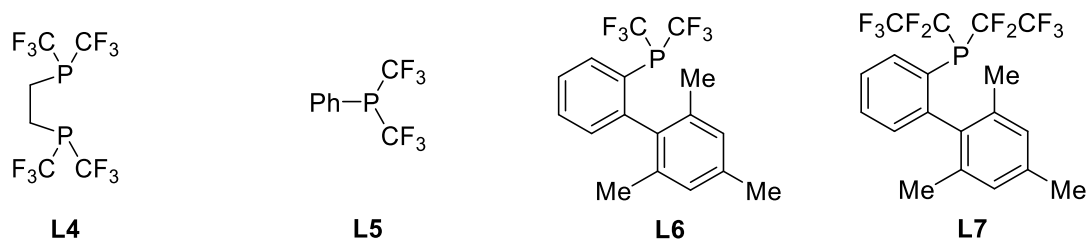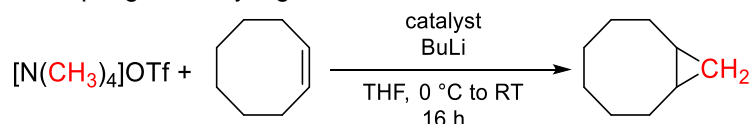
Figure 4.2. Strongly π-accepting ligands on trifluoromethyl groups.

Table 4.2. Strong π-Accepting Ancillary Ligands.[a]

Entry	Catalyst	Yield / %
1	1 mol% (Ph$_3$P)$_2$NiBr$_2$	25
2	1 mol% Ni(**L4**)$_2$	5
3	1 mol% (**L5**)$_2$Ni(cod)	17
4	1 mol% (dme)NiBr$_2$ / 1 mol% **L6**	6
5	1 mol% (dme)NiBr$_2$ / 2 mol% **L6**	8
6	1 mol% (dme)NiBr$_2$ / 1 mol% **L7**	7

[a]Standard conditions: 1 equiv [NMe$_4$]OTf, 1.05 equiv BuLi, 5 equiv COE, 0.05 M in THF.

4.4   3rd Generation - Allosteric Regulation through Remote Steric Effects

In chapter 3, we proposed a mechanistic model in which the substrate has to be coordinated to the catalyst in the resting state in order to be efficiently cyclopropanated. This led to a pre-equilibrium of alkene binding in competition with the phosphine ligand. This ancillary ligand is necessary to stabilize the Ni(0) species in absence of strongly binding alkenes, which presumably stabilize the Ni(0) sufficiently on their own. In line with this reasoning, no homoleptic, monodentate alkene-Ni(0) complex has been isolated with alkenes that have a binding constant lower than norbornene, according to Tolman (K = 4.4), such as terminal alkenes (K ≈ 0.5), at least to the best of our knowledge.[8]

In light of our pre-equilibrium model from chapter 3, we can postulate the following features of a successful ligand for our reaction. The ligand should bind to, and stabilize, Ni(0) as an ancillary ligand. The ligand should not saturate the catalyst to such an extent that the substrate cannot bind anymore. Thus, the ligand should have some form of 'self-recognition', i.e., the first ligand binds strongly to the metal but the coordination of subsequent ligands is hindered. This is reminiscent of allosteric

regulation in enzymes. The substrate itself should not be disfavored from binding however even in the presence of only one ancillary ligand. Indeed, the ancillary ligand might even enhance the binding of the substrate in a positive allosteric modulation.[9]

In this regard, a recent report by Wu and Doyle piqued our interest.[10] During their studies on nickel-catalyzed cross-couplings of acetals and aryl boroxines (**Figure 4.3**), they made the observation that many of the standard ligands for these types of transformations were ineffective. This includes ligands that we have also tried during our initial screening phase, such as Buchwald-type biaryl ligands and NHCs. While in their case PCy_3 was effective, PPh_3 afforded only traces of product. Even though they offer no mechanistic data, their hypothesis was that common ligands designed for Pd-catalyzed transformation sterically overcrowd the smaller coordination sphere of Ni. Hence, their conclusion was that their new ligands with remote bulk in the 3,5-positions (see **Figure 4.3**) "*probably permit coordination of reaction components to nickel while still discouraging the binding of multiple ligand equivalents and preventing bimetallic deactivation mechanisms*". Exactly what we were looking for!

They expressed this remote steric hindrance as large cone angle θ but small buried volume $\%V_{Bur}$ (see **Figure 4.4** and chapter 1 for a discussion of these concepts) and deconvoluted these two trends via multivariate regression analysis.

Indeed, Tolman had already made the point that the ligand has to be sterically bulky in order to be replaced efficiently by an alkene, albeit without the finer and likely important distinction of where the bulk is on the ligand with respect to the metal.[11]

Additionally, Pregosin and others have noted the "3,5-dialkyl meta-effect" as higher enantiomeric excess in enantioselective catalysis with chiral bidentate 3,5-dialkyl-substituted arylphosphines.[12] The effect was proposed to arise from a slightly larger and more rigid binding pocket.

The use of multivariate regression analyses to construct predictive models to improve catalyst design and explain its performance has been a field of intense focus in the past several years.[10, 13-14] By judicious choice of molecular descriptors, usually steric and electronic parameters, the reaction outcome can be correlated with the structure of the catalyst. In field of homogeneous catalyst, these descriptors are most commonly based on the ligand framework, e.g., in our case the steric properties of the phosphine ligand. The model output is a measurable reaction outcome. This can simply be the

yield as in our case, or in principle any possible selectivity such as chemo-, regio-, enantioselectivity etc. This allows to predict the performance of new ligands based on the chosen parameters and has the potential for a rational ligand design beyond trial and error. Additionally, with the proper choice of molecular parameters conclusions about the reaction mechanism itself can be inferred if these properties can be mapped onto specific steps of the catalytic cycle.[13] Thus, this approach has the potential to move beyond being useful for predictions but mechanistically opaque to an explanatory tool.
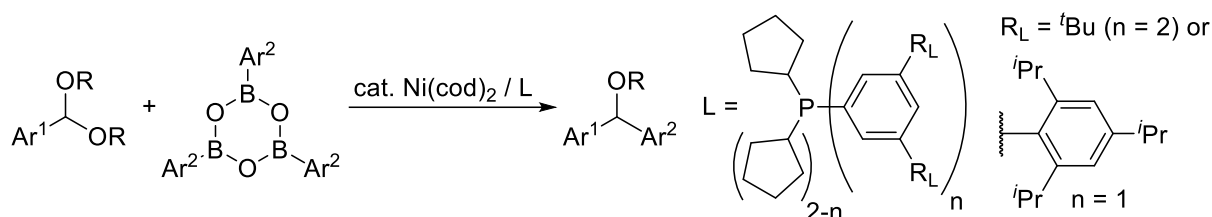
Figure 4.3. Nickel-catalyzed cross-coupling of acetals with aryl boroxines using phosphine ligands with remote steric hindrance according to Wu and Doyle.[10]
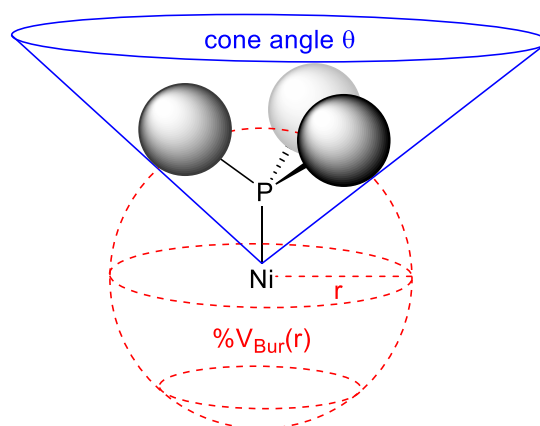
Figure 4.4. Schematic depiction of the buried volume $\%V_{Bur}$ and the cone angle θ. While the buried volume is dependent on the sphere radius r (dashed, red line), the cone angle θ has no such dependence (solid, blue line). This offers a complementary steric description of a ligand.

Because our most successful ligands up to this point were triarylphosphines, PPh_3 being standard, we designed ligands based on this framework in analogy to Doyle's work, that is, with large substituents in the 3,5-positions. Our synthetic efforts can be seen in **Figure 4.5**. We used both *tert*-butyl (**L8** to **L11**) and 2,4,6-tri-*iso*-propylphenyl(trip) (**L12** to **L13**) groups, which were also used by Doyle. Additionally, we synthesized ligands with silyl substituents (**L14** to **L16**). Due to the longer C–Si versus C–C bond, these groups are sterically more demanding, offer slightly different electronic effects ($\sigma_m(^tBu)$ = -0.10 versus $\sigma_m(SiMe_3)$ = -0.04)[15], and are, at the same

time, synthetically easily accessible via their corresponding electrophilic precursors (R_3SiCl, R_3SiOTf).
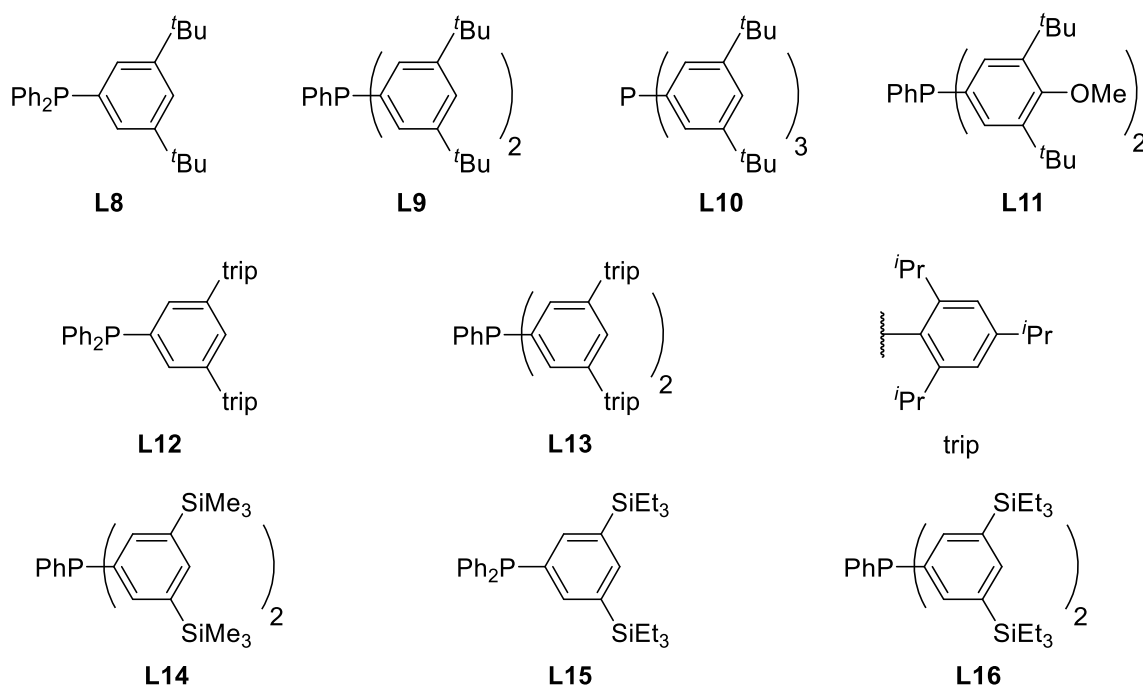

Figure 4.5. Newly designed triarylphosphines with remote steric hindrance by incorporation of large substituents in the 3,5-positions.

To our utmost delight, for the first time since the initial discovery phase we obtained yields better than the standard ligand PPh₃, as can be seen in **Table 4.3**. Indeed, we almost doubled the yield from 25% (PPh₃) to 48% (entry 2) and 49% (entry 4). **L9** is easily synthesized in one step from inexpensive, commercially available 1-bromo-3,5-di-*tert*-butylbenzene.

Table 4.3. Ligands with Remote Steric Hindrance.[a]

[N(CH₃)₄]OTf + (cyclooctene) → (bicyclic product with CH₂)

catalyst
BuLi
THF, 0 °C to RT
16 h
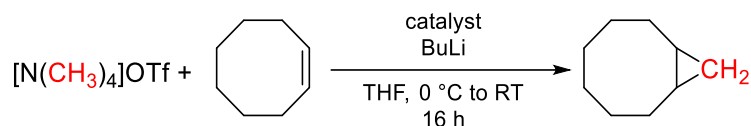
Entry	Catalyst	Yield / %
1	1 mol% (Ph₃P)₂NiBr₂	25
2	1 mol% (dme)NiBr₂ / 2 mol% **L8**	32
3	1 mol% (dme)NiBr₂ / 2 mol% **L9**	48
4	1 mol% (dme)NiBr₂ / 2 mol% **L10**	44
5	1 mol% (**L11**)₂NiBr₂	49
6	1 mol% (dme)NiBr₂ / 2 mol% **L12**	39
7	1 mol% (dme)NiBr₂ / 2 mol% **L13**	43
8	1 mol% Ni(cod)₂ / 2 mol% **L14**	40
9	1 mol% Ni(acac)₂ / 2 mol% **L14**	37
10	1 mol% Ni(acac)₂ / 2 mol% **L15**	30
11	1 mol% Ni(acac)₂ / 2 mol% **L16**	43

[a]Standard conditions: 1 equiv [NMe₄]OTf, 1.05 equiv BuLi, 5 equiv COE, 0.05 M in THF.

In analogy to Doyle, we wanted to see if our initial hypothesis was correct, i.e., that we need a large cone angle and a small buried volume %V_{Bur}, i.e., large remote steric hindrance. To do so, we chose a small subset of the ligands that we had tested that spanned both the steric parameter space as well as the yield space for the cyclopropanation of cyclooctene. We then optimized the geometries of the respective bis-ethene complexes, $(C_2H_4)_2Ni(PR_3)$, on the same level of theory as the DFT calculations in chapter 3.

With these structures in hand, we calculated the steric parameters exact ligand cone angle $\theta°$, exact ligand solid cone angle $\Theta°$, and the buried volume %V_{Bur} (**Table 4.4**). This was done with freely available tools, as described in the Introduction.[16-18] Additionally, these program packages allow for an easy visualization of the parameters as shown in **Figure 4.6** to **Figure 4.10**.

Table 4.4. Steric Parameters for Selected Ligands and Their Yields for the Cyclopropanation of Cyclooctene.[a]

Entry	Phosphine	Exact cone angle $\theta°$	Exact solid cone angle $\Theta°$	%V_{Bur}	Yield / %
1	PPhMe₂	138.947	122.863	26.5	3
2	PPh₂Me	155.594	129.365	28.6	0.3
3	PPh₃	168.196	135.023	30.4	25
4	PPh₂(3,5-di*t*BuPh) (**L8**)	188.849	142.790	31.2	32
5	PPh(3,5-di*t*BuPh)₂ (**L9**)	195.345	148.329	31.1	48

[a]Standard conditions: 1 equiv [NMe₄]OTf, 1.05 equiv BuLi, 5 equiv COE, 0.05 M in THF.

Next, we constructed univariate regression analyses with the parameter from **Table 4.4** to assess their correlation with the measured cyclopropanation yield (**Figure 4.11**). As can be seen from these linear regression models, all steric parameter correlate to some extent with the yield. While %V_{Bur} alone correlates only moderately well with the

yield, the exact cone angle $\theta°$ and the exact solid cone angle $\Theta°$ correlate much better. The exact solid cone angle $\Theta°$ was a slightly better predictor for the yield than the exact cone angle $\theta°$ ($R^2 = 0.90$ versus 0.87, respectively) and was thus used for the further analysis.
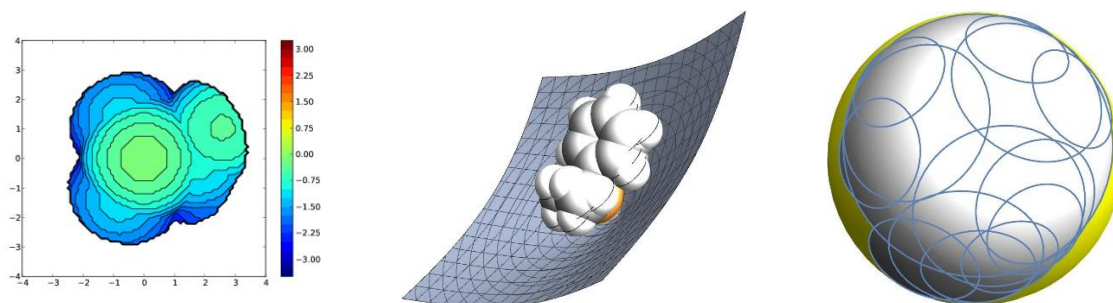

Figure 4.6. Steric map (left),.cone (middle), and 3D plot of the solid angle (right) of PPhMe$_2$.
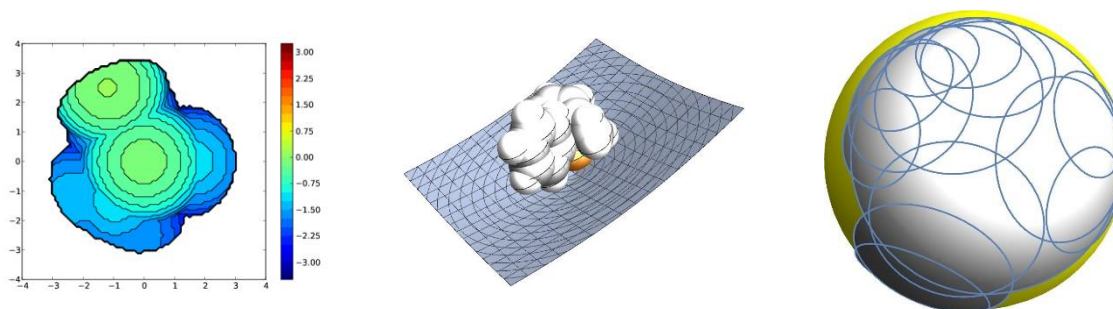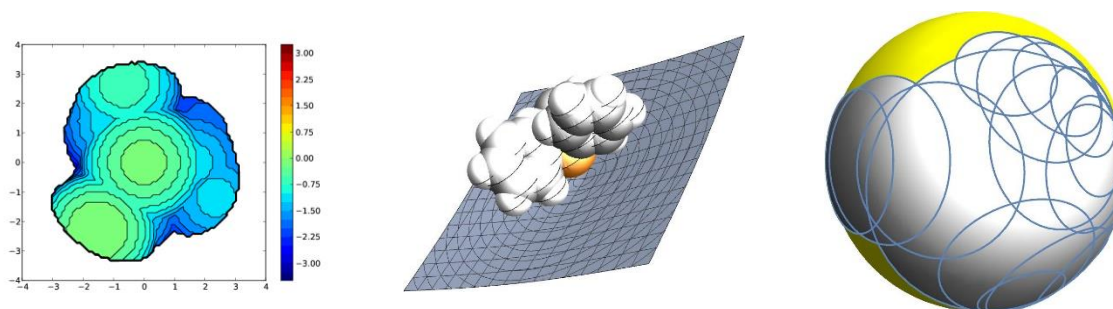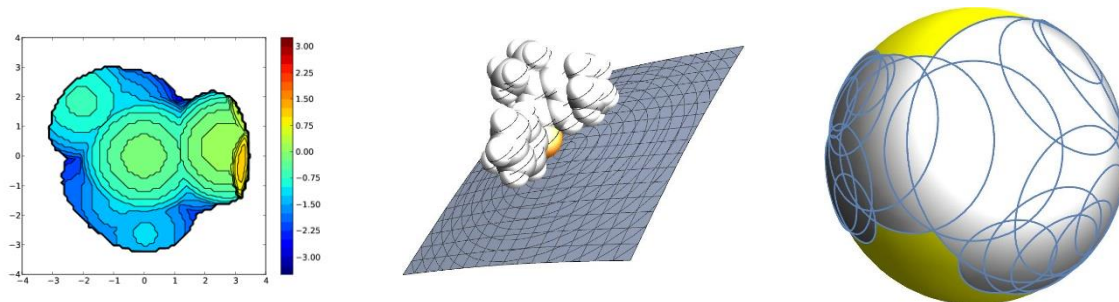

Figure 4.7. Steric map (left), cone (middle), and 3D plot of the solid angle (right) of PPh$_2$Me.

Figure 4.8. Steric map (left), cone (middle), and 3D plot of the solid angle (right) of PPh$_3$.

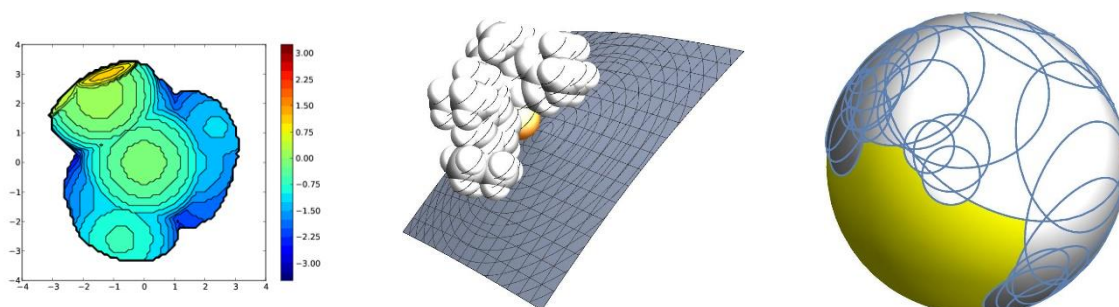**Figure 4.9.** Steric map (left), cone (middle), and 3D plot of the solid angle (right) of P(3,5-di^{t}BuPh)Ph$_2$ (**L8**).

Figure 4.10. Steric map (left), cone (middle), and 3D plot of the solid angle (right) of P(3,5-di^{t}BuPh)$_2$Ph (**L9**).
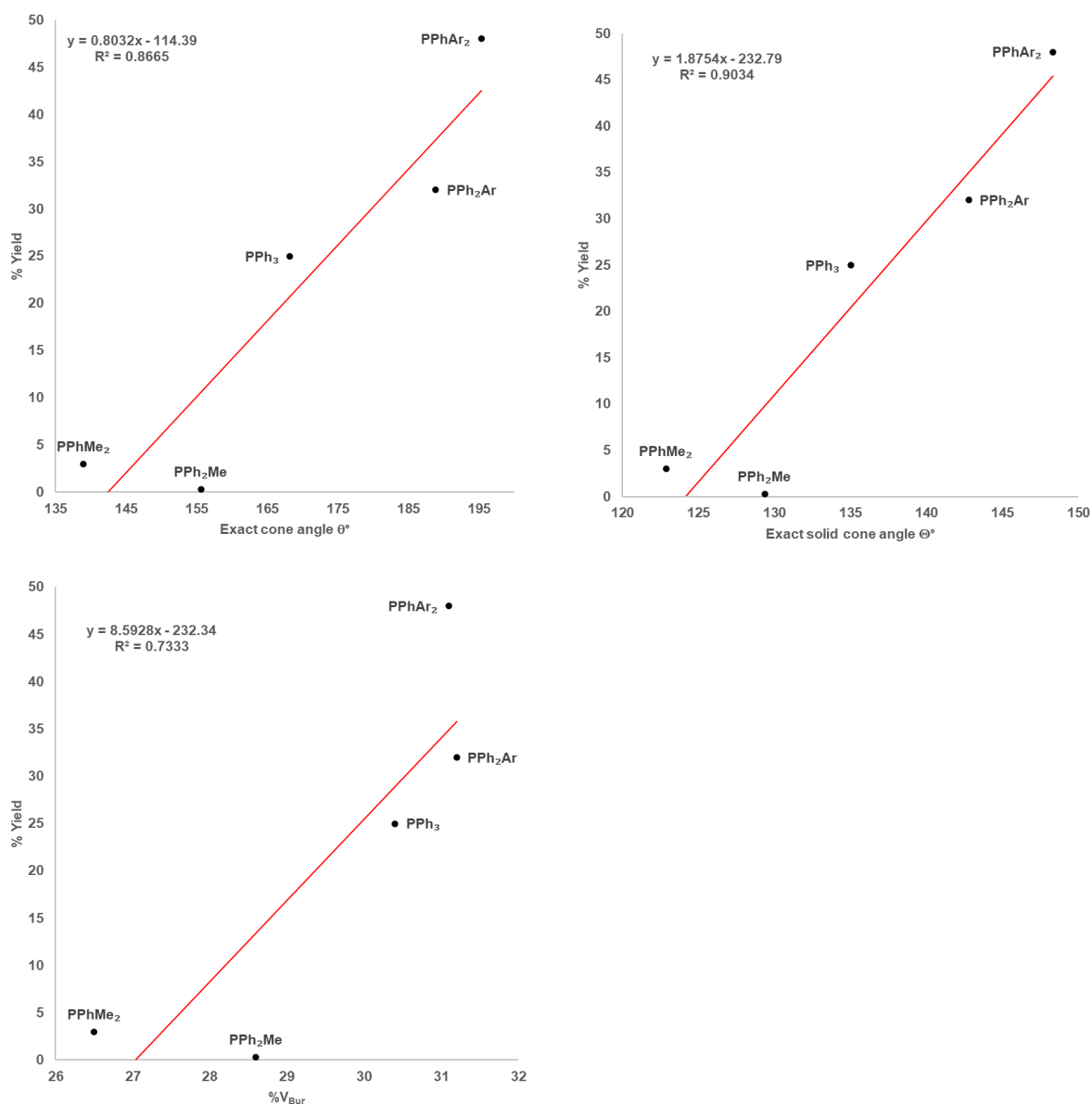
Figure 4.11. Univariate regression analyses for several steric parameter.

In the final step, we conducted a multivariate linear regression analysis to construct a steric-only model from the (non-normalized) exact solid cone angle $\Theta°$ and buried volume $\%V_{Bur}$ parameters (**Figure 4.12**). Already this, admittedly rather crude, model gives a good correlation between measured and predicted yields. Most importantly, the regression coefficients shown in **Figure 4.12** (top) give a qualitative corroboration of our assumption. A high yield is predicted when the ligand possesses both a large (solid) cone angle (positive coefficient) and a small buried volume $\%V_{Bur}$ (negative coefficient).
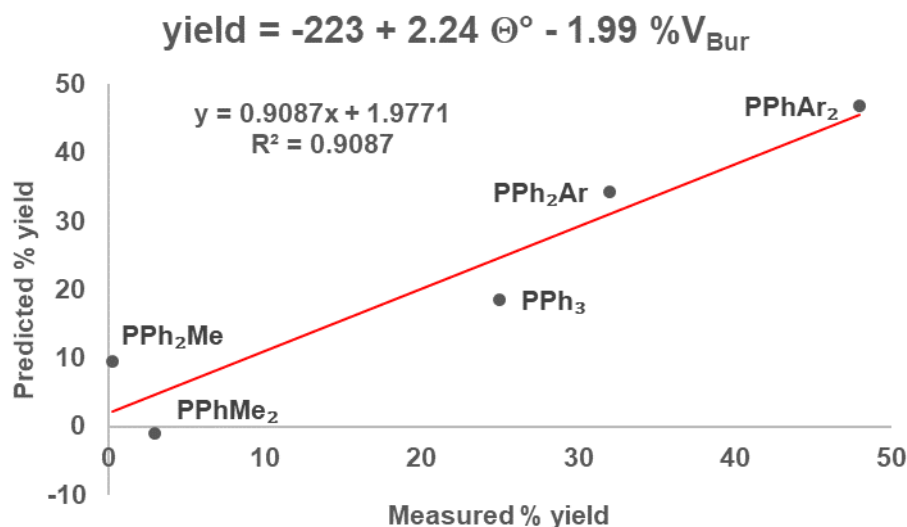
$$\text{yield} = -223 + 2.24 \, \Theta° - 1.99 \, \%V_{Bur}$$

Figure 4.12. Multivariate regression model for the cyclopropanation of cyclooctene using exact solid cone angle $\Theta°$ and buried volume $\%V_{Bur}$ as predictors.

4.4.1 Measured Binding Constants

With the ligand subset for the regression model in **Figure 4.12** in hand, we were interested in obtaining binding constants for these phosphines. In analogy to Tolman, we chose UV-Vis titrations as method to establish the binding constants. An excess of phosphine (ca. 20 equiv) was mixed with Ni(cod)$_2$ (1 equiv) in THF in a 10 mm quartz cuvette with septum screw cap. This was chosen as a simplification over isolation of the Ni(PR$_3$)$_3$ complex, the in situ formation of the nickel phosphine complex being operationally much simpler. Into this solution was titrated the alkene, and the disappearance of the starting complex in the visible region was observed.

This data was then fitted to the same equilibrium equation that was used for the mathematical model in chapter 3 (cf. chapter 6) to give the binding constants K in **Table 4.5**.

Table 4.5. Binding constants for different phosphine and alkenes.

Entry	Phosphine	K_{COE}	$K_{1\text{-Octene}}$	K_{NBE}
1	PPh$_3$	0.081	0.95	33
2	P(O-o-tolyl)$_3$ (Tolman)[a]	0.062	0.5	4.4
3	P(O-o-tolyl)$_3$	0.071	-	-
4	PPhMe$_2$	0.0014	-	-
5	PPh$_2$Me	0.0013	-	-
6	PPh$_2$(3,5-di^{t}BuPh) (**L8**)	0.11	-	-
7	PPh(3,5-di^{t}BuPh)$_2$ (**L9**)	0.090	-	-

[a]Values taken from ref. [3]

In chapter 3, we discussed the appropriateness in using Tolman's constants measured in benzene with P(O-o-tolyl)$_3$ instead of PPh$_3$ in THF. Only one comparison between these two ligands is available by Tolman for ethene and the constants are comparable (K$_{Ethene}$ = 250 and 300 for P(O-o-tolyl)$_3$ and PPh$_3$, respectively).[3, 19] Nevertheless, we argued that the Tolman's constants should be comparable and follow at least the correct trend. For us, the relative binding constants are important rather than the absolute values, so a systematic shift makes no difference.

Comparing entry 1 and 3 with entry 2 in **Table 4.5**, we can see that also with this extended data set our assumption is justified. K$_{COE}$ in entry 3 compares favorably with Tolman's data in entry 2 with a different solvent, THF in our case versus benzene, but the same ligand, P(O-o-tolyl)$_3$. Entry 1 and entry 3 compare three different alkenes with both different ligand and in THF instead of benzene. Nevertheless, we can see that all three binding constants K compare favorably as well. Our K$_{NBE}$ is slightly higher than Tolman's data. This might be an actual difference or a small measurement error (see discussion below).

To be able to conduct titration experiments, the reaction had to be carried out in cuvettes with 10 mm path length to allow for mixing. This necessitated the use of rather low concentrations of Ni (< 1 mM). It was found that Ni(PPh$_3$)$_3$ is not stable under these conditions and excess ligand was needed to keep Ni(0) stable. This circumstance has been observed previously.[19] Despite the low concentration of Ni, detector saturation can usually be seen below approximately 500 nm for the triarylphosphine complexes.

Figure 4.13 shows the titration of Ni(cod)$_2$/PPh$_3$ with COE to obtain the binding constant K. The titration curve is well fitted with the equilibrium equation for the alkene/phosphine equation derived in chapter 6.
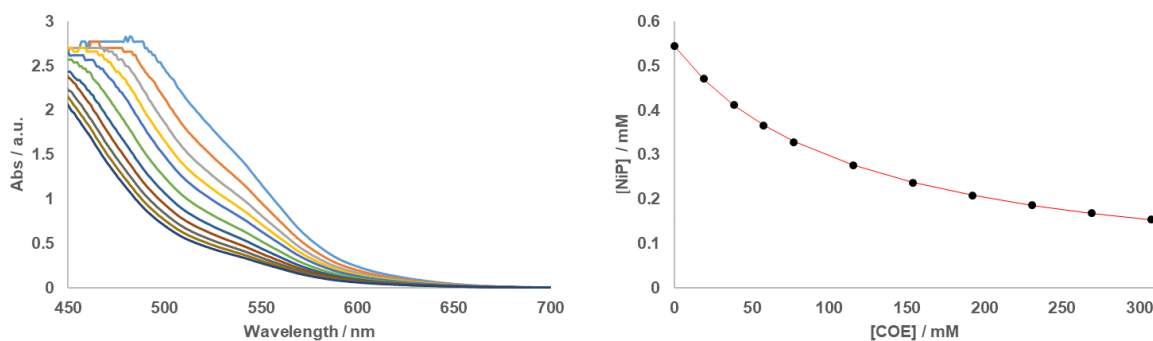
Figure 4.13. Left: UV-Vis titration of 9.91 mM PPh$_3$ and 0.55 mM Ni(cod)$_2$ in THF with COE. Right: Titration curve at 500 nm. Red curve depicts a fit to obtain the binding constant K.

Figure 4.14 shows the titration of Ni(cod)$_2$/PPh$_3$ with norbornene (NBE). Due to relatively large binding constant of NBE, the phosphine is quickly displaced by NBE even at a much lower concentration than employed for cyclooctene (COE, cf. **Figure 4.13**, right). This could have led to the relatively high K compared to Tolman's value rather than a true difference.
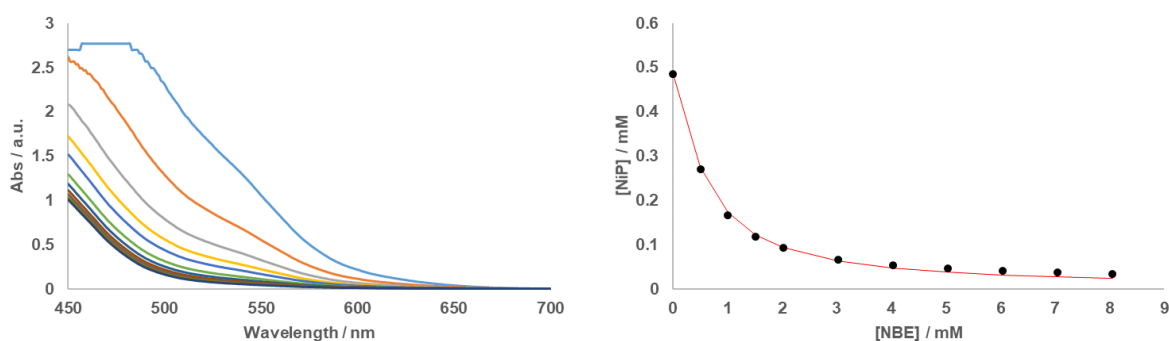

Figure 4.14. Left: UV-Vis titration of 12.77 mM PPh$_3$ and 0.48 mM Ni(cod)$_2$ in THF with NBE. Right: Titration curve at 500 nm. Red curve depicts a fit to obtain the binding constant K.

Figure 4.15 shows the titration of Ni(cod)$_2$/PPh$_2$Me with COE. Already the replacement of one phenyl group with a much smaller methyl group appears to changes the speciation in solution considerably. Indeed, what we abbreviated as [NiP] here is likely not Ni(PPh$_2$Me)$_3$ but the tetrakis-phosphine complex Ni(PPh$_2$Me)$_4$, especially with the added excess ligand.[20] In contrast, it is known that the solid denoted Ni(PPh$_3$)$_4$ dissociates one ligand in solution to give Ni(PPh$_3$)$_3$ and even addition of a large excess PPh$_3$ does not produced the tetrakis-phosphine species.[19]

Indeed, the absorbance was not corrected for the small volume change due to alkene addition. Thus, the binding constant both for PPh$_2$Me and PPhMe$_2$ are likely lower than the values in **Table 4.5**.
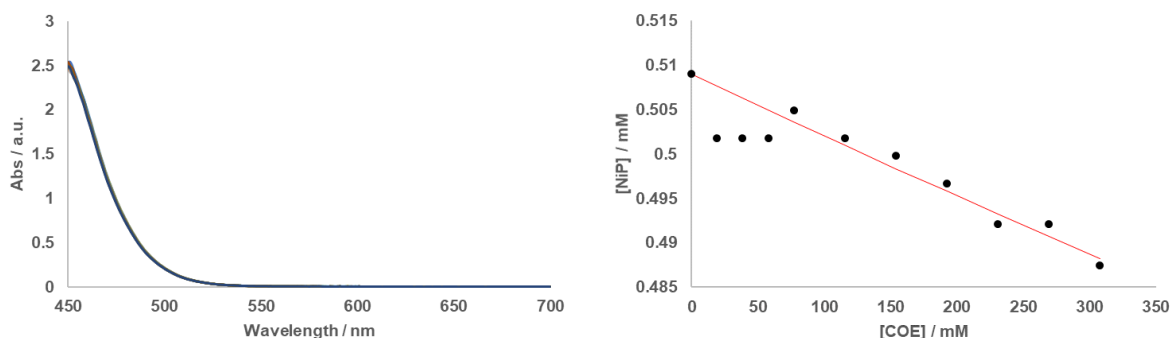
87

Figure 4.15. Left: UV-Vis titration of 9.99 mM PPh$_2$Me and 0.51 mM Ni(cod)$_2$ in THF with COE. Right: Titration curve at 460 nm. Red curve depicts a fit to obtain the binding constant K.

The new ligands PPh$_2$(3,5-di^{t}BuPh) (**L8**) and PPh(3,5-di^{t}BuPh)$_2$ (**L9**) are overall well behaved in the UV-Vis titration, similar to PPh$_3$ (**Figure 4.16** and **Figure 4.17**). This is in contrast to P(3,5-di^{t}BuPh)$_3$ (**L10**) (not shown), which seemingly did not form any NiL$_3$ complex at all in solution, based on its UV-Vis absorption spectrum, even before addition of any cyclooctene. Instead, very bulky ligands such as **L10** likely only form Ni(PR$_3$)$_2$L$_n$ (L ≠ PR$_3$) species in solution even with an excess of phosphine ligand present.
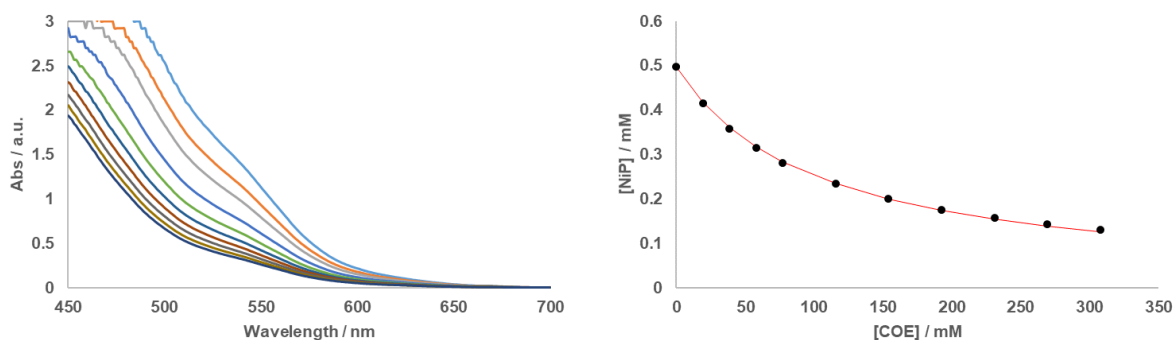

Figure 4.16. Left: UV-Vis titration of 11.88 mM PPh$_2$(3,5-di^{t}BuPh) (**L8**) and 0.50 mM Ni(cod)$_2$ in THF with COE. Right: Titration curve at 500 nm. Red curve depicts a fit to obtain the binding constant K..

The fit curve for **L9** in **Figure 4.17** does show small deviations from the experimental behavior. Whether this an experimental error or already indicates a small change in speciation as evidenced for **L10** is unclear at his point.
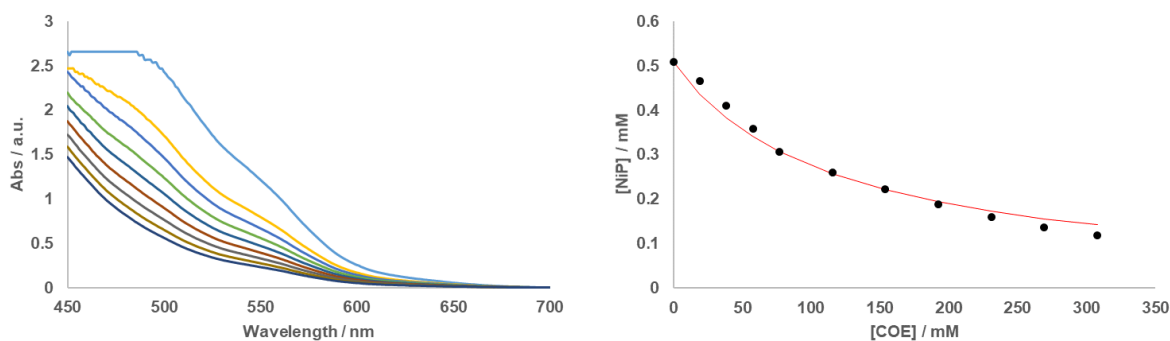
Figure 4.17. Left: UV-Vis titration of 10.89 mM PPh(3,5-di^{t}BuPh)$_2$ (**L9**) and 0.51 mM Ni(cod)$_2$ in THF with COE. Right: Titration curve at 500 nm. Red curve depicts a fit to obtain the binding constant K.

The above binding titrations give a highly valuable insight into the binding affinity of alkenes to various nickel phosphine complexes. For small ligands such as PPh$_2$Me it is likely that only an upper limit can be measured under these conditions. In contrast, ligands that are sterically too large (e.g. **L10**) do seemingly not form NiL$_3$ species in solution. In these cases, it would be necessary to use other techniques such as ^{31}P NMR to track the speciation in solution more precisely.

4.4.2 Comparison of Measured Binding Constants to Model

The binding constants of our ligand subset used in the steric-only regression model are plotted in **Figure 4.18** (cf. chapter 3). The new data (green diamonds) is in good agreement with the prediction of our mathematical model (red curve) from chapter 3. The small ligands PPh$_2$Me and PPhMe$_2$ agree well with the model even if the binding constants were to be smaller than we measured (see discussion above). PPh$_3$ and PPh$_2$(3,5-di^{t}BuPh) (**L8**) also corroborate the conclusion from our model. PPh(3,5-di^{t}BuPh)$_2$ (**L9**) does slightly deviate from our model. This might have several possible explanations.

First, it should be noted that the curve is sensitive to the variation in this region of K. A yield of 50% is already predicted for K ≈ 0.3 based on the model (K$_{COE}$(**L9**) = 0.09, **Table 4.5**). Thus, it might be that an experimental error contributes to the deviation. The slight deviation of the binding titration has been noted above and it might be necessary to isolate Ni(**L9**)$_3$ to obtain a more accurate number by titration. As noted above, the in-depth study of speciation for phosphines sterically bulkier than **L9** seem to be appropriate in general.

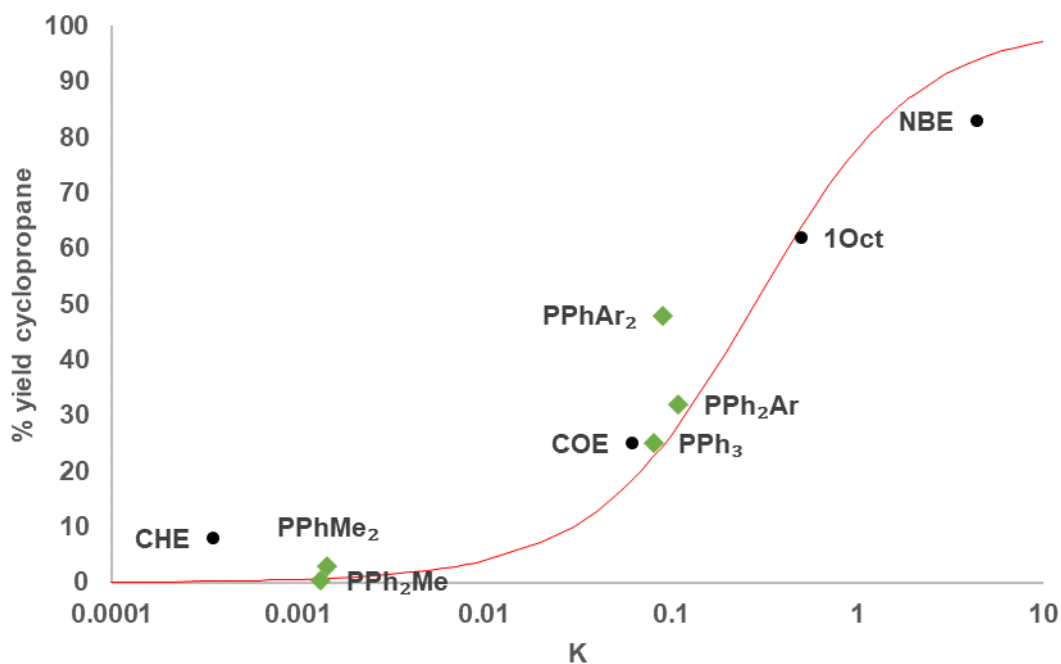Other possible factors are discussed below in chapter 4.4.3.

Figure 4.18. Plot of binding constant K (log scale) versus measured yields for the cyclopropanation with selected ligands and alkenes. Black circles represent yields of alkenes as indicated by the labels with PPh3 as ligand and K from Tolman and the corresponding fit to our model represented as red curve.[3] Green diamonds represent yields of COE with different phosphine ligands as indicated by the labels and K from **Table 4.5**. Ar = (3,5-di-^{t}BuPh), CHE = cyclohexene, COE, cyclooctene, 1Oct = 1-Octene, NBE = Norbornene.

Our binding model would also predict that an excess of phosphine entirely replaces the substrate from the catalyst and thereby suppressing the cyclopropanation completely. This was indeed the case by adding an excess of PPh3 (27 and 101 mol%) to the cyclopropanation of cyclooctene under otherwise standard conditions with 1 mol% (Ph3P)2NiBr2. While for the reaction with 27 mol% PPh3 traces of product were observed, none was observed for the reaction with 101 mol% PPh3 added. We also determined the fate of the phosphine. Most of the PPh3 stayed intact during the reaction as evidenced by ^{31}P NMR of the residue after evaporation of all volatiles. A small amount of PPh2Bn was detected, which likely formed via carbene transfer to PPh3 and subsequent phospha-Stevens rearrangement (see chapter 1 for discussion) and no [PPh3Me]$^+$ was observed.

It should be noted that Franzen and Wittig reported in their original Communication from 1960 that 'trimethylammonium methylide' was able to transfer the methylene unit to PPh3.[21] The evidence provided was the subsequent reaction with benzophenone to give 1,1-diphenylethene, which supposedly formed via a Wittig reaction with triphenylphosphonium methylide. No further evidence or experimental details were reported. Previous work in our group has shown that lithiomethyltrimethylammonium

90

triflate reacts with benzophenone to give the corresponding epoxide in high yield (see chapter 1).[22] Presumably, this was not observed by Franzen and Wittig. The detection of an epoxide was not reported.

4.4.3 Complementary and Contributing Factors

The above line of reasoning is based on the assumption that the increased yield is caused by disfavoring efficient binding of multiple phosphine ligands due to remote steric hindrance. Two additional factors that might contribute to the efficacy of this ligand class shall be discussed here briefly.

Both Hartwig and Buchwald and Liu noticed in recent reports the unique catalytic efficiency of the bulky ligand DTBM-SEGPHOS in two mechanistically related Cu-catalyzed hydrofunctionalization reactions of alkenes (**Figure 4.19**).[23-24]
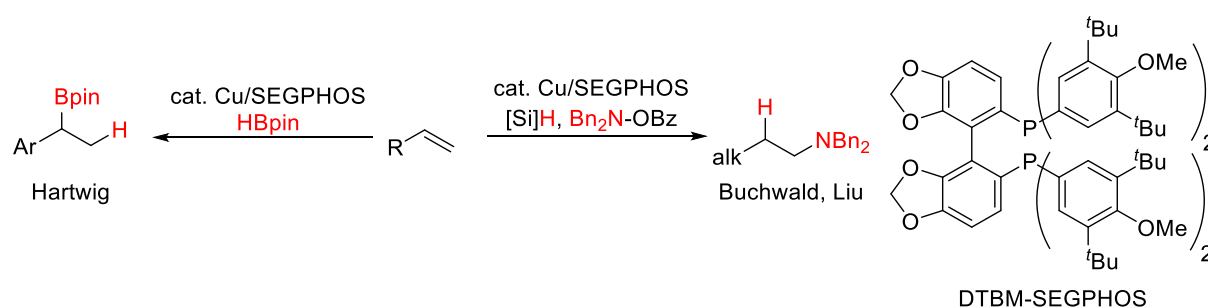

Figure 4.19. Hydrofunctionalization reactions of alkenes catalyzed by Cu/DTBM-SEGPHOS.

Hartwig et al. were able to show that the parent (phenyl-substituted) SEGPHOS ligand resulted in the formation of a dimeric CuH complex, which was not catalytically competent. The bulkier DTBM-SEGPHOS ligated complex stayed monomeric in solution and is thus a more reactive catalyst (**Figure 4.20**, left).

Mechanistic studies led Buchwald and Liu to suggest that the hydrocupration is the rate-determining step in their reaction. They performed DFT calculations on the hydrocupration transition state and proposed that stabilizing dispersion interactions between the *tert*-butyl groups on DTBM-SEGPHOS and the substituents on the double bond were the cause for the ligand's superior performance (**Figure 4.20**, right).
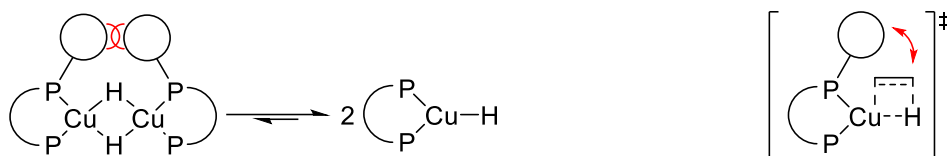
Figure 4.20. Left: Steric repulsion of large substituents on DTMB-SEGPHOS lead to a monomeric catalyst according to Hartwig. Right: Stabilizing dispersion interactions (red arrow) between large substituents on DTMB-SEGPHOS and alkene during the rate-determining hydrocupration step according to Buchwald and Liu.

How is this related to our system? We have already mentioned in chapter 3 that partial catalyst deactivation, either during the initial reduction or during the reaction, might be an issue. Thus, along Hartwig's reasoning, a contributing factor to the improved performance of our 3rd generation ligand design could be the prevention of bimetallic decomposition processes.

On the other hand, we propose the binding of an alkene and a phosphine to Ni(0) in the resting state of the catalytic cycle. Similar to the proposed dispersion interactions during the hydrocupration step, we might also have stabilizing, non-covalent interactions between the ancillary ligand and the alkene in the ground state. This could then lead to a higher binding constant of the alkene. We note that the systematic study of dispersion energy donors is a burgeoning field inter alia to stabilize unusual species and increase catalyst performance.[25-29] See also the discussion in chapter 4.4.2.

4.5 Conclusion

In this chapter, we traced the evolution of our ligand design from a 1st to a 3rd generation. The reasoning for every generation was guided by our mechanistic insights at that time. While the 1st and 2nd generation ligands were unsuccessful, the 3rd generation gave a more efficient catalyst system than with the simple PPh3. This raised the yield from 25% with PPh3 to almost 50% with **L9** and **L11** for the cyclopropanation of cyclooctene. We then corroborated our mechanism-guided ligand design for a subset of ligands through a steric-only multivariate regression model. This model confirmed the importance of the opposite trends of our two steric parameters, i.e., a large cone angle and a small buried volume are needed for a better performance. We further corroborated our proposed pre-equilibrium model by measuring binding constants of several alkenes and phosphines. First, this allowed us to be reassured that it is justified to use Tolman's constants. This already gave us a large, predictive

library of binding constants at hand. Second, we saw that the binding constant for different phosphines but the same alkene (the opposite base we modeled our data on in chapter 3) is consistent with our pre-equilibrium binding competition.

Unfortunately, it must be noted that we seemingly hit a plateau in our steric-only ligand design approach. The largest ligands we tried so far, **L10** and **L14** to **L16**, did not allow for a linear extrapolation from the mid-sized 'Goldilocks' ligands such as **L9**.

Even though some electronic effects have been observed by us and are known to influence the binding of alkenes to Ni(0),[11, 19] the electronic effects of the ancillary ligand remains underexplored.

Further conclusions and ligand design plans based on this chapter will be discussed in chapter 5.

4.6   References

1. Fischer, H. *Chem. Rev.* **2001,** *101*, 3581-3610.
2. Iluc, V. M.; Hillhouse, G. L. *J. Am. Chem. Soc.* **2014,** *136*, 6479-6488.
3. Tolman, C. A. *J. Am. Chem. Soc.* **1974,** *96*, 2780-2789.
4. Gabor, B.; Krüger, C.; Marczinke, B.; Mynott, R.; Wilke, G. *Angew. Chem.* **1991,** *103*, 1711-1713.
5. Pörschke, K.-R.; Jonas, K.; Wilke, G.; Benn, R.; Mynott, R.; Goddard, R.; Krüger, C. *Chemische Berichte* **1985,** *118*, 275-297.
6. Murphy-Jolly, M. B.; Lewis, L. C.; Caffyn, A. J. M. *Chemical Communications* **2005**, 4479-4480.
7. Brisdon, A. K.; Herbert, C. J. *Coordination Chemistry Reviews* **2013,** *257*, 880-901.
8. Jolly, P. W.; Wilke, G., CHAPTER V - Nickel-Olefin and -Alkyne Complexes. In *The Organic Chemistry of Nickel*, Jolly, P. W.; Wilke, G., Eds. Academic Press: 1974; pp 244-328.
9. Kovbasyuk, L.; Krämer, R. *Chem. Rev.* **2004,** *104*, 3161-3188.
10. Wu, K.; Doyle, A. G. *Nat Chem* **2017,** *9*, 779-784.
11. Tolman, C. A.; Seidel, W. C.; Gosser, L. W. *Organometallics* **1983,** *2*, 1391-1396.
12. Trabesinger, G.; Albinati, A.; Feiken, N.; Kunz, R. W.; Pregosin, P. S.; Tschoerner, M. *J. Am. Chem. Soc.* **1997,** *119*, 6315-6323.
13. Zhao, S.; Gensch, T.; Murray, B.; Niemeyer, Z. L.; Sigman, M. S.; Biscoe, M. R. *Science* **2018,** *362*, 670-674.
14. Santiago, C. B.; Guo, J.-Y.; Sigman, M. S. *Chemical Science* **2018,** *9*, 2398-2412.
15. Hansch, C.; Leo, A.; Taft, R. W. *Chem. Rev.* **1991,** *91*, 165-195.
16. Bilbrey, J. A.; Kazez, A. H.; Locklin, J.; Allen, W. D. *Journal of Computational Chemistry* **2013,** *34*, 1189-1197.
17. Bilbrey, J. A.; Kazez, A. H.; Locklin, J.; Allen, W. D. *Journal of Chemical Theory and Computation* **2013,** *9*, 5734-5744.
18. Falivene, L.; Credendino, R.; Poater, A.; Petta, A.; Serra, L.; Oliva, R.; Scarano, V.; Cavallo, L. *Organometallics* **2016,** *35*, 2286-2293.

19. Tolman, C. A.; Seidel, W. C.; Gerlach, D. H. *J. Am. Chem. Soc.* **1972,** *94*, 2669-2676.

20. Tolman, C. A.; Seidel, W. C.; Gosser, L. W. *J. Am. Chem. Soc.* **1974,** *96*, 53-60.

21. Franzen, V.; Wittig, G. *Angew. Chem.* **1960,** *72*, 417-417.

22. den Hartog, T.; Sarria Toro, J. M.; Couzijn, E. P.; Chen, P. *Chem Commun (Camb)* **2014,** *50*, 10604-10607.

23. Xi, Y.; Hartwig, J. F. *J. Am. Chem. Soc.* **2017,** *139*, 12758-12772.

24. Lu, G.; Liu, R. Y.; Yang, Y.; Fang, C.; Lambrecht, D. S.; Buchwald, S. L.; Liu, P. *J. Am. Chem. Soc.* **2017,** *139*, 16548-16555.

25. Schweighauser, L.; Strauss, M. A.; Bellotto, S.; Wegner, H. A. *Angewandte Chemie* **2015,** *54*, 13436-13439.

26. Wagner, J. P.; Schreiner, P. R. *Angewandte Chemie* **2015,** *54*, 12274-12296.

27. Rosel, S.; Becker, J.; Allen, W. D.; Schreiner, P. R. *J. Am. Chem. Soc.* **2018,** *140*, 14421-14432.

28. Thomas, A. A.; Speck, K.; Kevlishvili, I.; Lu, Z.; Liu, P.; Buchwald, S. L. *J. Am. Chem. Soc.* **2018,** *140*, 13976-13984.

29. Liptrot, D. J.; Power, P. P. *Nature Reviews Chemistry* **2017,** *1*, 0004.

5 Conclusion and Outlook

5.1 Conclusion

The foundation of this thesis can be tracked back to a publication by Franzen and Wittig in 1960. For the first and latest time in a very long time, the cyclopropanation of an alkene, cyclohexene, with 'trimethylammonium methylide' was demonstrated. After a de facto retraction of the result by Wittig without Franzen four years later, the case seemed to have been settled. Our group became nevertheless intrigued by the possibility that the reaction could have worked after all, catalyzed by some unknown contaminant. This led to the development of lithiomethyltrimethylammonium triflate – lithium is tightly coordinated to the ylide – as a methylene donor to imines, ketones, aldehydes and even double bonds in our group. Yet, only activated alkenes such as styrenes yielded cyclopropane in an uncatalyzed addition-ring closure sequence. Over 50 years later, the cyclopropanation of cyclohexene with an ammonium ylide was still elusive.

This thesis started with one more attempt to find an effective catalyst for a cyclopropanation reaction of unactivated alkenes. Nickel proved to be just that, and very uniquely effective. Early optimization dealt with the screening of other metals, which all proved to be ineffective, as well as ligands. Of all ligands tested in the initial phase, triphenylphosphine exhibited the best performance yielding 23 – 25% of bicyclo[6.1.0]nonane, the cyclopropane of cyclooctene, our standard test substrate. Cyclohexene was finally found to be a viable substrate, giving 8% yield with 5 equivalents of alkene, while norbornene was the highest yielding substrate with 79 – 83% yield. During this stage of the thesis, we also noted several odd observations. The yield was slightly dependent on whether the reaction was completely sealed or open to the Schlenk line. An observation that was also made previously for the uncatalyzed reaction. Polyethylene and cyclopropane (C_6H_6) were found as side products. The yield was highly substrate dependent. And most importantly, the amount of (pre)catalyst (($Ph_3P)_2NiBr_2$) had a significant, non-linear impact on the yield using cyclooctene. At low (<0.5 mol%) and high (>1 mol%) catalyst loading a suppressed yield was noticed, a maximum was reached at 0.5 to 1 mol%. These results have been discussed in chapter 2.

These observations, and most importantly our goal to improve the reaction based on a rational, mechanism-guided manner, led us to study the cyclopropanation reaction in greater detail. These efforts are summarized in chapter 3. Based on kinetics and other physical-organic methods and computational studies, we proposed a catalytic cycle and built a mathematical model thereupon. The reaction is based on a pre-equilibrium binding of the alkene in competition with the phosphine in a Curtin-Hammett-like scenario. This equilibrium is followed by ammonium ylide adduct formation (possibly also in an equilibrium and dependent on the other ligands on Ni(0)). Subsequent NMe_3 extrusion forms a nickel carbene. This reactive intermediate can either undergo intramolecular (inner-sphere) cyclopropanation if an alkene is coordinated or undergo homocoupling and subsequent side reactions if no substrate is present.

This can be expressed as a mathematical model, which takes into account binding constants of alkenes to Ni(0), as measured by Tolman, which was then fit to our observed yields. With this model in hand, we explained the substrate dependency. A higher alkene binding constant leads to more Ni(0) alkene complex in solution, which in turn favors cyclopropanation over homocoupling. The observed catalyst loading effect is explained in this framework, as the alkene (constant (initial) concentration in our experiments) loses out in the competition with higher phosphine concentrations brought about by the increased amount of the phosphine-containing precatalyst.

With this alkene-phosphine competition in mind, we began designing ligands that bind and stabilize Ni(0), yet do not saturate the catalyst for alkene binding. This 3rd ligand generation (and earlier ones) is highlighted in chapter 4. In our work, we were inspired by a recent report from the Doyle group, which introduced the concept of remote steric hindrance, i.e., a ligand that has steric bulk pointing away from the metal center. This results in a large cone angle but a small buried volume in the vicinity of the metal (see chapter 4 for a detailed explanation). The large cone angle serves as a self-recognition element between the phosphines themselves and disfavors binding of multiple ligands. The small buried volume still allows the coordination of the substrate, which does not 'feel' the remote steric hindrance. The design of this ligand generation led to a doubling of the yield for the test substrate cyclooctene from 25 to almost 50%. A preliminary multivariate regression analysis with the steric parameters introduced above

rationalized the observed effect of the ligand on the yield and serve as a rational basis for future ligand design campaigns.

Unfortunately, it cannot be stated that the reaction is synthetically useful at this point. Nevertheless, this thesis has opened up an elusive substrate class for this reagent, previously not possible. Mechanistic insights have been gained that might be applied to a broader set of reactions. And a way forward has been sketched upon rational, mechanism-guided ligand design. Yet again, nickel has proven to be a 'spirited horse'.[1]

5.2 Outlook

5.2.1 Ligand Design

The most promising and efficient way forward to improve ligand design is a multivariate regression analysis based on our preliminary results with the 3rd generation ligands. This work has already begun and parts were presented in chapter 4. The conclusion from the steric-only model was to leverage the effect of remote steric hindrance, i.e., a large cone angle and small buried volume.

Several points can be identified that should lead to an improvement of the model and its predictive ability. Only a small subset of all tested ligands were used with a limited number of steric variations on the ligand framework itself. Additionally, the description of the steric properties was done with a small set of descriptors. Going forward, the ligand library should be significantly expanded both in number and in variability. Additionally, a large range of molecular predictors need to be established and tested for their appropriateness. This is most conveniently done by DFT calculations.[2-5]

The analysis was mainly done on arylphosphines due to the good performance of PPh_3 up until the 3rd ligand generation. Besides that, there is no a priori reason why a triarylphosphine should be the ideal choice of ligand. With some guidance from the initial training set in hand, we are now able to computationally design new ligands that have the same steric features in terms of remote steric hindrance, but differ considerably in their framework. For example, an obvious choice is to move towards substituted benzyl phosphines, potentially offering interesting new reactivity similar to the switch of *tert*-butyl- to neopentyl-substituted alkyl phosphines.[6] Due to the additional methylene linker, the buried volume is expected to be already lower than for triarylphosphines. Nevertheless, the cone angle can easily be tuned by substitution on

the aryl ring. This also changes the electronic nature of the ligand. PBn_3 is a stronger donor than PPh_3.[7]

The electronic component has been mostly ignored for our initial regression models and the study of ligand electronic effects is underdeveloped. There is already some indication in Tolman's work that a more electron-rich ligand (P(*p*-tolyl)$_3$ versus PPh_3) results in a higher alkene binding constant, at least for ethene.[8] This might also explain the difference between PPh(3,5-diTMSPh)$_2$ (**L14**, 40%) and PPh(3,5-di*t*BuPh)$_2$ (**L9**, 48%). Despite that **L14** is bulkier than **L9**, it is less electron-rich, at least based on Hammett parameters of –$SiMe_3$ versus –*t*Bu, σ_m = -0.04 and σ_m = -0-10, respectively.[9] Some examples of ligands that have remote steric hindrance and stronger donor properties are shown in **Figure 5.1**.
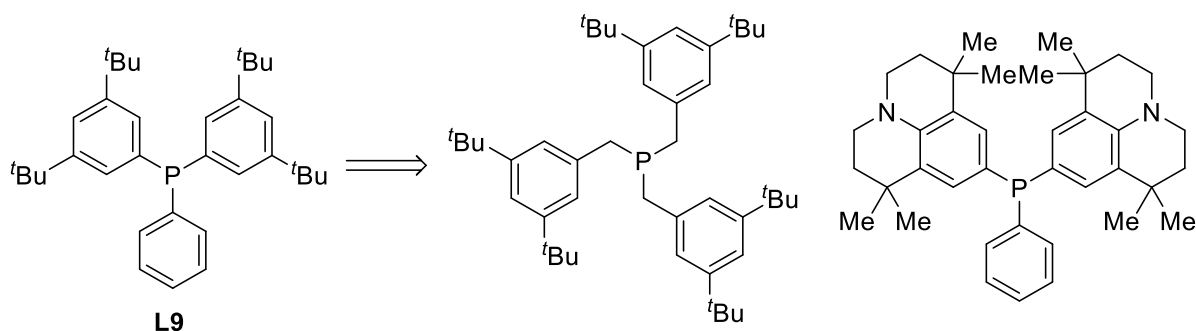
Figure 5.1. Ligand frameworks with large remote steric hindrance and higher donor abilities.

It could also be interesting to combine the approach of the 2nd and 3rd generation, strong π-acceptors and remote steric hindrance, respectively (**Figure 5.2**). While the strong π-accepting abilities of CF_3 groups might render the electronic nature of the alkene less dominant in terms of substrate binding (see chapter 4), the steric parameter space developed in the 3rd generation would modulate the binding affinity of the ligand such that no saturation of the catalyst occurs.
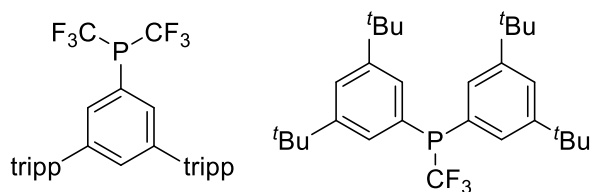

Figure 5.2. Proposed ligands that combine remote steric hindrance and strong π-accepting abilities.

Mechanistic investigations in chapter 3 have shown that amines have no influence on the cyclopropanation. Consistent with that observation, our 1st generation ligands with a hemilabile amino group had no beneficial influence on the yield. A likely explanation is that the nucleophilic amine is not reacting with the nucleophilic nickel carbene and thereby, no reversible trapping of the carbene occurs. By using an electrophilic arm, likely not hemilabile anymore with Ni(0), the carbene could be trapped such that no 'free' nickel carbene exists in solution (cf. Tebbe's reagent). An exemplary system is shown in **Figure 5.3**. Ambiphilic ligands combining both L- and Z-type ligands have found widespread interest, also in the context of catalysis.[10-11] A specific example for nickel is the reversible activation of H_2 across a Ni-B unit resulting in a bridged hydride, B-H-Ni.[12] This renders the B-ligand 'non-innocent' in the sense that it participates in the H_2 activation, or generally speaking in the transformation of the substrate or reagent as opposed to being purely a spectator ligand.
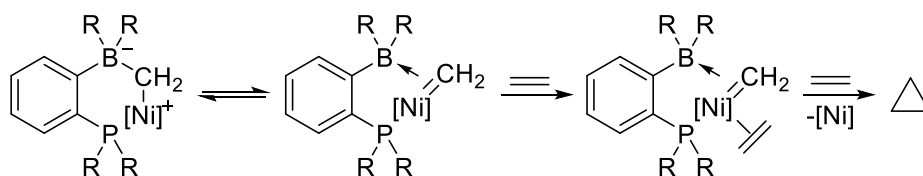

Figure 5.3. Proposed reversible trapping of nickel carbene by ambiphilic ligand.

A logical extension of this idea is the use of another metal as ligand or catalytic center in a dinuclear species. Besides mononuclear nickel carbene complexes, the Hillhouse group has also isolated dinuclear carbene species shown in **Figure 5.4**.[13] The geometry of the Ni-CPh2-Ni unit of **5.1Ph** in the crystal structure shows a pronounced asymmetry with respect to the nickel carbene fragment. One Ni-C is significantly shorter than the other by ca. 0.1 Å, while the other Ni center shows a close contact to the π-system of phenyl substituent on the carbene in an η^2 fashion (cf. **5.2**). Thus, the interaction should be thought of as the coordination of a nickel carbene to a second Ni center, rather than a truly bridging μ-CPh2 group. Interestingly, **5.1TMS** shows no such distortion in the solid-state with a symmetrically bridging μ-CH(TMS) group. Thus, it remains unknown whether the bonding asymmetry is a result of a secondary interaction with the π-system of the phenyl group or if the symmetry of **5.1TMS** is due to steric bulk of the TMS group not allowing a tilt of the carbene fragment without distorting the complex too much.

Another example we have already seen in the introduction (chapter 1). Uyeda and coworkers used a dinuclear nickel complex as catalyst for a cyclopropanation reaction. Changing the carbene source to diphenyl diazomethane allowed for the isolation of a bridged nickel carbene (**5.2**, **Figure 5.4**).[14] Analogous to **5.1Ph**, the Ni-CPh$_2$-Ni unit of **5.2** exhibits an asymmetry with a difference in Ni-C bond lengths of ca. 0.1 Å and a secondary η^2-interaction with the phenyl ring.

$R^1 = R^2 = Ph$ **5.1Ph**

$R^1 = H, R^2 = SiMe_3$ **5.1TMS**

5.2
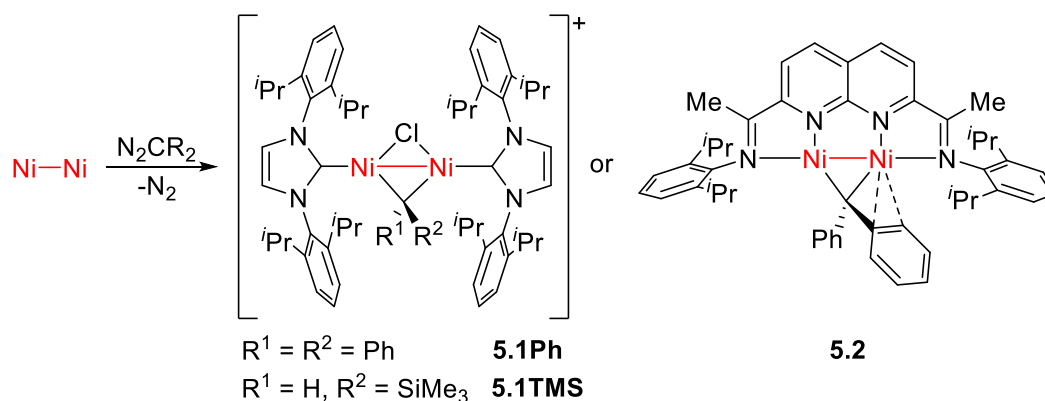
Figure 5.4. Examples of dinuclear nickel complexes with a bridging carbene.

The examples in **Figure 5.4** are arguably sterically less protected than the mononuclear nickel carbenes presented in the Introduction (chapter 1). It can be concluded that having a second metal center in close vicinity results in attenuated reactivity of the nickel carbene. Nevertheless, it has to be noted that both **5.1Ph** and **5.2** undergo carbene group transfer reaction with CO and ᵗBuNC, respectively, although, **5.2** did *not* cyclopropanate alkenes, not even ethene.[14]

The decreased steric protection of the ligand, yet unabated stability of the carbene, opens up the potential to study the carbene formation step in our system in detail. This step has so far been elusive in our hands (see chapter 3). The unequivocal, direct proof that a nickel carbene is formed from the ammonium ylide is unfortunately still a major missing piece in our mechanism. Thus, the reaction from a dimeric nickel species as shown in **Figure 5.5** would be an alternative approach to this challenge. Also, shifting the resting state to the metal carbene might, in general, offer different reactivity and selectivity for the cyclopropanation.
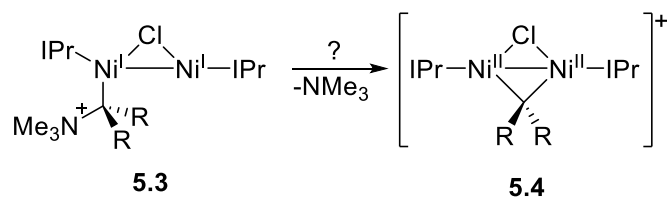
Figure 5.5. Potential formation of a stable, bridged nickel carbene from an ammonium ylide precursor.

The concept of a bimetallic catalyst could also be expanded to heterobimetallic systems. A very interesting report in this regard was recently published by Blum and coworkers.[15] They hypothesized that a carbophilic Lewis acid could activate an alkyne by lowering its LUMO (**Figure 5.5**, left) which allowed for an Au- and Pd-cocatalyzed vinylstannylation of alkynes. Both Au and Pd(0) were necessary for the catalysis to take place. Using only Pd(II) resulted in trace amounts of product. Even though a later mechanistic study favored the intermediacy of an Au-C σ-bond,[16] a conceptually similar example exists of $(Me_5C_5)_2Yb(\mu-C_2H_4)Pt(PPh_3)_2$.[17] A transfer of this concept to the current reaction would be interesting and is shown in **Figure 5.6** (middle). A heterobimetallic catalyst could activate both the ylide and the alkene substrate at the same time. Throughout this thesis, we have highlighted the substrate dependency and traced it, through literature precedent and our mechanistic studies, to the binding affinity of the substrate to Ni(0). This interaction is dominated by π-backbonding to the alkene LUMO. Thus, the proposed LUMO activation is an intriguing concept which could improve the cyclopropanation presented in this work.

In the context of Au, an isolated Au-ylide complex by Dr. Juan Manuel Sarria Toro (Chen group) is of great relevance (**Figure 5.6**, right).[18] This complex is exceedingly stable. Neither protic conditions (MeOH) nor cyclopropanation conditions at high temperature were reported to result in cyclopropanation or decomposition of the complex. Thus, it is possible that the ammonium ylide acts as a catalyst poison for the Lewis acid in this heterobimetallic system. Although, it should be noted that transmetallation between Au(I) and Ni, at least Ni(I) or Ni(II), is known in the context of cross-coupling.[19]
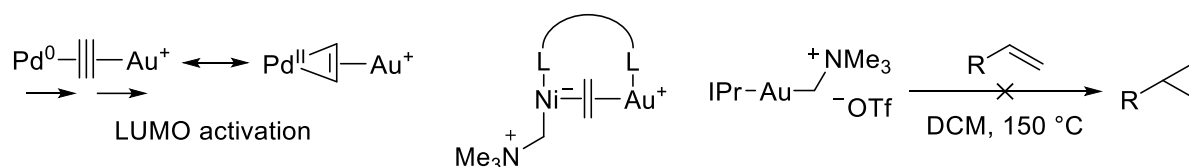
Figure 5.6. Left: LUMO activation by a carbophilic Lewis acid according to Blum (arrows depict push-pull arrangement).[15] Middle: Proposed heterobimetallic complex that activates both substrate and reagent. Right: Stable Au-ylide complex.

5.2.2 Ligand Screening

In section 5.2.1, we presented ligand parametrization and subsequent multivariate regression models as a rational way to understand and design an improved catalyst system for our cyclopropanation. Even though ligand descriptors can be calculated rather than experimentally determined, the initial training set to generate the model and the subsequent test set for verification purposes need to be synthesized. Thus, many interesting phosphines need to be first synthesized, often a laborious process, then separately tested to establish their performance. Of course, eventually the yield is the most direct quantity in which we are interested and the only value that determines if a ligand is good or bad.

Nevertheless, having our mechanistic data at hand, we can already speculate what might be a sign of a successful ligand, namely that an alkene binds strongly to the nickel-ligand complex. With this idea in mind, having a method that rapidly screens ligands with this feature could lead to a massive reduction in time consumption. Such an idea is presented in **Figure 5.7**.
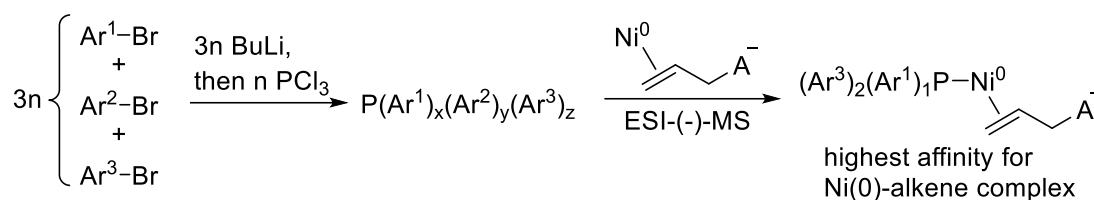

Figure 5.7. One-pot synthesize of phosphine library and subsequent binding affinity screening by ESI-MS.

First, a library of phosphines is synthesized by halogen-lithium exchange of a mixture of aryl bromides. Subsequent reaction with PCl_3 results in a statistical mixture of triarylphosphines. A mixture of this library together with an appropriate Ni(0) source and an anionic charge-tagged alkene is then analyzed by ESI-MS. Fishing out the $[(R_3P)Ni(alkene)]^-$ complex(es) identifies the candidate(s) that are worthwhile to synthesize separately and test in the reaction. This is an alternative and

complementary approach to the ligand parametrization model. Ligands can subsequently be fed into the training or test set.

Mass spectrometry-aided catalyst screening has been successfully applied including combinatorial catalyst preparation.[20-22]

Preliminary results have shown the triarylphosphine library generation to be straightforward but the subsequent analysis by ESI-MS to be problematic, as no Ni(0) was observed, even in the negative mode to prevent oxidation during the spray process. Indeed, throughout this work, no Ni(0) species has ever been observed by ESI-MS despite numerous attempts. While several examples are known for Pd(0) with anionic charge-tagged ligands,[23-25] the literature is ominously devoid of Ni(0) examples.

5.2.3 Substituted Methylene Transfer Reagents

The aim of this thesis was the use of tetramethylammonium salts as methylene donors for the cyclopropanation of unactivated alkenes. Part of our motivation was to circumvent the use of diazomethane due to its hazardous nature (see chapter 1). This severe drawback is present even for many substituted diazomethane compounds. Only the highly stabilized ethyldiazoacetate and similar, carbonyl-stabilized diazo reagents as well as trimethylsilyldiazomethane are commercially available and relatively stable.

The in situ formation of diazomethane has found widespread interest in the literature (see chapter 1) and the extension of this methodology to substituted diazomethane reagents has been noted. This includes the formation of F_3C-[26], F_2HC-[27], EtO_2C-[28], NC-substituted[29] diazomethane and subsequently their reaction with alkenes to give the corresponding cyclopropanes. Unfortunately, the substrate scope for these reactions is commonly limited to styrenes.

Therefore, it is of general synthetic interest to introduce substituted methylene units to obtain cyclopropanes with a more diverse substitution pattern than from this limited set of reagents and alkene substrates. This would especially be the case, if shelf-stable reagents were available. Substituted tetramethylammonium salts might offer such an alternative (**Figure 5.8**).
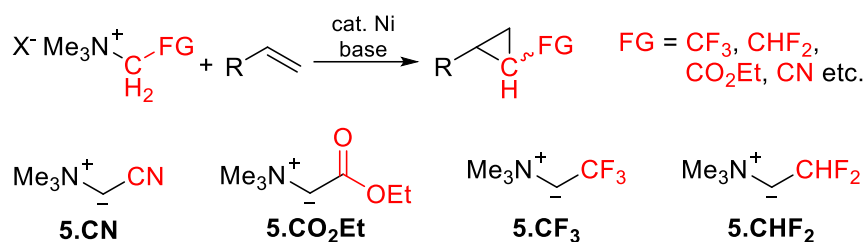
Figure 5.8. Functional group bearing tetramethylammonium reagents to synthesize functionalized cyclopropanes.

Several issues potentially arise from such a reagent in the context of our reaction, namely, the question of transfer selectivity, stability of the ylide, and the reactivity with Ni(0). If the selectivity were to be thermodynamically controlled, one would expect the most stable anionic site to be transferred. In our case, this would conveniently be the functional group-substituted carbon. The resonance stabilized ylides **5.CN** and **5.CO₂Et** have the strongest conjugate acids with pK_a values of 20.6 (-CN) and 20.0 (-CO₂Et) in DMSO, respectively.[30] The pK_a of NMe_4^+ was estimated by extrapolation to give a value of 42. Deprotonation at the substituted site is therefore thermodynamically highly favored. Although the acidities for the F_3C- and F_2HC-substituted tetramethylammonium salts are not known, they should still be considerably acidified through an inductive effect.

In chapter 1, we discussed the interaction of the ylide with Ni(0) as a push-pull system, i.e., the stability of the adduct is partly determined by the σ-donation/nucleophilicity of the ylide. The least nucleophilic ylide studied by Pörschke et al. in this context is the sulfoxonium ylide $[Me_2S(O)CH_2]$ with a pK_a of 18.2. At least in the solid state upon (violent) decomposition at 0 °C, $[Me_2S(O)CH_2]Ni(C_2H_4)_2$ is capable of forming cyclopropane.[31] Thus, for the above-proposed substituted ammonium ylides an interaction with Ni(0) is predicted based upon their pK_a.

A third issue can be identified as the likely instability of the fluorine-substituted ylides **5.CF₃** and **5.CHF₂** without resonance stabilization. β-F elimination is a potential decomposition pathway that might prohibit the use of these reagents.

In a similar vein, carboxylate (betaine) or redox-active ester substituted ammonium salts might open up the possibility of ylide generation via photocatalysis. The combination of photocatalysis and traditional transition metal-catalyzed reactions have found an enormous interest in the past years. A seminal publication with respect to the present case is a dual catalytic cross-coupling of carboxylic acids and aryl halides

(**Figure 5.9**, left).[32] The Ir photocatalyst is proposed to decarboxylate the substrate to give a radical intermediate that is trapped by a nickel(II) aryl species, which has formed by oxidative addition of the aryl halide. Reductive elimination closes the cycle. The reaction is proposed to go through a Ni(0)/Ni(II)/Ni(III)/Ni(I) cycle. With this precedent, there might be a chance that, if the ylide radical can be generated (**Figure 5.9**, right), it will be captured by Ni^n and possibly react further to the carbene in a Ni(I)/Ni(III) cycle.
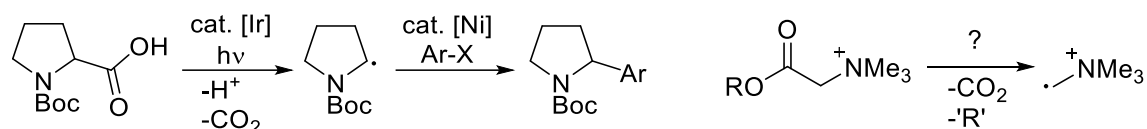
Figure 5.9. Left: Photodecarboxylation and subsequent cross-coupling under Ir/Ni catalysis.[32] Right: Potential formation of the trimethylammonium methyl radical from a carboxylic acid or redox-active ester precursor.

There is at least one example in the literature for the decarboxylation of betaine ($O_2CCH_2NMe_3$, inner salt) using a stoichiometric amount of Fe(III) porphyrin and a high-intensity Xenon light source (300 W, $\lambda > 390$ nm).[33] Although, preliminary results using typical 'modern' photoredox conditions (Ir, Ru, and organic-based photocatalysts and white LEDs) have not led to any cyclopropanation, finding photodecarboxylation conditions would offer many benefits inherent in these types of transformations. Especially the circumvention of a strongly basic and nucleophilic organolithium reagent should be highlighted and holds great promise.

5.3   References

1. Ananikov, V. P. *ACS Catalysis* **2015,** *5*, 1964-1971.
2. Brethome, A. V.; Fletcher, S. P.; Paton, R. S. *Acs Catalysis* **2019,** *9*, 2313-2323.
3. Durand, D. J.; Fey, N. *Chemical reviews* **2019**.
4. Zhao, S.; Gensch, T.; Murray, B.; Niemeyer, Z. L.; Sigman, M. S.; Biscoe, M. R. *Science* **2018,** *362*, 670-674.
5. Santiago, C. B.; Guo, J.-Y.; Sigman, M. S. *Chemical Science* **2018,** *9*, 2398-2412.
6. Raders, S. M.; Moore, J. N.; Parks, J. K.; Miller, A. D.; Leißing, T. M.; Kelley, S. P.; Rogers, R. D.; Shaughnessy, K. H. *The Journal of organic chemistry* **2013,** *78*, 4649-4664.
7. Tolman, C. A. *Chem. Rev.* **1977,** *77*, 313-348.
8. Tolman, C. A.; Seidel, W. C.; Gerlach, D. H. *J. Am. Chem. Soc.* **1972,** *94*, 2669-2676.
9. Hansch, C.; Leo, A.; Taft, R. W. *Chem. Rev.* **1991,** *91*, 165-195.
10. Bouhadir, G.; Bourissou, D. *Chemical Society Reviews* **2016,** *45*, 1065-1079.
11. You, D.; Gabbaï, F. P. *Trends in Chemistry*.
12. Harman, W. H.; Peters, J. C. *J. Am. Chem. Soc.* **2012,** *134*, 5080-5082.
13. Laskowski, C. A.; Hillhouse, G. L. *Chemical Science* **2011,** *2*, 321.

14. Maity, A. K.; Zeller, M.; Uyeda, C. *Organometallics* **2018,** *37*, 2437-2441.

15. Shi, Y.; Peterson, S. M.; Haberaecker, W. W.; Blum, S. A. *J. Am. Chem. Soc.* **2008,** *130*, 2168-2169.

16. Shi, Y.; Ramgren, S. D.; Blum, S. A. *Organometallics* **2009,** *28*, 1275-1277.

17. Burns, C. J.; Andersen, R. A. *J. Am. Chem. Soc.* **1987,** *109*, 915-917.

18. Sarria Toro, J. M. Discovery, Development and Study of Carbenoid Mediated Reactions From Olefin. ETH Zürich, 2014.

19. Hirner, J. J.; Blum, S. A. *Organometallics* **2011,** *30*, 1299-1302.

20. Chen, P. *Angewandte Chemie International Edition* **2003,** *42*, 2832-2847.

21. Fleischer, I.; Pfaltz, A. **2010,** *16*, 95-99.

22. Isenegger, P. G.; Bachle, F.; Pfaltz, A. *Chemistry* **2016,** *22*, 17595-17599.

23. Janusson, E.; Zijlstra, H. S.; Nguyen, P. P. T.; MacGillivray, L.; Martelino, J.; McIndoe, J. S. *Chemical Communications* **2017,** *53*, 854-856.

24. Vikse, K. L.; Henderson, M. A.; Oliver, A. G.; McIndoe, J. S. *Chemical Communications* **2010,** *46*, 7412-7414.

25. Vikse, K. L.; Woods, M. P.; McIndoe, J. S. *Organometallics* **2010,** *29*, 6615-6618.

26. Morandi, B.; Carreira, E. M. *Angewandte Chemie International Edition* **2010,** *49*, 938-941.

27. Hock, K. J.; Mertens, L.; Koenigs, R. M. *Chemical Communications* **2016,** *52*, 13783-13786.

28. Morandi, B.; Dolva, A.; Carreira, E. M. *Org. Lett.* **2012,** *14*, 2162-2163.

29. Hock, K. J.; Spitzner, R.; Koenigs, R. M. *Green Chemistry* **2017,** *19*, 2118-2122.

30. Zhang, X. M.; Bordwell, F. G. *J. Am. Chem. Soc.* **1994,** *116*, 968-972.

31. Pörschke, K.-R. *Chemische Berichte* **1987,** *120*, 425-427.

32. Zuo, Z.; Ahneman, D. T.; Chu, L.; Terrett, J. A.; Doyle, A. G.; MacMillan, D. W. *Science* **2014,** *345*, 437-440.

33. C. Gilbert, B.; R. Lindsay Smith, J.; F. Parsons, A.; K. Setchell, P. *Journal of the Chemical Society, Perkin Transactions 2* **1997**, 1065-1074.

6 Experimental Part

Parts of this chapter have been published as the Supporting Information for and figures adapted or reprinted with permission from:

Künzi, S. A.; Sarria Toro, J. M.; den Hartog, T.; Chen, P. Nickel-Catalyzed Cyclopropanation with NMe$_4$OTf and nBuLi. *Angew. Chem. Int. Ed.* **2015**, *54*, 10670-106704.

Künzi, S. A.; Gershoni-Poranne, R.; Chen, P. Mechanistic Studies on the Nickel-Catalyzed Cyclopropanation with Lithiomethyltrimethylammonium Triflate. *Organometallics* **2019**, *38*, 1928-1938.

6.1 General Methods

Note: All flasks and glass-coated stir bars (self-made or commercially available) used for cyclopropanation reactions were cleaned consecutively in a KOH/^{i}PrOH base bath, *aqua regia* and dried overnight in an oven at 150 °C. As noted previously, the lithiomethyl trimethylammonium reagent is prone to decomposition even when low concentrations of undesired trace metals are present in the reaction mixture.[1] Additionally, all cyclopropanation reactions were conducted in a closed Schlenk flask to allow no gas exchange, unless noted otherwise.

All reactions were conducted in a glove box with N$_2$-atmosphere or using standard Schlenk techniques under Ar if not noted otherwise.[2]

Concentration of solutions of air-stable compounds was conducted using a rotary evaporator at 40 °C. ^{1}H, ^{13}C, ^{31}P and ^{19}F NMR spectra were recorded at 300 or 400 MHz (Bruker AV300 or AVIII400 spectrometers).

Chemical shifts were determined relative to the residual solvent peaks. The following abbreviations are used to indicate signal multiplicity: s, singlet; d, doublet; t, triplet; q, quartet; m, multiplet. GC-FID analysis was performed on a Finnigan Focus CG with a Zebron ZB-5MS, 30m*0.25 mm column. Headspace analysis was performed on a Thermo Scientific Trace1300 GC/ISQ Single Quad MS with a Phenomenex Zebron ZB-1MS (60 m) column using a isothermal temperature program at 40 °C by Daniel

Zindel (LPC, ETH Zürich). UV-Vis measurements were performed on a Hitachi U-2010 spectrophotometer. IR spectra were recorded on a PerkinElmer FT-IR spectrometer Spectrum Two with ATR cell. GPC analysis was performed on a Polymer Laboratories PL GPC-220 with a PLgel 5 µm MIXED-D column using 1,2,4-trichlorobenzene as eluent at 150 °C. Elemental analyses and high resolution mass spectrometry were performed by the Molecular and Biomolecular Analysis Service MoBiAS, ETH Zürich. Anhydrous THF was distilled from Na/benzophenone under N_2 prior to use. Anhydrous THF-d_8 was distilled from CaH_2 under Ar and degassed by freeze-pump-thaw cycles prior to use.

Dibromobis(triphenylphosphine)nickel(II) (99%) was purchased from Sigma-Aldrich, stored in the glove box and used as received. *n*-BuLi (2.0 M in cyclohexane or 1.6 M in hexanes) was purchased from Sigma-Aldrich and used as received. Cyclooctene was purchased from Sigma-Aldrich (95%) or TCI (>95%), distilled from Na under Ar and degassed by freeze-pump-thaw cycles prior to use. Cyclohexene was purchased from Sigma-Aldrich (≥99%), distilled from Na under Ar and degassed by freeze-pump-thaw cycles prior to use. Norbornene (99%) and 4-phenyl-1-butene (99%) were purchased from Sigma-Aldrich, stored in the glove box and used as received. Commercial 3,4-dihydro-2*H*-pyrane was distilled prior to use. α-Pinene (98%) was purchased from Sigma-Aldrich and used as received. Trimethylamine (1 M in THF) was purchased from Acros. Cyclooctane was purchased from TCI and used as received. *n*-Undecane (≥ 99.8%, analytical standard) was purchased from Fluka and used as received. Tetramethylammonium chloride (≥ 98%) was purchased from Sigma-Aldrich, dried under vacuum and stored in the glove box. Iodomethane-[13]C (99 atom% [13]C) was purchased from Sigma-Aldrich and used as received. Tetramethyl-d_{12}-ammonium chloride was purchased from Cambridge Isotope Laboratories (98%) or Sigma-Aldrich (98 atom % D), dried under vacuum, and used immediately or stored in the glove box. Silver(I) trifluoromethanesulphonate was purchased from ABCR (99%) or TCI (>98.0%) and used as received. PBnPh$_2$ (99%) was purchased from Strem, stored in the glove box and used as received.

All other chemicals were purchased from commercial suppliers and used as received. Authentic products, exo-tricyclo[3.2.1.0[2,4]]octane, bicyclo[6.1.0]nonane, bicyclo[4.1.0]heptane, and hexylcyclopropane, were prepared following reported procedures and matched reported data.[3-5]

Juan Manuel Sarria Toro and Tim den Hartog (Chen group) are thanked for the preparation of exo-tricyclo[3.2.1.0^{2,4}]octane, bicyclo[6.1.0]nonane, and (2-cyclopropylethyl)benzene and their GC calibration curves and [NMe$_4$]BArF$_{24}$.

Augustin A. S. W. Tchawou (Chen group) is thanked for the preparation of authentic heptylcyclopropane and its GC calibration curve.[6]

Tetramethylammonium triflate was prepared as reported previously, dried under vacuum and stored in the glove box.[1, 3]

Ammonium salts were synthesized by exhaustive methylation with MeI and/or subsequent anion exchange with AgOTf.

Ligands **L1** and **L2** were synthesized according to known procedure.[7-8] **L3** is commercially available.

Ligands **L4** to **L7** were synthesized from their respective phenoxy precursors with TMSCF$_3$/CsF or TMSC$_2$F$_5$/CsF via a known procedure.[9] The purification of **L4** and **L5** from by-products proved difficult. The products were obtained heavily contaminated with most likely PhOTMS. (**L5**)$_2$Ni(cod) and Ni(**L4**)$_2$ were used as crude products but with much less contamination.

Ligands **L8** to **L16** were synthesized by halogen-lithium exchange with BuLi and the appropriate aryl halide at -78 °C and subsequent addition of PCl$_n$Ph$_{3-n}$.

5'-Bromo-2,2'',4,4'',6,6''-hexaisopropyl-1,1':3',1''-terphenyl, 3,5-bis(trimethylsilyl) bromobenzene and 3,5-bis(triethylsilyl) bromobenzene were synthesized according to literature procedures.[10-11] Bis(3,5-di-tert-butyl-4-methoxyphenyl)chlorophosphine is commercially available.

All data was analyzed with Microsoft Excel 2016 and/or OriginLab OriginPro 2016 or 2019.

6.2   Standard Conditions for Cyclopropanation

Inside the glove box, an oven-dried 5 mL Schlenk flask equipped with a Teflon tap and a glass-coated stir bar was charged with [NMe$_4$]OTf (22.3 mg, 0.1 mmol, 1 equiv), alkene (0.5 mmol, 5 equiv), catalyst in THF (prepared as stock solution), and THF (tot. vol. THF: 2 mL, 0.05 M). The flask was removed from the glove box, cooled to 0 °C in an ice/water bath, and BuLi (0.105 mmol, 1.05 equiv; 2 M in cyclohexane or 1.6 M in hexanes) was added dropwise via micro syringe under a counterflow of Ar. The flask

was sealed (no gas exchange). After 16 h (or overnight), undecane (10 µL; internal standard) was added and an aliquot (ca. 0.2 mL) was partitioned between 2 mL pentane and 2 mL water. After vigorous mixing of the aliquot with a vortex mixer, the organic phase was filtered through a plug of $MgSO_4$ and analyzed by GC-FID. The yield was determined by the integral ratio of the product versus undecane as internal standard using a previously determined calibration curve.

6.3 In Situ and Preformation of Lithiomethyltrimethylammonium Triflate for Kinetic Measurements
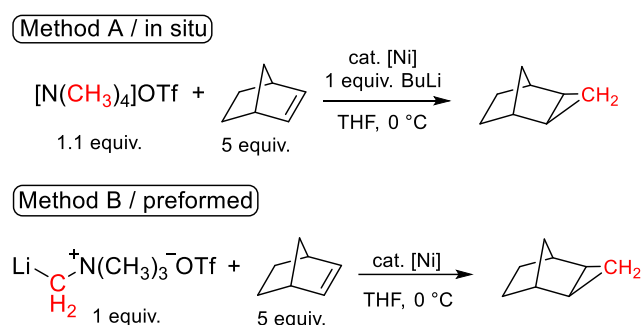
Figure 6.1. Two different methods employed to generate the active reagent [LiCH$_2$NMe$_3$]OTf, either after (A) or before (B) addition of catalyst.

We used two different Methods, A and B, that differ in the generation of the ammonium ylide reagent, either in situ (A) or preformed (B).

For method A, [NMe$_4$]OTf (1.1 equiv), alkene and catalyst were mixed together, cooled to 0 °C, then BuLi (1 equiv) was added to form the ylide in situ. Under these conditions, a small induction phase was observed, most likely due to a non-instantaneous deprotonation of the not fully soluble ammonium salt in THF.

For method B, the ammonium salt was deprotonated first (in the *presence or absence of alkene*) before the catalyst was added to the preformed ylide to initiate the cyclopropanation/ylide decomposition. In this case, no induction phase was observed.

In general, we had opted to use method A due to the more convenient reaction set up. In cases where we studied the consumption of ylide, method B was used to simplify the kinetics by having the maximum concentration of ylide present upon addition of catalyst.

We have only observed two significant differences between method A and B. For method A, we observe a small induction phase due to the deprotonation as mentioned above. Method B appears to form a smaller amount of active catalyst, likely due to the reduction with the ylide itself instead of BuLi. A more detailed discussion of the tetramethylammonium deprotonation can be found in section 6.23.

6.3.1 General Kinetic Protocol - Method A (Direct Deprotonation)

Inside the glove box, an oven-dried 50 mL Schlenk flask equipped with a J. Young inlet valve, glass stopper, screw cap with septum and a glass-coated stir bar was charged with [NMe$_4$]OTf (245.5 mg, 1.1 mmol, 1.1 equiv), (Ph$_3$P)$_2$NiBr$_2$ or Ni(PPh$_3$)$_4$ in THF (prepared as stock solution, added dropwise by difference with a 2.5 mL gastight Hamilton syringe (previously dried at 50 °C in a vacuum oven)) and norbornene (471 mg, 5.0 mmol, 5 equiv). The flask was removed from the glove box and attached to a Schlenk line. Dry THF (x mL THF + (catalyst in THF) mL = 19.5 mL THF) was added via syringe. Undecane (50 μL) was added via a 50 μL micro syringe as internal standard. The flask was immersed in an ice bath and the reaction allowed to equilibrate (over ca. 20 min).

Then, an aliquot (ca. 0.2 mL) was taken with a disposable 1 mL plastic syringe (flushed several times with Ar) and immediately quenched by injection into 2 mL H$_2$O / 2 mL pentane (t = 0 min).

BuLi (500 μL, 1 mmol, 1 equiv; 2 M in cyclohexane) was added dropwise over ca. 30 s via a 1 mL gastight Hamilton syringe (by difference; previously dried at 50 °C in a vacuum oven) (t = 0 min with first drop).

After the addition was completed, the flask was sealed/closed to the Schlenk line again and only opened when an aliquot was taken.

After vigorous mixing of the aliquot with a vortex mixer, the organic phase was filtered through a plug of MgSO$_4$ and analyzed by GC-FID. The yield was determined by the integral ratio of the product versus undecane as internal standard using a previously determined calibration curve.

6.3.2 General Kinetic Protocol - Method B (Preformed Ylide)

Inside the glove box, an oven-dried 50 mL Schlenk flask equipped with a J. Young inlet valve, glass stopper, screw cap with septum and a glass-coated stir bar was charged

with [NMe₄]OTf (245.5 mg, 1.1 mmol, 1.1 equiv) and norbornene (471 mg, 5.0 mmol, 5 equiv). The flask was removed from the glove box and attached to a Schlenk line. Dry THF (x mL THF + (catalyst in THF) mL = 19.5 mL THF) was added via syringe. Undecane (50 μL) was added via a 50 μL micro syringe as internal standard. The flask was immersed in an ice bath and the reaction allowed to equilibrate (over ca. 20 min). BuLi (500 μL, 1 mmol, 1 equiv; 2 M in cyclohexane) was added dropwise over ca. 30 s via a 1 mL gastight Hamilton syringe (by difference; previously dried at 50 °C in a vacuum oven). The flask was sealed/closed to the Schlenk line unless reagents were added or aliquots collected.

After 15 min, an aliquot (ca. 0.2 mL) was taken with a disposable 1 mL plastic syringe (flushed several times with Ar) and immediately quenched by injection into 2 mL H₂O / 2 mL pentane (t = 0 min).

Then, (Ph₃P)₂NiBr₂ or Ni(PPh₃)₄ (x mol%) in THF (prepared as stock solution inside the glove box) was added dropwise by difference with a 2.5 mL gastight Hamilton syringe (previously dried at 50 °C in a vacuum oven) over ca. 30 s (t = 0 min with first drop). After the addition was completed, the flask was sealed/closed to the Schlenk line again and only opened when an aliquot was taken.

After vigorous mixing of the aliquot with a vortex mixer, the organic phase was filtered through a plug of MgSO₄ and analyzed by GC-FID. The yield was determined by the integral ratio of the product versus undecane as internal standard using a previously determined calibration curve.

6.4   Kinetic Measurements of Norbornene Cyclopropanation with (Ph₃P)₂NiBr₂ – Method A (Direct Deprotonation)
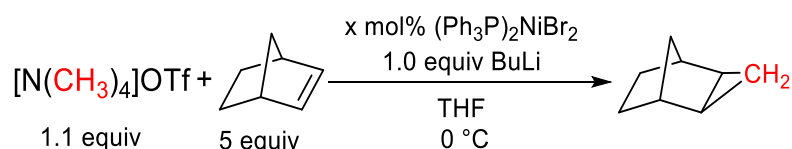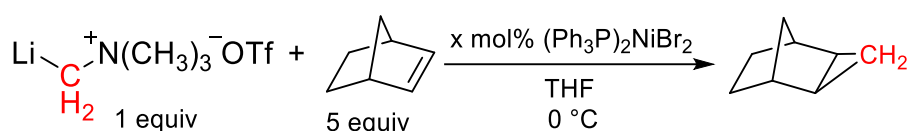

Figure 6.2. Reaction scheme for the determination of the order in catalyst using Method A.

The reaction was conducted according to Method A in section 6.3.1. Reaction profiles and the order plot are shown in **Figure 6.3**.
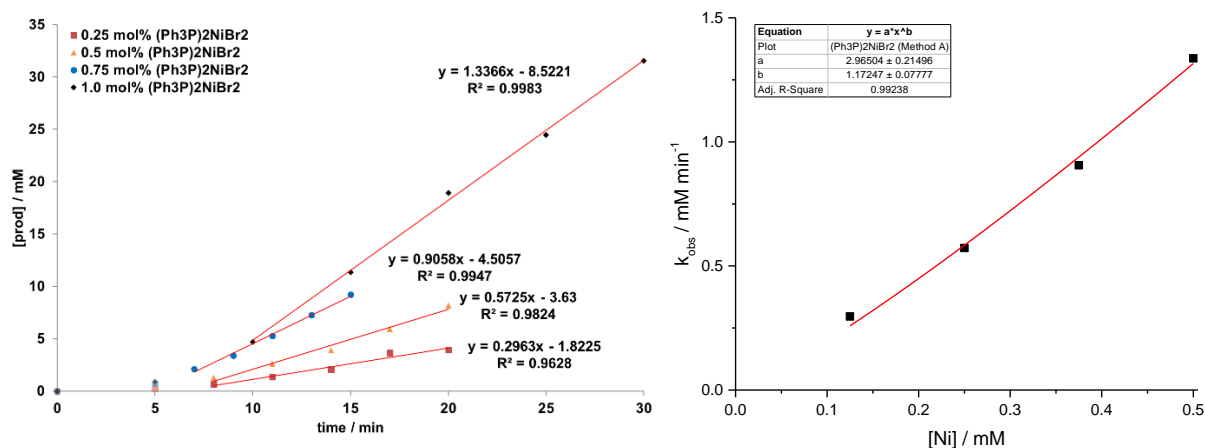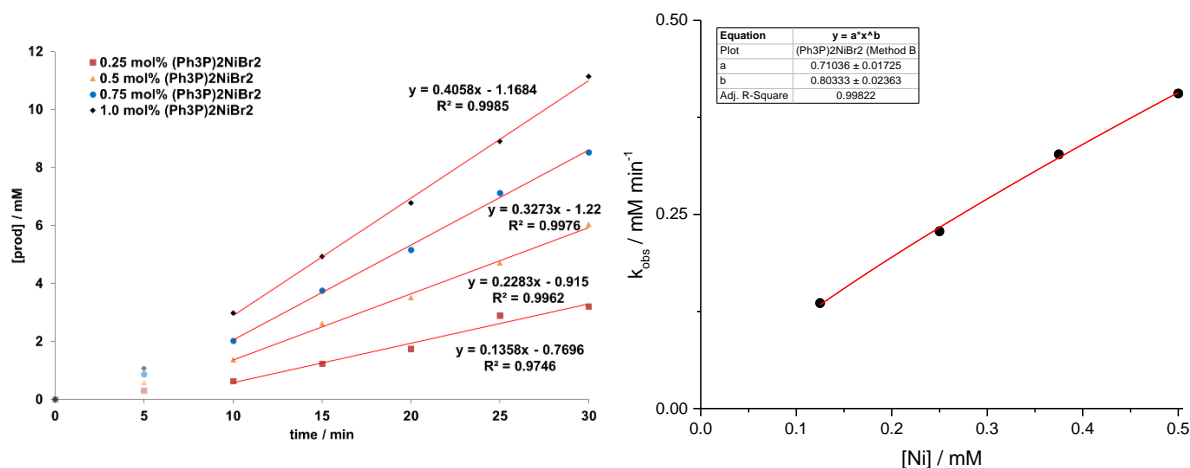
Figure 6.3. Left: Plot of time versus product concentration for four different catalyst concentrations of $(Ph_3P)_2NiBr_2$. The red lines depict an initial rate fit with omission of the first few data points of the induction phase (lightly shaded) to obtain k_{obs}. Right: Plot of the catalyst concentration [Ni] of $(Ph_3P)_2NiBr_2$ versus k_{obs} for product formation with in situ deprotonation (Method A). The red curve depicts a fit to the function $y = ax^b$ to establish the order in [Ni], $b = 1.17 \pm 0.08$.

6.5 Kinetic Measurements of Norbornene Cyclopropanation with $(Ph_3P)_2NiBr_2$ – Method B (Preformed Ylide)
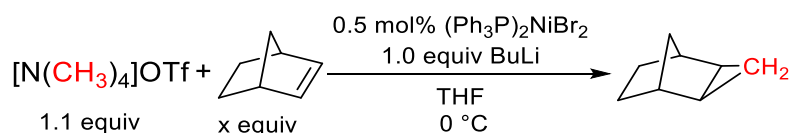

Figure 6.4. Reaction scheme for the determination of the order in catalyst using Method B.

The reaction was conducted according to Method B in section 6.3.2. Reaction profiles and the order plot are shown in **Figure 6.5**.
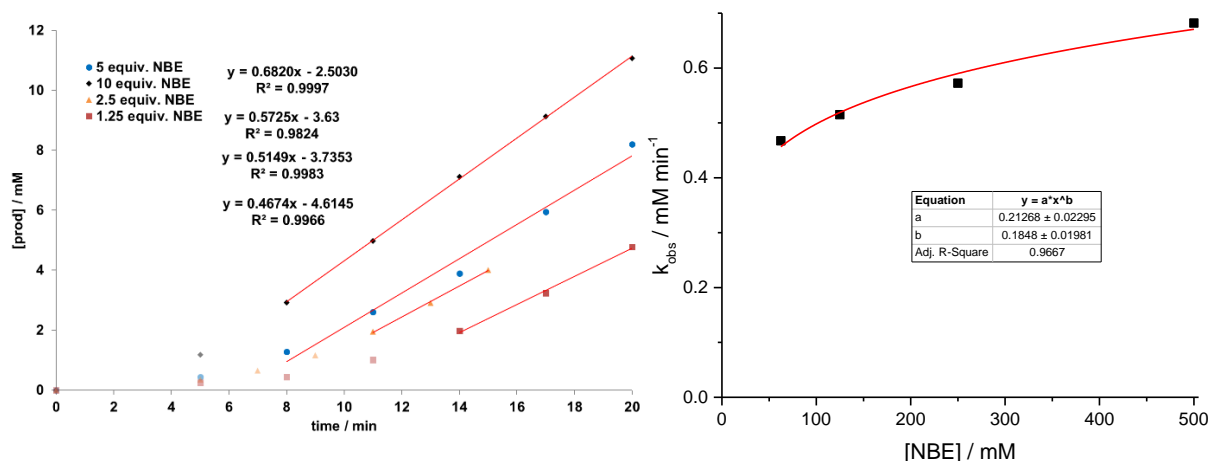
Figure 6.5. Left: Plot of time versus product concentration for four different catalyst concentrations of $(Ph_3P)_2NiBr_2$. The red lines depict an initial rate fit with omission of the first few data points of the induction phase (lightly shaded) to obtain k_{obs}. Right: Plot of the catalyst concentration [Ni] of $(Ph_3P)_2NiBr_2$ versus k_{obs} for product formation using the preformed ylide (Method B). The red curve depicts a fit to the function $y = ax^b$ to establish the order in [Ni], $b = 0.80 \pm 0.02$.

6.6 Determination of Secondary KIE with [N(CD_3)_4]OTf – Method A
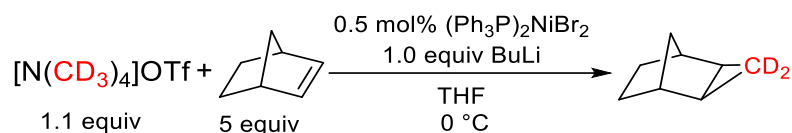
Figure 6.6. Reaction scheme for the determination of a secondary KIE using $[N(CD_3)_4]OTf$.

The reaction was conducted according to Method A in section 6.3.1 with $[N(CD_3)_4]OTf$ (258.8 mg, 1.1 mmol, 1.1 equiv). The same response factor for the product-d_2 was assumed. Reaction profiles are shown in **Figure 6.7** and the secondary KIE is shown in **Table 6.1**.
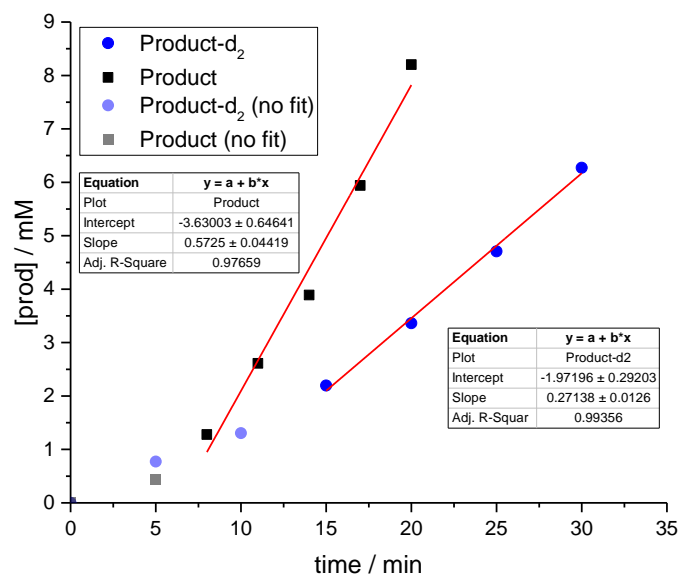
Figure 6.7. Plot of time versus product concentration using tetramethylammonium triflate or tetramethylammonium-d$_{12}$ triflate to probe a possible secondary KIE. The red lines depict an initial rate fit with omission of the first few data points of the induction phase (lightly shaded) to obtain k_{obs}, i. e. k_H and k_D, for the protiated and deuterated tetramethylammonium reagent, respectively.

Table 6.1. Determination of the Secondary KIE using Tetramethylammonium-d12 Triflate.

k_H / mM min^{-1}	k_D / mM min^{-1}	k_H/k_D
0.57 ± 0.04	0.27 ± 0.01	2.1 ± 0.3

## 6.7 Kinetic Measurements of Norbornene Cyclopropanation with (Ph$_3$P)$_2$NiBr$_2$ – Order in NBE

Figure 6.8. Reaction scheme for the determination of the order in norbornene.

The reaction was conducted according to Method A in section 6.3.1. Reaction profiles and the order plot are shown in **Figure 6.9**.
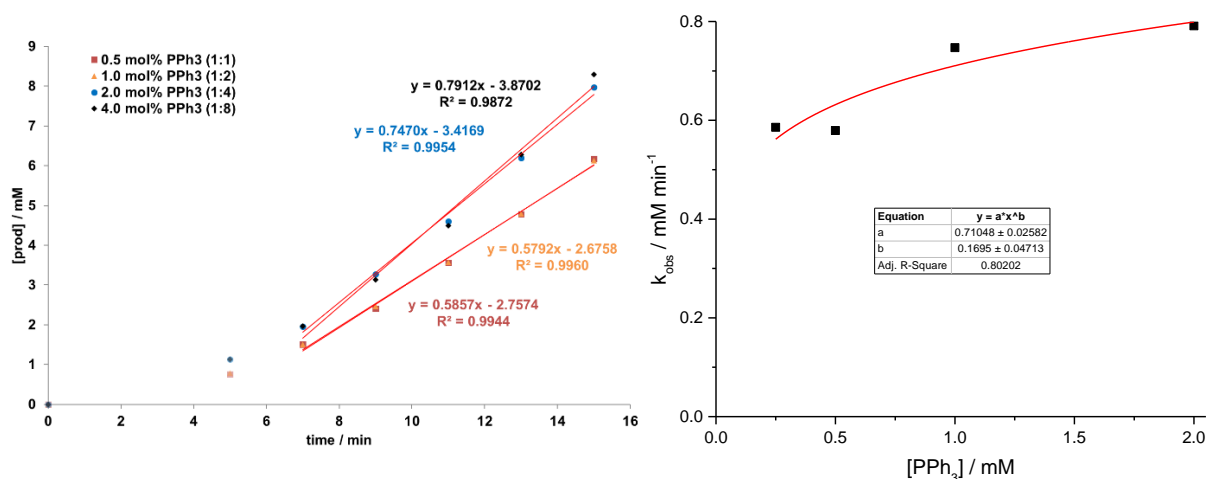
Figure 6.9. Left: Plot of time versus product concentration for four different norbornene (NBE) concentrations. The red lines depict an initial rate fit with omission of the first few data points of the induction phase (lightly shaded) to obtain k_{obs}. Right: Plot of the norbornene concentration [NBE] versus k_{obs} for product formation. The red curve depicts a fit to the function $y = ax^b$ to establish the order in [NBE], $b = 0.18 \pm 0.02$.

## 6.8 Kinetic Measurements of Norbornene Cyclopropanation with Ni(acac)$_2$/PPh$_3$ – Order in PPh$_3$
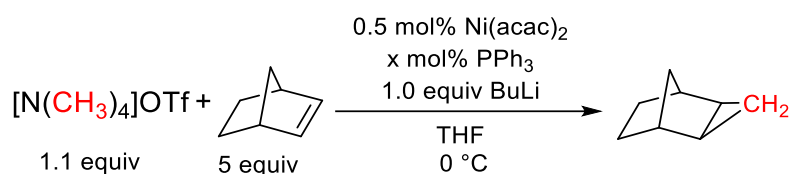
Figure 6.10. Reaction scheme for the determination of the order in PPh$_3$.

The reaction was conducted according to Method A in section 6.3.1 with a PPh$_3$ stock solution. Reaction profiles and the order plot are shown in **Figure 6.11**.

Figure 6.11. Left: Plot of time versus product concentration for four different triphenylphosphine concentrations with constant nickel concentration. The black lines depict an initial rate fit with omission of the first few data points of the induction phase (lightly shaded) to obtain k_{obs}. Right: Plot of the triphenylphosphine concentration [PPh3] versus k_{obs} for product formation. The red curve depicts a fit to the function $y = ax^b$ to establish the order in [PPh3], $b = 0.17 \pm 0.05$.

6.9 Kinetic Measurements of Norbornene Cyclopropanation with (Ph₃P)₂NiBr₂ – Method B (Preformed Ylide) – Order in Ylide
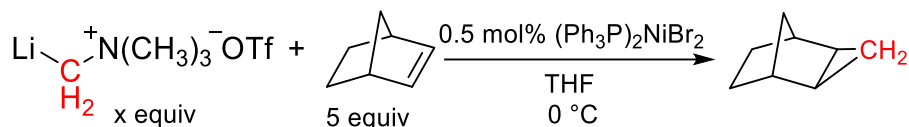
Figure 6.12. Reaction Scheme for the determination of the order in ylide using Method B.

The reaction was conducted according to Method B in section 6.3.2 with [NMe₄]OTf ((x+0.1) mmol, (x + 0.1) equiv) and BuLi (x mmol, x equiv; 2 M in cyclohexane). The order plot is shown in chapter 3.

The order in ylide shows a complex behavior which can be appreciated by the work of Pörschke et al. regarding the Lewis acidic nature of Ni(0).[12-14] The stability of the Ni(0) adduct depends on the nucleophilicity of the carbanion to and the (π-)acceptor strength of the ligands in a temperature-dependent equilibrium. The qualitative order was given as LiCH₃ > [Me₃PCH₂] > [Ph₃PCH₂] > [Me₂(O)SCH₂] for the carbanion and as Ni(CO)₃ > Ni(C₂H₄)₂ > Ni(CDT) for the Ni(0) fragment (CDT = *all-trans*-1,5,9-Cyclododecatriene).[12-14]

From this one can assume that the ylide binding is affect by the alkene and its concentration, the ylide concentration and the ancillary ligand without changing the turnover-limiting transition state.

117

This can be observed by the reaction profile for the consumption of ylide in the *absence* of substrate. The reaction follows a well-behaved 1st order decay (**Figure 6.14**) due to the weak acceptor fragment Ni(0)(PPh$_3$)$_2$ and the ylide not coordinated in the resting state. With a relatively strong π-acceptor, norbornene, the reaction rate is longer constant for product formation than one would expect for a simple 1st order dependence on ylide (see, e.g., **Figure 6.17**) with a switch from 0th to 1st order in ylide at high conversion.

6.10 Kinetic Measurements of Ylide decomposition / Homocoupling with Ni(PPh$_3$)$_4$ in the Absence of Alkene
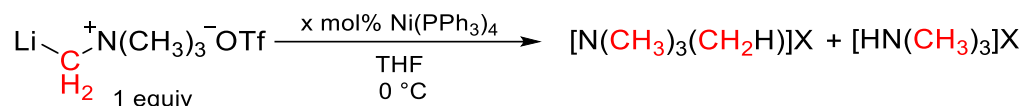
Figure 6.13. Reaction scheme for the determination of the order in catalyst in the absence of added alkene.

The reaction was conducted according to a modified version of Method B in section 6.3.2.

Inside the glove box, an oven-dried 50 mL Schlenk flask equipped with a J. Young inlet valve, glass stopper, screw cap with septum and a glass-coated stir bar was charged with [NMe$_4$]OTf (245.5 mg, 1.1 mmol, 1.1 equiv). The flask was removed from the glove box and attached to a Schlenk line. Dry THF (x mL + (catalyst in THF) mL = 19.5 mL THF) was added via syringe. Cyclooctane (100 μL) was added via a 100 μL micro syringe as internal standard. The flask was immersed in an ice bath and the reaction allowed to equilibrate (over ca. 20 min).

BuLi (500 μL, 1 mmol, 1 equiv; 2 M in cyclohexane) was added dropwise over ca. 30 s via a 1 mL gastight Hamilton syringe (by difference; previously dried at 50 °C in a vacuum oven). The flask was sealed/closed to the Schlenk line unless reagents were added or aliquots collected.

After 15 min, an aliquot (ca. 0.2 mL) was taken with a disposable 1 mL plastic syringe (flushed several times with Ar) and immediately quenched by injection into 0.2 mL 1 M TFA in DCM (t = 0 min).

Then, Ni(PPh$_3$)$_4$ (x mol%) in THF (prepared as stock solution inside the glove box) was added dropwise by difference with a 2.5 mL gastight Hamilton syringe (previously dried at 50 °C in a vacuum oven) over ca. 30 s (t = 0 min with first drop). After the addition

118

was completed, the flask was sealed/closed to the Schlenk line again and only opened when an aliquot was taken.

Aliquots were diluted with 0.3 mL CD_3OD and analyzed by ^1H NMR. Spectra were subsequently analyzed with MestReNova. The integrated 'Full Auto (Bernstein Polynomials)' baseline correction was applied. The spectrum was referenced to the residual solvent peak of CD_3OD ($\delta = 3.31$). Signals of cyclooctane ($\delta = 1.55$, s) and trimethylammonium ($\delta = 2.90$, s) were integrated using the peak integration function. The signal of tetramethylammonium ($\delta = 3.20$, t) was integrated using the sum function. The integral ratio of tetramethylammonium to cyclooctane at t = 0 min was set to 55 mM and all other integral ratios at later time points were referenced to that value.

The integral ratio of trimethylammonium to cyclooctane was also referenced to the integral ratio of tetramethylammonium to cyclooctane at t = 0 min and scaled by 4/3 to account for the number of protons.
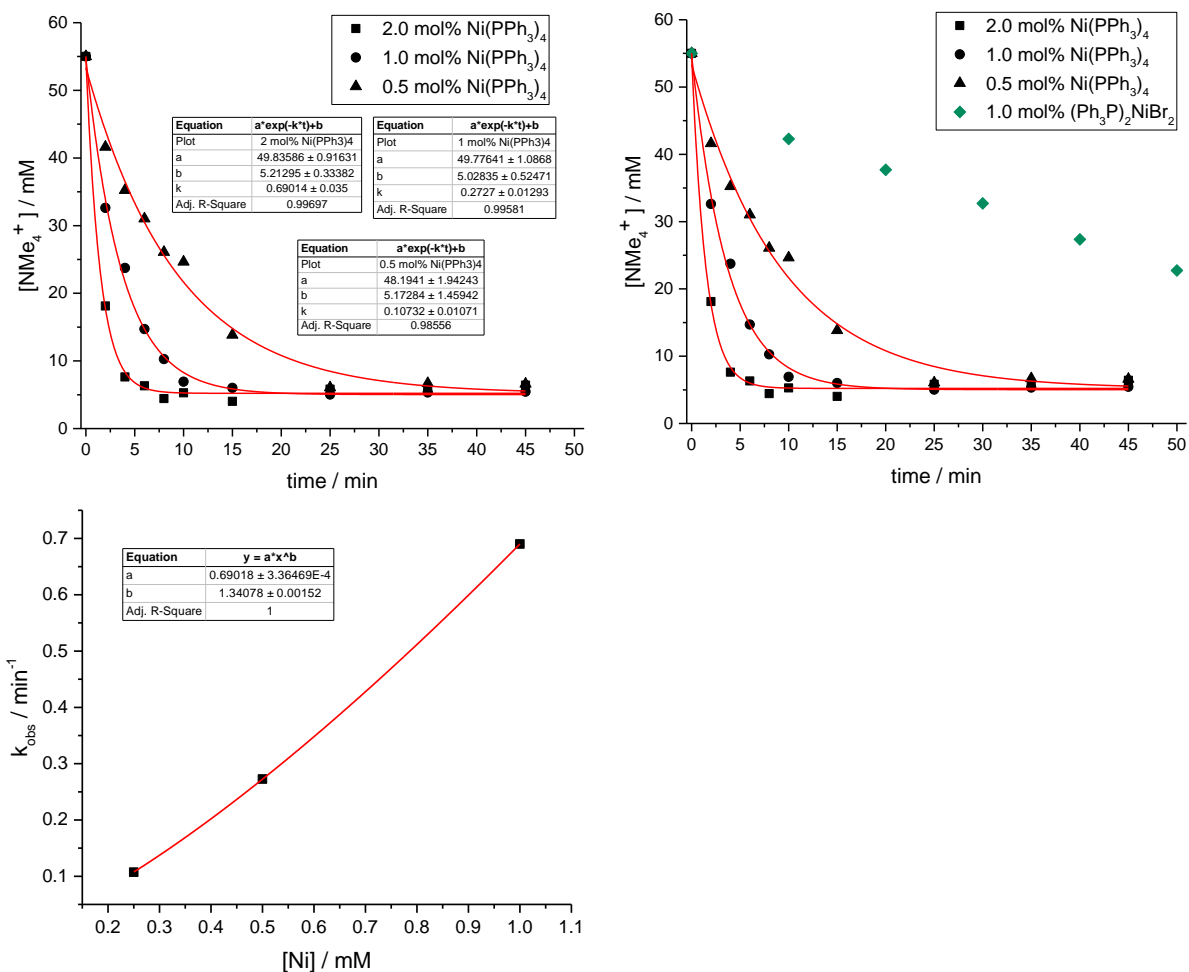
Figure 6.14. Top, left: Plot of time versus tetramethylammonium concentration for three different catalyst concentrations. The red curves depict a fit to the function $y = a\,e^{-kt}+b$ to obtain k_{obs}. Top, right: Plot of time versus tetramethylammonium concentration for three different $Ni(PPh_3)_4$ concentrations and one $(Ph_3P)_2NiBr_2$ concentration as comparison. The red curves depict a fit to the function $y = a\,e^{-kt}+b$ to obtain k_{obs}. Bottom: Plot of the catalyst concentration [Ni] of $Ni(PPh_3)_4$ versus k_{obs} for tetramethylammonium disappearance. The red curve depicts a fit to the function $y = ax^b$ to establish the order in [Ni], $b = 1.341 \pm 0.002$.
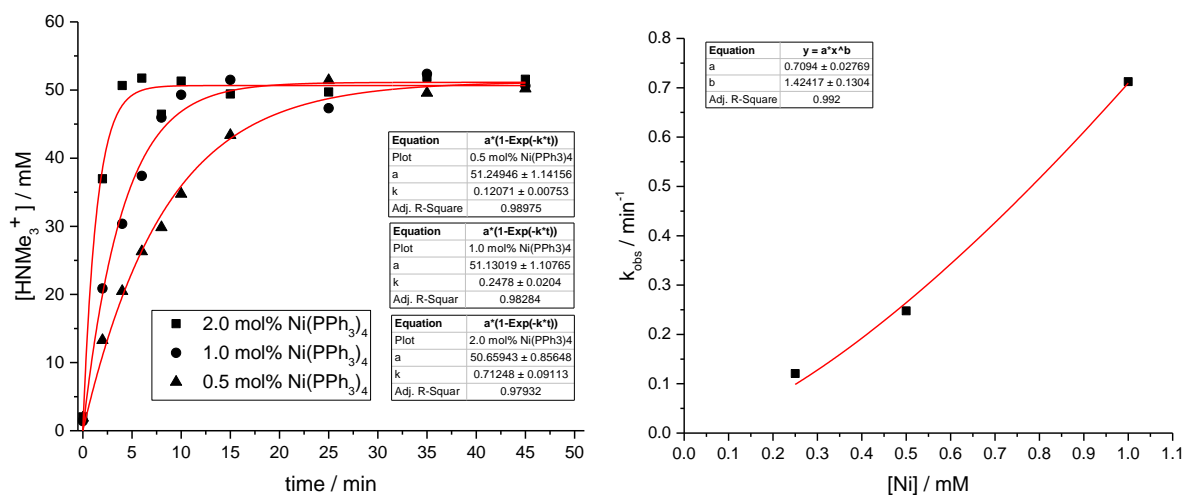
Figure 6.15. Left: Plot of time versus trimethylammonium concentration after an acidic quench for three different catalyst concentrations. The red curves depict a fit to the function $y = a(1-e^{-kt})$ to obtain k_{obs} for the formation of trimethylamine. Right: Plot of the catalyst concentration [Ni] of Ni(PPh$_3$)$_4$ versus k_{obs} for trimethylammonium formation after an acidic quench. The red curve depicts a fit to the function $y = ax^b$ to establish the order in [Ni], $b = 1.4 \pm 0.1$.

6.11 Kinetic Measurements of Norbornene Cyclopropanation with Ni(PPh$_3$)$_4$

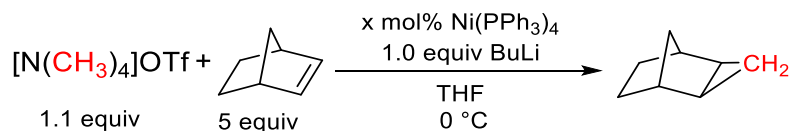**Figure 6.16.** Reaction scheme for the determination of the order in catalyst using Ni(PPh$_3$)$_4$.

The reaction was conducted according to Method A in section 6.3.1. Ni(PPh$_3$)$_4$ was added after the reaction was allowed to equilibrate in an ice bath (over ca. 20 min). Reaction profiles and the order plot are shown in **Figure 6.17**.
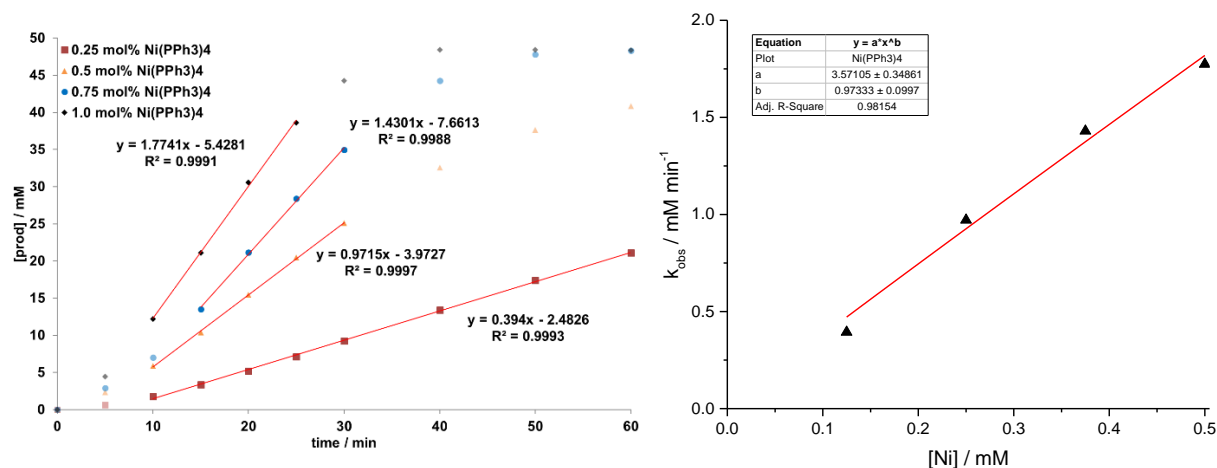
Figure 6.17. Left: Plot of time versus product concentration for four different catalyst concentrations. The red lines depict an initial rate fit with omission of the first few data points of the induction phase and the later data points at high conversions (lightly shaded) to obtain k_{obs}. Right: Plot of the catalyst concentration [Ni] of Ni(PPh$_3$)$_4$ versus k_{obs} for product formation. The red curve depicts a fit to the function $y = ax^b$ to establish the order in [Ni], $b = 1.0 \pm 0.1$.

6.12 Influence of Catalyst Loading on the Cyclopropanation of Different Alkenes
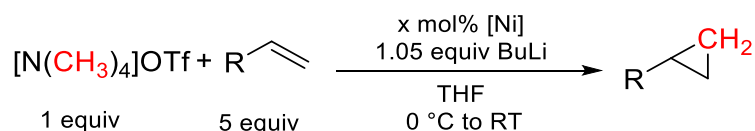

Figure 6.18. Influence of different precatalyts and loading on product formation.

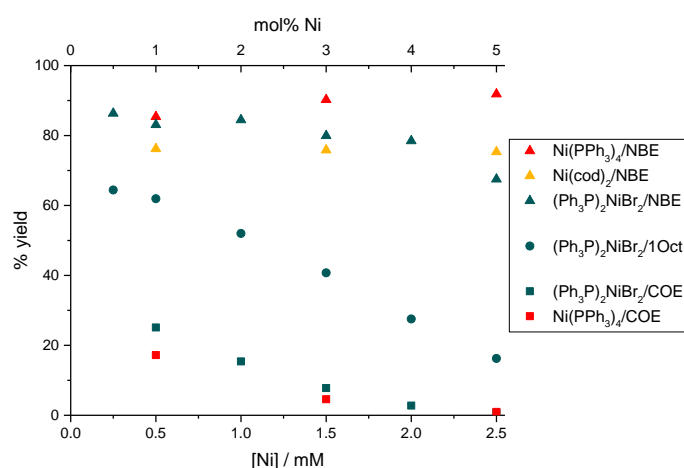The reaction was conducted according to the standard conditions in section 6.2.

Figure 6.19. Plot of catalyst concentration [Ni]$_{tot}$ versus % yield of product for three different alkenes, cyclooctene (COE, squares), 1-octene (1Oct, circles), and norbornene (NBE, triangles), and three different catalysts, (Ph$_3$P)$_2$NiBr$_2$ (green), Ni(PPh$_3$)$_4$ (red), and Ni(cod)$_2$ (yellow).

Table 6.2. Influence of Catalyst Loading on the Cyclopropanation of Different Alkenes.

Entry	Alkene	Precatalyst	[Ni] / mM	Yield / %
1	Norbornene	$Ni(PPh_3)_4$	0.5	85.4
2			1.5	90.2
3			2.5	91.9
4		$Ni(cod)_2$	0.5	76.2
5			1.5	75.8
6			2.5	75.3
7		$(Ph_3P)_2NiBr_2$	0.25	86.3
8			0.5	83.1
9			1.0	84.5
10			1.5	79.9
11			2.0	78.4
12			2.5	67.5
13	1-Octene	$(Ph_3P)_2NiBr_2$	0.25	64.4
14			0.5	61.9
15			1.0	52.0
16			1.5	40.7
17			2.0	27.5
18			2.5	16.3
19	Cyclooctene	$Ni(PPh_3)_4$	0.5	17.2
20			1.5	4.6
21			2.5	1.0
22		$(Ph_3P)_2NiBr_2$	0.5	25.1
23			1.0	15.4
24			1.5	7.8
25			2.0	2.8
26			2.5	0.8

6.13 Fit for k_{CP}/k_H for Different Catalyst Loadings

Data was taken from **Table 6.2** using $(Ph_3P)_2NiBr_2$ as catalyst and norbornene (K = 4.4), 1-octene (K = 0.5), or cyclooctene (K = 0.062) as the substrate. The experimental data was fit to equation (6.25) using k_{CP}/k_H as parameter for each catalyst concentration separately.
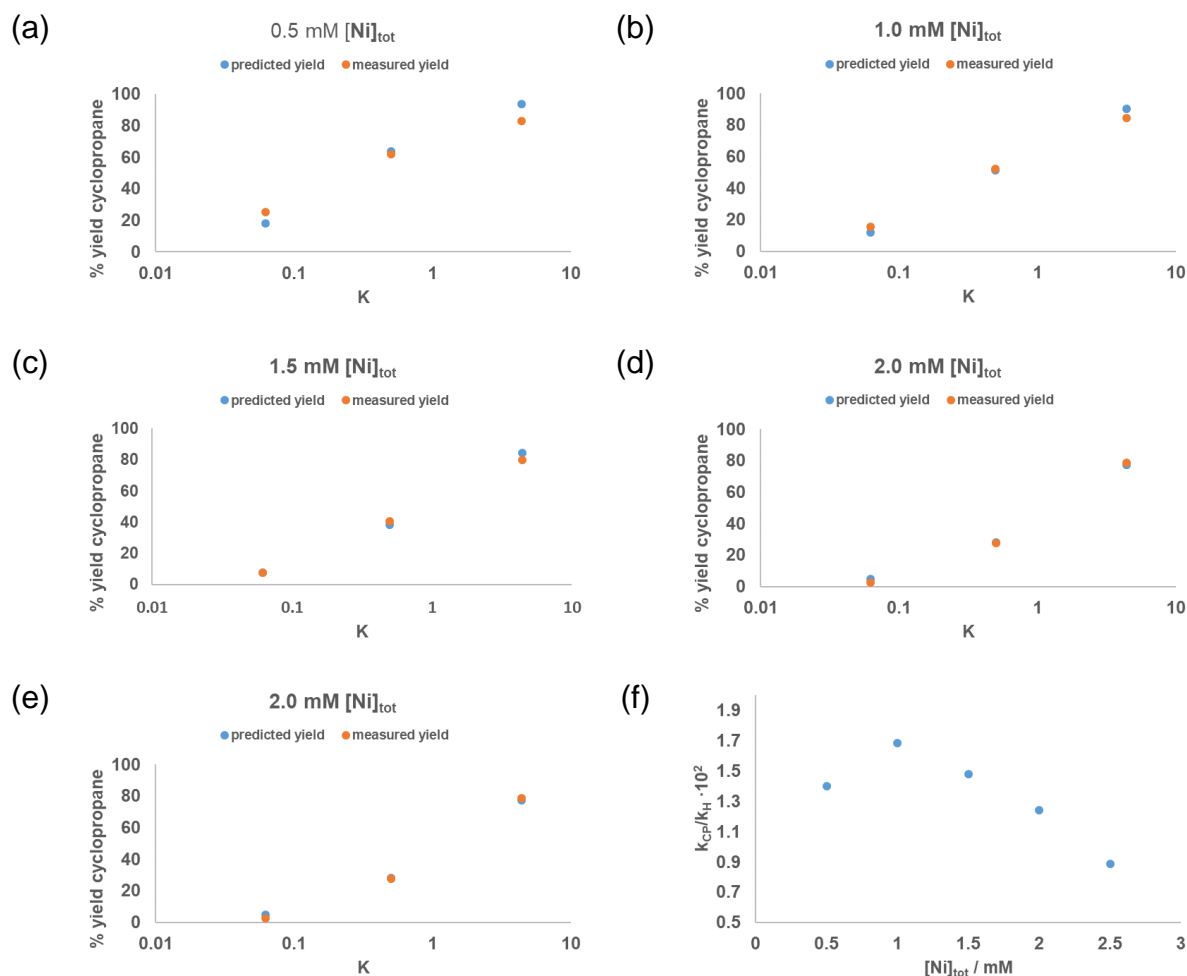
Figure 6.20. a)-e) Plots of K (log scale) versus the experimental yield and the predicted yield based on equation (6.25) for different concentrations of (Ph$_3$P)$_2$NiBr$_2$ as catalyst. f) Plot of k$_{CP}$/k$_H$ versus catalyst concentration [Ni]$_{tot}$

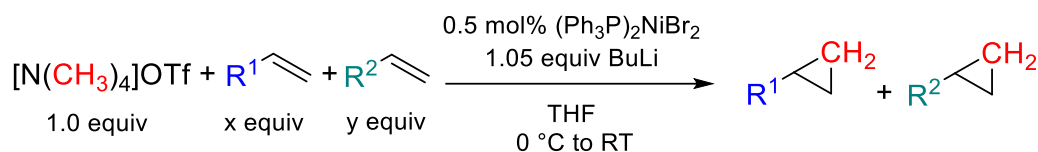## 6.14 Method of Continuous Variation – Alkene Competition

Figure 6.21. MCV competition experiment between two alkenes.

The reaction was conducted according to the standard conditions in section 6.2. For (NBE/1Oct), the reaction was worked up after 6 h. For (NBE/COE) and (1Oct/1Non), the reaction was quenched with 0.1 mL H$_2$O after 30 min. The total concentration of added alkene 1 and alkene 2 was kept constant, [A1]$_{tot}$ + [A2]$_{tot}$ = 250 mM. Additional discussion is provided in chapter 3.

Table 6.3. MCV Alkene Competition Experiment with Norbornene and Cyclooctene.

X_{NBE}	$[NBE]_{tot}$ / mM	$V_{NBEstock}$ / mL	$[COE]_{tot}$ / mM	$V_{COEstock}$ / mL	$[P_{NBE}]/[P_{COE}]$
0.1	25	0.1	225	0.9	1.464770072
0.2	50	0.2	200	0.8	2.485806392
0.3	75	0.3	175	0.7	3.716750536
0.4	100	0.4	150	0.6	5.382796308
0.5	125	0.5	125	0.5	7.202673907
0.6	150	0.6	100	0.4	12.87358766
0.7	175	0.7	75	0.3	17.697543
0.8	200	0.8	50	0.2	26.31536905
0.9	225	0.9	25	0.1	53.71648742

Table 6.4. MCV Alkene Competition Experiment with Norbornene and 1-Octene.

X_{NBE}	$[NBE]_{tot}$ / mM	$V_{NBEstock}$ / mL	$[1Oct]_{tot}$ / mM	$V_{1Octstock}$ / mL	$[P_{NBE}]/[P_{1Oct}]$
0.1	25	0.1	225	0.9	0.25236
0.2	50	0.2	200	0.8	0.576194
0.3	75	0.3	175	0.7	0.91573
0.4	100	0.4	150	0.6	1.550245
0.5	125	0.5	125	0.5	2.096557
0.6	150	0.6	100	0.4	4.033734
0.7	175	0.7	75	0.3	7.189614
0.8	200	0.8	50	0.2	14.03366
0.9	225	0.9	25	0.1	34.18419

Table 6.5. MCV Alkene Competition Experiment with 1-Octene and 1-Nonene.

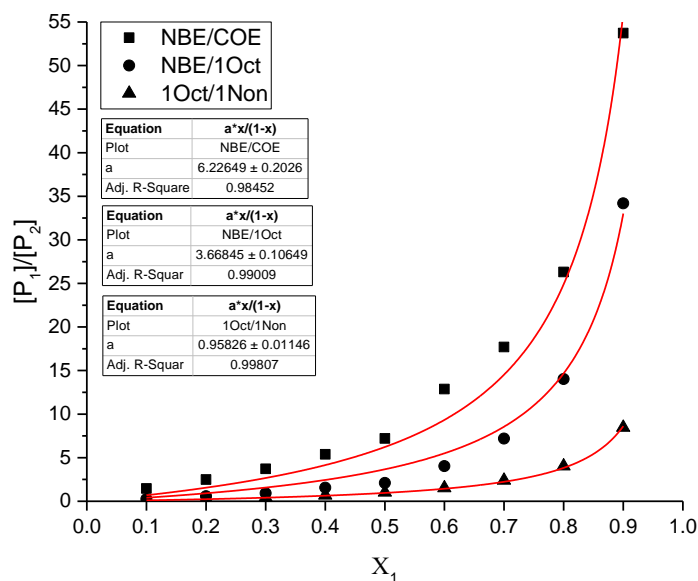| X_{1Oct}	$[1Oct]_{tot}$ / mM	$V_{1Octstock}$ / mL	$[1Non]_{tot}$ / mM	$V_{1Nonstock}$ / mL	$[P_{1Oct}]/[P_{1Non}]$
0.1	25	0.1	225	0.9	0.114310346
0.2	50	0.2	200	0.8	0.257989186
0.3	75	0.3	175	0.7	0.435932707
0.4	100	0.4	150	0.6	0.679684628
0.5	125	0.5	125	0.5	1.021350891
0.6	150	0.6	100	0.4	1.533079553
0.7	175	0.7	75	0.3	2.403979384
0.8	200	0.8	50	0.2	4.036792419
0.9	225	0.9	25	0.1	8.462446599

Figure 6.22. Plot of mole fraction of alkene 1 X_1 versus product ratio $[P_1]/[P_2]$ derived from alkene 1 and alkene 2. Nummeration is as follows: 1: Norbornene (NBE), 2: Cyclooctene (COE) (squares); 1: Norbornene, 2: 1-Octene (1Oct) (circles); 1: 1-Octene, 2: 1-Nonene (1Non) (triangles). The red curves depict a fit to the function $y = aX_1/(1-X_1)$ (equation (6.10)).

6.15 Kinetic Measurements of Cyclopropanation with Norbornene and Cyclooctene – Competition Experiment
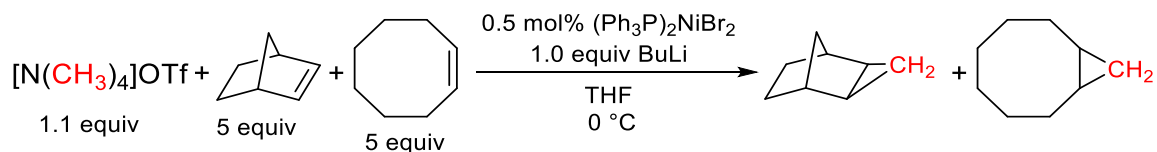

Figure 6.23. Competition experiment between norbornene and cyclooctene.

The reaction was conducted according to Method A in section 6.3.1 with cyclooctene (650 µL, 5.0 mmol, 5 equiv), and norbornene (471 mg, 5.0 mmol, 5 equiv). The reaction profile and additional discussion is provided in chapter 3.

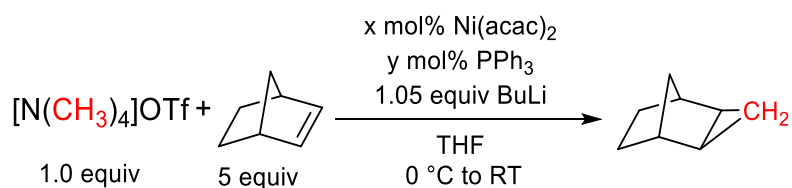## 6.16 Method of Continuous Variation – Ni/PPh₃

Figure 6.24. MCV experiment with varying ratio of Ni to PPh₃.

The reaction was conducted according to the standard condition in section 6.2. The total concentration of added Ni and PPh$_3$ was kept constant, [Ni]$_{tot}$ + [PPh$_3$]$_{tot}$ = 0.5 mM.

Table 6.6. MCV Alkene Competition Experiment with 1-Octene and 1-Nonene.

| X_{Ni}	[Ni]$_{tot}$ / mM	$V_{Nistock}$ / mL	[PPh$_3$]$_{tot}$ / mM	V_{Pstock} / mL	% yield 30 min	% yield 16 h
0.1	0.05	0.02	0.45	0.18	6.768188684	90.733705
0.2	0.1	0.04	0.4	0.16	14.63634768	92.883315
0.3	0.15	0.06	0.35	0.14	22.08597692	85.754546
0.4	0.2	0.08	0.3	0.12	27.66665363	85.441463
0.5	0.25	0.1	0.25	0.1	31.13132601	83.052698
0.6	0.3	0.12	0.2	0.08	38.3908584	
0.7	0.35	0.14	0.15	0.06	39.92518041	83.611353
0.8	0.4	0.16	0.1	0.04	43.74514148	
0.9	0.45	0.18	0.05	0.02	43.4492871	
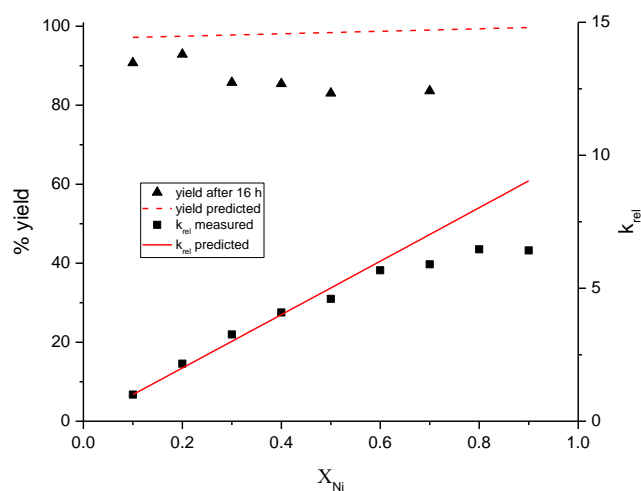
Figure 6.25. Plot of mole fraction of nickel X_{Ni} (using Ni(acac)$_2$) versus the measured rate (squares) and predicted rate (red solid curve) (approximated as initial yield after 30 min) based on our model (eqs (6.25) and (6.27)) and the measured (triangles) and predicted yield (red dashed curve) (after 16 h) for the cyclo-propanation of NBE, all with no further adjustment of parameters. kCP/kH = 0.014, [Ni]tot + [P]tot = 0.5 mM, [A]tot = 250 mM.

6.17 Derivation for Alkene Competition Equation

See chapter 3 for mechanistic scheme. We assume that alkene i is coordinated in the resting state of the cyclopropanation cycle, NiAi. The rate of cyclopropanation to give product Pi is given by

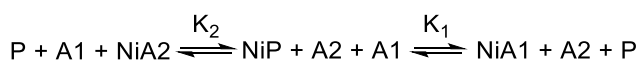$$\frac{d[Pi]}{dt} = k_i[NiAi][Y] \tag{6.1}$$

127

where [Y] is the concentration of ylide. The product ratio [P1]/[P2] for two competing alkenes A1 and A2 is given by

$$\frac{[P_1]}{[P_2]} = \frac{k_1[NiA1][Y]}{k_2[NiA2][Y]} = \frac{k_1[NiA1]}{k_2[NiA2]} \tag{6.2}$$

We make the assumption that both alkene complexes react analogously with the ylide. Further we assume that a pre-equilibrium is established between NiA1 and NiA2 when the alkenes compete for the Ni catalyst ([A1], [A2] >> [Ni]) before the rate-determining nickel carbene formation.

As discussed in chapter 3, we approximate the equilibrium constant K_i by Tolman's values (with Ni(P(O-o-tolyl)$_3$ as hypothetical reference compound).[15]

$$K_1 = \frac{[NiA1][P][A2]}{[NiP][A1][A2]}$$

$$= \frac{[NiA1][P]}{[NiP][A1]} \tag{6.3}$$

$$P + A1 + NiA2 \underset{}{\overset{K_2}{\rightleftharpoons}} NiP + A2 + A1 \underset{}{\overset{K_1}{\rightleftharpoons}} NiA1 + A2 + P$$

$$K_2 = \frac{[NiA2][P][A1]}{[NiP][A2][A1]}$$

$$= \frac{[NiA2][P]}{[NiP][A2]} \tag{6.4}$$

$$K = \frac{K_1}{K_2} = \frac{[NiA1][P][NiP][A2]}{[NiP][A1][NiA2][P]}$$

$$= \frac{[NiA1][A2]}{[A1][NiA2]} \tag{6.5}$$

$$[NiA2] = \frac{K_2}{K_1} \frac{[NiA1][A2]}{[A1]} \tag{6.6}$$

Inserting equation (6.6) into the equation (6.2) gives

$$\frac{[P_1]}{[P_2]} = \frac{k_1[NiA1]}{k_2[NiA2]} = \frac{k_1 K_1}{k_2 K_2} \frac{[NiA1][A1]}{[NiA1][A2]} = \frac{k_1 K_1}{k_2 K_2} \frac{[A1]}{[A2]} \tag{6.7}$$

To construct a Job plot, the total alkene concentration [A]$_{tot}$ is kept constant, i.e. [A]$_{tot}$ = [A1] + [A2] = const., and the molar fractions are defined as follows

$$X_1 = \frac{[A1]}{[A]_{tot}} \qquad (6.8) \qquad X_2 = \frac{[A2]}{[A]_{tot}} = 1 - X_1 \qquad (6.9)$$

Rearranging equations (6.8) and (6.9) and inserting in equation (6.7) gives

$$\frac{[P_1]}{[P_2]} = \frac{k_1 K_1}{k_2 K_2} \frac{[A1]}{[A2]} = \frac{k_1 K_1}{k_2 K_2} \frac{X_1 [A]_{tot}}{X_2 [A]_{tot}} = \frac{k_1 K_1}{k_2 K_2} \frac{X_1}{X_2} = \frac{k_1 K_1}{k_2 K_2} \frac{X_1}{(1 - X_1)} \qquad (6.10)$$

6.18 Derivation for Alkene-Ligand Competition Equation

See chapter 3 for mechanistic scheme. We define the cyclopropanation rate and the homocoupling rate as

$$\frac{d[P_{CP}]}{dt} = k_{CP}[NiA][Y] \qquad (6.11) \qquad \frac{d[P_H]}{dt} = k_H[NiP][Y] \qquad (6.12)$$

, respectively. NiA is the resting state of the cyclopropanation reaction and NiP is the resting state of the homocoupling reaction with no ligated alkene (that would undergo cyclopropanation).

Before the rate-determining step a pre-equilibrium is established between alkene and phosphine binding.

$$A + NiP \underset{}{\overset{K}{\rightleftharpoons}} NiA + P \qquad\qquad K = \frac{[NiA][P]}{[NiP][A]} \qquad (6.13)$$

We can also define the following boundary conditions with the total concentrations. [Ni]$_{tot}$ (precatalyst concentration) is distributed over the resting state manifold NiA/NiP:

$$[Ni]_{tot} = [NiA] + [NiP] \qquad (6.14) \qquad\qquad \rightarrow [NiA] = [Ni]_{tot} - [NiP] \qquad (6.15)$$

The phosphine is either bound to Ni or free:

$$[P]_{tot} = [P] + [NiP] \qquad (6.16) \qquad\qquad \rightarrow [P] = [P]_{tot} - [NiP] \qquad (6.17)$$

The alkene is either bound to Ni or free:

$$[A]_{tot} = [A] + [NiA] \qquad (6.18) \qquad \rightarrow [A] = [A]_{tot} - [NiA]$$
$$= [A]_{tot} - [Ni]_{tot} + [NiP] \qquad (6.19)$$

Inserting this boundary conditions into equation (6.13) gives

$$K = \frac{[P][NiA]}{[A][NiP]} \xrightarrow{boundary\ cond.} K = \frac{([P]_{tot} - [NiP])([Ni]_{tot} - [NiP])}{([A]_{tot} - [Ni]_{tot} + [NiP])[NiP]} = \frac{[P]_{tot}[Ni]_{tot} - ([P]_{tot}+[Ni]_{tot})[NiP] + [NiP]^2}{([A]_{tot} - [Ni]_{tot})[NiP] + [NiP]^2} \qquad (6.20)$$

Rearranging equation (6.20) leads to a quadratic equation that can be solved for NiP or NiA.[16]

$$[NiP] = \frac{([P]_{tot} + K[A]_{tot} + (1-K)[Ni]_{tot}) - \sqrt{([P]_{tot} + K[A]_{tot} + (1-K)[Ni]_{tot})^2 - 4(1-K)[P]_{tot}[Ni]_{tot}}}{2(1-K)} \qquad (6.21)$$

$$[NiA] = \frac{-([P]_{tot} + K[A]_{tot} + (K-1)[Ni]_{tot}) + \sqrt{([P]_{tot} + K[A]_{tot} + (K-1)[Ni]_{tot})^2 + 4K(1-K)[A]_{tot}[Ni]_{tot}}}{2(1-K)} \qquad (6.22)$$

We can further define the cyclopropane yield by assuming that all ylide (full conversion) reacts either to cyclopropane P_{CP} or homocoupling-derived side-products P_H according to our mechanistic scheme.

$$\frac{[P_{CP}]}{[P_H]} = \frac{k_{CP}[NiA][Y]}{k_H[NiP][Y]} = \frac{k_{CP}[NiA]}{k_H[NiP]}$$
$$= \frac{k_{CP}}{k_H} \frac{([Ni]_{tot} - [NiP])}{[NiP]} \qquad (6.23)$$

$$\frac{\% \ yield}{100} = \frac{[P_{CP}]}{[P_{CP}] + [P_H]} \qquad (6.24)$$

Rearranging and inserting equations (6.21) and (6.23) into (6.24) gives finally

$$\frac{\% \ yield}{100} = \frac{\frac{k_{CP}}{k_H}([Ni]_{tot} - \frac{([P]_{tot} + K[A]_{tot} + (1-K)[Ni]_{tot}) - \sqrt{([P]_{tot} + K[A]_{tot} + (1-K)[Ni]_{tot})^2 - 4(1-K)[P]_{tot}[Ni]_{tot}}}{2(1-K)})}{\frac{k_{CP}}{k_H}[Ni]_{tot} + (1 - \frac{k_{CP}}{k_H})\frac{([P]_{tot} + K[A]_{tot} + (1-K)[Ni]_{tot}) - \sqrt{([P]_{tot} + K[A]_{tot} + (1-K)[Ni]_{tot})^2 - 4(1-K)[P]_{tot}[Ni]_{tot}}}{2(1-K)}} \qquad (6.25)$$

A full derivation of equation (6.25) can be found elsewhere.[16]

Relative rates can further be defined as

$$k_{obs} = k_{CP}[NiA] \qquad (6.26) \qquad k_{rel,n} = \frac{k_{obs,n}}{k_{obs,1}} = \frac{k_{CP}[NiA]_n}{k_{CP}[NiA]_1} = \frac{[NiA]_n}{[NiA]_1} \qquad (6.27)$$

The rate $k_{rel,1}$ is usually normalized to the first k_{obs} (e.g. lowest $[Ni]_{tot}$) in a series of measurements.

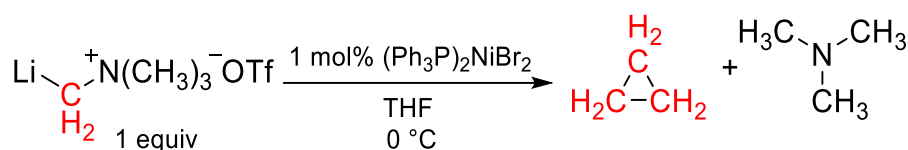## 6.19 Headspace Analysis

Figure 6.26. Headspace analysis in the absence of added alkene.

The reaction was conducted according to a modified version of Method B in section 6.3.2.

Inside the glove box, an oven-dried 50 mL Schlenk flask equipped with a J. Young inlet valve, glass stopper, screw cap with septum and a glass-coated stir bar was charged with [NMe$_4$]OTf (245.5 mg, 1.1 mmol, 1.1 equiv). The flask was removed from the glove box and attached to a Schlenk line. Dry THF (18.5 mL) was added via syringe. Cyclooctane (100 μL) was added via a 100 μL micro syringe as internal standard. The flask was immersed in an ice bath and the reaction allowed to equilibrate (over ca. 20 min).

BuLi (500 μL, 1 mmol, 1 equiv; 2 M in cyclohexane) was added dropwise over ca. 30 s via a 1 mL gastight Hamilton syringe (by difference; previously dried at 50 °C in a vacuum oven). The flask was sealed/closed to the Schlenk line unless reagents were added or aliquots collected.

After 15 min, an aliquot (ca. 0.2 mL) was taken with a disposable 1 mL plastic syringe (flushed several times with Ar) and immediately quenched by injection into 0.2 mL 1 M TFA in DCM (t = 0 min).

Then, (Ph$_3$P)$_2$NiBr$_2$ (1 mol%, 0.01 mmol) in 1 mL THF (prepared as stock solution inside the glove box) was added dropwise by difference with a 2.5 mL gastight Hamilton syringe (previously dried at 50 °C in a vacuum oven) over ca. 30 s (t = 0 min with first drop). After the addition was completed, the flask was sealed/closed to the Schlenk line again until *after* the headspace aliquot was taken.

After 60 min, the headspace was sampled with a 2.5 mL gastight Hamilton syringe (previously dried at 50 °C in a vacuum oven). Another aliquot (t = 60 min) was then taken as described above.

The headspace sample (ca. 1 mL gas volume) was then analyzed by GC-MS.

Aliquots were diluted with 0.3 mL CD₃OD and analyzed by NMR.

An analogous reaction was conducted with $[N(CD_3)_4]OTf$ (258.8 mg, 1.1 mmol, 1.1 equiv).
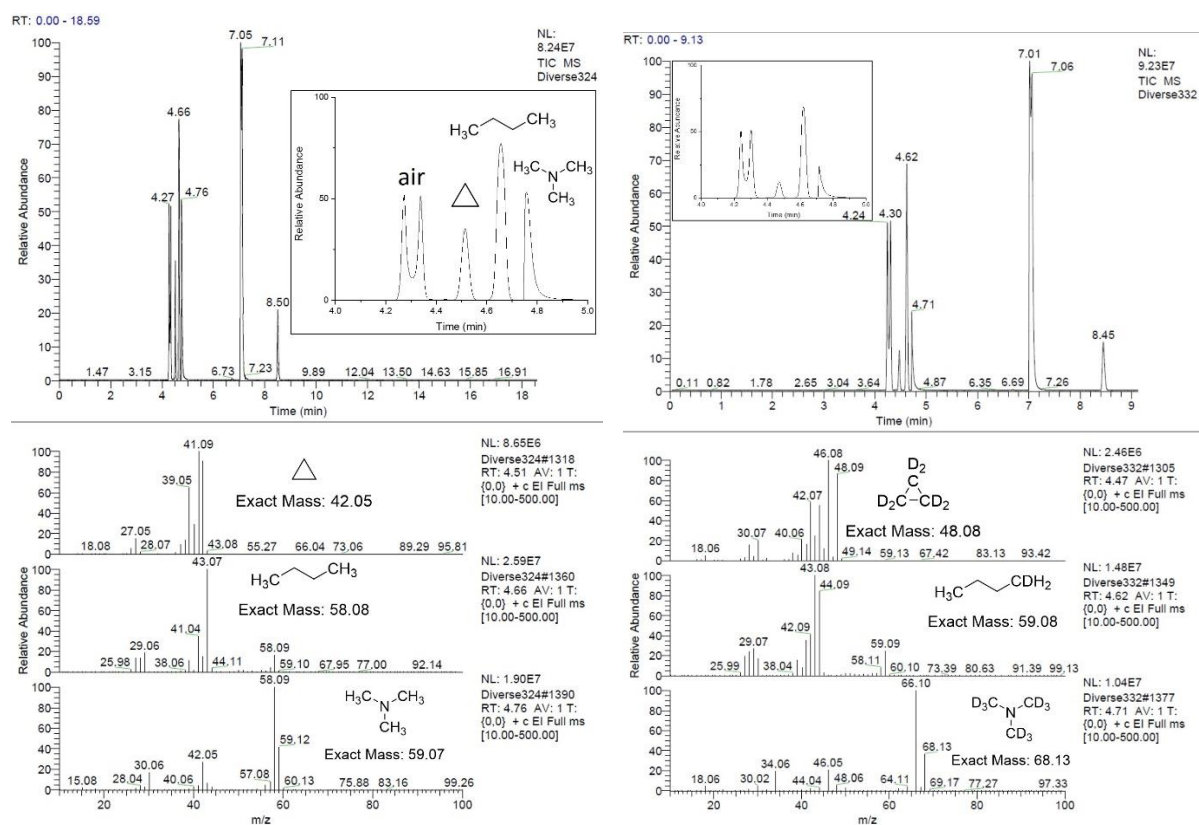

Figure 6.27. Top left: GC-MS chromatogram of a headspace sample after 60 min as described above with $[N(CH_3)_4]OTf$. Peaks at t = 7.05 and 7.11 min are THF. Peak at t = 8.50 min is cyclohexane. Double peaks are due to detector overload (air (inset) and THF). Top left, inset: Magnified chromatogram between 4 and 5 min with labeled peaks. Bottom left: Mass spectra of selected compounds and their assigned structures with mass. Top right: GC-MS chromatogram of a headspace sample after 60 min as described above with $[N(CD_3)_4]OTf$. Peaks at t = 7.01 and 7.06 min are THF. Peak at t = 8.45 min is cyclohexane. Double peaks are due to detector overload (air (inset) and THF). Top right, inset: Magnified chromatogram between 4 and 5 min with analogous peak assignment as left. Bottom right: Mass spectra of selected compounds and their assigned structures with mass.
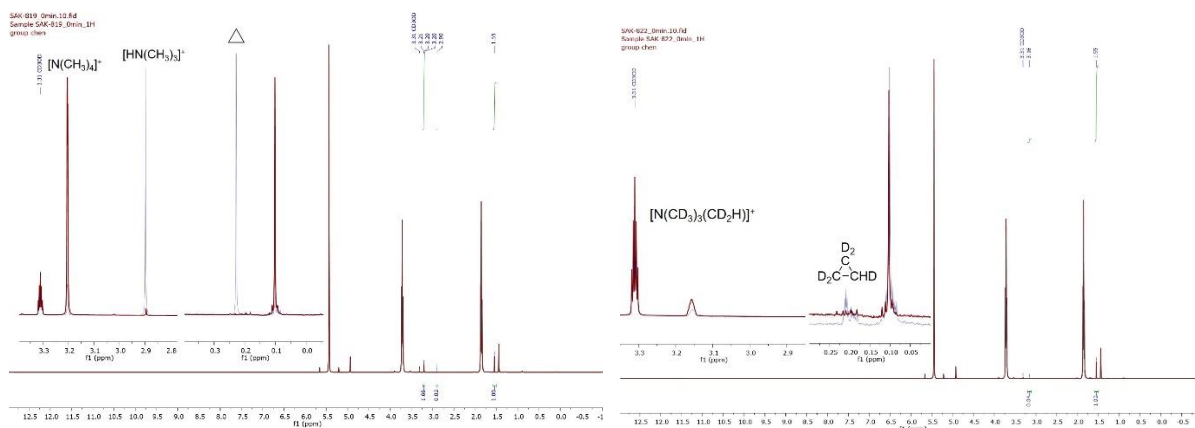
Figure 6.28. Left: Overlaid ^{1}H NMR spectra of aliquots taken after 0 min (red, before addition of catalyst) and 60 min (see above for detailed description) using [N(CH$_3$)$_4$]OTf. Inset: Enlarged regions show disappearance of [N(CH$_3$)$_4$]$^+$, formation of [HN(CH$_3$)$_3$]$^+$, and formation of cyclopropane C$_3$H$_6$ (assignment based on GC-MS and D-labelling). Right: Overlaid ^{1}H NMR spectra of aliquots taken after 0 min (red, before addition of catalyst) and 60 min (see above for detailed description) using [N(CD$_3$)$_4$]OTf. Inset: Enlarged regions show disappearance of [N(CD$_3$)$_3$(CHD$_2$)]$^+$ (from H$^+$ quench) and formation of cyclopropane C$_3$HD$_5$ (assignment based on GC-MS and D-labelling).

6.20 Trapping Experiments with BnNMe$_2$
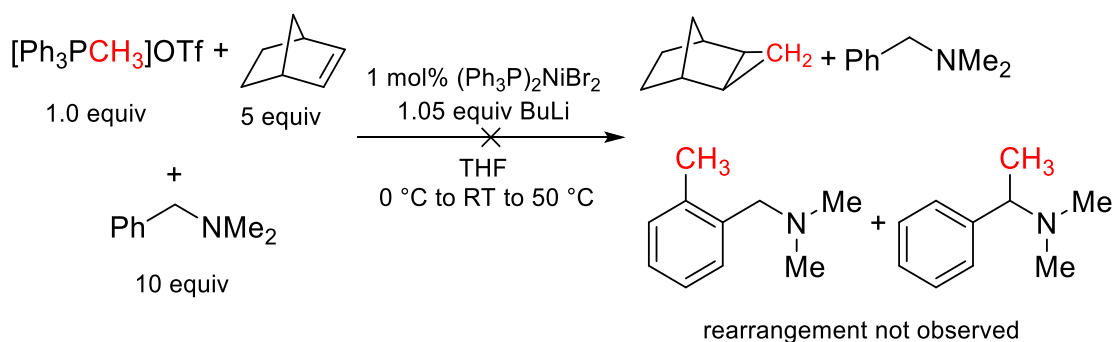
Figure 6.29. Attempted cyclopropanation of norbornene with methyltriphenylphosphonium triflate in the presence of *N,N*-dimethylbenzylamine.

The reaction was conducted according to the standard conditions in section 6.2. BnNMe$_2$ (150 μL, 1.0 mmol, 10 equiv) was added before addition of BuLi. After BuLi addition, the reaction was stirred at room temperature for 2 h, then at 50 °C for an additional 14 h. No product formation was observed. The reaction was repeated in the absence of norbornene. In both cases no rearrangement product stemming from carbene trapping and formation of *N,N,N*-trimethylbenzylammonium ylide was observed, namely *N,N*-dimethyl-1-(*o*-tolyl)methanamine and/or *N,N*-dimethyl-1-phenylethan-1-amine.
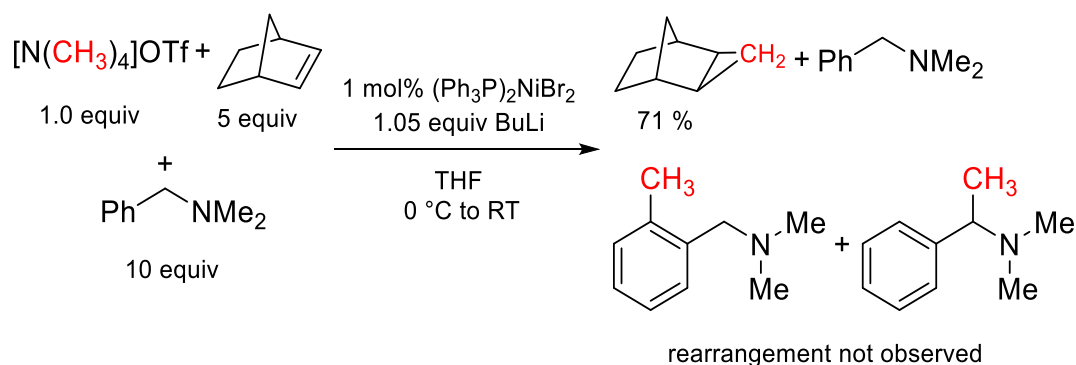
Figure 6.30. Cyclopropanation of norbornene in the Presence of *N,N*-dimethylbenzylamine.

The reaction was conducted according to the standard conditions in section 6.2. 10 min after BuLi addition, BnNMe$_2$ (150 µL, 1.0 mmol, 10 equiv) was added, followed immediately by (Ph$_3$P)$_2$NiBr$_2$ in 0.2 mL THF (1 mol%, prepared as stock solution). The reaction was repeated in the absence of norbornene. In both cases no rearrangement product stemming from carbene trapping and formation of N,N,N-trimethylbenzylammonium ylide was observed, namely *N,N*-dimethyl-1-(*o*-tolyl)methanamine and/or *N,N*-dimethyl-1-phenylethan-1-amine.
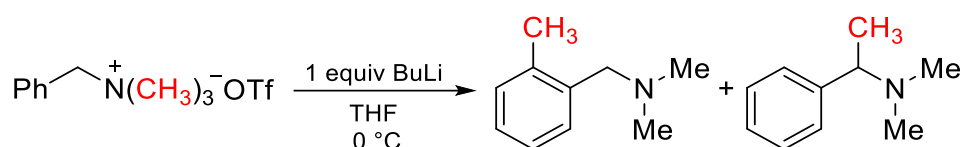

Figure 6.31. Rearrangement of *N,N,N*-trimethylbenzylammonium ylide.

The reaction was conducted according to the standard conditions in section 6.2 with [BnNMe$_3$]OTf (29.9 mg, 0.1 mmol, 1 equiv). After 45 min, the reaction was quenched with a few drops of CD$_3$OD. The products were identified by GC-MS (**Figure 6.32**) and by comparison to literature NMR data.[17-18]

134
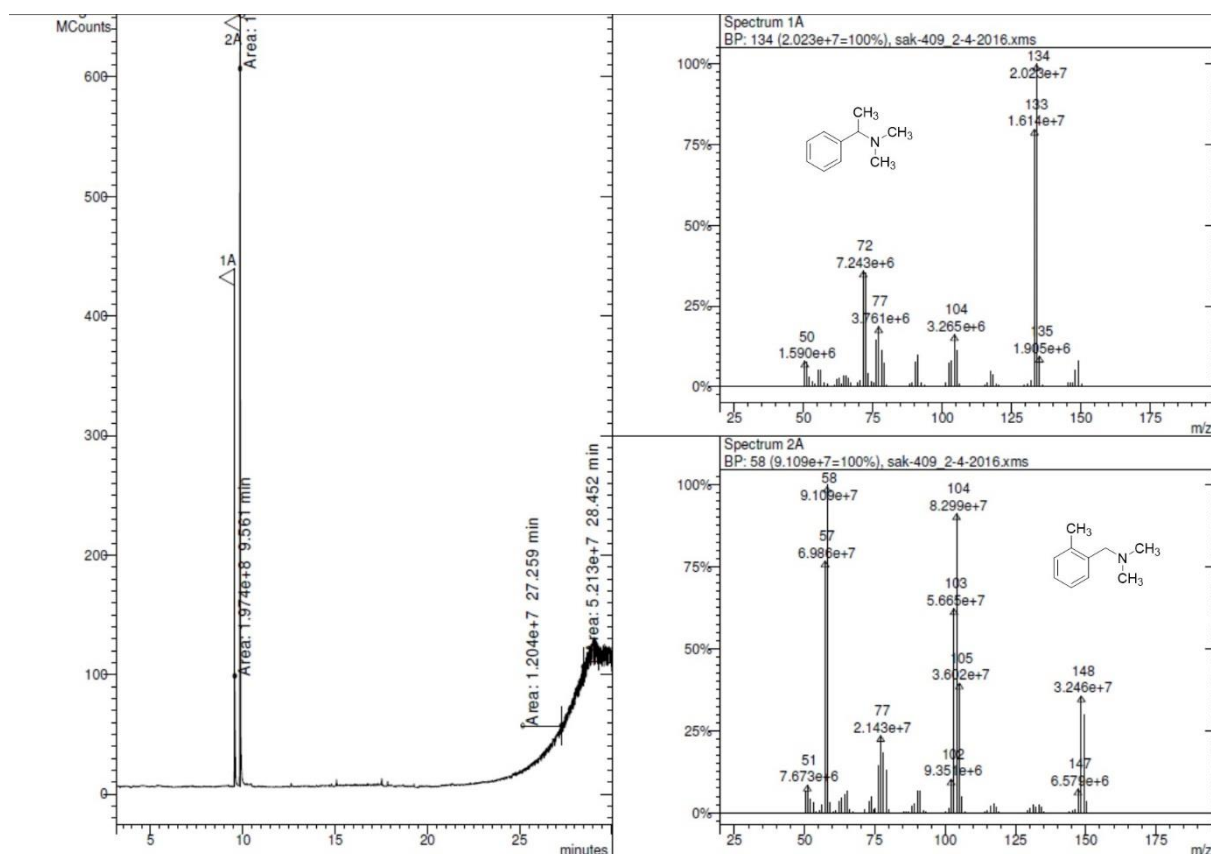
Figure 6.32. Left: GC-MS chromatogram of the *N,N,N*-trimethylbenzylammonium ylide rearrangement after 45 min. Right: Mass spectra of the rearrangement products.

6.21 Addition of Excess PPh$_3$
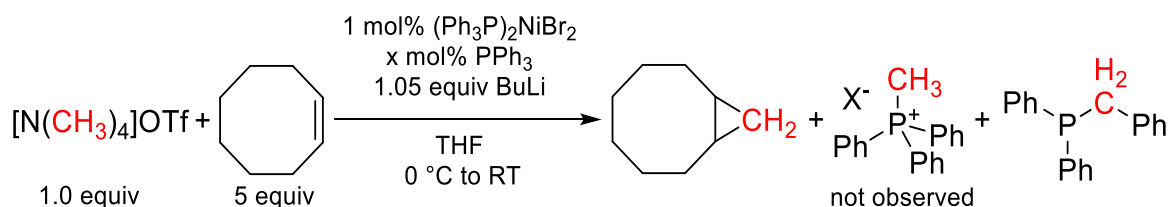
Figure 6.33. Cyclopropanation of cyclooctene in the presence of excess PPh$_3$.

The reaction was conducted according to the standard conditions in section 6.2 with additional PPh$_3$ (A: 7.2 mg, 0.027 mmol, 27 mol% *or* B: 26.6 mg, 0.101 mmol, 101 mol%). After 16 h, the reaction was quenched with 0.1 mL CD$_3$OD. The remaining reaction mixture was evaporated to dryness on the Schlenk line. The solid residue was dissolved in CD$_3$OD/CDCl$_3$ (0.35 mL/0.35 mL) and analyzed by NMR. (Some solid remained undissolved, most likely polyethylene. Solubility tests showed [PMePh$_3$]Br, [NMe$_4$]OTf, and PPh$_3$ to be soluble in this solvent mixture at comparable concentrations).

135

Mixtures of authentic samples of [PMePh$_3$]Br/PPh$_3$, PBnPh$_2$/PPh$_3$, and [NMe$_4$]OTf/PPh$_3$ were prepared in the same solvent mixture at comparable concentration (ca. 0.1 mmol / 0.7 mL per compound) and analyzed by NMR (**Figure 6.34**).

Addition of an excess of PPh$_3$ resulted in a strongly or even completely suppressed cyclopropanation of COE. A small amount of PBnPh$_2$ (>10:1 PPh$_3$:PBnPh$_2$ by ^{31}P NMR) had formed, likely via a Ni(0)-promoted/catalyzed phospha-Stevens rearrangement of a small amount of in situ formed Ph$_3$P=CH$_2$.[19-20]
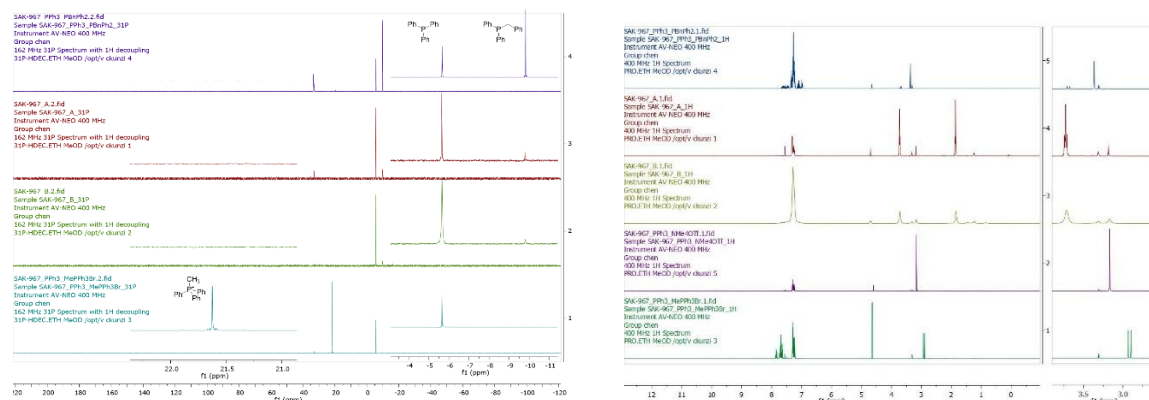
Figure 6.34. Left: Stacked [31]P{[1]H spectra plot for a mixture of authentic PPh$_3$ and PBnPh$_2$ (Spectrum 4), reaction A with additional 27 mol% PPh$_3$ (Spectrum 3), reaction B with additional 101 mol% PPh$_3$ (Spectrum 2), and a mixture of authentic PPh$_3$ and [PMePPh$_3$]Br (Spectrum 1). Left inset: Expansion of the [PMePh$_3$]$^+$ region. Right inset: Expansion of the PPh$_3$/PBnPh$_2$ region. Right: Stacked ^{1}H spectra plot for a mixture of authentic PPh$_3$ and PBnPh$_2$ (Spectrum 5), reaction A with additional 27 mol% PPh$_3$ (Spectrum 4), reaction B with additional 101 mol% PPh$_3$ (Spectrum 3), a mixture of authentic PPh$_3$ and [NMe$_4$]OTf (Spectrum 2), and a mixture of authentic PPh$_3$ and [PMePPh$_3$]Br (Spectrum 1). Right inset: Expansion of the P(CH_2Ph)Ph$_2$/[PPh$_3$(CH_3)]$^+$/[N(CH_3)$_4$]$^+$ region.

6.22 Synthesis of Ammonium Salts

6.22.1 Synthesis of [(CH$_3$)$_3$N^{13}CH$_3$]OTf
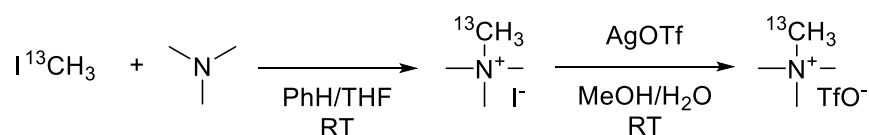
A 100 mL round bottom flask under Ar was charged with 14 mL benzene and ^{13}CH$_3$I (99 atom% ^{13}C; 1 g, 7 mmol, 1 equiv.). The flask was immersed in a water bath at RT and NMe$_3$ (~0.8 M in THF; 35 mL, 28 mmol, 4 equiv.) was added via syringe over 10 min. The reaction was stirred for 15 h at RT, then all volatiles were removed under

vacuum to give $(CH_3)_3N^{13}CH_3I$ as off-white solid (quantitative yield) which was used for the next step without further purification.

In the dark, a 50 mL round bottom flask under air was charged with $(CH_3)_3N^{13}CH_3I$ (606 mg, 3 mmol, 1 equiv.). The solid was dissolved in 30 mL MeOH and 7 mL H_2O at 60 °C. To this vigorously stirred solution was added a solution of AgOTf (771 mg, 3 mmol, 1 equiv.) in 2 mL MeOH in one portion (rinsed with 1 mL MeOH). The reaction was cooled to RT, stirred for another 15 min, and then filtered through a plug of Celite. The solvent was evaporated under reduced pressure and the solid residue was further dried under vacuum. The crude product was dissolved in a minimal amount of boiling *i*PrOH (distilled from CaH_2 under N_2). The crystals were filtered off after storage at -20 °C overnight and rinsed with cold *i*PrOH (2 x 2 mL). Drying under vacuum overnight afforded the product as white powder (0.455 g, 2 mmol, 66 % yield) which was stored in the glove box.

Elemental analysis: Found: C, 26.71; H, 5.54; N, 6.24; S, 14.42; F, 25.29. Calc. for $C_4^{13}CH_{12}F_3NO_3S$: C, 21.43; ^{13}C, 5.80; H, 5.39, N, 6.25; O, 21.41; F, 25.42; S, 14.30. ^{13}C determined as ^{12}C: C, 26.90.

^{1}H NMR (300 MHz, CD$_3$OD): δ 3.43-2.95 (m, 12H).

^{13}C NMR (75 MHz, CD$_3$OD): δ 121.8 (q, $^1J_{(C-F)}$ = 319 Hz), 55.9 (t, $^1J_{(C-N)}$ = 4 Hz).

^{19}F NMR (282 MHz, CD$_3$OD): δ -80.1.

6.22.2 Synthesis of [N(CD$_3$)$_4$]OTf

Tetramethylammonium-d$_{12}$ triflate was prepared in analogy to the protiated compound as reported previously, dried under vacuum and stored in the glove box.[1, 3]

The elemental analysis values for C, H are outside the tolerance, most likely due to the level of deuteration. All other analysis techniques confirmed the purity.

Elemental analysis: Found: C, 25.02; H, 4.61; N, 6.05. Calc. for $C_5D_{12}F_3NO_3S$: C, 25.52; D, 10.27, N, 5.95; O, 20.40; F, 24.22; S, 13.63. D determined as H: H, 5.42.

^{1}H NMR (400 MHz, CD$_3$OD): δ 3.15 (m, small amount of $[N(CD_3)_3(CD_2H)]^+$).

^{1}H NMR (600 MHz, D$_2$O): δ 3.16 (m, small amount of $[N(CD_3)_3(CD_2H)]^+$).

^{2}H NMR (92 MHz, D$_2$O): δ 3.04 (s).

^{13}C NMR (100 MHz, CD$_3$OD): δ 121.8 (q, $^1J_{(C-F)}$ = 319 Hz), 54.7 (m).

^{13}C NMR (150 MHz, D$_2$O): δ 119.6 (q, $^1J_{(C-F)}$ = 317 Hz), 54.1 (m).

¹⁹F NMR (376 MHz, CD₃OD): δ -80.1.

¹⁹F NMR (470 MHz, D₂O): δ -78.8.

HRMS (ESI, M⁺, [N(CD₃)₄]⁺): m/z calcd for $C_4D_{12}N$ 86.1717; Found 86.1716 (100%), 85.1655 (2.7%, [N(CD₃)₃(CD₂H)]⁺).

6.22.3 Characterization of other Ammonium Salts

***N,N*-Dimethylpyrrolidinium Triflate:** **¹H NMR (400 MHz, CD₃OD):** δ 3.58 – 3.49 (m, 4H), 3.17 (s, 6H), 2.30 – 2.21 (m, 4H). **¹³C NMR (100 MHz, CD₃OD):** δ 121.81 (q, J = 318.5 Hz), 67.01 – 66.75 (m), 52.55 – 52.19 (m), 22.90 (s). **¹⁹F NMR (376 MHz, CD₃OD):** δ -80.08 (s).

***N,N*-Dimethylmorpholinium Triflate:** **¹H NMR (400 MHz, CD₃OD):** δ 4.02 – 3.96 (m, 4H), 3.51 – 3.45 (m, 4H), 3.25 (s, 6H). **¹³C NMR (100 MHz, CD₃OD):** δ 127.12 – 116.43 (m, q of -OTf not resolved), 62.54 – 62.35 (m), 61.78 (s), 52.37 (s). **¹⁹F NMR (376 MHz, CD₃OD):** δ -80.10 (s).

***N,N,N*-Trimethyl-1-adamantylammonium Triflate:** **¹H NMR (400 MHz, CD₃OD):** δ 3.02 (s, 9H), 2.34 – 2.27 (m, 3H), 2.11 (d, J = 3.1 Hz, 6H), 1.86 – 1.65 (m, 6H). **¹³C NMR (100 MHz, CD₃OD):** δ 121.82 (q, J = 318.6 Hz), 73.80 (s), 48.55 – 48.43 (m), 36.06 (s), 35.64 (s), 31.72 (s). **¹⁹F NMR (376 MHz, CD₃OD):** δ -80.03 (s).

***N,N,N*-Trimethylneopentylammonium Triflate:** **¹H NMR (400 MHz, CD₃OD):** δ 3.34 (s, 2H), 3.23 (s, 9H), 1.22 (s, 9H). **¹³C NMR (100 MHz, CD₃OD):** δ 126.80 – 116.80 (m, q of -OTf not resolved), 78.23 – 78.01 (m), 56.10 – 55.82 (m), 34.31 (s), 29.99 (s). **¹⁹F NMR (376 MHz, CD₃OD):** δ -80.07 (s).

Tetramethylammonium Nonaflate: **¹H NMR (400 MHz, CD₃OD):** δ 3.20 – 3.19 (m, 12H). **¹³C NMR (100 MHz, CD₃OD):** δ 55.93 – 55.79 (m). No signal for nonaflate. **¹⁹F NMR (376 MHz, CD₃OD):** δ -82.54 (tt, J = 10.3, 2.8 Hz), -115.63 – -116.14 (m), -122.35 – -122.98 (m), -126.68 – -127.60 (m). **Elemental analysis**: Calc. for $C_8H_{12}NO_3F_9S$: C, 25.74; H, 3.24; N, 3.75; O, 12.86; F, 45.81; S, 8.59. Found: C, 25.48; H, 3.31; N, 3.79; F, 45.75; S, 8.52.

Tetramethylammonium Trifluoroacetate: ^{1}H NMR (400 MHz, CD$_3$OD): δ 3.20 – 3.19 (m, 12H). **^{19}F NMR (376 MHz, CD$_3$OD):** δ -77.25 (s). **^{13}C NMR (100 MHz, CD$_3$OD):** δ 161.65 (q, J = 36.6 Hz), 55.96 – 55.78 (m). (No signal for F$_3$*C*CO$_2^-$.)

Butyltrimethylammonium Triflate: ^{1}H NMR (400 MHz, CD$_3$OD): δ 3.38 – 3.28 (m, 2H, overlaps with solvent signal), 3.16 – 3.07 (m, 9H), 1.84 – 1.70 (m, 2H), 1.42 (dq, J = 14.8, 7.4 Hz, 2H), 1.02 (t, J = 7.4 Hz, 3H). **^{19}F NMR (376 MHz, CD$_3$OD):** δ -80.09 (s). **^{13}C NMR (100 MHz, CD$_3$OD):** δ 121.80 (q, J = 318.5 Hz), 67.76 – 67.53 (m), 53.62 – 53.31 (m), 25.83 (s), 20.92 – 20.41 (m), 13.87 (s).

6.23 Deprotonation Kinetics of [N(CH$_3$)$_4$]OTf and [N(CD$_3$)$_4$]OTf

6.23.1 Deprotonation Kinetics of [N(CH$_3$)$_4$]OTf

Figure 6.35. Deprotonation and deuterium quench with subsequent analysis by ^{1}H NMR.

Inside the glove box, an oven-dried 50 mL Schlenk flask equipped with a J. Young inlet valve, glass stopper, screw cap with septum and a glass-coated stir bar was charged with [NMe$_4$]OTf (245.5 mg, 1.1 mmol, 1.1 equiv). The flask was removed from the glove box and attached to a Schlenk line. Dry THF (19.5 mL) was added via syringe. The flask was immersed in an ice bath and the reaction allowed to equilibrate (over ca. 20 min).

An aliquot (ca. 0.2 mL) was taken and immediately quenched by injection into 0.2 mL 1 M DCl / D$_2$O (t = 0 min).

BuLi (500 μL, 1 mmol, 1 equiv; 2 M in cyclohexane) was added dropwise over ca. 30 s via a 1 mL gastight Hamilton syringe (by difference; previously dried at 50 °C in a vacuum oven) (t = 0 min with the first drop). The flask was sealed/closed to the Schlenk line unless aliquots collected.

Aliquots (ca. 0.2 mL) were taken with a disposable 1 mL plastic syringe (flushed several times with Ar) and immediately quenched by injection into 0.2 mL 1 M DCl / D$_2$O (t = 0 min).

Aliquots were diluted with 0.3 mL CD₃OD and analyzed by ^{1}H NMR. Spectra were subsequently analyzed with MestReNova. The integrated 'Full Auto (Bernstein Polynomials)' baseline correction was applied. The spectrum was referenced to the residual solvent peak of CD₃OD (δ = 3.31). Signals of cyclooctane (δ = 1.55, s) and the signal of [N(C*H*₃)₄]⁺ (δ = 3.24, t) (overlap with [N(C*H*₃)₃(CH₂D)]⁺) and [N(CH₃)₃(C*H*₂D)]⁺ (δ = 3.23, br m) were integrated using the sum function.

Exemplary ^{1}H NMR spectra are shown in **Figure 6.36**. The deprotonation progress is shown in **Figure 6.37** (left).

Figure 6.36. ^{1}H NMR spectrum expanded from 3.35 ppm to 3.10 ppm after 0 min (left, before BuLi addition), after 2 min (middle) ,and after (15 min). Residual solvent signal of CD₃OD at 3.31 ppm, [N(CH₃)₄]⁺ at 3.24 ppm overlapping with [N(CH₃)₃(CH₂D)]⁺, and [N(CH₃)₃(CH₂D)]⁺ at 3.23 ppm.
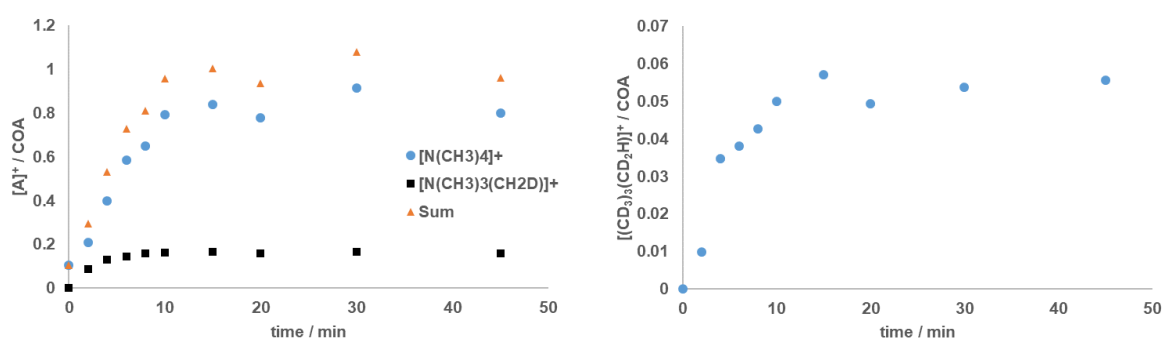
Figure 6.37. Left: Plot of time versus integral ratio of ammonium species [A]⁺ to COA (cyclooctane, internal standard) with the following integral areas of ammonium species: [N(CH₃)₃(C*H*₂D)]⁺ (black squares), [N(C*H*₃)₄]⁺ plus [N(CH₃)₃(C*H*₂D)]⁺ (blue circles), sum of both species, [N(C*H*₃)₄]⁺ plus [N(C*H*₃)₃(C*H*₂D)]⁺ (orange triangles). Right: Plot of time versus integral ratio of [N(CD₃)₃(CD₂*H*)]⁺ to COA (cyclooctane, internal standard).

6.23.2 Deprotonation Kinetics of [N(CD₃)₄]OTf

$$[\text{N(CD}_3)_4]\text{OTf} \xrightarrow[\substack{\text{THF} \\ 0\,°C}]{\substack{\text{1) 1.0 equiv BuLi} \\ \text{2) 1 M TFA / DCM} \\ \text{quench after t}}} [\text{N(CD}_3)_3(\text{CD}_2\text{D})]^+ \;+\; [\text{N(CD}_3)_4]^+$$

1.1 equiv

Figure 6.38. Deprotonation of tetramethylammonium-d₁₂ and proton quench with subsequent analysis by ^{1}H NMR.
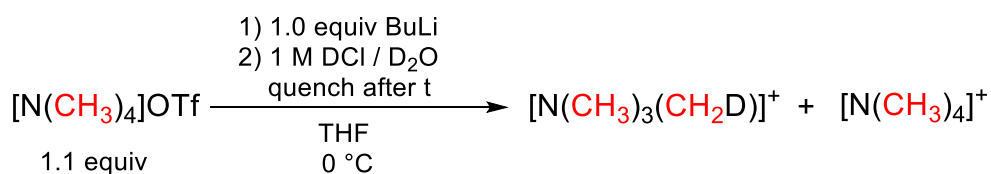
Inside the glove box, an oven-dried 50 mL Schlenk flask equipped with a J. Young inlet valve, glass stopper, screw cap with septum and a glass-coated stir bar was charged with [N(CD$_3$)$_4$]OTf (258.8 mg, 1.1 mmol, 1.1 equiv). The flask was removed from the glove box and attached to a Schlenk line. Dry THF (19.5 mL) was added via syringe. The flask was immersed in an ice bath and the reaction allowed to equilibrate (over ca. 20 min).

An aliquot (ca. 0.2 mL) was taken and immediately quenched by injection into 0.2 mL 1 M TFA in DCM (t = 0 min).

BuLi (500 μL, 1 mmol, 1 equiv; 2 M in cyclohexane) was added dropwise over ca. 30 s via a 1 mL gastight Hamilton syringe (by difference; previously dried at 50 °C in a vacuum oven) (t = 0 min with the first drop). The flask was sealed/closed to the Schlenk line unless aliquots collected.

Aliquots (ca. 0.2 mL) were taken with a disposable 1 mL plastic syringe (flushed several times with Ar) and immediately quenched by injection into 0.2 mL 1 M TFA in DCM.

Aliquots were diluted with 0.3 mL CD$_3$OD and analyzed by ^{1}H NMR. Spectra were subsequently analyzed with MestReNova. The integrated 'Full Auto (Bernstein Polynomials)' baseline correction was applied. The spectrum was referenced to the residual solvent peak of CD$_3$OD (δ = 3.31). Signals of cyclooctane (δ = 1.55, s) and the signal of tetramethylammonium-d$_{11}$ [N(CD$_3$)$_3$(CD$_2$H)]$^+$ (δ = 3.16, m) were integrated using the sum function.

The integral ratio of [N(CD$_3$)$_3$(CD$_2$H)]$^+$ to cyclooctane (internal standard) is taken as the extent of deprotonation.

Exemplary ^{1}H NMR are shown in **Figure 6.39**. The deprotonation progress is shown in **Figure 6.37** (right).
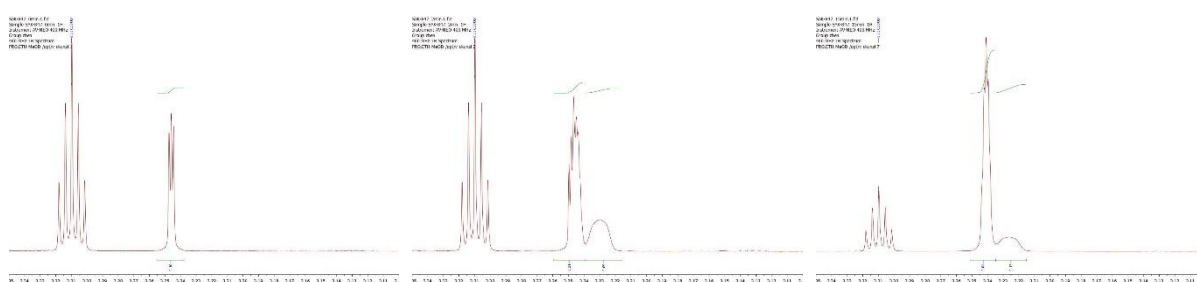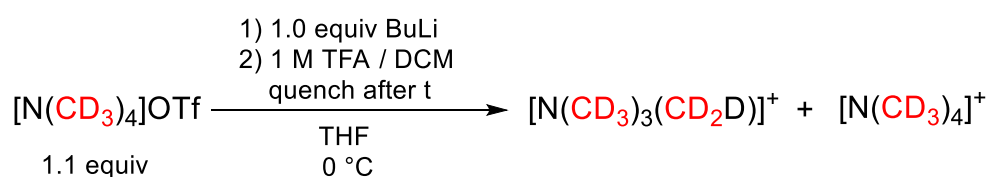

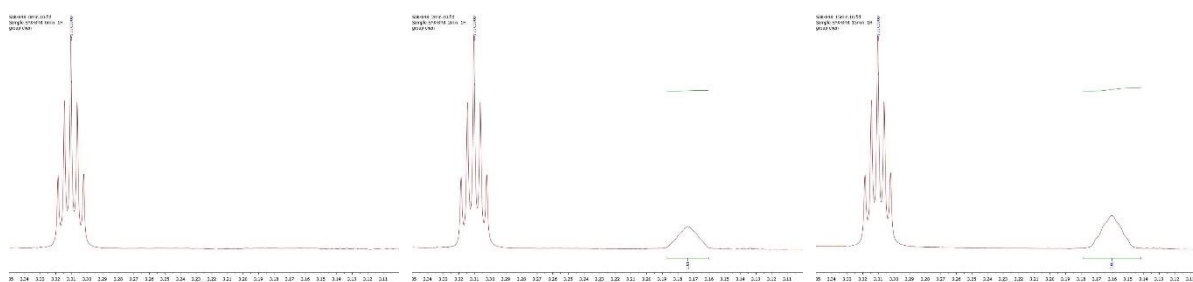**Figure 6.39.** ^{1}H NMR spectrum expanded from 3.35 ppm to 3.10 ppm after 0 min (left, before BuLi addition), after 2 min (middle) ,and after (15 min). Residual solvent signal of CD$_3$OD at 3.31 ppm and [N(CD$_3$)$_3$(CD$_2$H)]$^+$ at 3.16 ppm.

For all deprotonation experiments one can see that the ylide-derived species after quenching, either $[N(CH_3)_3(CH_2D)]^+$ or $[N(CD_3)_3(CD_2H)]^+$, reaches its maximum concentration after about 10 to 15 min (**Figure 6.37**). After that time, the concentration is approximately constants at least up to 45 min. There is no apparent difference in the deprotonation rate between the perprotiated and the perdeuterated tetramethylammonium salt. Thus, there is no observable primary KIE for the deprotonation under these conditions and the rate appears to be dictated by the limited solubility of the ammonium reagent in THF.

6.24 NMR Experiments with unlabeled and ^{13}C-enriched [NMe$_4$]OTf

In the glove box, an oven-dried J. Young NMR tube was charged with $(CH_3)_3N^{13}CH_3OTf$ (6.2 mg, 0.0275 mmol, 1.1 equiv.) or $N(CH_3)_4OTf$ (6.1 mg, 0.0275 mmol, 1.1 equiv.), cyclooctene (16 µL, 0.135 mmol, 5 equiv.) and $(PPh_3)_2NiBr_2$ (~0.2 mg, 0.00025 mmol, 0.01 equiv.; prepared as stock solution) in 0.1 mL THF-d_8, and 0.6 mL THF-d_8. The NMR tube was cooled to -30 °C and n-BuLi (1.6 M in hexane; 16 µL, 0.025 mmol, 1 equiv.) was added via micro syringe. The NMR tube was quickly sealed, vigorously shaken for 5 min while being kept at ca. -30 °C, and then removed from the glove box and placed in an ice bath. The reaction was allowed to slowly warm in the ice bath overnight. ^{1}H and ^{13}C NMR spectra were taken after 23 h. Undecane (3 µL) was added and an aliquot (0.1 mL) was analyzed by GC-FID. The yield was determined by the integral ratio of bicyclo[6.1.0]nonane vs undecane as internal standard (10.2% and 9.3% yield for the ^{13}C-enriched and unlabeled reagent, respectively; yields are typically lower than on normal scale). NMR spectra overlays are shown in chapter 2.

6.25 Isolation of Polymer

An oven-dried 500 mL three-neck round bottom flask equipped with a rubber septum, an argon inlet, a thermometer and a glass-coated stir bar under Ar was charged with NMe$_4$OTf (4.425 g, 20 mmol, 1 equiv.; weighed in the glove box) and $(PPh_3)_2NiBr_2$ (148.6 mg, 0.2 mmol, 0.01 equiv.; weighed in the glove box). 200 mL THF (0.1 M) was added via cannula (Teflon tubing). The reaction was cooled to 0 °C in an ice bath and cyclooctene (13 mL, 100 mmol, 5 equiv.; degassed by sparging with Ar for 30 min) was added via syringe. n-BuLi (1.6 M in hexane; 13.1 mL, 21 mmol, 1.05 equiv.) was added dropwise via syringe over 20 min (temperature constant at ~2 °C). After stirring for 5 min, the Ar inlet was closed to allow no gas exchange and reaction was allowed to

warm to RT inside the ice/water bath overnight. After 23 h, acetic acid (114 μL, 2 mmol, 0.1 equiv.) and TMEDA (60 μL, 0.2 mmol, 0.01 equiv.) were added. All volatiles were removed under vacuum and the solid residue was suspended in 10 mL MeOH, centrifuged and decanted (3 x) and once in 10 mL hexane. The remaining solid was dried under vacuum overnight at RT, 14 h at 60 °C and 12 h at 90 °C to give a beige powder (48 mg, 3.42 mmol, 17% yield calc. as $(CH_2)_n$). (Comparable yields of polymer and bicyclo[6.1.0]nonane have been obtained at 0.05 M, but the polymer was less pure.)

GPC traces are shown in **Figure 6.40** and IR spectra are shown in chapter 2.
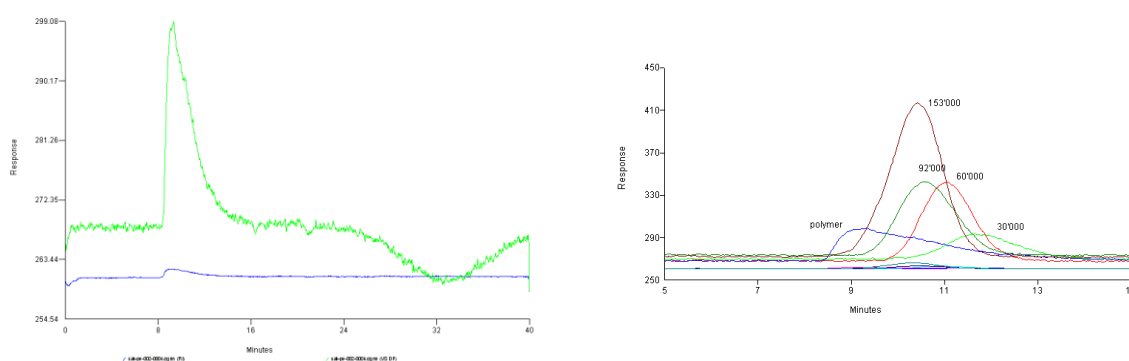
Figure 6.40. Left: GPC trace of the isolated polymer. Right: GPC traces of the isolated polymer and polyethylene standards with M_w indicated in the figure.

6.26 UV-Vis Alkene Binding Titrations

Inside the glove box, a vacuum-oven dried quartz cuvette (10 mm path length) with septum screw cap was charged with phosphine (ca. 10 mM, 20 equiv relative to Ni, see below) and 1.8 mL THF. To this solution was added $Ni(cod)_2$ in 0.2 mL (prepared as stock solution, ca. 4.1 mg in 3 mL THF, ca. 0.5 mM, see below). A separate oven-dried 4 mL vial with septum screw cap was charged with alkene, either neat or as stock solution in THF. The cuvette and vial were removed from the glove box and wrapped with parafilm. The vial containing the alkene was placed under an N_2-atmosphere using a needle inlet. The first measurement was taken without any added alkene and denoted as '0 μL alkene'. Then, alkene was added (by difference) using a gastight 25 μL Hamilton microsyringe and the cuvette was agitated for several seconds to mix. Measurements were taken at room temperature.

The data was analyzed by measuring the absorbance at a specific wavelength as indicated (see below), converting this value to [NiP], the phosphine-only ligated Ni species, using $[NiP]_0$ (no alkene added) = $[Ni(cod)_2]$. The resulting plot of [alkene] versus [NiP] is fitted to equation (6.21) in Excel using a least square method with the binding constant K as fit parameter. ($[Ni]_{tot}$ = $[Ni(cod)_2]$, $[A]_{tot}$ = [alkene], $[P]_{tot}$ = [phosphine]). The volume increase by adding alkene was neglected for the concentration.

The binding constants K are given in tabular form in chapter 4 together with exemplary UV-Vis spectra and titration curves.

6.27 Synthesis and Evaluation of New Ligands
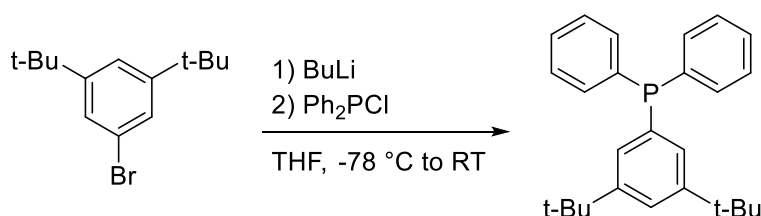
(3,5-Di-*tert*-butylphenyl)diphenylphosphane (L8). A flame-dried 50 mL Schlenk flask with rubber septum was charged with 1-bromo-3,5-di-*tert*-butylbenzene (424 mg, 1.58 mmol, 1.05 equiv), evacuated and refilled with Ar (3x). Dry THF (15 mL) was added via syringe and the reaction was cooled to -78 °C before BuLi (0.75 mL, 2 M in cyclohexane, 1.5 mmol, 1 equiv) was added dropwise via syringe over ca. 2 min. The solution became slightly turbid. The reaction was stirred at -78 °C for 1 h, then Ph₂PCl (277 μL, 1.5 mmol, 1 equiv) was added dropwise via syringe over ca. 2 min. The reaction was stirred at -78 °C for 1 h, removed from the cooling bath and stirred at RT for an additional 30 min. Silica (3 g) was added and all volatiles were removed under vacuum. The residue was loaded on a short column (SiO₂, length: 5 cm, diameter: 2 cm), and eluted with hexane (3x10 mL), then toluene (3x10 mL) using vacuum. The combined toluene fractions were evaporated to dryness and further dried under vacuum to give a colorless, viscous oil (503 mg, 1.34 mmol, 90 %). (The oil is prone to oxidation.)

¹H NMR (400 MHz, CDCl₃): δ 7.40 (t, *J* = 1.8 Hz, 1H), 7.36 – 7.30 (m, 10H), 7.17 (dd, *J* = 8.5, 1.8 Hz, 2H), 1.25 (s, 18H). **³¹P{¹H} NMR (162 MHz, CDCl₃):** δ -3.89. **¹³C{¹H} NMR (100 MHz, CDCl₃):** δ 150.77 (d, *J* = 6.9 Hz), 138.01 (d, *J* = 10.9 Hz), 135.67 (d, *J* = 8.8 Hz), 133.80 (d, *J* = 19.1 Hz), 128.64 (s), 128.47 (d, *J* = 6.8 Hz), 128.37 (d, *J* = 20.2 Hz), 122.89 (s), 35.07 (s), 31.52 (s). **HRMS (ESI, [M+H]⁺):** m/z calcd for C₂₆H₃₂P 375.2236; Found 375.2235. **Elemental analysis**: Calc. for C₂₆H₃₁P: C, 83.39; H, 8.34, P, 8.27. Found: C, 83.49; H, 8.40.
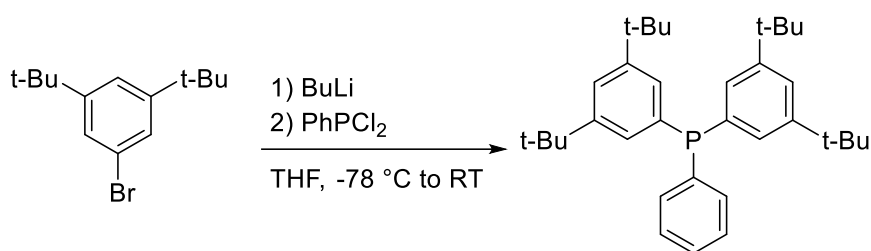
Bis(3,5-di-*tert*-butylphenyl)(phenyl)phosphane (L9). A flame-dried 50 mL Schlenk flask with rubber septum was charged with 1-bromo-3,5-di-*tert*-butylbenzene (848 mg, 3.15 mmol, 2.1 equiv), evacuated and refilled with Ar (3x). Dry THF (15 mL) was added via syringe and the reaction was cooled to -78 °C before BuLi (1.5 mL, 2 M in cyclohexane, 3.0 mmol, 2 equiv) was added dropwise via syringe over ca. 5 min. Within several minutes a white precipitate formed. After 70 min at -78 °C, PhPCl₂ (102 μL, 1.5 mmol, 1 equiv) was added dropwise via syringe. (The precipitate dissolved again within 30 min). The reaction was stirred at -78 °C for 1 h, then removed from the cooling bath and stirred at room temperature for 30 min. Silica (4 g) was added and all volatiles were removed under vacuum. The residue was loaded on a short column (SiO₂, length: ca. 5 cm, diameter: 2 cm), eluted with hexane (3x10 mL), then toluene (3x10 mL). The combined toluene fractions were evaporated to give the product as colorless oil that solidified to a white solid upon drying under vacuum (550 mg, 1.13 mmol, 75 %).

¹H NMR (400 MHz, CDCl₃): δ 7.41 (td, *J* = 1.9, 0.6 Hz, 2H), 7.36 – 7.33 (m, 5H), 7.18 (dd, *J* = 8.3, 1.9 Hz, 4H), 1.27 (s, 36H). **³¹P{¹H} NMR (162 MHz, CDCl₃):** δ -3.11 (s). **¹³C{¹H} NMR (100 MHz, CDCl₃):** δ 150.62 (d, *J* = 6.8 Hz), 138.67 (d, *J* = 11.1 Hz), 136.34 (d, *J* = 9.0 Hz), 133.65 (d, *J* = 18.8 Hz), 128.42 (s), 128.30 (d, *J* = 6.7 Hz), 128.26 (d, *J* = 19.8 Hz), 122.65 (s), 35.03 (s), 31.53 (s). **HRMS (ESI, [M+H]⁺):** m/z

calcd for $C_{34}H_{48}P$ 487.3488; Found 487.3486. **Elemental analysis**: Calc. for $C_{34}H_{47}P$: C, 83.90; H, 9.73, P, 6.36. Found: C, 84.15; H, 9.73.
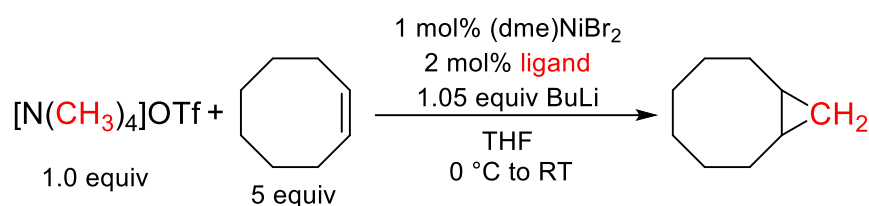
Figure 6.41. Evaluation of new ligands.

The reaction was conducted according to the standard conditions in section 6.2.

Table 6.7. Evaluation of New Ligands.

Entry	Ligand	Yield / %
1	P(3,5-di^{t}BuPh)Ph$_2$	32
2	P(3,5-di^{t}BuPh)$_2$Ph	48

6.27.1 Characterization of Other Ligands

2-(Diphenylphosphaneyl)-N,N-dimethylethan-1-amine (L1)[8]: ^{1}H NMR (400 MHz, CDCl$_3$): δ 7.48 – 7.40 (m, 4H), 7.38 – 7.30 (m, 6H), 2.48 – 2.35 (m, 2H), 2.29 – 2.19 (m, 8H). **^{31}P{^{1}H} NMR (162 MHz, CDCl$_3$):** δ -19.88 (s).

1-(2-(Diphenylphosphaneyl)ethyl)pyrrolidine (L2): ^{1}H NMR (400 MHz, CDCl$_3$): δ 7.51 – 7.41 (m, 4H), 7.36 – 7.28 (m, 6H), 2.65 – 2.54 (m, 2H), 2.55 – 2.46 (m, 4H), 2.37 – 2.26 (m, 2H), 1.80 – 1.72 (m, 4H). **^{31}P{^{1}H} NMR (162 MHz, CDCl$_3$):** δ -19.44 (s). **^{13}C{^{1}H} NMR (100 MHz, CDCl$_3$):** δ 138.55 (d, J = 12.8 Hz), 132.71 (d, J = 18.7 Hz), 128.56 (s), 128.43 (d, J = 6.7 Hz), 53.99 (s), 52.96 (d, J = 23.3 Hz), 27.85 (d, J = 11.5 Hz), 23.46 (s). **HRMS (ESI, [M+Na]$^+$):** m/z calcd for $C_{18}H_{22}NNaP$ 306.1382; Found 306.1382. **Elemental analysis**: Calc. for $C_{18}H_{22}NP$: C, 76.30; H, 7.83; N, 4.94. Found: C, 76.02; H, 7.91; N, 5.12.

1,2-Bis(bis(trifluoromethyl)phosphaneyl)ethane (L4)[9]: ^{1}H NMR (400 MHz, C$_6$D$_6$): δ 1.68 – 1.54 (m, 4H). (Impure, likely PhOTMS ca. 200 mol%). **^{31}P{^{1}H} NMR (162 MHz, C$_6$D$_6$):** δ 1.75 – -3.57 (m). **^{19}F NMR (376 MHz, C$_6$D$_6$):** δ -53.90 – -55.00 (m).

Ni(L4)$_2$: ^{1}H NMR (400 MHz, C$_6$D$_6$): δ 1.51 (d, J = 13.5 Hz, 4H). **^{31}P{^{1}H} NMR (162 MHz, C$_6$D$_6$):** δ 66.97(br). **^{19}F NMR (376 MHz, C$_6$D$_6$):** δ-58.87 – -59.59 (m).

Phenylbis(trifluoromethyl)phosphane (L5)[9]: ^{1}**H NMR (400 MHz, C$_6$D$_6$):** δ 7.48 (dd, J = 9.9, 7.7 Hz, 1H), remaining peaks hidden under impurity (13 % pure). ^{31}**P{**^{1}**H} NMR (162 MHz, C$_6$D$_6$):** δ -0.04 (hept, J = 79.3 Hz). ^{19}**F NMR (376 MHz, C$_6$D$_6$):** δ -53.35 (d, J = 79.3 Hz).

(L5)$_2$Ni(cod): ^{1}**H NMR (400 MHz, C$_6$D$_6$):** δ 7.45 (t, J = 8.6 Hz, 4H), 6.95 − 6.74 (m, 6H), 5.12 (d, J = 7.4 Hz, 4H), 2.42 − 2.20 (m, 4H), 1.90 (t, J = 9.2 Hz, 4H). ^{31}**P{**^{1}**H} NMR (162 MHz, C$_6$D$_6$):** δ 55.22 − 52.51 (m). ^{19}**F NMR (376 MHz, C$_6$D$_6$):** δ -55.41 − -55.74 (m).

Bis(trifluoromethyl)(2',4',6'-trimethyl-[1,1'-biphenyl]-2-yl)phosphane (L6): ^{1}**H NMR (400 MHz, C$_6$D$_6$):** δ 8.11 − 8.01 (m, 1H), 7.06 (tt, J = 7.5, 1.2 Hz, 1H), 6.94 (td, J = 7.7, 1.5 Hz, 1H), 6.85 (ddd, J = 7.3, 5.4, 1.5 Hz, 1H), 6.78 (s, 2H), 2.14 (s, 3H), 1.85 (s, 6H). ^{31}**P{**^{1}**H} NMR (162 MHz, C$_6$D$_6$):** δ -9.60 (hept, J = 81.2 Hz). ^{19}**F NMR (376 MHz, C$_6$D$_6$):** δ -52.63 (d, J = 81.5 Hz). **HRMS (ESI, [M+H]$^+$):** m/z calcd for C$_{17}$H$_{16}$F$_6$P 365.0888; Found 365.0892. **HRMS (MALDI, [M+H]$^+$):** m/z calcd for C$_{17}$H$_{16}$F$_6$P 365.0888; Found 365.0888. The compound ionizes poorly by ESI and MALDI.

Bis(perfluoroethyl)(2',4',6'-trimethyl-[1,1'-biphenyl]-2-yl)phosphane (L7): ^{1}**H NMR (400 MHz, C$_6$D$_6$):** δ 8.05 (ddd, J = 8.0, 3.1, 1.4 Hz, 1H), 7.05 (tt, J = 7.5, 1.2 Hz, 1H), 6.98 − 6.83 (m, 2H), 6.77 (q, J = 0.7 Hz, 2H), 2.09 (s, 3H), 1.88 (s, 6H). ^{31}**P{**^{1}**H} NMR (162 MHz, C$_6$D$_6$):** δ -5.83 − -8.22 (m). ^{19}**F NMR (376 MHz, C$_6$D$_6$):** δ -81.78 − -82.30 (m), -106.06 − -113.58 (m). ^{13}**C{**^{1}**H} NMR (100 MHz, CDCl$_3$):** δ 151.33 (d, J = 43.0 Hz), 138.04 (s), 136.80 (s), 136.44 (d, J = 9.3 Hz), 136.33 (d, J = 1.9 Hz), 133.43 (d, J = 1.5 Hz), 131.56 (d, J = 8.6 Hz), 128.31 (s), 127.72 (d, J = 1.8 Hz), 21.29 (s), 20.24 (s). (Not all C$_{Ar}$, CF$_2$, CF$_3$ visible and/or resolved.) **HRMS (ESI, [M+H]$^+$):** m/z calcd for C$_{19}$H$_{16}$F$_{10}$P 465.0824; Found 465.0821. **HRMS (MALDI, [M+H]$^+$):** m/z calcd for C$_{19}$H$_{16}$F$_{10}$P 465.0824; Found 465.0824. The compound ionizes poorly by ESI and MALDI. **Elemental analysis**: Calc. for C$_{19}$H$_{15}$F$_{10}$P: C, 49.15; H, 3.26. Found: C, 46.35; H, 2.94. Possibly incomplete combustion due to perfluoroethyl groups.

Tris(3,5-di-tert-butylphenyl)phosphane (L10)[21]: ^{1}**H NMR (400 MHz, CDCl$_3$):** δ 7.36 (td, J = 1.9, 0.5 Hz, 3H), 7.08 (dd, J = 8.1, 1.8 Hz, 6H), 1.22 (s, 54H). ^{31}**P{**^{1}**H} NMR (162 MHz, CDCl$_3$):** δ -3.40. ^{13}**C{**^{1}**H} NMR (100 MHz, CDCl$_3$):** δ 150.52 (d, J = 6.6 Hz), 136.96 (d, J = 8.5 Hz), 128.11 (d, J = 19.2 Hz), 122.41 (s), 35.01 (s), 31.53 (s). **HRMS**

(ESI, [M+H]⁺): m/z calcd for $C_{42}H_{64}P$ 599.4740; Found 599.4733. **Elemental analysis**: Calc. for $C_{42}H_{63}P$: C, 84.23; H, 10.60. Found: C, 84.03; H, 10.52.

Bis(3,5-di-tert-butyl-4-methoxyphenyl)(phenyl)phosphane (L11): ¹H NMR (400 MHz, CDCl₃): δ 7.37 (d, J = 11.0 Hz, 4H), 7.55 – 7.43 (m, 5H), 3.71 (s, 6H), 1.35 (s, 36H). ³¹P{¹H} NMR (162 MHz, CDCl₃): δ -6.65 (s), impurity: 35.44 (s), likely phosphine oxide, 84% purity. **(L11)₂NiBr₂: Elemental analysis**: Calc. for $C_{72}H_{102}O_4P_2NiBr_2$: C, 65.91; H, 7.84. Found: C, 65.21; H, 7.82. Likely phosphine oxide impurity.

(2,2'',4,4'',6,6''-Hexaisopropyl-[1,1':3',1''-terphenyl]-5'-yl)diphenylphosphane (L12): ¹H NMR (400 MHz, C₆D₆): δ 7.50 – 7.37 (m, 4H), 7.40 (dd, J = 7.4, 1.6 Hz, 2H), 7.15 (s, 4H, overlapping with solvent signal), 7.14 – 6.88 (m, 8H), 2.99 (hept, J = 7.0 Hz, 4H), 2.84 (hept, J = 6.8 Hz, 2H), 1.26 (d, J = 6.9 Hz, 12H), 1.21 (d, J = 6.9 Hz, 12H), 1.12 (d, J = 6.9 Hz, 12H). (Aromatic region not properly resolved.) ³¹P{¹H} NMR (162 MHz, C₆D₆): δ -5.83 (s). ¹H NMR (400 MHz, CDCl₃): δ 7.41 – 7.34 (m, 4H), 7.32 – 7.28 (m, 6H), 7.11 (dd, J = 7.6, 1.6 Hz, 2H), 6.99 (s, 4H), 6.97 (t, J = 1.6 Hz, 1H), 2.89 (hept, J = 6.9 Hz, 2H), 2.71 (hept, J = 6.8 Hz, 4H), 1.27 (d, J = 6.9 Hz, 12H), 1.05 (appt t, J = 6.7 Hz, 24H). ³¹P{¹H} NMR (162 MHz, CDCl₃): δ -4.89 (s). ¹³C{¹H} NMR (100 MHz, CDCl₃): δ 147.98 (s), 146.45 (s), 140.71 (d, J = 6.8 Hz), 137.50 (d, J = 11.2 Hz), 137.33 (d, J = 11.6 Hz), 136.69 (s), 133.89 (d, J = 19.6 Hz), 132.83 (d, J = 18.6 Hz), 131.81 (s), 128.88 (s), 128.61 (d, J = 7.1 Hz), 120.56 (s), 34.37 (s), 30.62 (s), 24.24 (s), 24.22 (s), 24.19 (s). **HRMS (ESI, [M+H]⁺):** m/z calcd for $C_{48}H_{60}P$ 667.4427; Found 667.4419.

(L12)₂NiBr₂: Elemental analysis: Calc. for $C_{96}H_{118}P_2NiBr_2$: C, 74.27; H, 7.66. Found: C, 74.24; H, 7.64.

Bis(2,2'',4,4'',6,6''-hexaisopropyl-[1,1':3',1''-terphenyl]-5'-yl)(phenyl)phosphane (L13): ¹H NMR (400 MHz, CDCl₃): δ 7.29 (dd, J = 8.1, 1.6 Hz, 4H), 7.24 – 7.22 (m, 5H), 6.99 (appt t, J = 1.6 Hz, 2H), 6.97 (s, 8H), 2.89 (hept, J = 7.0 Hz, 4H), 2.62 (appt dp, J = 13.3, 6.6 Hz, 8H), 1.27 (d, J = 6.9 Hz, 24H), 1.01 (appt t, J = 6.5 Hz, 24H), 0.95 (d, J = 6.8 Hz, 12H), 0.87 (d, J = 6.9 Hz, 12H). ³¹P{¹H} NMR (162 MHz, C₆D₆): δ -4.28 (s). ¹³C{¹H} NMR (100 MHz, CDCl₃): δ 147.97 (s), 146.43 (d, J = 1.6 Hz), 140.85 (d, J = 7.6 Hz), 136.62 (s), 133.42 (d, J = 20.2 Hz), 133.12 (d, J = 18.1 Hz), 132.23 (s), 128.47 (d, J = 6.2 Hz), 128.32 (s), 120.51 (d, J = 4.8 Hz), 34.44 (s), 30.57 (s), 24.25

(s), 24.22 (s), 24.21 (s), 24.18 (s), 24.08 (s). (iPr groups appear slightly inequivalent, not all aromatic C are resolved and/or appear as apparent doublets.) **HRMS (ESI, [M+H]$^+$):** m/z calcd for $C_{78}H_{104}P$ 1071.7870; Found 1071.7856. **Elemental analysis**: Calc. for $C_{78}H_{103}P$: C, 87.42; H, 9.69. Found: C, 87.28; H, 9.80.

Bis(3,5-bis(trimethylsilyl)phenyl)(phenyl)phosphane (L14): ^{1}H NMR (400 MHz, CDCl$_3$): δ 7.62 (q, *J* = 1.2 Hz, 2H), 7.42 (dd, *J* = 7.6, 1.2 Hz, 4H), 7.35 – 7.28 (m, 5H), 0.18 (s, 36H). **^{31}P{^{1}H} NMR (162 MHz, CDCl$_3$):** δ -5.60 (s). **^{13}C{^{1}H} NMR (100 MHz, CDCl$_3$):** δ 139.58 (d, *J* = 5.1 Hz), 139.43 (d, *J* = 18.9 Hz), 138.42 (s), 138.00 (d, *J* = 10.9 Hz), 135.48 (d, *J* = 12.0 Hz), 133.65 (d, *J* = 18.8 Hz), 128.61 (s), 128.40 (d, *J* = 6.7 Hz), -1.03 (s). **HRMS (ESI, [M+H]$^+$):** m/z calcd for $C_{30}H_{48}PSi_4$ 551.2565; Found 551.2576. **Elemental analysis**: Calc. for $C_{30}H_{47}Si_4P$: C, 65.39; H, 8.60. Found: C, 65.16; H, 8.58.

(3,5-Bis(triethylsilyl)phenyl)diphenylphosphane (L15): ^{1}H NMR (400 MHz, CDCl$_3$): δ 7.59 (q, *J* = 1.2 Hz, 1H), 7.42 – 7.38 (m, 2H), 7.38 – 7.30 (m, 10H), 0.96 – 0.86 (m, 18H), 0.77 – 0.68 (m, 12H). **^{31}P{^{1}H} NMR (162 MHz, CDCl$_3$):** δ -5.55 (s). Impurity at -5.13 (s), likely Ar$_2$P(3-Br-5-TESPh). (Purity: 90%). **^{13}C{^{1}H} NMR (100 MHz, CDCl$_3$):** δ 140.51 (s), 140.18 (d, *J* = 18.9 Hz), 137.84 (d, *J* = 10.9 Hz), 136.41 (d, *J* = 5.0 Hz), 134.85 (d, *J* = 11.2 Hz), 133.78 (d, *J* = 19.1 Hz), 128.68, 128.50 (d, *J* = 6.8 Hz), 7.52 (s), 3.50 (s). **HRMS (ESI, [M+H]$^+$):** m/z calcd for $C_{30}H_{44}PSi_2$ 491.2714; Found 491.2722.

Bis(3,5-bis(triethylsilyl)phenyl)(phenyl)phosphane (L16): ^{1}H NMR (400 MHz, CDCl$_3$): δ 7.58 (q, *J* = 1.2 Hz, 2H), 7.39 – 7.30 (m, 9H), 0.95 – 0.84 (m, 36H), 0.78 – 0.65 (m, 24H). **^{31}P{^{1}H} NMR (162 MHz, CDCl$_3$):** δ -5.91 (s). Impurity at -5.39 (s), likely Ar$_2$P(3-Br-5-TESPh). (Purity: 90%). **^{13}C{^{1}H} NMR (100 MHz, CDCl$_3$):** δ 140.41 (s), 140.07 (d, *J* = 18.6 Hz), 138.03 (d, *J* = 10.7 Hz), 136.25 (d, *J* = 5.0 Hz), 135.39 (d, *J* = 11.4 Hz), 133.68 (d, *J* = 18.7 Hz), 128.52 (s), 128.36 (d, *J* = 6.8 Hz), 7.50 (s), 3.49 (s). **HRMS (ESI, [M+H]$^+$):** m/z calcd for $C_{42}H_{72}PSi_4$ 719.4443; Found 719.4439.

6.28 Ligand Parametrization Model

The steric parameters are given in **Table 6.8** for the DFT-optimized $(C_2H_4)_2Ni(PR_3)$ complexes. Multivariate ligand parametrization models were generated using the *Multiple Linear Regression* fit as implemented in the OriginPro software package.

Table 6.8. Steric Parameters, Binding Constants and Yields with COE for Several Phosphines.

Phosphine	Exact cone angle $\theta°$	Exact solid cone angle $\Theta°$	$\%V_{Bur}$	K	% Yield
PPhMe$_2$	138.947	122.863	26.5	0.0014	3[a]
PPh$_2$Me	155.594	129.365	28.6	0.0013	0.3[a]
PPh$_3$	168.196	135.023	30.4	0.081	25
P(3,5-di^{t}BuPh)Ph$_2$	188.849	142.79	31.2	0.11	32
P(3,5-di^{t}BuPh)$_2$Ph	195.345	148.329	31.1	0.090	48

6.29 Computational Details

The computations in this thesis have been performed by Dr. Renana Gershoni-Poranne.

Gaussian 09 Revision D was used for all calculations.[22] All geometries were optimized and frequencies calculations were performed to ensure real minima for the intermediates (i.e., $N_{imag} = 0$) and first-order saddle points for the transition states (i.e., $N_{imag} = 1$). The energies reported are zero-point corrected energies. Density functionals and basis sets were benchmarked by comparison to literature-known crystal structures of compounds [(PMDTA)Li][MeNi(C_2H_4)$_2$] and nickel carbenes **1.2** and **1.3** (see chapter 1). M06L/def2-SVP was chosen as optimal choice of accuracy and computational cost.

The computed energies are shown in **Table 6.9**. The catalytic cycle and energy profile are shown in chapter 3. Model systems with two PH_3 and two ethenes as ligands showed similar reactivity.[16]

Table 6.9. Computed Energies for the Cyclopropanation Reaction with a Model System.

Entry	Step	Energy / kcal mol^{-1}
1	I + II to III	-42.78
2	III to TSIII-IV	15.02
3	TSIII-IV to IV + LiOTf·NMe$_3$	-12.37
4	IV to TSIV-V	9.47
5	TSIV-V to V	-19.22
6	V + C$_2$H$_4$ to VI	-29.23
7	VI to TSVI-VII	3.81
8	TSVI-VII to (VII + I)	-9.54

6.30 References

1. Sarria Toro, J. M.; den Hartog, T.; Chen, P. *Chem Commun (Camb)* **2014,** *50*, 10608-10610.
2. Sarria Toro, J. M.; Garcia-Morales, C.; Raducan, M.; Smirnova, E. S.; Echavarren, A. M. *Angewandte Chemie* **2017,** *56*, 1859-1863.
3. Kunzi, S. A.; Sarria Toro, J. M.; den Hartog, T.; Chen, P. *Angewandte Chemie* **2015,** *54*, 10670-10674.
4. Friedrich, E. C.; Domek, J. M.; Pong, R. Y. *The Journal of organic chemistry* **1985,** *50*, 4640-4642.
5. den Hartog, T.; Toro, J. M.; Chen, P. *Organic letters* **2014,** *16*, 1100-1103.
6. Tchawou, A. A. S. W.; Raducan, M.; Chen, P. *Organometallics* **2017,** *36*, 180-191.
7. Habtemariam, A.; Watchman, B.; Potter, B. S.; Palmer, R.; Parsons, S.; Parkin, A.; Sadler, P. J. *Journal of the Chemical Society, Dalton Transactions* **2001**, 1306-1318.
8. Malet, R.; Moreno-Mañas, M.; Parella, T.; Pleixats, R. *The Journal of organic chemistry* **1996,** *61*, 758-763.
9. Murphy-Jolly, M. B.; Lewis, L. C.; Caffyn, A. J. M. *Chemical Communications* **2005**, 4479-4480.
10. Wu, K.; Doyle, A. G. *Nat Chem* **2017,** *9*, 779-784.
11. Sevov, C. S.; Hartwig, J. F. *J. Am. Chem. Soc.* **2014,** *136*, 10625-10631.
12. Pörschke, K.-R.; Jonas, K.; Wilke, G.; Benn, R.; Mynott, R.; Goddard, R.; Krüger, C. *Chemische Berichte* **1985,** *118*, 275-297.
13. Pörschke, K.-R.; Wilke, G.; Mynott, R. *Chemische Berichte* **1985,** *118*, 298-312.
14. Pörschke, K.-R. *Chemische Berichte* **1987,** *120*, 425-427.
15. Tolman, C. A. *J. Am. Chem. Soc.* **1974,** *96*, 2780-2789.
16. Künzi, S. A.; Gershoni-Poranne, R.; Chen, P. *Organometallics* **2019,** *38*, 1928-1938.
17. Cai, G.; Fu, Y.; Li, Y.; Wan, X.; Shi, Z. *J. Am. Chem. Soc.* **2007,** *129*, 7666-7673.
18. Liang, R.; Li, S.; Wang, R.; Lu, L.; Li, F. *Org. Lett.* **2017,** *19*, 5790-5793.
19. Heydenreich, F.; Mollbach, A.; Wilke, G.; Dreeskamp, H.; Hoffmann, E. G.; Schroth, G.; Seevogel, K.; Stempfle, W. *Israel Journal of Chemistry* **1972,** *10*, 293-319.
20. Herbert, D. E.; Lara, N. C.; Agapie, T. *Chemistry - A European Journal* **2013,** *19*, 16453-16460.
21. Cinderella, A. P.; Vulovic, B.; Watson, D. A. *J. Am. Chem. Soc.* **2017,** *139*, 7741-7744.
22. Frisch, M. J.; Trucks, G. W.; Schlegel, H. B.; Scuseria, G. E.; Robb, M. A.; Cheeseman, J. R.; Scalmani, G.; Barone, V.; Petersson, G. A.; Nakatsuji, H.; Li, X.; Caricato, M.; Marenich, A. V.; Bloino, J.; Janesko, B. G.; Gomperts, R.; Mennucci, B.; Hratchian, H. P.; Ortiz, J. V.; Izmaylov, A. F.; Sonnenberg, J. L.; Williams; Ding, F.; Lipparini, F.; Egidi, F.; Goings, J.; Peng, B.; Petrone, A.; Henderson, T.; Ranasinghe, D.; Zakrzewski, V. G.; Gao, J.; Rega, N.; Zheng, G.; Liang, W.; Hada, M.; Ehara, M.; Toyota, K.; Fukuda, R.; Hasegawa, J.; Ishida, M.; Nakajima, T.; Honda, Y.; Kitao, O.; Nakai, H.; Vreven, T.; Throssell, K.; Montgomery Jr., J. A.; Peralta, J. E.; Ogliaro, F.; Bearpark, M. J.; Heyd, J. J.; Brothers, E. N.; Kudin, K. N.; Staroverov, V. N.; Keith, T. A.; Kobayashi, R.; Normand, J.; Raghavachari, K.; Rendell, A. P.; Burant, J. C.; Iyengar, S. S.; Tomasi, J.; Cossi, M.; Millam, J. M.; Klene, M.; Adamo, C.; Cammi, R.; Ochterski, J. W.; Martin, R. L.; Morokuma, K.; Farkas, O.; Foresman, J. B.; Fox, D. J. *Gaussian 09 Rev. D.01*, Wallingford, CT, 2016.